Intelligent and Cost-effective Protection Schemes for Improved Reliability of Large-Scale Wind Farms

by
Nima Rezaei

A thesis submitted in partial fulfilment of the requirement for the degree of
Doctor of Philosophy at
Department of Electrical Engineering
Lakehead University
Thunder Bay, Ontario, Canada
March 2021

Abstract

Recently, wind power has become a reliable and cost-effective renewable energy source of electricity due to the foreseeable exhaustion of fossil fuel-based power generations and its growing adverse effects on the environment as it is the main source of greenhouse gases. Doubly fed induction generator (DFIG) based wind farm gets the popularity due to its ability for variable speed operation, reactive power control, and reduced converter ratings. Traditional protection schemes result in huge protection failure during fault and abnormality incidents for wind farms since wind turbine fault analysis behavior is different from conventional synchronous generators. Thus, the simple conventional settings for relays would result in maloperation and miscoordination between relays for wind farms and hence, the existing wind farms protection schemes need to be significantly improved. The specific problems with wind farm protection relaying that this thesis aims to solve are presented below:

1. Overcurrent protection relays: Non-optimal settings, resulting in delayed operation of relays or false tripping resulting in stress in power quality, unnecessary disconnection of healthy feeders, severe damage to power apparatus, and endanger personnel safety.

2. Coordination of protective relays: Miscoordination and maloperation of protection relays as a result of dynamic behavior of wind farms.

3. Distance protection relays: Inaccurate impedance measurement, causing: maloperation, false tripping, over-reaching and under-reaching, delayed operation and miscoordination between different zones of protection.

4. Differential protection relays: Implementation of this technique could be extremely costly, since installing several microprocessor-based differential protection relays (MDPRs) with extensive communication links at a large-scale wind farms could be quite expensive.

Thus, in order to solve the aforementioned wind farm protection issues, a multifold approach has been implemented that involves both power system protection and application of artificial intelligence and machine learning techniques. The first problem is successfully addressed by developing an Overcurrent Relay (OCR) based on IEC60255-151:2009 standard, along with a user-friendly graphical interface and coding in Matlab. The relay settings and coordination criteria are defined based on conventional nonlinear time-current relay curve optimization method and then in order to improve the relay operation time, settings and coordination, a Genetic Algorithm (GA)-based new optimization technique by formulating an objective function (OF) is developed. In order to address the second problem associated with adverse effect of dynamic behavior of DFIG based wind farms on protective relays performance, a new adaptive and optimal overcurrent protection for large-scale wind farms using hybrid Grey Wolf Optimizer and rule-based Fuzzy Logic Controller (GWO-FLC) protection scheme is proposed. The GWO is implemented to attain optimal OCR coordination for the defined quadruple group settings for all relays, and the FLC is developed to provide adaptive feature for the relays to cope with the variation in wind speeds. The proposed GWO-FLC performance has been found to be robust, reliable, efficient and extremely satisfactory.

In order to address the third and fourth problems, digital differential protection scheme is developed and designed for providing adequate protection for the intertie section of wind farms. Furthermore, a cost-effective and more reliable differential protection relay is designed for wind farms using a field-programmable gate array (FPGA). The performance of the proposed FPGA-based digital differential protection relay (FPGA-DDPR) is verified in the lab environment using DE2-115 FPGA board equipped with Cyclone IV E (EP4CE115F29C7). The experimental results show that the proposed FPGA-DDPR can successfully detect fault locations, trips the internal

faults and even faults with extremely high resistance, while ignores the external fault. Thus, the proposed FPGA-DDPR protection scheme would be a cost-effective alternative to MDPRs. Finally, a new Bayesian-based optimized Support Vector Machine (SVM) as a supervised machine learning classifier approach is developed to take into account both the dynamic behaviors of wind speed and the current measured by the current transformers. The performance of the proposed method is compared to several other successful classification-based machine learning techniques. It is found the proposed SVM-DDPR had superior performance with an astonishing average accuracy of 99.8% in the context of distinguishing the normal operation, internal and external faults that helps the protective relays to avoid any false tripping.

Acknowledgment

This thesis becomes a reality with the kind support and encouragement of many individuals. I would like to extend my sincere thanks to all of them.

First, I would like to express my deep and sincere gratitude to my parents for their consistent encouragement, patience, selflessness and support which gave me a peace of mind to carry out my work.

It is a genuine pleasure to express my deep sense of appreciation and gratitude to my research supervisor, Dr. M. N. Uddin for his support, guidance and valuable advices during all these years. His wisdom and supervision were the main reason behind the successful writing of this thesis, many publications, and completion of my Ph.D. program. I learned many things from him during my research, his prompt inspirations and timely suggestions with kindness helped me a lot to grow as a better researcher.

I wish to thank the members of my supervisory committee, Dr. K. Natarajan and Dr. Qiang Wei, as well as the graduate coordinator of department of electrical engineering, Dr. A. Tayebi, for all their valuable feedbacks, insightful suggestions, and academic advice.

Finally, it is my privilege to thank my collogues, lab mates, and friends in both Thunder Bay and Barrie campus for their unconditional help and cooperation. My special thanks go to Dr. Md. M. Hasan as well as many other professors, students and the staff of Lakehead University and Georgian college who helped me a lot in numerous occasions during my Ph.D. study.

Table of contents

List of Figures

XII

XIII

XV

List of Tables

List of Acronyms

DG   Distributed generation

DFIG   Doubly fed induction generator

NERC   North American electric reliability corporation

MPR   Microprocessor-based protection relay

MDPR   Microprocessor-based differential protection relay

OCR   Overcurrent relay

GA   Genetic algorithm

OF   Objective function

GWO   Grey wolf optimizer

FLC   Fuzzy logic controller

GWO-FLC   Grey wolf optimizer based fuzzy logic controller

FPGA   Field-programmable gate array

DBPR   Differential-based protection relay

DDPR   Digital differerntial protection relay

DDPS   Digital differential protection scheme

FPGA-DDPR   Field-programmable gate array based digital differential protection relay

FPGA-DDPS   Field-programmable gate array based digital differential protection scheme

SVM	Support vector machine
SVM-DDPR	Support vector machine based digital differential protection relay
SVM-DDPS	Support vector machine based digital differential protection scheme
WWEA	World wind energy association
WTG	Wind turbine generator
VAWT	Vertical-axis wind turbine
HAWT	Horizontal-axis wind turbine
GE	General Electric
MPPT	Maximum power point tracking
P&C	Protection and control
CB	Circuit breaker
VT	Voltage transformer
CT	Current transformer
PT	Potential transformer
FCL	Fault current limiter
LVRT	Low voltage ride through
FRT	Fault ride through
LP	Linear programming
NLP	Nonlinear programming

GAMS	General algebraic modeling system
AI	Artificial intelligence
NIA	Nature inspired algorithm
ANN	Artificial neural network
ABC	Artificial bee colony
HSA	Harmony search algorithm
HBA	Honey bee algorithm
PSO	Particle swarm optimization
IEC	International Electrotechnical Commission
IEEE	Institute of Electrical and Electronics Engineers
RMS	Root mean square
GOOSE	Generic object-oriented substation event
SCIG	Squirrel cage induction generator
TMS	Time multiplier setting
PF	Power factor
PU	Per unit
HV	High voltage
EHV	Extra high voltage
SLG	Single line to ground

RSC	Rotor side converter
GSC	Grid side converter
WRIG	Wound rotor induction generator
PMSG	Permenent magnet synchronous generator
TCC	Time current characteristics
PS	Plug setting
PMS	Plug multiplier setting
CTI	Coordination time interval
SEL	Schweitzer Engineering Laborotary
RSI	Relay setting current
FLA	Full load amperage
ML	Machine learning
ADC	Analog to digital converter
DAC	Digital to analog converter
MUX	Multiplexer
DSP	Digital signal processing
IC	Integrated circuit
HDL	Hardware desciption language
FIL	FPGA-in-the-loop

HIL	Hardware-in-the-loop
RIL	Relay-in-the-loop
GP	Gaussian Process
UCB	Upper confidence band
MPI	Maximum probablity of improvement
EI	Expected improvement
CDF	Cumulative distribution function
PDF	Probability density function

Chapter 1

Introduction

1.1 Background

Over the last couple of decades, popularity of renewable energy sources is increasing rapidly to cope with the proliferation in power demand and thus, decreasing the dependence on fossil fuels to reduce the greenhouse gas emission. Among various renewable resources, wind energy converted to electric energy has emerged as the leading source due to its easy availability and environment-friendly nature [1]. Wind power plants have been widely employed as the means of power generation in smart grids and microgrids as a distributed generation (DG) system. Undoubtedly, wind power has dominated as the mainstream of renewable energy systems in most developed countries as a reliable and financially reasonable source of electricity. The contribution of wind energy to power generation has reached a considerable share even on the worldwide level [2]. According to world wind energy association (WWEA), the overall capacity of all wind turbines installed worldwide by the end of 2018 and 2019 reached, 591 and 650.8 Gigawatt (GW) respectively, while this remarkable growth was hindered in 2020 due to COVID-19 pandemic [3]. This remarkable trend, updated at the time of writing this thesis, is depicted in Fig. 1.1.

It is estimated that 6% of the global energy demand can be provided by all wind turbines installed by the end of 2019 and this rate is slowly but steadily increasing annually which signifies the eminence of wind energy as a reliable source of power. The leading countries in harnessing wind energy, in order, by the end of 2019 are: China, US, Germany, India, Spain, UK, France,

Brazil, Canada and Italy [4]. In the years to come, there will be more and more wind power plants connected to the grid, thus, with the goal of 20% global wind penetration by 2030, the wind farm's operation should be well planned. The power system switchgear and power system protection for wind power plants should be carefully designed to be compatible with the operation of conventional synchronous generators connected to the same grid.
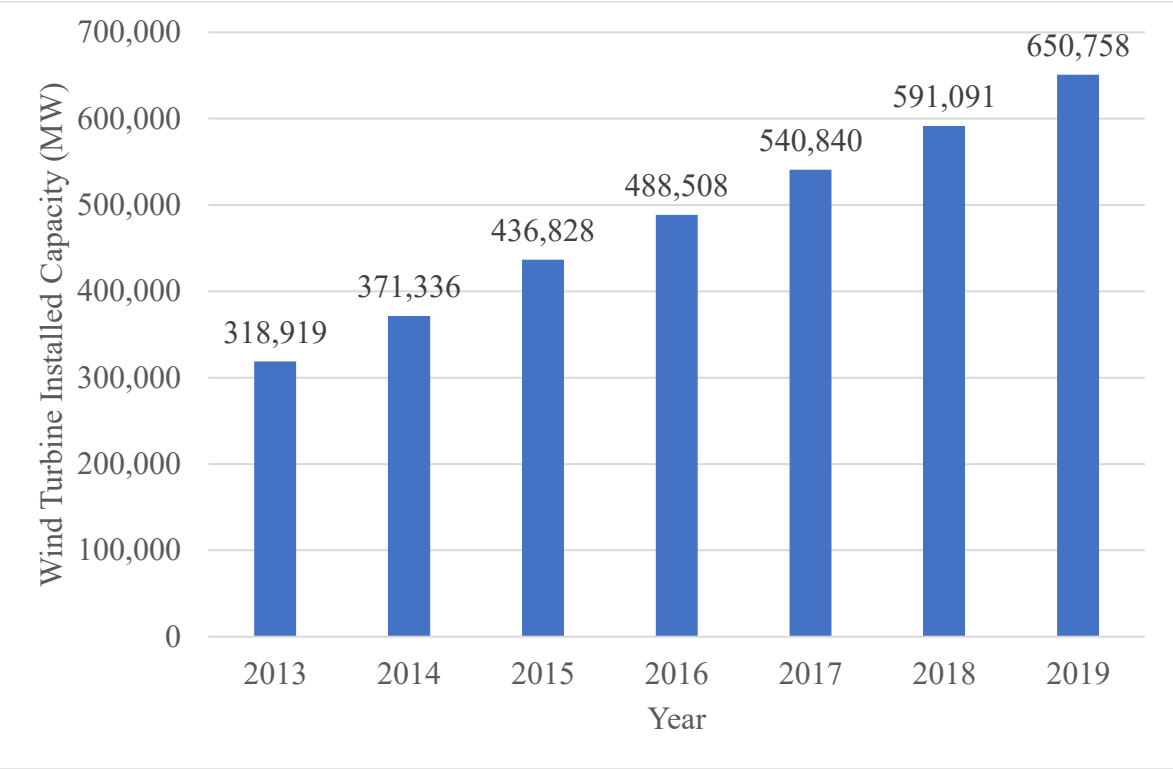
Fig. 1.1. Total worldwide wind turbine installed capacity.

1.2   Wind Farms

A wind farm which is interchangeably used as "wind park", "wind power plant", depending on its size, consists of a few to hundreds of wind turbine generators (WTGs) installed in a wide land and each turbine with respect to the geography of the area, is placed with some specific

distance away from each other to use the most of the accessible wind energy. The two most common types of wind turbines mostly used in wind farms are vertical-axis wind turbine (VAWT) and horizontal-axis wind turbine (HAWT). A schematic of these wind turbines is presented in Fig. 1.2. VAWT technology, as the name suggests, has a vertical axis of rotation which enables the wind turbine to capture wind energy from any direction without the need to reposition the rotor with respect to change in the direction of wind [5]. This is one of the main advantages of VAWT over HAWT, however, these turbines are less predominant in the modern wind farms due to some serious disadvantages related to this technology such as lacking self-starting mechanism, having significantly less power coefficient (compared to HAWT), strong suspension of rotations due to periodic changes in the lift force and unsatisfactory regulation of power.
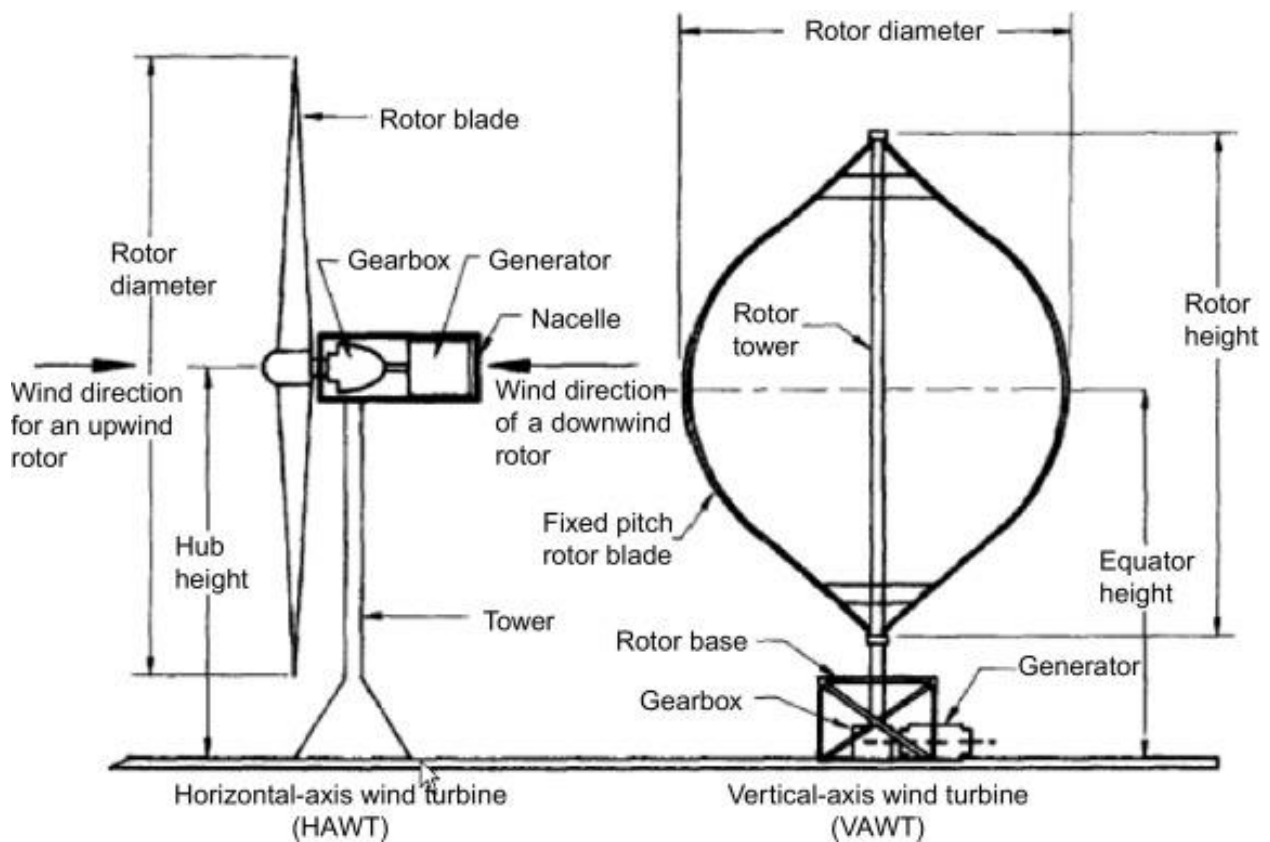
Fig. 1.2. Schematic of two most common types of wind turbines installed in wind farms [6].

On the other hand, HAWT are by far the most common design and therefore are prevalently used in wind farms. They utilize aerodynamic blades known as airfoils, fitted to a rotor, which can be positioned either upwind or downwind. HAWTs are typically either two or three-bladed and operate at high blade tip speeds. Machines with upwind rotors require a yaw, or tail vane, to help them orient into the wind while downwind rotors have blades that are coned allowing the turbine to orient on its own [7]. The electric generator and the rotor shaft, are placed on the top of a tall tower. The blades of the rotor are forced to rotate due to the air flow. The rotor shaft meshes with the generator, and consequently, the rotor shaft rotation leads to electricity generation. This type of turbine is usually designed to ensure that the rotor blades are facing the wind, thus it utilizes wind sensor and servo motor. High wind speeds could be dangerous and may cause damage to the wind turbine; to prevent that, the turbine is fitted with a brake to reduce rotor shaft speed [8]. Currently, available HAWT sizes are between 1 MW and 14 MW, where the world's most powerful and efficient offshore wind turbine generator as of now, is HALIADE-X manufactured by General Electric (GE) renewable energy company, which has a massive 14 MW power capacity and 61% capacity factor (i.e., the factor that compares how much energy was generated against the maximum that could have been produced at continuous full power operation during a specific period of time) [9].

The generated power of a wind farm highly depends on the wind variability, where its dispatch capability is based on wind forecasting. Large-scale wind farms are located in high-wind resource regions, and these may be far from the load center. Since a wind farm covers a very large area, there are usually some power output diversities found, since each WTG is located at different electrical distances from the substation (i.e., diversity in line impedance), and also each turbine may be driven by different instantaneous wind speeds. Hence, not only the entire wind farm power

generation fluctuates during different seasons, days, hour to hour and minute to minute, but also each WTG may feed fairly assorted power to the grid, that's why wind farms are considered as highly intermittent DG source, which have attracted many researchers and engineers to carry out abundant studies on power management, maximum power point tracking (MPPT), power quality, and intelligent protection and control (P&C) of these entities.

1.3   Overview of Wind Farm Protection and Challenges

The impressive growth in the utilization of wind energy has consequently spawned active research activities in a wide variety of technical fields. Progressive amplification of grids by wind farms has led to the emergence of some significant electrical issues including security, protection, stability, reliability and power quality. Among these issues, protection aspect plays an important role that has drawn the attention of researchers. Although protection of wind farms is very critical and intricate, wind power plants still implement simple protection schemes which lead to different levels of damages to power components in the plant under faulty conditions. Moreover, most of the researches conducted on wind farm protection have been dominantly restricted to literature and methodologies as opposed to implementation and reducing damages to the power apparatus [10]. In [11]–[14], the authors reported different levels of damage, but the drawbacks of the associated protection systems have been skipped. Although there are partial analysis of centralized protection [15], an overall protection scheme has yet to be developed to overcome the protection crisis in wind power plants [16].

A schematic diagram of a typical wind farm is shown in Fig. 1.3. The entire wind farm must be protected from any over/under voltage, frequency, current disturbances, unexpected

insulation failure, lightning and most importantly electrical faults. A common practice in power system protection is to define several zones known as "protection zone" for every section of the network that is required to be protected. Some protective equipment used in wind farm protections such as fuse, protective relay, circuit breaker (CB), reclosers, voltage transformer (VT) also known as potential transformer (PT) and, current transformer (CT) is briefly described below.
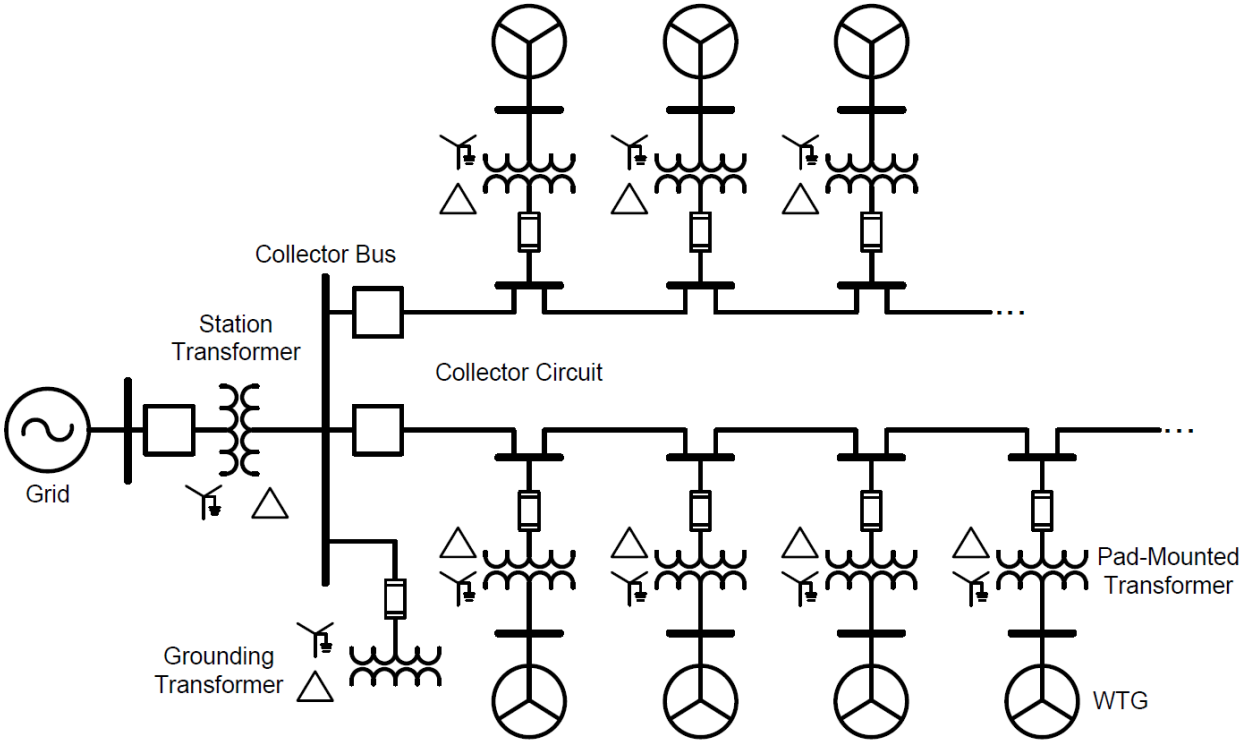
Fig. 1.3. A single line diagram of a typical wind farm [17].

A wind farm has many protection zones where each should be carefully designed to provide adequate protection and security for the power apparatus. This concept is shown in Fig. 1.4. Each protection zone may have one or more protective relays in conjunction with other elements of protection such as fuses and fault current limiters (FCLs) [18].

6
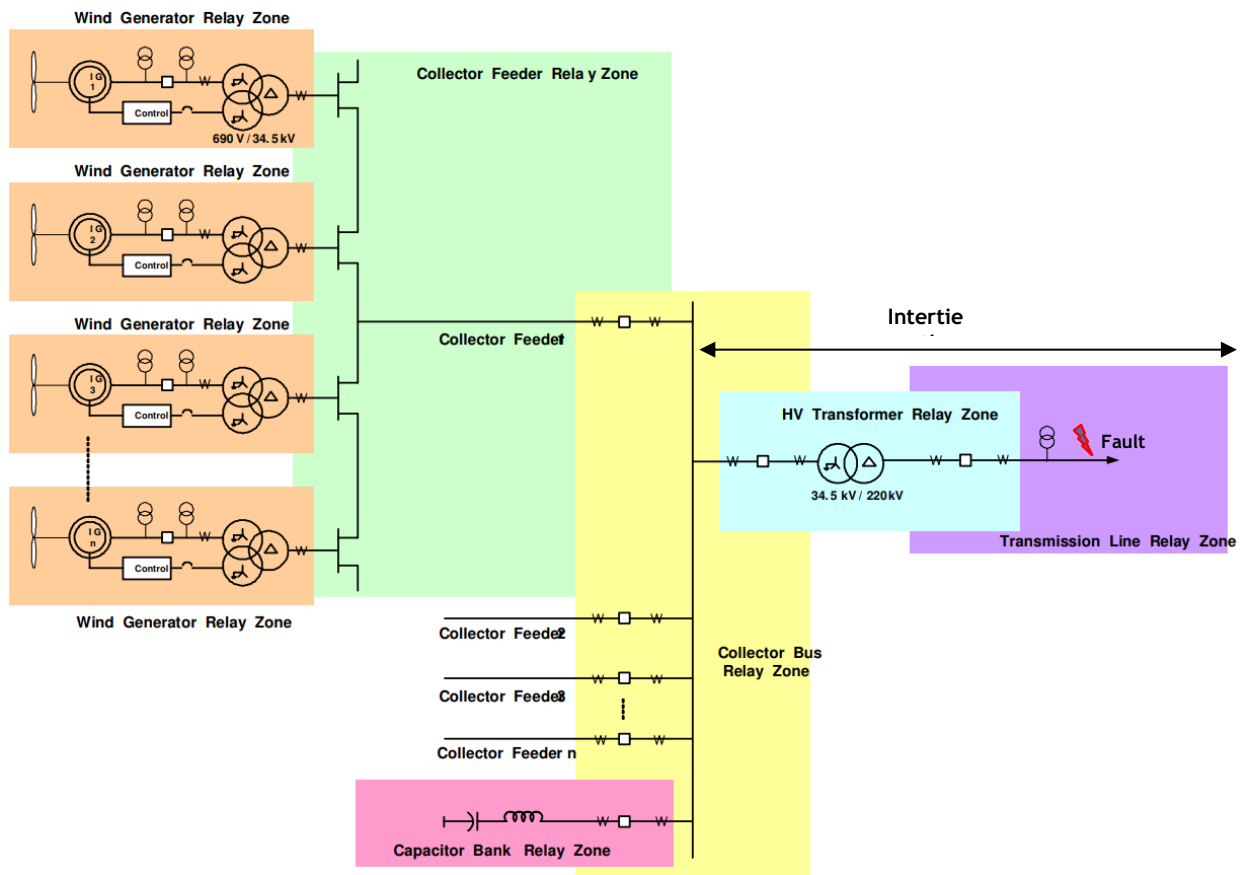
Fig. 1.4. Protection zones for a small section of a wind farm [18].

At the turbine section, the WTG generates at low voltage levels which is typically in the standard range of 480 V, 575 V or 690 V. The WTG which typically includes an induction generator (type I, II and III wind turbine technologies) or synchronous generator (type IV wind turbine technology), power electronics converter, control system, and step-up power transformer and are all protected by one protective relay. In early days, due to employment of small power transformers at WTG, usually (<1 MW), power fuses used to be installed at the high voltage side of the transformer which occasionally resulted in unnecessary miscoordination between transformer fuse and WTG relay during high fault current or significant voltage dip and eventual disconnection of the entire subfeeder connected to the collector feeder. This protection issue is

7

counterproductive against the modern grid standards such as low voltage ride through (LVRT) and fault ride through (FRT), which require the wind turbines to remain connected to the grid for some specific time during fault incidence or voltage dip due to grid disturbances [19], [20]. Hence, nowadays for modern wind farms, instead of a fuse, a multifunctional relay is implemented to provide protection for the entire WTG feeder as shown by orange color in Fig. 1.4.

The collector system consists of line feeders where each feeder can also include several WTGs, connects the high side of the pad-mounted transformer to the substation. Usually, wind turbines are divided into groups of turbines connected in a daisy-chain fashion using underground cables. These groupings are then connected to the substation by either underground cables or overhead lines at 34.5 kV. These protection zones are shown by green and yellow colors in Fig. 1.4. It is very important that the protection relay and coordination for these zones are set optimally, so that during a fault at any feeder, the adjacent feeder protection relays do not operate at the same time, otherwise, instead of only one feeder, multiple feeders with WTGs would be disconnected by mistake which is an unsatisfactory outcome of non-optimal protection systems. [21]–[24].

Finally, the entire wind farm is connected to the power grid through a step-up power transformer and transmission line. These zones which are shown by blue and purple color in Fig. 1.4, are of significant importance since maloperation of protection scheme could result in serious damage to the costly high voltage power apparatus and also disconnection of the entire wind farm, which would not only cause loss of bulk power to the grid, and consequently loss of revenue, but also the reconnection of the wind farm back to the grid, considering voltage and frequency synchronization complying with standard grid codes, could be challenging and time consuming.

Therefore, the role of power system protection in power networks is of significant importance, and it is absolutely necessary to design and implement highly reliable and efficient

protection schemes for every zone of wind farm, to protect power systems from unexpected faults and abnormalities, prevent damage to the power equipment, and meanwhile, minimize the disconnection of affected area, to preserve power quality and stability for the rest of the plant. However, despite the aforementioned statement, simple and inefficient protection schemes are still being implemented for wind farms which have been found unreliable [25]. For example, a recent report by North American Electric Reliability Corporation (NERC) has inferred that 28% of protective relays maloperation in wind farms are due to improper settings and logic errors. These errors prevalently resulted from the existing relay testing procedures that do not provide a proper mechanism to easily and effectively evaluate the performance of all settings, logics, and the simple protection system as a whole [26]. Thus, the protection schemes for wind farms must be significantly improved to provide adequate protection for power apparatus in a wind power plant.

1.4   Literature Review and Research Motivation

In the following section, a brief literature review on several protection schemes, i.e., overcurrent protection and coordination (adaptive and non-adaptive), distance protection and differential protection for wind farms including significant challenges associated with each technique, pros and cons, and the research motivation of this thesis are presented.

1.4.1   Overcurrent protection and coordination

Overcurrent protection is one of the most crucial areas of protection in wind power systems. One of the conventional protection apparatus is overcurrent relay (OCR) which is responsible for

protecting power systems from impending faults. OCRs are mostly used as primary and backup protection in many regions of power networks and power plants. To provide comprehensive protection, the relays must be adequately coordinated with each other, not only to prevent damage to power devices due to current faults but also to limit the disconnected district to the faulty feeders [27]. Proper power system protective relaying for doubly-fed induction generator (DFIG)-based wind farms and relay coordination is immensely challenging which have not been addressed adequately in the literature. The conventional protective relay settings and techniques provided for wind farms are not the best possible settings and schemes available, and there are scopes for improvement regarding relay operation time and relay coordination. Moreover, due to dynamic nature of wind energy and its effect on power generation and current characteristics, protective relays should be able to manage these behaviors and avoid false tripping. This topic requires solicitous attention and negligence in proper protection would compromise the reliability and stability of power systems and severe personnel health injuries [28]. Besides, optimal coordination of overcurrent relays is hugely demanding and considered as a highly constrained nonlinear programming problem specifically in complex power systems such as (DFIG)-based wind farms [29].

1.4.1.1   Non-adaptive overcurrent protection and coordination

Among different approaches the most prominent and successful method is the use of artificial intelligence to improve the function and coordination of OCRs in power systems [30]. Initially, trial-and-error method was implemented to coordinate relays with each other, however, in order to achieve a proper relay setting, a large number of iterations should be provided, thus

leading to a very slow convergence rate [31]. The best way to do this was to divide the loops at certain locations called breakpoints and start the coordination of OCRs at these points. In this technique, the most challenging part is to find the breakpoints and accomplish the coordination of OCRs [32]. The other approach is called topological analysis which is based on graph theory and functional computations. This method was considered to be a better approach than trial-and-error, however the lack of optimization was the shortcoming in this method [33]. This means that the time settings of relays in this approach are obtained in high values, which is considered non-optimal and unsatisfactory. The other disadvantage of these two methods is the requirement for a high period of time to set the relay settings.

Recently, several optimization techniques based on artificial intelligence (AI) algorithm and the nature inspired algorithm (NIA) have attracted researchers to achieve improved and optimized relay settings [34]. The advantage of these intelligent optimization techniques over the aforementioned conventional OCR coordination methods is that there is no necessity of determining the breakpoint. Unsophisticated techniques such as dual simplex and two-phase simplex linear programming (LP) method, nonlinear programming (NLP), mixed integer nonlinear programming of the general algebraic modeling system (GAMS), Big M, are some of the techniques that have been proposed to address the solution of the optimal coordination for distribution power system protection [35]–[38]. These methods have several drawbacks such as trapping into local minimum and difficulty to reach at optimal global value [39]–[42].

In order to provide coordination of both directional OCRs and non-directional OCRs, optimal solutions must be provided to protect the wind farms from faults within shortest possible time. The most recent trend in implementing modern artificial intelligence (AI) algorithm and the nature inspired algorithm (NIA) in solving engineering problems, are implementation of various

AI algorithms such as, fuzzy expert systems, rule-based expert systems, genetic algorithm (GA) and evolutionary programming, grey wolf optimizer (GWO), artificial neural network (ANN), artificial bees colony (ABC), harmony search algorithm (HSA), honey bee algorithm (HBA), particle swarm optimization (PSO) and etc., it is found that GA and GWO provides more reliable and optimal solution for highly constrained nonlinear problems [43]–[47].

Both GA and GWO are able to address the nonlinear characteristic of overcurrent relays and optimize the operation time of relays. Moreover, if these algorithms are appropriately developed, the most optimal solution could be achieved. Despite the massive success of these techniques in the protection of power system components, they were never extensively used to improve the wind farm protection which leaves a considerable gap in electrical power protection study. Hence, the GA and GWO based optimization algorithms with the formulation of a proper objective function and suitable parameter constraints are proposed in this thesis. The relay settings are optimized by minimizing the time and current settings concerning IEC standards to procure the best possible operating time and coordination for all the overcurrent relays. To verify the efficacy of the developed technique, they are tested under various fault condition at different locations of the power network. Furthermore, a comparison between the standard conventional protection and coordination method [48], and the developed protection schemes are presented which will be discussed later in Chapter 3.

1.4.1.2   Adaptive overcurrent protection and coordination

Besides the AI or NIA-based optimal protection, another significant aspect of protection that should be considered for intermittent power generation plants, e.g., wind farms, is adaptive

protection that has been drastically neglected in the previous wind farm overcurrent protection studies. The purpose of implementing adaptive protection is primarily to update the relay settings according to the changes imposed to a power system [49]. This type of protection scheme has been previously applied to microgrids where the fault current during grid connected and islanded mode of operation are extensively different and there is an immense necessity to update the relay settings accordingly [50]. In wind farms, since the wind speed is intermittent, the power and current characteristic are dynamic as well. Moreover, during high and low wind speed, there is a huge difference between the generated currents. Furthermore, since the fault current and nominal root mean square (RMS) values of current profiles are used for setting OCRs, existence of only one group set of settings for the relays would cause drastic miscoordination and false tripping when the wind speed is drastically altered. Thus, there should be an intelligent mechanism devised in order for OCR settings to be updated according to the dynamic changes of the wind farm operation, based on the data collected at site, so that only proper coordination settings are adopted.

In some studies, a simple non-communication based dual overcurrent and voltage-based protection was proposed, which was tested for radial distribution systems with high penetration of DG systems [51]. Some other studies, focused heavily on numerical and complex mathematical approaches to provide adaptive-like feature for relays, in order to improve their performance and maintain their coordination specific for networks that have highly varying generating stations or highly varying load demand [52]–[55]. The advantages of such offline adaptive protection systems are to avoid using FCL and any communication infrastructures, which would reduce the costs and simplify the protection schemes. On the other hand, the main disadvantage of this technique is the lack of communication between relays and control center where during event of fault, if a relay maloperates, no communication is made between the main and backup relays, and none of the

relays are updated with the new optimal settings [56], [57]. Thus, offline adaptive protection would not be the best candidate for implementation in large-scale wind farms.

Online adaptive protection schemes are mainly reliant on IEC 61850 standards where the relays communicate with each other through a standard protocol known as generic object-oriented substation event (GOOSE) [58]. The recent modern microprocessor-based protective relays implemented in smart grids are all equipped with such capability to enhance their performance and also improve their reliability by reducing false trips. For example, in a recent study that focused on implementation of online adaptive protection based on IEC 61850 and GOOSE protocol, directional overcurrent protection relays with peer-to-peer communication capability were employed to provide adequate protection for medium voltage (MV) distribution network [59]. Similar works have also been carried out by other researchers for different power systems, such as microgrids, solar plants, photovoltaic farms, distributed networks with high penetration of DGs and etc., where the attained results showed that by introducing an online adaptive protection to the network, the performance of relays was improved and relays were able to detect faults in a shorter time [60]–[64]. In spite of the promising advantages associated with applying online adaptive protection, this type of protection requires modern power networks (smart grids), extensive communication infrastructures, and microprocessor-based protective relays, therefore it's rather an expensive protection scheme, yet highly efficient and reliable.

The current literature on adaptive overcurrent protection in power systems is still limited and more research is required to apply such techniques for various power systems, most specifically for wind farms. Moreover, many of the reported techniques are extremely sophisticated, and may not be applicable to many scenarios since the initial protection scheme was constrained with the availability of DG technology, specific power network under study, and the

14

unnecessarily complicated techniques employed. Nevertheless, the most important attributes of power system protection and relaying is its simplicity, reliability and applicability of the proposed technique for various power systems [65], [66], contrary to recent trend in the literature. Adaptive protection should be simple and easy to implement, so the relays are updated in fraction of second and avoid unnecessary communication delay between relays and the central control unit.

Thus, this thesis proposes a new adaptive and optimal overcurrent protection technique for large-scale wind farms using hybrid grey wolf optimizer and fuzzy logic controller (GWO-FLC) scheme to significantly improve the protection, and reliability of wind farm operation. The hybrid GWO-FLC consists of two parts where the GWO is responsible for minimizing the time and current settings of the OCRs, hence minimizing the operation time of protective relays. The second part of the proposed technique consists of the implementation of FLC, which is responsible for adaptive protection. Due to dynamic behavior of wind farms, OCR settings and coordination can be an extremely challenging task. The existing single group setting for the entire wind farm is not acceptable anymore and can cause severe miscoordination, maloperation, false tripping or even delayed tripping during fault incidence. Thus, in order to solve this issue, adaptive protection was proposed in this study as an inevitable procedure to provide adaptive feature for the relays so that the OCR settings are updated online and group settings for each relay are adopted according to the variation of wind speed, which will be discussed in Chapter 4.

1.4.2   Protection of Intertie Zone of Wind Farms

The intertie section of wind farms, where the entire wind power plant is connected to the power grid through a step-up power transformer and a power transmission line, are usually

equipped with several layers of protection. Distance protection relay is the most effective method implemented for power transmission lines; thus, these protection relays are also being applied to wind farm transmission lines. Overcurrent relays are used as backup protection scheme and are coordinated with the distance protection relay and also with the next overcurrent relay in either upstream or downstream depending on the topology of the wind farm. Transformer protections within the intertie system are equipped with differential relay as the primary protection and overcurrent relay as a backup protection.

1.4.2.1   Distance Protection

Distance protection relays are an inevitable part of transmission lines and provide proper protection in the presence of faults or grid abnormalities [67]. Distance protective relays as the name suggests, rely on the impedance at each relay which is simply measured by the division of voltage over current at the relay location [68]. During setting the distance relay, one important procedure that should be carried out is to define several zones, usually 3 zones based on the priority and significance of that particular section, and also set the settings of protection for each zone by considering the "overreaching" characteristic of relay to provide adequate and reliable protection which is of substantial importance in power system protective relaying. Although these relays are extremely effective for stable power systems, they are not as equally effective and reliable for the power systems where the source is unstable and drastically intermittent e.g., wind farm intertie systems. This is mainly due to the reason that the distance protection relay performance is drastically affected by variations in the output voltage of wind farms, source impedance and

variations in the frequency of voltages and currents on occurrence of fault on the transmission line [69].

In a recent study [70] conducted for DFIG protection system, distance protection relays were used as the primary protection unit for intertie and collector system. However, the fault analysis inferred that distance protection relay failed to operate properly for faults on intertie section connected to DFIG wind turbines. The maloperation of the relays were resulted from incorrect impedance measurement due to difference in frequencies of voltage and current which stem from the DFIG-based wind farm unique behavior. In another research [71] carried out using distance-based protection comprising both distance principle and pilot distance protection for a large-scale wind farm, performance of distance protection relay was unsuccessful and did not operate due to small power source characteristic of wind farm. At the very beginning of fault cycles, the decaying DC offset component has a large current and frequency magnitude, while the power frequency component is rather negligible and unstable. This would result in inaccurate power frequency component extraction from Fourier algorithm by distance protection, consequently, the impedance between the relay and fault location is derived incorrectly, leading to maloperation of distance protection relay. Incompetency of distance relays is not only limited to DFIG-based wind farms, but also in a research carried out on squirrel cage induction generator (SCIG)-based wind farms, the impedance measured by distance relay, failed to represent the fault location and caused maloperation of the relay on zone 1 of protection [72].

According to the research in [73], [74], distance protection relays poor performance are mainly due to poor selectivity, low sensitivity and miscoordination between distance and overcurrent relays during fault incidence. Poor selectivity results from weak feed characteristics of wind generator, the proportion of positive and negative sequence components is much smaller

than the proportion of zero sequence component in the collector system side short-circuit current. Thus, the traditional distance protection relay may operate incorrectly. Meanwhile, since the lengths of the collector lines differ from one another, it is not easy for the setting values of line distance protection to cooperate with each other, which may result in poor selectivity. Low sensitivity is due to the reason that since wind farm intertie section are grounded via resistance or arc suppression coil, consequently during fault occurrence, the fault resistance will greatly affect the operation performance of distance protection and result in lower sensitivity to unsymmetrical faults, specifically, single line to ground fault due to its smaller fault current magnitude compared to symmetrical three phase faults. Lastly, miscoordination among several distance relays and with other overcurrent relays may also occur due to aforementioned problems, which would result in wrong tripping and catastrophic maloperation of relays within or outside the intertie system. Moreover, distance protection relays may operate at a longer time, and if its operation is delayed to an extent that the backup overcurrent protection acts instead of primary distance protection relay, it could cause miscoordination, compromised power quality and also unnecessary disconnection of extended healthy feeders [75]. Thus, based on the existing problems associated with distance protection relays for the intertie section, it is extremely essential to study new protection schemes to guarantee the safe operation of wind farm intertie system and power grid.

1.4.2.2   Differential Protection

Differential protective relays are usually employed to provide protection for a single unit commonly employed for power transformers, generators, buses, and recently, power transmission lines. However, in wind farms since there is a necessity to provide adequate protection for several

18

zones rather than only a single unit, differential zone protection including required numbers of relays and measurement sensors i.e., CTs and VTs, for each specific zone must be implemented. Differential protection operation is reliably fast, usually close to 5 ms, which could contribute to fast tripping and provide robust security for the wind farm intertie section [76].

The performance problems of distance protection relays, explained in the previous section could be successfully solved by implementing differential-based protection relay (DBPR) for intertie system due to its high sensitivity, swift operation and, immunity to power swings. Moreover, the differential based protection acts like a unit protection-based scheme that is extremely advantageous compared to distance relays since it is not required to cope with "underreach" and "overreach" characteristics, resulting in less false tripping [77]. However, since wind farms are intermittent sources of power generation, and hence, the generated power and current depends on the behavior of wind profile, it could have a detrimental effect on the performance of differential protection relays. Because, these relays are sensitive to difference between incoming and outgoing currents measured at two sides of a power apparatus to be protected, for example two sides of a power transformer or transmission line, and any drastic change in wind velocity, could simply cause this differential current exceeds the threshold value and would consequently cause maloperation during normal operation. This problem is more prevailing if the slope ratio of differential relay is not properly selected. Thus, a differential protection relay must be able to cope with this issue and avoid false tripping during normal operation.

Some researchers have proposed digital signal processing, wavelet-alienation coefficient technique, least square curve fitting method to analyze the frequency characteristics during fault to help the differential relay detect the fault better, however such techniques were proved to have

lack of accuracy, consequently during external faults, false tripping was occurred since the proposed protection scheme was not able to discriminate between internal and external faults [78]–[80]. The failure of differential protection relay is not just limited to the intertie protection zone, but also some research has showed that the existing method has an adverse effect on the operation of reclosers during auto-reclosing [81]. This problem itself, could significantly compromise the stability of large-scale wind farms connected to the grid and is totally unacceptable by grid standards. A recent study was conducted on improving the performance of differential relays for the intertie section of wind farms by applying a central relaying unit based on principle of operation of differential relay [82]. The proposed method was able to provide better protection for the wind farm and discriminate between fault at the wind turbine and grid side, however, the resistance of the fault was not considered at all. Usually the fault resistance, diminishes the fault current drastically, which would cause the relays to ignore the fault or at the best scenario, the backup overcurrent relay may be able to detect the fault but operates with a significant delay.

Most recently, some researchers proposed differential protection with extensive communication to improve the protection of wind farms [83]. Although differential protection was found to be successful, implementation of this technique could be extremely costly, since installing several microprocessor-based differential protection relays at a large-scale wind farms might be quite expensive. In other studies, effectiveness of differential protection for offshore wind farms were analyzed and several recommendations were made to improve the sensitivity of relay against various fault types [84], [85]. Unfortunately, there has been very limited research conducted on the implementation of differential protection relays for wind farms, but based on the available literature, it is evident that differential protection schemes is a viable and effective protection method for wind farms connected to power grid, and is a better candidate compared to distance

protection relays for protecting the intertie zone of wind farms [86]. However, such protection schemes have its own specific challenges and limitations as was discussed earlier. Moreover, it is found that only a very few of the previous proposed methods considered the adverse effect of wind farms dynamic behavior, and fault resistance in their differential protection scheme, which would result in blinding, maloperation, and lack of discrimination between external and internal faults. Another major drawback is the cost of implementing microprocessor-based differential relays since for large distribution, transmission or power plants, various different requirements of protection are necessary to ensure coordination and reliability are provided, thus, employing large number of digital microprocessor-based differential relays would drastically increase the cost. The aforementioned problem could be escalated for large-scale wind farms connected to the power grid, that their size is gradually increasing and so are the costs of implementing, installing and maintenance of modern protective relays.

Therefore, in order to successfully address the present distance and differential protection issues in wind farms, two novel protection schemes are proposed. Firstly, a cost-effective and more reliable differential protection relay is designed in a field-programmable gate array (FPGA) and is proposed as an alternative protection scheme for wind farms. The performance of the proposed FPGA-based digital differential protection relay (FPGA-DDPR) is verified in the lab environment using DE2-115 FPGA board equipped with Cyclone IV E (EP4CE115F29C7). Secondly, a new Bayesian-based optimized Support Vector Machine (SVM) as an intelligent supervised machine learning classifier approach is developed to take into account both the dynamic behaviors of wind speed and the current measured by the current transformers. The performance of the two proposed protection schemes is also compared to other existing protection schemes, which will be discussed thoroughly in Chapter 5.

1.5   Objectives of the Thesis

This thesis aims to tackle the existing protection challenges by proposing novel intelligent and robust, yet simple, effective and practical protection schemes to improve the reliability and security of large-scale wind farms.

The main objectives of this research are as follows:

a) To develop and design OCRS, calculation of relay settings and coordination for all protective relays by applying load flow and fault analysis, and test the relays performance by designing a large-scale wind farm.

b) To develop and design an optimal overcurrent protection and coordination scheme to achieve the following objectives:

> ➤ Improvement of the protection of the wind farms by enhancing the coordination between relays, by optimizing the relay settings according to IEC 60255-151:2009 standard through the optimization of time multiplier setting (TMS), and subsequently the operation time of each relay.

> ➤ Implementation of GA and GWO, as a powerful optimization branch of AI and NIA, to obtain improved relay settings based on their coordination criteria. Each relay operation time and TMS are optimized by using GA and GWO method, which would consequently contribute to the enhanced protection for wind farms.

c) To develop and design an intelligent adaptive overcurrent protection and coordination scheme by proposing a hybrid GWO-FLC scheme, along with optimized quadruple group settings for each relay, to operate as an online adaptive mechanism during various wind speeds.

d) To develop and design a differential-based protection relay (DBPR) as a simple, yet practical protection scheme, and an ideal replacement to unreliable distance protection, specific for the intertie zone of wind farms.

e) To develop and design a cost-effective FPGA-based digital differential protection scheme (FPGA-DDPR), as a robust zonal protection scheme for wind farms.

f) To develop and design a support vector machine digital differential protection relay (SVM-DDPR) as comprehensive and intelligent differential protection mechanism based on machine learning techniques, which is aimed to be represented as a modern data-driven protection approach for wind farms.

g) To develop a prototype protection scheme incorporating FPGA DE2-115 board with built-in Cyclone IV E (EP4CE115F29C7), in a laboratory environment to test and validate the effectiveness of the proposed differential and overcurrent protection techniques for the protection of wind farm against various types of fault at different locations and with different fault resistances.

1.6 Organization of the Chapters

The chapters of this thesis are organized as follows.

In Chapter 1, an overview of wind farm operation, and associated protection challenges with these entities are presented. Furthermore, a brief but comprehensive literature review on specific wind farm protection issues is provided with thorough explanation, and the research motivation for each specific protection scheme is also presented at the end of each section. Finally,

the main objectives of this research with respect to addressing the present problems in wind farm protection, are mentioned concisely.

Chapter 2 is entirely dedicated to design of the wind farm model as a case study for protection analysis. Moreover, short-circuit current contribution of various types of wind turbines, with emphasis on DFIG type is explained. Finally, with regards to short-circuit current calculation for a DFIG, usually powerful and explicit industrial software are used to provide an accurate calculation of fault current within a power system, however in this chapter, a sample of hand calculation for short-circuit current of a DFIG as a verification for the software analysis is also provided.

Design and development of OCRs, determining the settings for each relay, along with their coordination is fully detailed in Chapter 3. Moreover, a few samples of hand calculations for relay settings and coordination are provided. Furthermore, the application of two artificial intelligence optimization technique e.g., GA and GWO, along with their coding, objective function formulation, and their development are explained thoroughly. Additionally, their application on optimizing the relay settings with the optimization process is presented. Finally, the operation of optimal overcurrent protection and coordination is tested and analyzed to validate the developed protection scheme.

In Chapter 4, the proposed intelligent adaptive protection and coordination for large-scale wind farms, and development of hybrid GWO-FLC is presented. Furthermore, the performance of this protection scheme under test and validation for various wind speed cases even during drastic wind speed variation for examining the robustness and effectiveness of the proposed method is also illustrated. Finally, in a laboratory environment the proposed protection scheme is implemented in real-time using FPGA DE2-115 board equipped with Cyclone IV-E device

(EP4CE115F29C7). The performance of the proposed hybrid GWO-FLC is also tested in both simulation and experimental setups to examine the robustness, reliability, efficiency of the protection scheme.

Chapter 5 is an extensive chapter which covers several topics including, design and development of several differential protection schemes particularly for intertie zone of wind farms including digital differential protection scheme, cost-effective FPGA-DDPR, and Intelligent SVM-DDPR. All of these techniques are explained thoroughly and the step-by-step design and development of each technique. Additionally, the performance of each novel protection scheme is inspected for various types of faults, at different locations and different fault resistances. Besides, the experimental hardware-in-the-loop operation of FPGA-based protection using FPGA DE2-115 board to validate the developed protection scheme and simulation results is also provided.

Finally, a concise summary and contributions of this research along with the suggestions for future works are highlighted in Chapter 6.

Chapter 2

Wind Farm Modelling and Short-circuit Current Analysis

2.1   Background

There are several types of feeder topologies currently applied in wind farms. Radial, bifurcated radial, feeder-subfeeder, and looped topologies are the most common types employed, each yielding their own distinct advantages and disadvantages. The selection of wind-farm feeder topology depends on several factors such as the wind turbine technology with respect to the converters and generators, mode of operation either grid-connected or islanded (where the wind farm operates autonomously), wind profiles, available tower placement, costs, etc. The most common wind farm topology used in many countries is feeder-subfeeder topology due to its protection criteria advantage compared to its counterparts. Feeder-subfeeder topologies are typically employed where clusters of towers are distributed over large areas. They are typically comprised of a single cable feeding remotely located switchgear with several subfeeder.

The significant protection advantage of this type of wind farm topology is that, during a fault incidence at any feeder, only the faulty feeder will be disconnected from the intertie system and the rest of the other feeders and wind turbines will remain connected. However, in other types of wind farm topologies such as loop or radial, any fault on the feeder, may result in disconnection of the entire wind turbines from the power grid which is a catastrophic situation that would compromise power quality, reliability and integrity of the wind farm as a reliable source of DG.

There are four main types of WTGs available in wind farms which are:

- Type I: fixed-speed turbine with a squirrel-cage induction generator (SCIG).

- Type II: variable-speed turbine with a wound-rotor induction generator (WRIG) that has a variable resistor in series with the rotor winding.

- Type III: variable-speed turbine with a doubly fed induction generator (DFIG).

- Type IV: variable-speed turbine with a permanent magnet synchronous generator (PMSG) and full-scale AC-DC-AC power electronic converter.

Nowadays there are many variable-speed wind turbine technologies, where Type III wind turbines mostly known as DFIG, is currently the one with the largest growth, both in capacity as in units sold, in wind farm application. It is justified due to the low power converters, which have a fraction of the rated power of the machine, and its flexibility of operation at variable speed. Thus, the DFIG-based wind farm is considered in this thesis for further investigation on protection issues.

2.2   Wind Farm Model

The typical wind farm modelled and simulated by MATLAB/Simulink as one of the most common type of wind farm topology available in many countries is shown in the Fig. 2.1. The wind power plant modelled in this research, consists of 40 Type-III wind turbines based on doubly fed induction generator (DFIG), in 4 clusters, where each cluster includes 10 wind turbines, where each wind turbine is protected by circuit breaker, as modelled in Fig. 2.2. Each individual DFIG (wind turbine) generates 1.5 MVA apparent power at 0.85 power factor (PF); hence, the entire wind farm provides 60 MVA power to the utility grid. Each DFIG operates at the voltage and frequency of 575V and 60 Hz respectively. Transformers corresponding to each wind turbine has

voltage ratio of 575V/35KV in star-delta configuration where the star side is earthed. Furthermore, the wind farm is connected to the grid through a step-up transformer, boosting voltage from 35 kV to 220 kV and also a 50 km transmission line, where the line is designed as a π-circuit model. Additionally, a grounding transformer has also been installed next to the intertie line in order to manage the unbalanced load on the power system as well as to handle high magnitude of excessive current during single line to ground fault. The wind turbine generator model is shown in Appendix A.1, and the characteristics of each wind turbine generator with respect to turbine output power over turbine speed at generator synchronous speed, in per-unit (pu) value and for wind speed 5 m/s - 16.2 m/s is shown in Fig. 2.3.
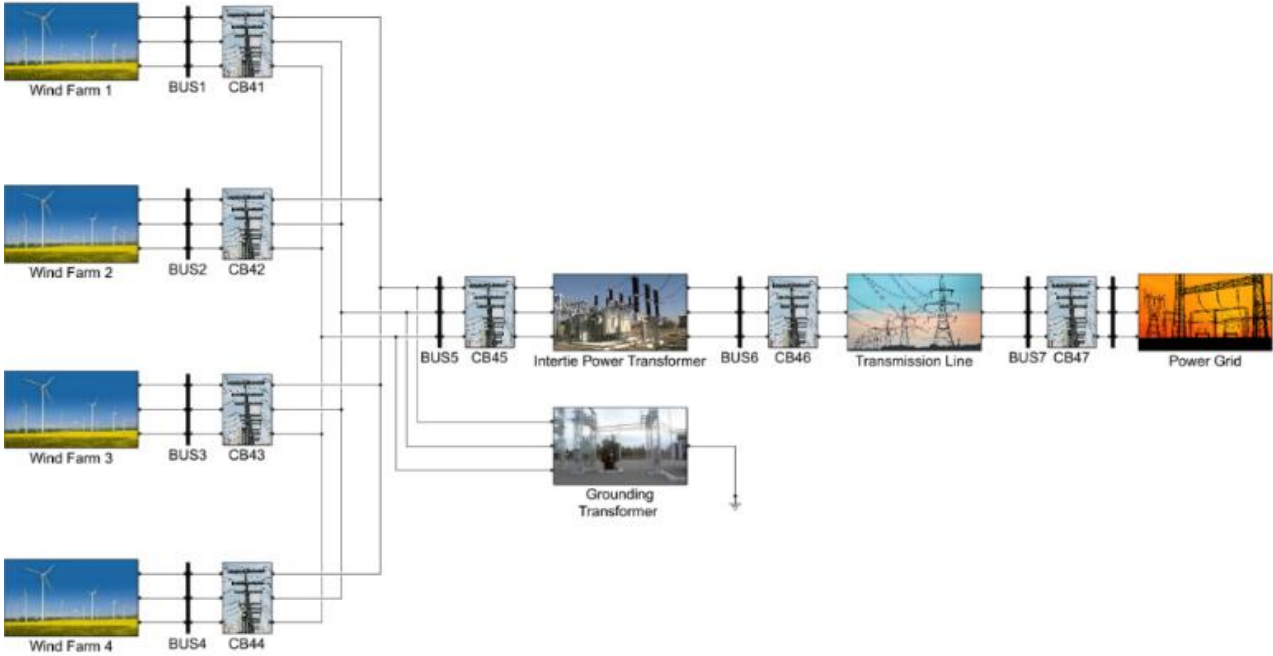
Fig. 2.1. Simplified conceptual model of a large-scale wind farm developed for protection study.
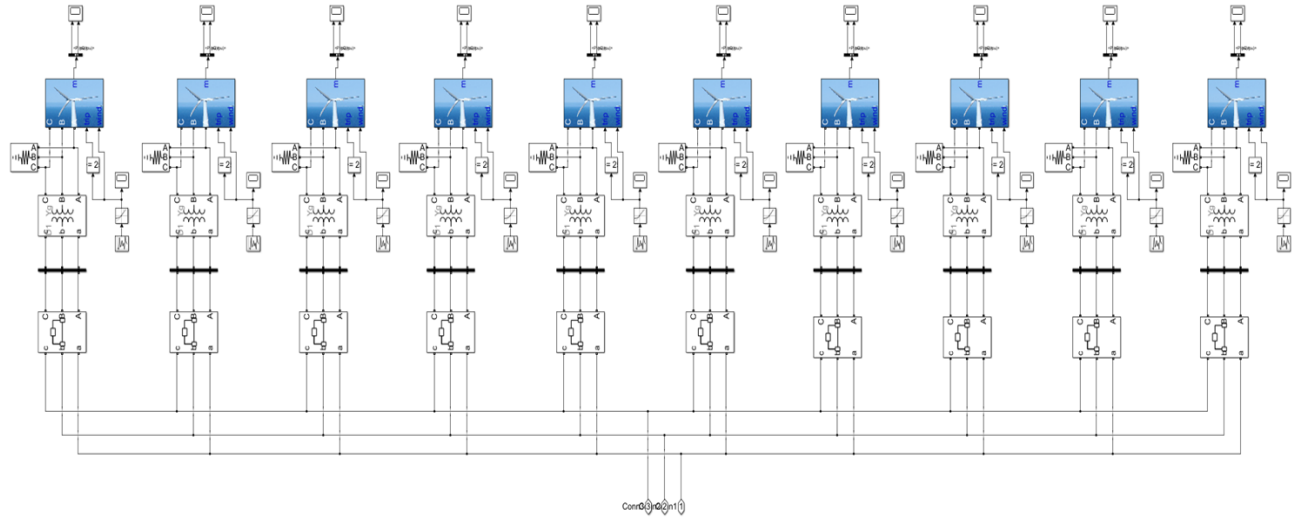
Fig. 2.2 Each main feeder consists of 10 wind turbines where each wind turbine generating near 1.25 MW power ("A", "B", and "C" notations represents primary side, while "a", "b", and "c" notations represents secondary side).
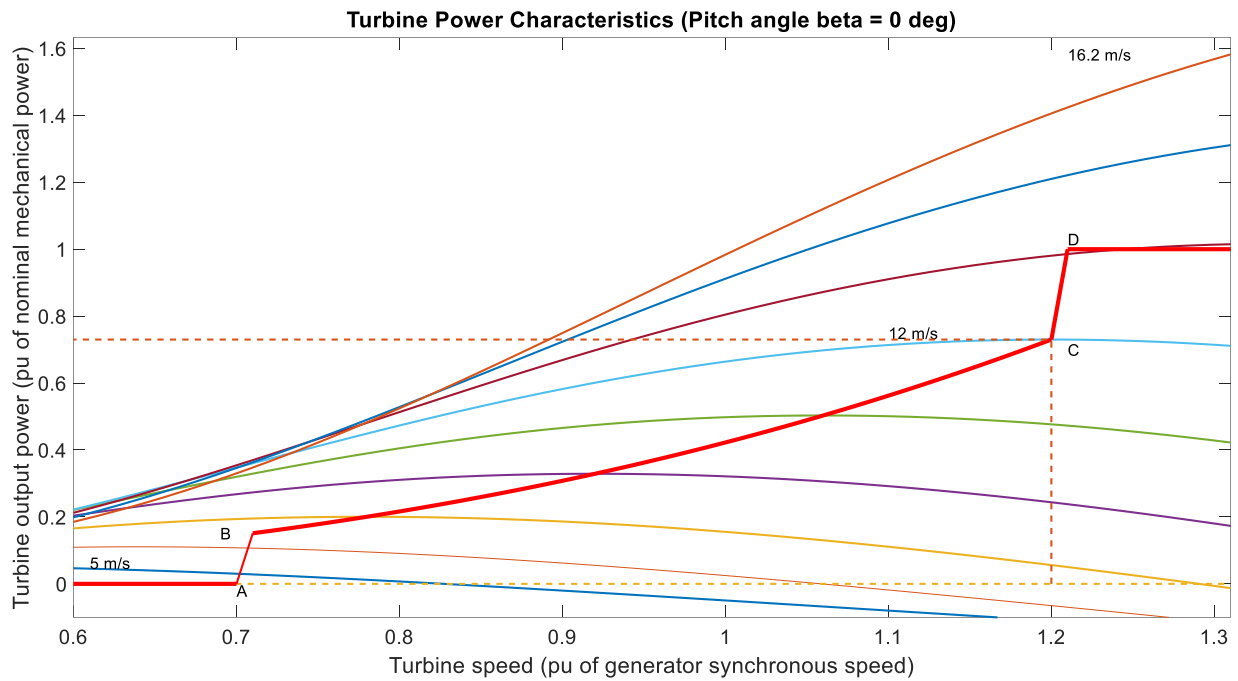
Fig. 2.3 Wind turbine generator output power characteristics [87].

In wind power plants, since the wind speed is not always stable and essentially fluctuates all the time, therefore, the current generated by the wind turbines also varies according to the wind velocity. The minimum adequate wind speed for wind turbines to produce electricity is usually in the range of 3.5 m/s to 5 m/s, however the maximum wind speed that DFIG-based wind turbines can tolerate are typically 25 m/s. If the wind velocity exceeds that specific value, then it will cause severe damage to the wind turbine generators and control system. In order to protect the wind turbines from high wind speed in this study, an instantaneous protection relay is located to trip the wind turbine as soon as the wind speed exceeds 25 m/s to avert any potential damage to the generator and converter systems. Wind speed in this research is selected to be varying in the range of 5 to 25m/s, in order to study the protection of wind farm during all possible wind characteristics. The natural variation of wind speed for a short duration of 25 seconds is simulated and is shown in Fig. 2.4 that we considered an extreme case of gust wind where the wind speed was changing rapidly. This is considered to show the application of protection schemes to protect the DFIG-based wind farm in the case when wind velocity is out of the safe operating zone 5m/s-25m/s, which will be studied and analyzed in subsequent chapters.
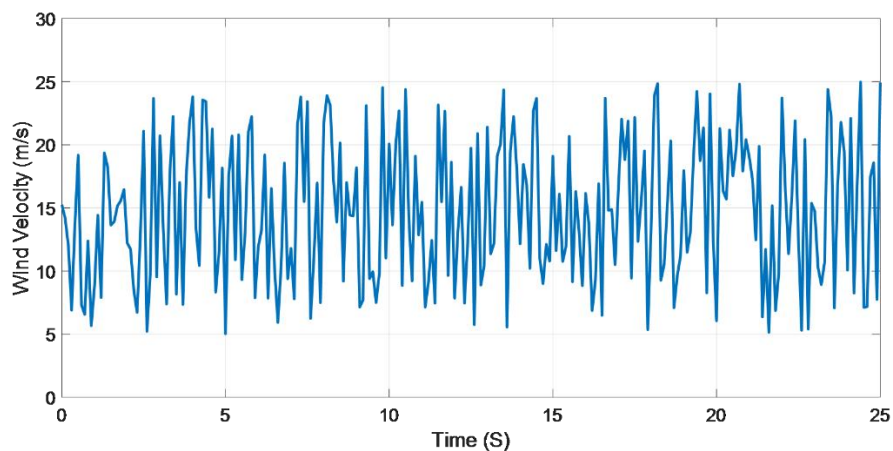
Fig. 2.4. Instantaneous behavior of wind speed over a short duration of time.

The positive, negative and zero sequence of the designed wind farm model is shown in Fig. 2.5. that can be used to determine the short-circuit characteristics at any location required on the wind farm. For simplicity, the aggregated reactances are shown, where X^+, X^-, and X^0 are the aggregated positive, negative and zero sequences, respectively.
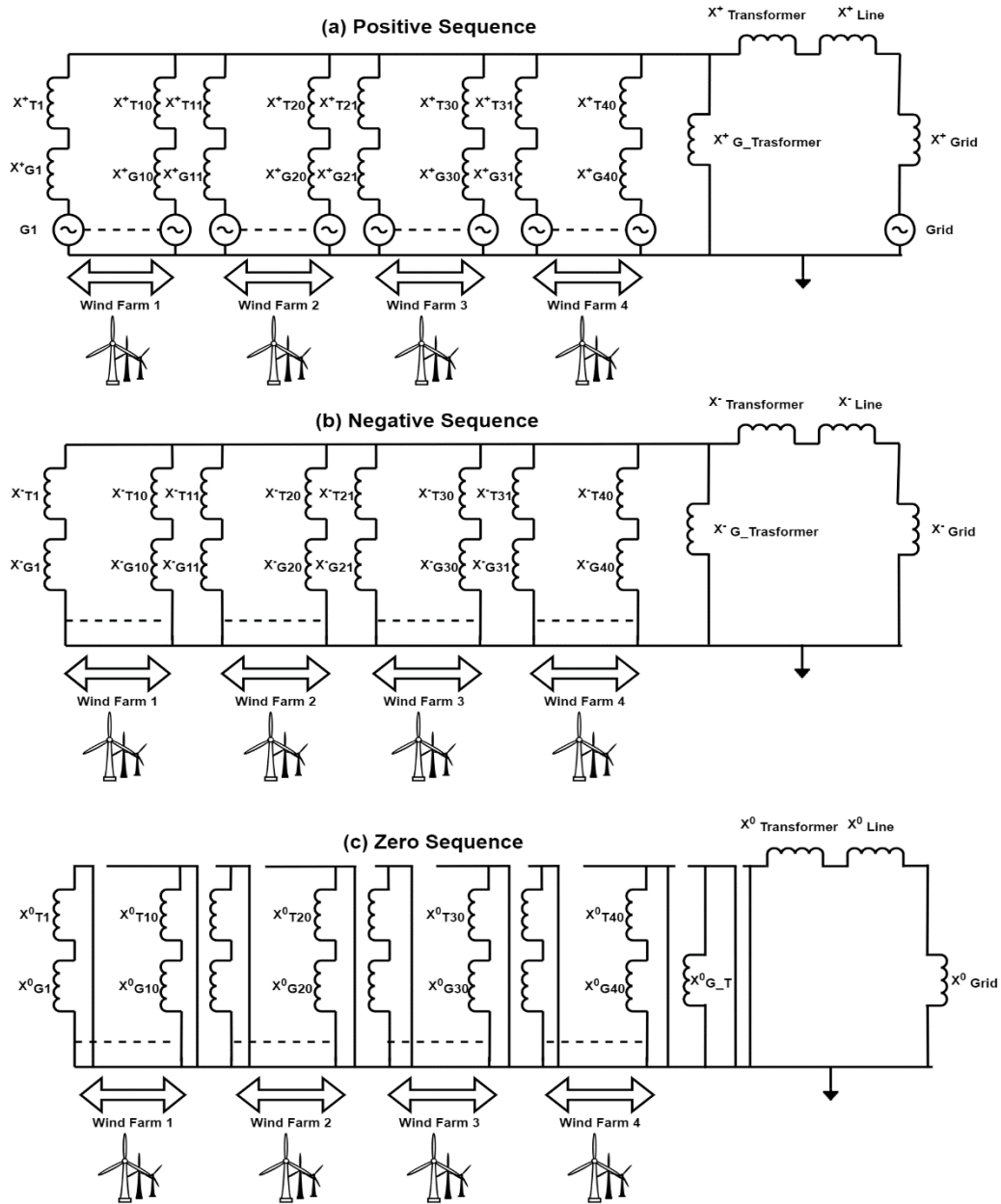
Fig. 2.5. The aggregated model for the wind farm: (a) Positive sequence, (b) Negative sequence, and (c) Zero sequence.

2.3 Short-circuit Current Phenomena

Short-circuits is a detrimental phenomenon in power systems that transpires when equipment insulation fails due to system overvoltages caused by lightning or switching surges, insulation contamination, e.g., salt spray or pollution, or other mechanical causes. The resulting short-circuit or so-called "fault" current is determined by the internal voltages of the electric machines and by the system impedances between the machine voltages and the fault. Short-circuit currents may be several orders of magnitude larger than normal operating currents and, if allowed to persist, may cause thermal damage to equipment. Windings and busbars may also suffer mechanical damage due to high magnetic forces during faults. Thus, the fault sections of a power system need to be isolated as soon as possible. Standard extra high voltage (EHV) protective equipment is designed to clear faults within 3 to 4 cycles, i.e., about 50 ms at 60 Hz. Lower voltage protective equipment operates more slowly, for instance, 5 to 20 cycles [88].

There are several different types of fault that are prevalent in power systems and wind farms, where the probability of occurrence for each type of fault, and the severity of the fault current differs from each other [89]. For example, three phase faults have the least probability of occurrence, however they are the most severe fault type since they impose the highest fault current in a power system. Therefore, protective relays must be able to detect such abnormal conditions at the shortest possible time and isolate the faulty section accordingly. On the other hand, single line to ground fault which are usually known as SLG, or L-G, are the most common type of fault with high probability of occurrence, however they are the least severe of all, since the fault current is significantly less compared to other types of faults. Nonetheless, protective relays must be sensitive enough to detect such faults, since their prolonged duration of these faults might cause

damage to the power cables, deformation of transformer windings, and etc. An overview of different types of faults with respect to their probability of occurrence is tabulated in Table 2.1.

Table 2.1 Different types of faults in power systems and the probability of occurrence for each case [66].

No.	Type of fault	Short form	Symmetrical or unsymmetrical	Probability of occurrence
1	Three phase line to line	3L-L	Symmetrical	<1%
2	Three phase line to ground	3L-G	Symmetrical	2-3%
3	Line to line	L-L	Unsymmetrical	8-10%
4	Double line to ground	L-L-G	Unsymmetrical	10-17%
5	Single line to ground	SLG (L-G)	Unsymmetrical	70-80%

2.4 Short-circuit Current Behavior of Wind Turbines

Conventional power plants including fossil-fueled, nuclear, and hydro plants consist of single or several synchronous generating units, wherein for each unit the rotational speed is fixed and the magnetic flux is controlled via exciter windings; the magnetic flux and the rotor rotate synchronously. The short-circuit current analysis of such power systems are very simple and its detailed discussion can be found in [90]. On the other hand, with regard to wind turbines, their short-circuit current behavior and calculation is somewhat different from the conventional power plants [91], [92]. Usually, a wind farm consists of several wind turbine generators, which are dispersed over a wide geographical area, and their fault contribution to the grid, depending on the type and technology of the wind turbine, could be drastically high. A brief description of DFIG technology and discussion on short-circuit current calculation of DFIG are presented below:

33

2.4.1   Type III Wind Turbine Technology

The schematic diagram of a typical a DFIG-based WTG is shown in Fig. 2.6. The DFIG topology employs two static converters. While the machine stator circuit is directly connected to the grid, the rotor circuit is fed through the two converters, on back-to-back topology, interconnected by a DC bus [93]. The rotor side converter (RSC) is connected to the rotor of the machine, while the grid side converter (GSC) is connected to the network through a filter and a power transformer. During the time that the induction machine speed is below the synchronous speed, the back-to-back converter receives active power from the grid. On the contrary, if the machine speed increases beyond the synchronous speed, then active power from the rotor would be transferred to the grid via the back-to-back converter, which is the ideal performance of DFIG during normal operation [94]. The typical connection diagram for a DFIG-based WTG is shown in Fig. 2.6.

The power converter connected to the rotor winding should be able to withstand the currents induced by the dc and ac components flowing in the stator winding. However, the components of the power converter (IGBT, diode, capacitor, etc.) are designed to handle only normal currents and normal dc bus voltage [95]. Therefore, a crowbar system is usually devised for protecting the power electronics converter from overvoltage and thermal breakdown during short-circuit faults. The operation of a crowbar is very simple, a crowbar is generally employed to allow the addition of resistance into the rotor winding to avert the short circuit current in the rotor winding from damaging the susceptible power converters. Additional dynamic braking on the DC bus is also used to limit the dc bus voltage [96].
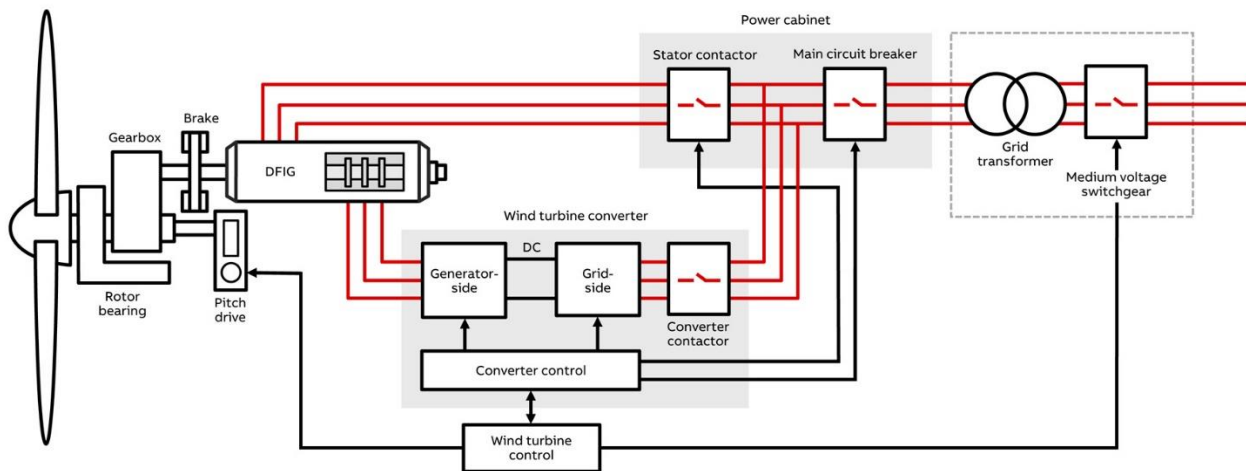
Fig. 2.6. Schematic for Type III WTG technology [97]**.**

2.4.2   Short-circuit Current behavior of a DFIG

In order to provide adequate protection for the entire wind farm, the relay settings should be calculated based on fault current level. Therefore, it is extremely important to calculate the short-circuit current contributed to the grid by each DFIG. Short-circuit current of Type III wind turbines consists of two main components such as, the transient and steady-state. In order to set the relay settings, the maximum short-circuit current should be calculated by considering stator and rotor reactances, transient reactances, stator and rotor coupling factor, leakage factor, and damping time constant.

The equivalent electrical diagram of a DFIG is shown in Fig.2.7. It is very similar to one for a regular induction generator except for additional rotor voltage, representing voltage produced by a power converter. Under normal operation, this voltage is actually from a current-controlled

power converter with the ability to control the real and reactive power output instantaneously and independently.
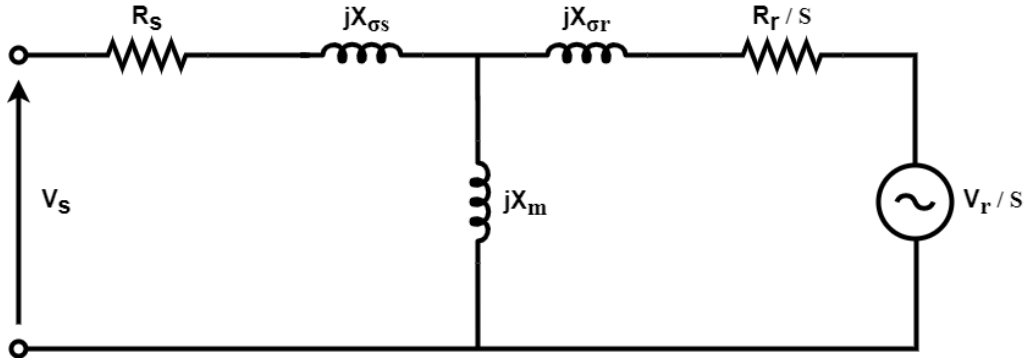
Fig. 2.7. Simplified equivalent circuit of a DFIG for short-circuit current calculation.

Considering the simplified equivalent circuit of a DFIG above, the following parameters are defined shown in Table 2.2 below.

Table 2.2 Definition of parameters of DFIG equivalent circuit for short-circuit current calculation

Parameters	Definition
R_s, X_s	Stator resistance and reactance
R_r, X_r	Wound rotor resistance and reactance
$X_{s\sigma}$, $X_{r\sigma}$	Stator and rotor leakage reactance
X_m	Magnetizing reactance
X_s', X_r'	Stator and rotor transient reactance
K_s, K_r	Stator and rotor coupling factor
σ (sigma)	Leakage factor
T_s', T_r'	Time constant for the damping of the DC component in Stator and rotor
V_s	Stator voltage
R_{ext}, X_{ext}	External resistance and reactance
R_{cb}	Crowbar resistance

The stator and rotor reactance of a DFIG can be represented as:

$$X_s = X_{s\sigma} + X_m \tag{2.1}$$

$$X_r = X_{r\sigma} + X_m \tag{2.2}$$

Also, the equivalent stator and rotor transient reactance could be derived as shown below:

$$X_s' = X_{s\sigma} + \frac{X_{r\sigma} * X_m}{X_{r\sigma} + X_m} \tag{2.3}$$

$$X_r' = X_{r\sigma} + \frac{X_{s\sigma} * X_m}{X_{s\sigma} + X_m} \tag{2.4}$$

Furthermore, the stator and rotor coupling factor, could be calculated by:

$$K_s = \frac{X_m}{X_s} \tag{2.5}$$

$$K_r = \frac{X_m}{X_r} \tag{2.6}$$

By knowing the magnetizing reactance, and stator and rotor reactances, the leakage factor of the machine can be determined by:

$$\sigma = 1 - \frac{X_m^2}{X_s * X_r} \tag{2.7}$$

Another important characteristic that significantly affect the behavior of short-circuit current of a DFIG, are the damping time constants of the DC components of both the stator and the wound rotor of the generator which can be calculated as follows:

$$T_s' = \frac{X_s' + X_{ext}}{\omega_s (R_s + R_{ext})} \tag{2.8}$$

$$T_r' = \frac{X_r'}{\omega_s (R_r + R_{cb})} \tag{2.9}$$

37

The short-circuit fault can occur anywhere in the wind farm, and also in any fault type. But for simplicity, a symmetrical 3L-G is considered in this section. In order to find the short-circuit current of a DFIG system, an equivalent diagram of a power system under fault condition, representing as a R-L circuit is considered as shown in Fig. 2.8. The location of the fault is indicated by a shorting switch at the end of the line.
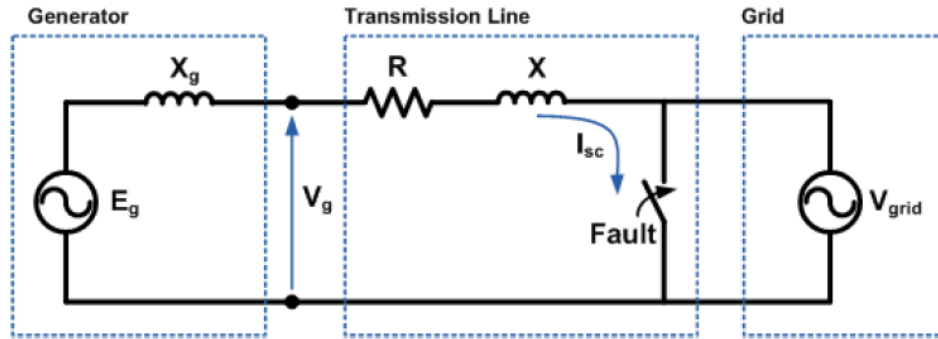
Fig. 2.8. Equivalent diagram of R-L circuits representing a power system with symmetrical fault at the end of the line.

As soon as the fault takes place, a significant level of current is produced by the generator. By considering R and L as transmission line resistance and inductance, and also u_g as the instantaneous voltage on the terminal of the generator, the short-circuit current contribution from the generator can be found from:

$$u_g = L\frac{di}{dt} + iR \tag{2.10}$$

And solving the above equation to derive the current:

$$i = \frac{V_g}{Z}\sin(\omega t + \alpha - \varphi) - e^{-\frac{R}{L}t}[\frac{V_g}{Z}\sin(\alpha - \varphi)] \tag{2.11}$$

Where, V_g and α represent peak voltage and voltage phase of the generator, and the impedance of the line is shown by Z which consists of R and X, thus, $Z = \sqrt{R^2 + X^2}$. Also, the impedance angle at the location of the fault is shown by φ, where $\varphi = \text{atan}\left(\frac{X}{R}\right)$. Equation (2.11) consists of two different signals. The first signal is a continuous sinusoidal waveform, and indicates the steady-state behaviour of the fault current contributed by the generator, while the second signal, has an exponential element that causes the waveform to decay exponentially with a time constant of $\frac{R}{L}$, which represents the DC component of the current and is the natural response of the circuit without the excitation produced by E_g, in Fig. 2.8.

In order to calculate the steady-state fault current in RMS value, only the first component of the above equations is considered. Thus, the magnitude of the short-circuit current would be:

$$I_{sc} = \frac{V_g/\sqrt{2}}{\sqrt{R^2 + X^2}} \tag{2.11}$$

The short-circuit current of a DFIG system is similar to the equation 2.10, only the crowbar and slip should also be considered. The entire derivation of the DFIG short-circuit current are documented in [98], and therefore is not repeated here. By referencing to all the parameters shown above, the approximate behavior of short-circuit current (3L-G fault) of a single DFIG can be obtained by [99]:

$$i(t) = \frac{\sqrt{2}\,V_s}{\sqrt{(X_s' + X_{ext})^2 + R_{cb}^2}} \left[e^{-\frac{t}{T_s'}} \sin(\alpha) - (1 - \sigma)\, e^{-\frac{t}{T_r'}} \sin(\omega t + \alpha) \right] \tag{2.12}$$

Where α is the voltage phase angle, σ is the leakage factor, and T_s' and T_r' are the stator and rotor time constants which represents the damping of the DC component in stator and rotor windings.

Additionally, since the industrial protective relays are set according to the maximum fault current contribution of a power generation unit, the above equation can be simplified to a term that only presents the maximum fault current, which is shown below:

$$I_{sc,max\ magnitude} = 2\frac{\sqrt{2}\ V_s}{X_s'} \tag{2.13}$$

2.4.3   A General Comparison Between Short-circuit Current for Different Types of WTG

The short circuit current contribution from different types of WTGs is not equally the same. Additionally, the maximum value of the magnitude of the short circuit current is immensely affected by various factors, where the furthermost critical ones are, the transient reactance, the pre-fault voltage, the effective rotor resistances, and also the instance the fault occurs. Also, the short-circuit current transient behavior could be affected by the stator time constant and the rotor time constant for Type I through Type III WTGs. For example, since Type I, II, and III wind turbines are equipped with induction generators, the short circuit current gradually declines as the fault progresses and eventually decays to a very small value, usually near zero, due to the depletion of the rotor flux.

On the other hand, for Type IV WTGs, since this technology implements synchronous generator, the short-circuit current is maintained constant, in other words, the Type IV WTG can generate constant current during the event of fault. It's almost similar to synchronous generators in conventional power plants, however thanks to employment of power electronics, the level of

short-circuit current is extremely small and is usually constrained to less than two orders of maximum full-load current.

With reference to equation (2.12), Table 2.3 is tabulated below to summarize different fault impedance, along with transient rotor time constants for different types of WTG technologies. Therefore, it is obvious that any change in those parameters could alter the behavior and magnitude of short-circuit current for any wind turbine. Table 2.4 shows the maximum and minimum possible values of the short-circuit current for different types of WTGs. In summary, with respect to Type I and Type II WTGs, the maximum and the minimum short-circuit current depends on timing of the fault, the parameters and the operating condition of the induction generator, while for Type III WTGs, the magnitude of short-circuit current could be affected by the control and the operation of the converter. Finally, with regard to Type IV WTGs, the fault current could be controlled by the power converters, and that is why the fault current is usually very small in comparison to other types of WTGs.

Table 2.3 Modified values for short-circuit current calculation for different types of WTGs

WTG	Type I	Type II	Type III
Z_s'	$X_s' = \omega L_s'$	$\sqrt{x_s'^2 + R_{ext}^2}$	$\sqrt{x_s'^2 + R_{CB}^2}$
T_r'	$\dfrac{L_r'}{R_r}$	$\dfrac{L_r'}{R_r + R_{ext}}$	$\dfrac{L_r'}{R_r + R_{CB}}$

Table 2.4 Maximum and minimum possible values of the short-circuit current for different types of WTGs

WTG	Type I	Type II	Type III	Type IV
Maximum short-circuit current	$2\dfrac{\sqrt{2}V_s}{X'_s}$	$2\dfrac{\sqrt{2}V_s}{X'_s}$	$2\dfrac{\sqrt{2}V_s}{X'_s}$	$[1.1 \sim 1.5] * I_{rated}$
Minimum short-circuit current	$\dfrac{\sqrt{2}V_s}{X'_s}$	$\dfrac{\sqrt{2}V_s}{\sqrt{x_s'^2 + (9R_r')^2}}$	$1.1 * I_{rated}$	0

Among all available WTGs, the DFIG-based wind farms are the most difficult and challenging to protect, since there are many variables that could alter the fault current, as discussed previously, and could cause the protective relays to maloperate or impose miscoordination between overcurrent relays. For example, during a fault, if the voltage dips 50% (0.5pu) as wind speed increases, active power will also increase, however reactive power will remain the same. In this case, the voltage will be changed extremely marginally, however, the short-circuit current is increased as wind speed is escalated. However, during fault where the voltage at the fault location is dipped to zero (100% voltage drop), as wind speed is increased, the WTG active power will be increased, but the fault current will not change much. Therefore, these important aspects must be considered during designing protection schemes. This problem will be further discussed in Chapter 4, where intelligent adaptive protection schemes are proposed.

2.4.4 Short-circuit Current Calculation of a DFIG

Now by knowing all the parameters, explained in sections 2.4.2 and 2.4.3, the DFIG unknown parameters can be calculated accordingly and thus, the magnitude of short-circuit current would be determined for setting protection relays, as shown below:

- Stator and rotor reactance:

$$X_s = X_{s\sigma} + X_m = 0.171 + 2.9 = 3.071pu$$

$$X_r = X_{r\sigma} + X_m = 0.156 + 2.9 = 3.056pu$$

- Stator and rotor transient reactance:

$$X_s' = X_{s\sigma} + \frac{X_{r\sigma} * X_m}{X_{r\sigma} + X_m} = 0.171 + \frac{0.156 * 2.9}{0.156 + 2.9} = 0.319pu$$

$$X_r' = X_{r\sigma} + \frac{X_{s\sigma} * X_m}{X_{s\sigma} + X_m} = 0.156 + \frac{0.171 * 2.9}{0.171 + 2.9} = 0.317pu$$

- Stator and rotor coupling factor:

$$K_s = \frac{X_m}{X_s} = \frac{2.9}{3.071} = 0.944pu$$

$$K_r = \frac{X_m}{X_r} = \frac{2.9}{3.056} = 0.948pu$$

- Leakage factor:

$$\sigma = 1 - \frac{X_m^2}{X_s * X_r} = 1 - \frac{(2.9)2}{3.071 * 3.056} = 0.103pu$$

- Damping time constant:

$$T_s' = \frac{X_s' + X_{ext}}{\omega_s (R_s + R_{ext})} = \frac{0.319 + 0.285}{(2\pi60)(0.007 + 0.018)} = 0.064s$$

$$T_r' = \frac{X_r'}{\omega_s (R_r + R_{cb})} = \frac{0.317}{(2\pi60)(0.005)} = 0.168s$$

- 3 L-G Short-circuit current:

$$I(t) = \frac{\sqrt{2} V_s}{\sqrt{(X_s'+X_{ext})^2 + R_{cb}^2}} [e^{-\frac{t}{T_s}} \sin(\alpha) - (1 - \sigma) e^{-\frac{t}{T_r}} \sin(\omega t + \sigma)]$$

$$I_{sc,max\ pu\ magnitude} = 2\frac{\sqrt{2} V_s}{X_s'} = 8.86\ pu$$

$$I_{FLA} = \frac{S}{\sqrt{3}*V} = \frac{1.5 * 10^6}{\sqrt{3} * 575} = 1506.13\ A$$

$$I_{sc} = I_{FLA} * I_{sc,max\ pu\ magnitude} = 1506.13 * 8.86 = 13344.31\ A\ (RMS\ value)$$

$$I_{sc,\ peak} = I_{SC} * \sqrt{2} = 13344.31* \sqrt{2} = 18871.7\ A\ (Peak\ value)$$

The waveform of the calculated short-circuit current of a the DFIG is presented in Fig. 2.9. The short-circuit current is 8.89 pu which is very close to the one that was calculated that was 8.86 pu. During the fault incidence at 0.2 S, the magnitude of the fault current is extremely high due to DC offset, unsymmetrical sub-transient and transient of induction machine, however they decay to zero shortly after the fault incidence and only symmetrical steady state component remains. The AC symmetrical steady state short-circuit current is significantly smaller compared to the total fault current; however, it is large enough to cause drastic damage to power apparatus within a wind farm. Therefore, the overcurrent relay must be able to detect any form of faults, even faults with high resistance, to ensure maximum protection and security is provided and at the same time, minimum disconnection of faulty zone from the plant is made. This important phenomenon is studied in the next chapter.
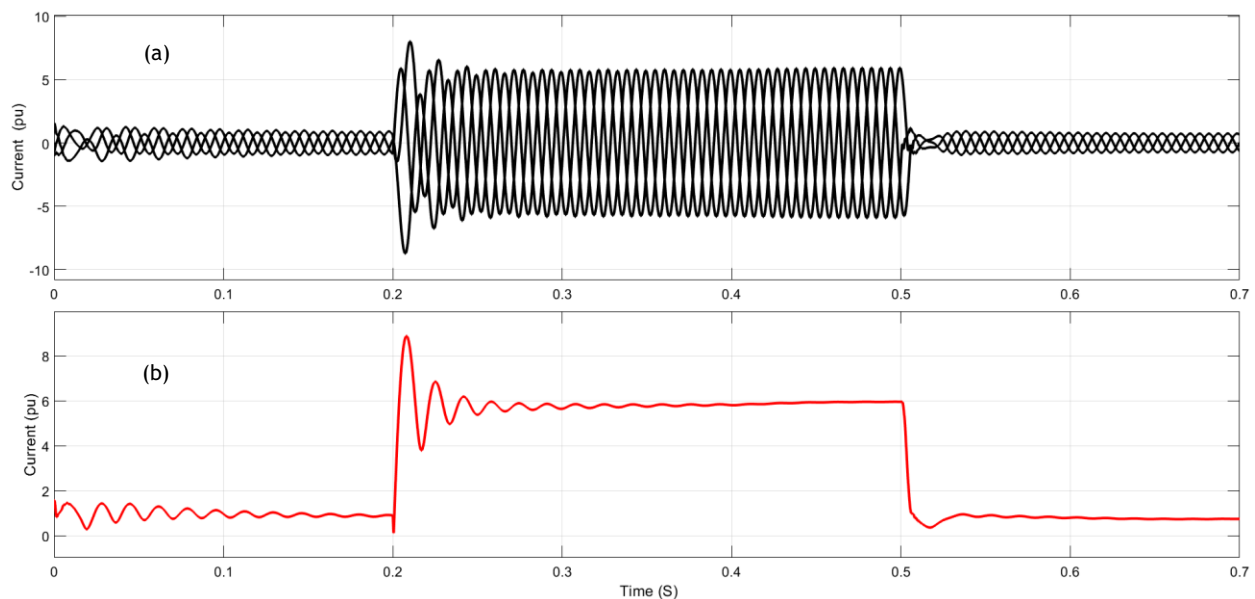
Fig. 2.9. Calculated short-circuit current waveform of a DFIG: (a) behavior of bolted 3 phase fault current (b) magnitude of the fault current.

2.5　Conclusion

In this Chapter, a brief description of the design of the wind farm model that will be used for power system protection studies in the subsequent Chapters was provided. An explanation of short-circuit current contribution for various types of wind turbines, with emphasis on DFIG-based WTG technology was provided in this Chapter. Furthermore, a sample of hand calculation for short-circuit current of a DFIG was done as a verification for the software analysis. In the next Chapter, the design, implementation and coordination of overcurrent relays, along with proposed optimal settings for each relay using AI, will be discussed.

Chapter 3

Optimal Overcurrent Protection and Coordination Schemes for Wind Farms

3.1   Overcurrent Protective Relays

OCRs have the same basic I/O signal operation as other types of relays. In these relays, if the incoming current is higher than the pre-set current value, the relay will send out an output signal (either instantaneously or after a calculated delay) to the circuit breaker (CB) to disconnect the circuit in order to protect the power components from the result of excess current. There are three main types of OCRs used in power systems, which are: definite current relay (also known as instantaneous relay), definite time relay, and inverse time relay. The most common type is inverse time relay which has an inverse characteristic curve that means the relay operates faster as the current increases. These types of relays operate instantaneously when the current reaches a high limit magnitude thus eliminating the damage to the power components[100]. Modern protective relays are equipped with both the inverse characteristic and instantaneous element, which help the relay to have the capability of time-current sensitivity, as well as instantaneous tripping function, specific for during the time the fault current is very high and no delay in operation is tolerated.

Inverse time OCRs based on their sensitivity to the current and time, can again have several characteristics depending on the applications. These OCR types, according to IEC 60255-151:2009 standard is presented in Table 3.1 below [101]. Also, the time current characteristics (TCC) curve

of a typical protective relay is shown in Fig. 3.1. These standard curves could be set differently by changing the type of OCR according to the previous table, and thus, a proper operation expected from the relay could provide protection and security for a specific power apparatus or at a large scale for a large protection zone, i.e., feeders, transmission lines, wind turbines (generator and transformer together), and etc.
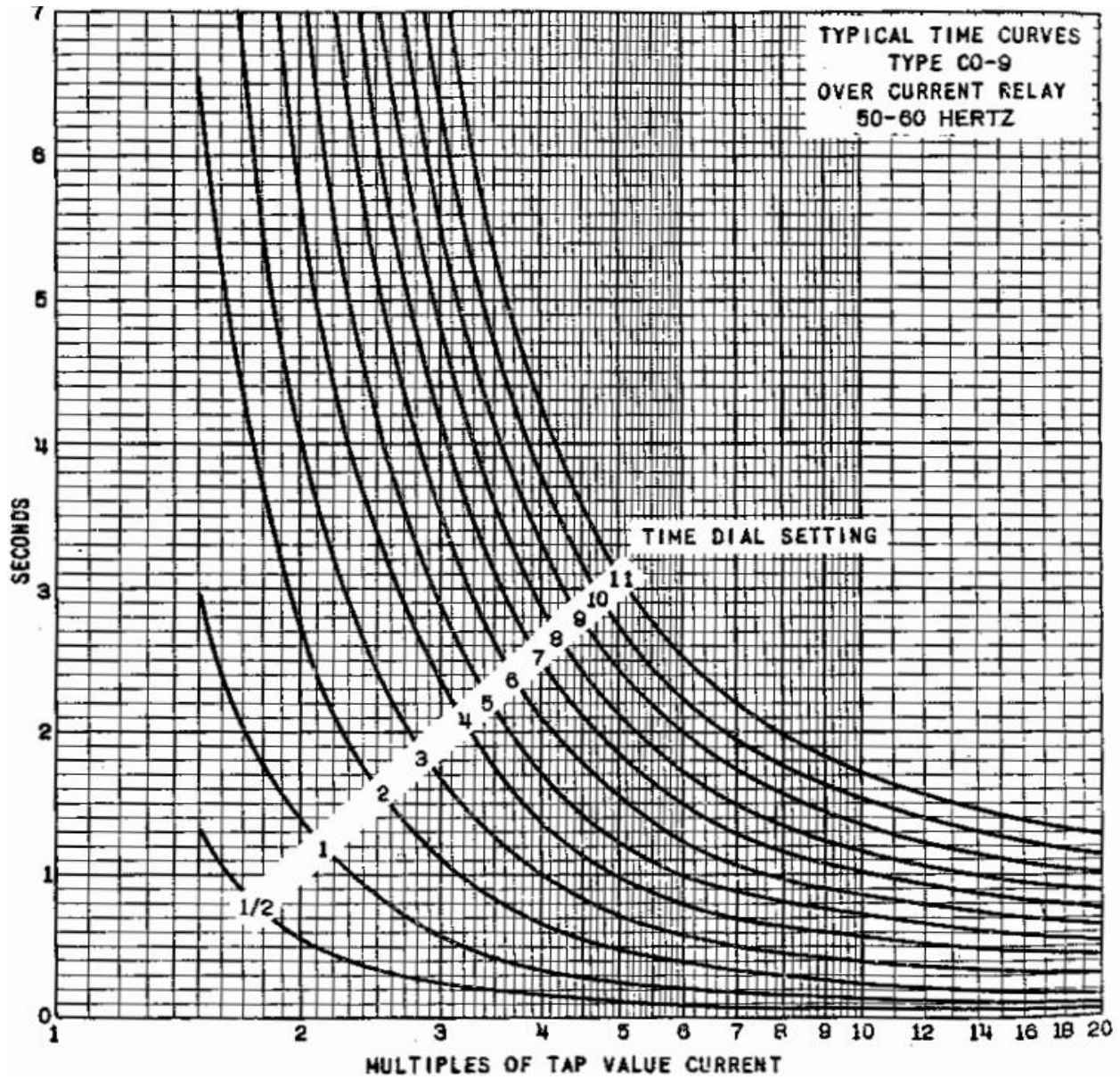
Fig. 3.1. TCC curve of a typical OCR [65]**.**

Table 3.1 Types of OCRs according to IEC 60255-151:2009 standard

Type of Overcurrent Relay	Operation Time
Normally-Inversed	$T = \dfrac{0.14 * \text{TMS}}{(I/Ipickup)^{0.02} - 1}$
Very Inversed	$T = \dfrac{13.5 * \text{TMS}}{(I/Ipickup)^{1} - 1}$
Extremely Inversed	$T = \dfrac{80 * \text{TMS}}{(I/Ipickup)^{2} - 1}$
Long time-Inversed	$T = \dfrac{120 * \text{TMS}}{(I/Ipickup)^{1} - 1}$

3.2   Coordination of Several OCRs

In power systems, the entire OCRs must be properly coordinated with each other in order to protect the power elements from the fault current. To do so, the critical settings of OCRs such as, plug multiplier setting (PMS) and time multiplier setting (TMS), must be properly calculated and selected for each relay. PMS is varied in the range of 50% to 200% and in steps of 25%. This setting is only used for inverse current relays which detect phase to phase fault [102]. For the relays that detect phase to ground fault, the PMS is quite different. It is varied in in the range of 10% to 40% in steps of 10%, or in the range of 20% to 80% in steps of 20%. The point that should be taken into consideration is that the higher the value of PMS for the relay is selected, the higher current the relay requires to sense for tripping. TMS ranges from 0 to 1 in steps of 0.1. However, sometimes it varies in steps of 0.05, for better sensitivity. Thus, the maximum value for TMS could be selected is 1 and the minimum is 0.1 or 0.05 (depending on the manufacturer). The higher the value of TMS for the relay is selected, the longer it takes for the relay to trip. Thus, the TMS for

the first relay that coordination starts from, is usually selected as minimum value, which is 0.05. This would help proper coordination with minimum delayed time for the subsequent protection relays. In order to coordinate OCRs with each other, there is a time interval between a primary relay and a backup relay operation and this is called the coordination time interval (CTI). This time interval is usually set in the range of 0.3 and 0.5 seconds for most of the conventional relays, while for modern digital relays it is set at 0.2 seconds, which means the backup relay is able to operate faster compared to conventional relays. So, in order to coordinate relays with each other, both CTI, and the relay operation time which are the constraint of TMS and PMS, must be taken into consideration.

The concept of coordination of OCRs means that the closest relay to the fault location, which is referred to as the primary relay, must first trip the CB, and in the case when the primary relay does not trip or malfunctions, the adjacent relay closest to the primary relay, which is called the backup relay, must trip instead. This coordination is extremely crucial and is conducted in order to decrease the expanded power loss and avert power quality compromise. The coordination phenomenon is depicted in the Fig. 3.2, which shows a simple radial power system. In this figure, by imposing a fault at the end of the line, OCR_1 as primary protection must trip to the fault. In case of any relay malfunction, or blinding situation, OCR_2 as backup protection should trip. Furthermore, if OCR_2 does not operate, OCR_3 as the second backup protection must trip and disconnect the feeder.
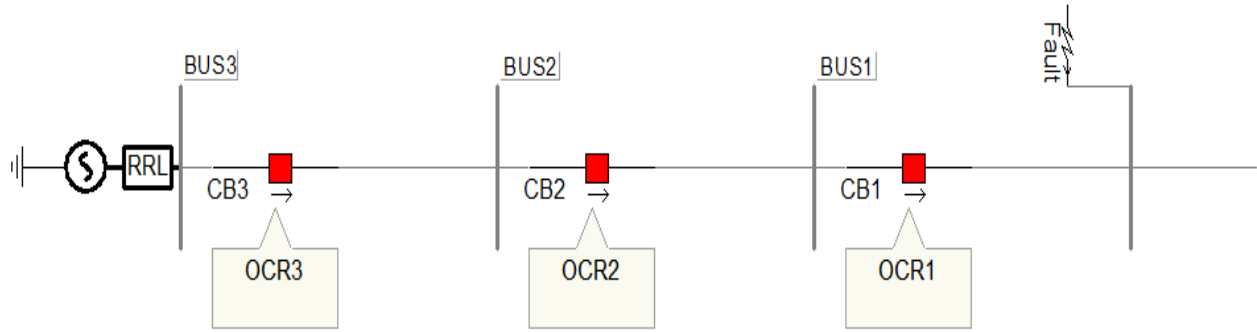
Fig. 3.2. Overcurrent relay coordination concept.

3.3 Design and Development of the proposed OCR

In order to analyze the OCR setting and coordination, a digital OCR protection scheme has been developed in Matlab/Simulink, where its operation is designed based on industrial SEL-751 protective relays. The proposed relay operates according to IEC 60255-151:2009 standard and can be set for various TCC curves where the relay operation time is calculated precisely according to IEC standard which was shown in the previous section. The coding used for developing the operation of the relay, along with the codes for plotting the TCC curve for each relay mode of operation, as well as codes for defining the type of OCR are shown in Appendix A.2 – A.4. Furthermore, the simplified version of the relay model created in Matlab is shown in Fig. 3.3, while the user-friendly graphical interface of the developed relay for easier relay settings has been established and presented in Fig. 3.4. According to the developed relay, in order to set the OCR, the CT primary and secondary, along with TCC operation mode, pickup current, maximum fault current, plug setting (PS - which determines the pickup current), PMS and TMS can be modified and the OCR would react accordingly. Another feature of this scheme is that the TCC curve for each OCR can be plotted to ensure that relays have been set properly and are well coordinated with each other. In Appendix A.5 and A.6., the overview of the proposed centralized overcurrent

protection and coordination scheme, which consists of 47 OCRs, implemented for the protection of wind farms are presented.
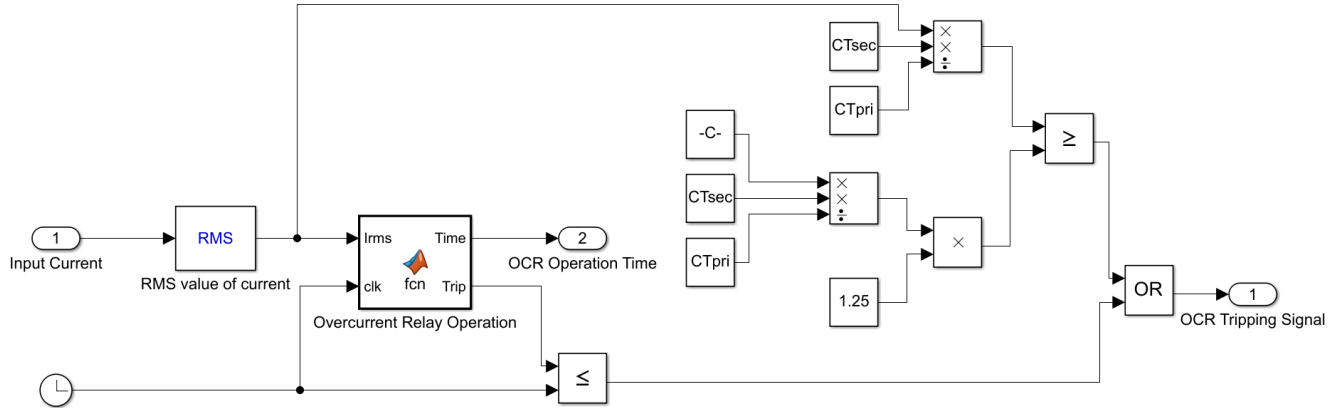
Fig. 3.3. Simplified version of the relay model created in Matlab.
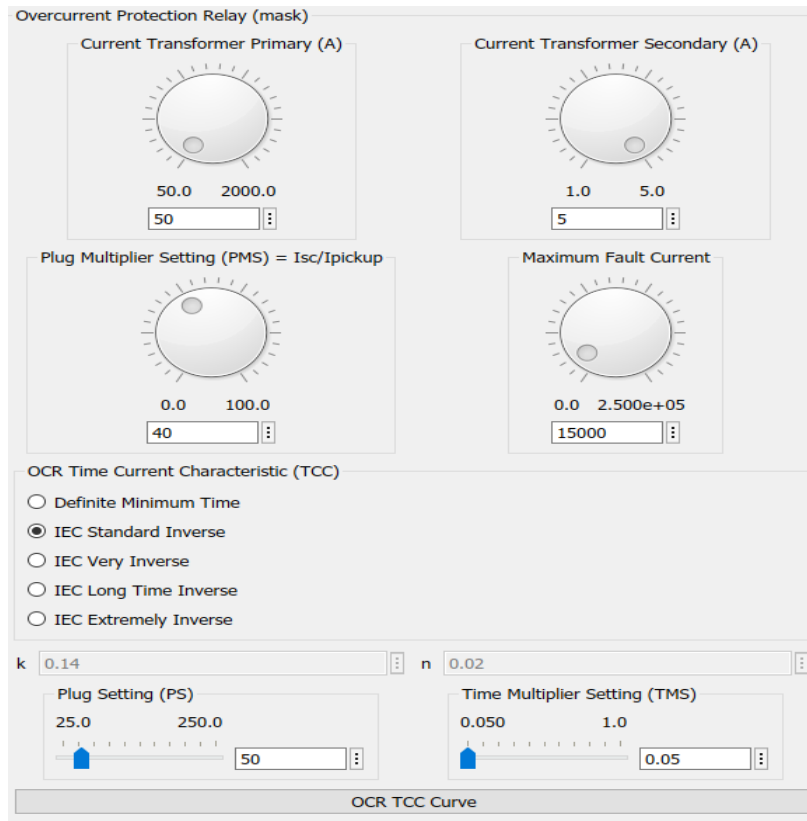
Fig. 3.4. The graphical interface of the developed OCR based on industrial SEL-751 protective relay in Matlab/Simulink.

3.4   Relay Settings and Coordination Calculation

In this research, it is possible to design the coordination of the relay settings in two different ways. One way of doing it is to consider the relay next to the power grid as the primary relay, and start the coordination from that protection zone, to the last relay located at each wind turbine generator. This practice is suitable and applicable for numerous power systems, such as distribution networks; however, the disadvantage of implementing such coordination for wind farms is that, such protection scheme has less selectivity and could create miscoordination between the main and backup relays at the end of the protection zone. For example, if a fault occurs near one of the wind turbines, due to this specific coordination implemented, the entire wind farm would be disconnected from the grid, which is totally unacceptable. Therefore, in order to prevent such calamity, in this research, coordination starting from each DFIG to the main grid is proposed, so that during any fault incidence at the wind turbines, or even the feeders containing several wind turbines, only the faulty section is tripped by the CBs and therefore the minimum disconnection is exercised.

The relay settings and coordination has been calculated for all 47 protective relays employed for the wind farm based on the fault behaviour that was discussed in previous Chapter, however due to massive number of calculations and large space required to present all the calculations, only the samples of two relay setting calculations are presented below:

3.4.1   Relay 1 Settings

The first relay is responsible for the wind turbine protection zone that includes the DFIG and the local power transformer. The relay should be able to detect the fault at the shortest possible

time, to avoid the extended disconnection of the entire feeder. In order to set the relay settings, relay setting current (RSI), need to be calculated, which is generally 1.25 to 1.5 times of full load amperage (I_{FLA}) [103], However, in this work to achieve maximum sensitivity RSI of 1.25 times of I_{FLA} is considered. I_{FLA} was calculated in Chapter 2 for a single DFIG, which was 1506.13 A, for the LV side of transformer (575V). Therefore, since the OCR is located on the HV side (35kV), the IFLA for the HV side should be considered which would be 24.74 A. By running the simulation, the I_{FLA} is found to be 28.69 A, which is close to the hand calculation. This small error is not significant, since I_{FLA} will be rounded to a standard value for relays as will be shown later. Since all the protection relays are developed in MATLAB, the simulation results for I_{FLA} will be considered for setting the relays. Therefore, the RSI on the HV side would be:

$$RSI = 1.25 * I_{FLA} = 1.25 * 28.69 = 35.86 \ A$$

Afterwards, the PS of the relay by considering a proper CT ratio is calculated. For the above RSI, CT ratio of 50:5 is selected, which is determined by the closest CT ratio available for 1.5 times of the calculated RSI. Usually, the output of CT secondary should be less than 5A [104]. Also, in order to avoid saturation, the fault current on the secondary should be limited to maximum 100A. Considering this condition, then the best selected CT ratio would be 250:5. However, in this specific case, since the focus is on the relay coordination, it is assumed that CT is ideal and does not get saturated during fault current, and the previous CT ratio of 50:5 is selected. Thus:

$$RSI = (PS * CT_{pri}) / 100 => 35.86 = (PS * 50) / 100 => PS = 71.72 \ \%$$

As mentioned before, PS is varied in the range of 50% to 200% and in steps of 25%. Therefore, PS should be standardized as below:

$$PS = 71.72 \ \% \approx 75 \ \%$$

Next, the pickup current both on the primary and secondary side of the CT which will be monitored by the relay are calculated as:

$$I_{pickup\text{-}pri} = (75 * 50) / 100 = 37.5 \ A$$

$$I_{pickup\text{-}sec} = (37.5 * 5) / 50 = 3.75 \ A$$

Now by knowing the pickup current (I_{pickup}), and short circuit current (I_{sc}) calculated in previous chapter, the relay operation time can be determined. It should be noted that, for the coordination studies, the TMS for the first relay should always be selected as the minimum value, so the relay operates as soon as possible, and also reduce the operation time of subsequent backup protective relays. Therefore, the least possible value for TMS which is 0.05, is selected for this relay. As discussed in Chapter 2, if a fault occurs at the DFIG, then the maximum short-circuit current on the LV side 18871.7 A, therefore in the HV side where the relay is located, the fault current would be reduced to 310.02 A. In order to protect the WTG, a differential protection relay could be placed, which will be discussed in Chapter 5. However, if a fault occurs on the HV side of the transformer, since the fault location is close to the OCR, then OCR would be responsible for protecting the WTG and its entire feeder. After running the fault simulation on HV side, the fault current would be 9051.61A on the primary side of the CT. The fault current at this point is significantly high which is due to the contribution of other wind turbines to the fault location. Thus, the current on the primary and secondary side of the selected CT would be:

$$I_{sc\text{-}pri} = 9051.61 \ A$$

$$I_{sc\text{-}sec} = (9051.61 * 5) / 50 = 905.16 \ A$$

So, the operation time of the relay will be:

$$T = \frac{0.14 * TMS}{\left(\frac{Isc}{Ipickup}\right)^{0.02} - 1} = \frac{0.14 * 0.05}{\left(\frac{905.16}{3.75}\right)^{0.02} - 1} = 0.06 \text{ s}$$

Finally, PMS for the first relay, which is the ratio of short-circuit current over pickup current, and is a unitless quantity, is calculated as:

$$PMS = 905.16 / 3.75 = 241.37$$

3.4.2 Relay 2 Settings

The second relay, is the backup relay for the first relay, as well as the main protection relay for the entire feeder protection zone, where 10 wind turbines are connected to this feeder. For a fault on the HV side of the WTG, close the Relay 1, then Relay 2 should only operate in case the main relay for each wind turbine doesn't detect the fault, or there is severe fault current on the main feeder. The procedure for calculating the pickup current relay setting for the backup relay is the same as the first relay. By knowing the IFLA of a single WTG is 28.73A, then the aggregated I_{FLA} for the entire feeder consisting of 10 WTG, would be 287.32 A. so we shall have:

$$RSI = 1.25 * 287.32 = 359.15 \text{ A}$$

$$RSI = (PS * 450) / 100 => PS = 79.81 \% \approx 100 \%$$

$$I_{pickup\text{-}pri} = (100 * 450) / 100 = 450 \text{ A}$$

$$I_{pickup\text{-}sec} = (450 * 5) / 450 = 5 \text{ A}$$

The procedure for calculating the operation time of the backup relay is slightly different from the primary relay. The reason is that, for the second relay, we do not have the TMS information and it should be calculated based on both relay 1 and relay 2 operation times. In order

to do that, based on the coordination principles, the operation time of the backup relay should be more than the operation of the first relay, therefore, a CTI setting should be defined. In this study, the minimum value for CTI which is 0.3 S is selected, thus the operation time of the backup relay (second relay) shown by T_{R2} would be:

$$T_{R2} = CTI + T_{R1} = 0.3 + 0.06 = 0.36\ S$$

Now by knowing the approximate operation time of the backup relay, short-circuit current of both the primary and secondary relay, and also the pickup current of the backup relay, the TMS and PMS setting for the backup relay is calculated. As shown in last section, the short-circuit current near Relay 1 is 9051.61 A. The short-circuit current near Relay 2, is 8666.45 A, which is somewhat smaller due to impedance of the underground cable. Thus:

Relay 1: Primary side $\qquad\qquad I_{sc,pri} = 9051.61\ A$

Relay 1: Secondary side $\qquad\qquad I_{sc,sec} = (9051.61 * 5) / 450 = 100.57\ A$

Relay 2: Primary side $\qquad\qquad I_{sc,pri} = 8666.45\ A$

Relay 2: Secondary side $\qquad\qquad I_{sc,sec} = (8666.45 * 5) / 450 = 96.29\ A$

$$PMS = 96.29 / 5 = 19.25$$

$$TMS = \frac{T * \left(\frac{Isc}{Ipickup}\right)^{0.02} - 1}{0.14} = \frac{0.36 * \left(\frac{100.57}{5}\right)^{0.02} - 1}{0.14} = 0.159$$

As mentioned before, TMS varies in the range of 0.05 to 1 and in steps of 0.05. Thus, TMS should be standardized as below:

$$TMS = 0.159 \approx 0.2$$

Finally, based on the new TMS and PMS values, the backup relay operation time would be:

$$T = \frac{0.14 * TMS}{\left(\frac{Isc}{Ipickup}\right)^{0.02} - 1} = \frac{0.14 * 0.2}{\left(\frac{96.29}{5}\right)^{0.02} - 1} = 0.46 \ s$$

The same procedure has been carried out for all protective relays with respect to their protection zone, and their responsibility (main or backup), and their coordination settings are tabulated in Table 3.2 below. It should be noted that, the settings for all wind turbines relays (R1-40) are the same, since the parameters for all DFIG are exactly the same. Also, the settings for all four feeders (R41-44) are also the same, since each feeder consists of 10 wind turbines with identical parameters. R45 is the relay responsible for the main feeder protection zone, while the R46 and R47 are responsible for the intertie protection zone where the main power transformer and transmission line are located.

Table 3.2 Calculated relay settings and coordination for all OCRs

Relay Number	Full Load Current	CT Ratio	Relay Setting Current	Pickup Current	Plug Setting	Plug Multiplier Setting	Time Multiplier Setting	Relay Operation Time
R	I_{FLA}	CT	RSI	I_{pickup}	PS	PMS	TMS	T
1-40	28.69	50/5	37.5	3.75	75%	241.37	0.05	0.06
41-44	287.32	450/5	450	5	100%	19.25	0.2	0.45
45	1145.06	2000/5	1500	3.75	75%	4.93	0.2	0.86
46	181.6	300/5	300	5	100%	3.92	0.55	2.78
47	178.51	300/5	225	3.75	75%	5.06	0.75	3.18

Based on the calculated relay settings and coordination above, these settings were used to successfully set the relay parameters on the developed OCR, where the TCC curve for each relay

are shown in Fig. 3.5 – 3.9. Also, later all the relays coordination in one plot will be shown in section 3.6, in Fig. 3.22.
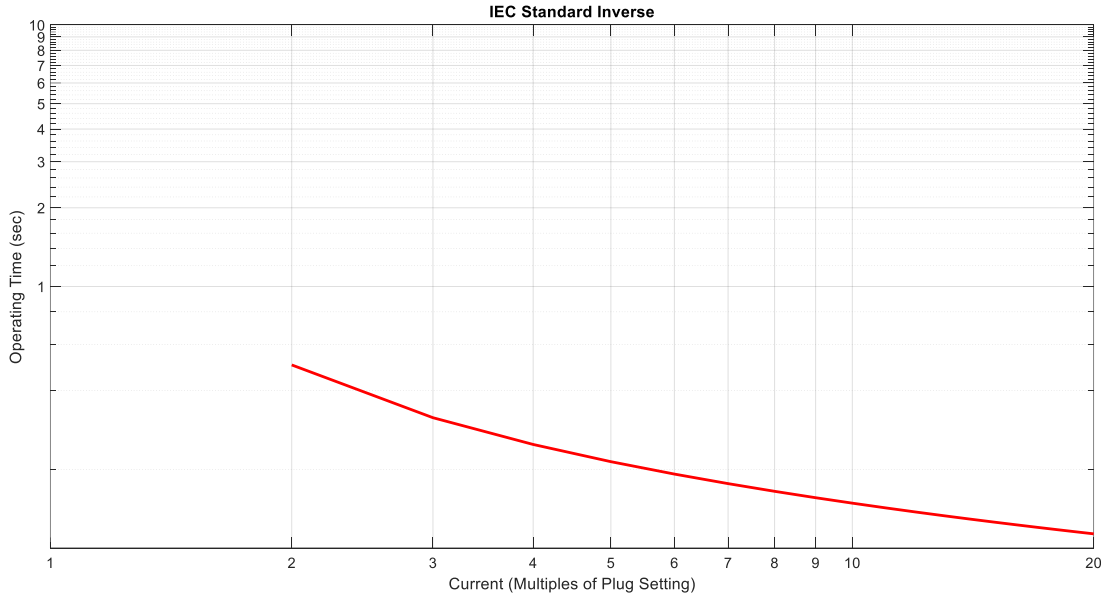
Fig. 3.5. TCC curve for OCR1-40.
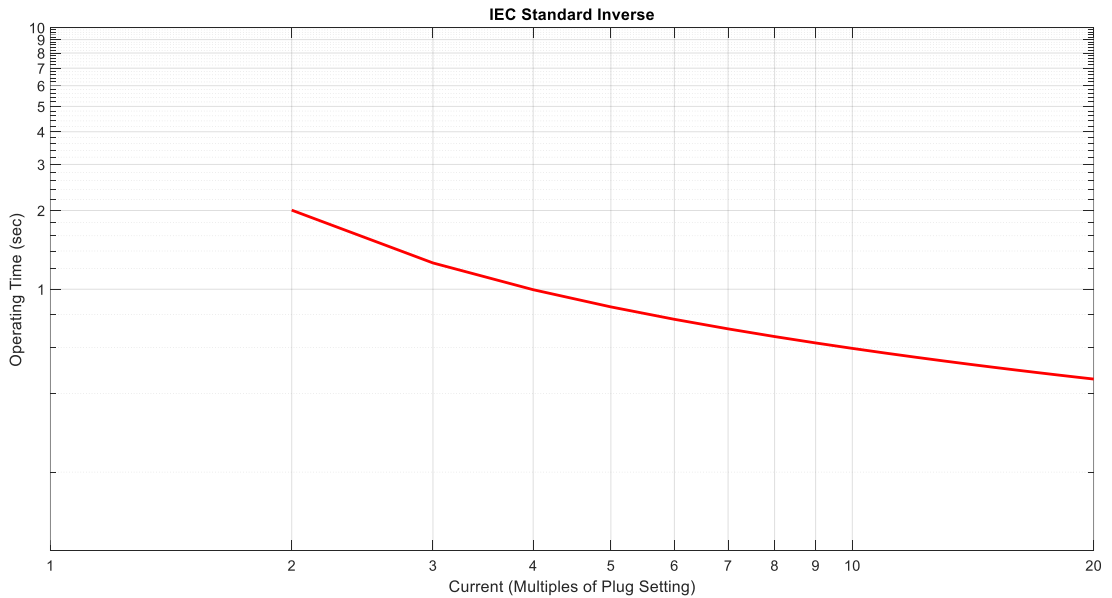
Fig. 3.6. TCC curve for OCR41-44.

IEC Standard Inverse
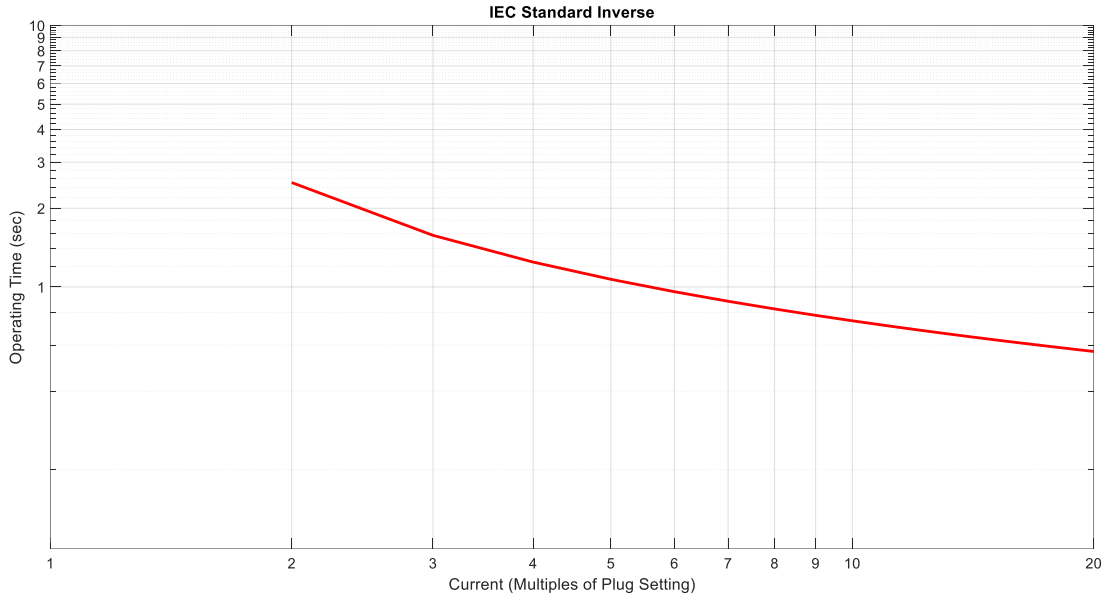
Fig. 3.7. TCC curve for OCR45.

IEC Standard Inverse
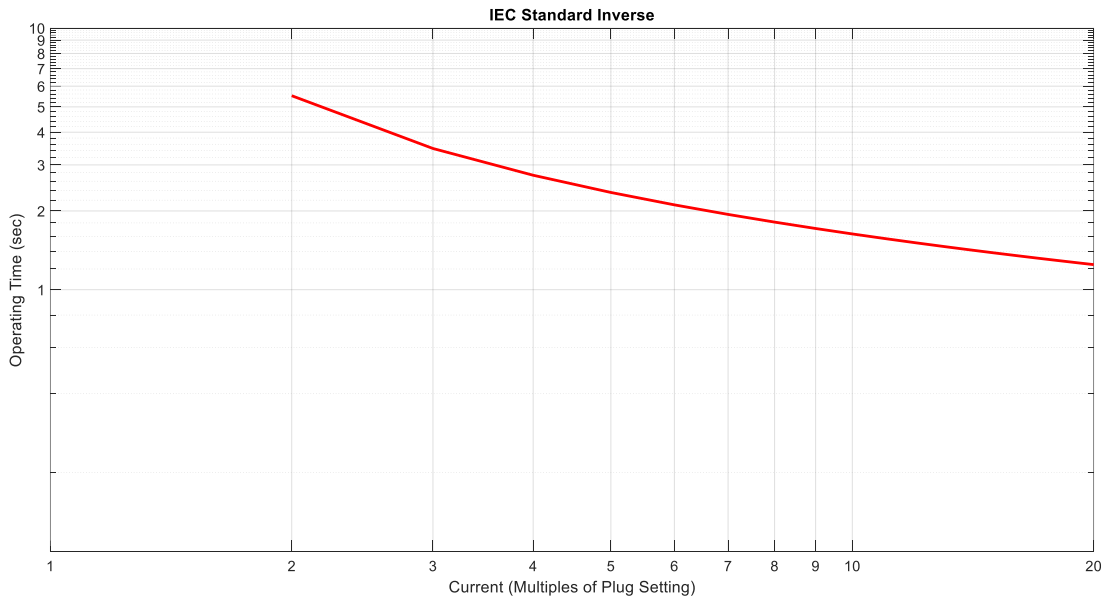
Fig. 3.8. TCC curve for OCR46.
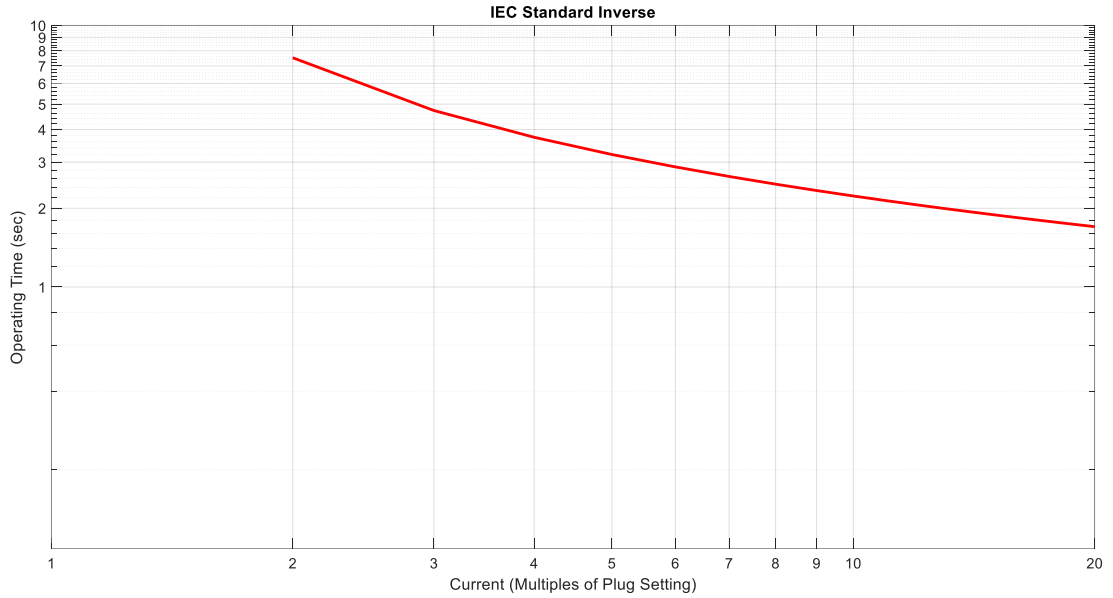
Fig. 3.9. TCC curve for OCR47.

3.5   Optimal Coordination of OCRs

In the previous sections, the settings for all protective relays for the wind farm was calculated and their parameters were tested on the developed OCR, where the TCC curves for each relay was also successfully plotted. In this section, with the purpose of optimizing the operation of OCRs, two AI optimization techniques such as GA and GWO, are developed and implemented to provide a better protection and security for large-scale wind farms.

3.5.1 Genetic Algorithm Based Optimization of OCR Coordination for Wind Farms

GA is an advanced and practical method that can be used for variety of applications to optimize the solutions including problems where the objective functions (OF) are discontinuous stochastic, and non-differentiable or non-linear. GA can also be implemented for problems of mixed integer programming where some elements are constrained to be integer valued.

In the GA module, there are four important terminologies which are population, chromosomes, genes, and finally allele where a generalized form of such entity is shown in Fig. 3.10. Population is the subset of possible solutions, which contains numerous chromosomes. A chromosome is actually one possible solution to the given problem, which consists of several genes. Meanwhile, each gene is basically one element position of the chromosome that contains a value, that is referred to allele.
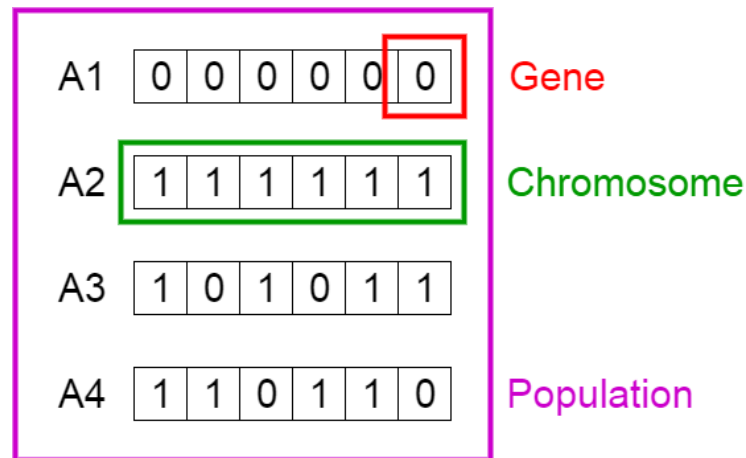
Fig. 3.10. GA module terminologies.

GA fulfill three types of rules at each step to produce the next generation from the in-progress population which are called selection, crossover and mutation. In selection stage,

individuals are selected, that are named as parents, to contribute to the population at the next generation. Crossover is then used to combine two parents to create children for the next generation. At the end mutation is implemented in order to apply random changes to individual parents to generate children. The steps are explained in the following subsections and the flowchart for GA approach has also been depicted in the Fig. 3.11.
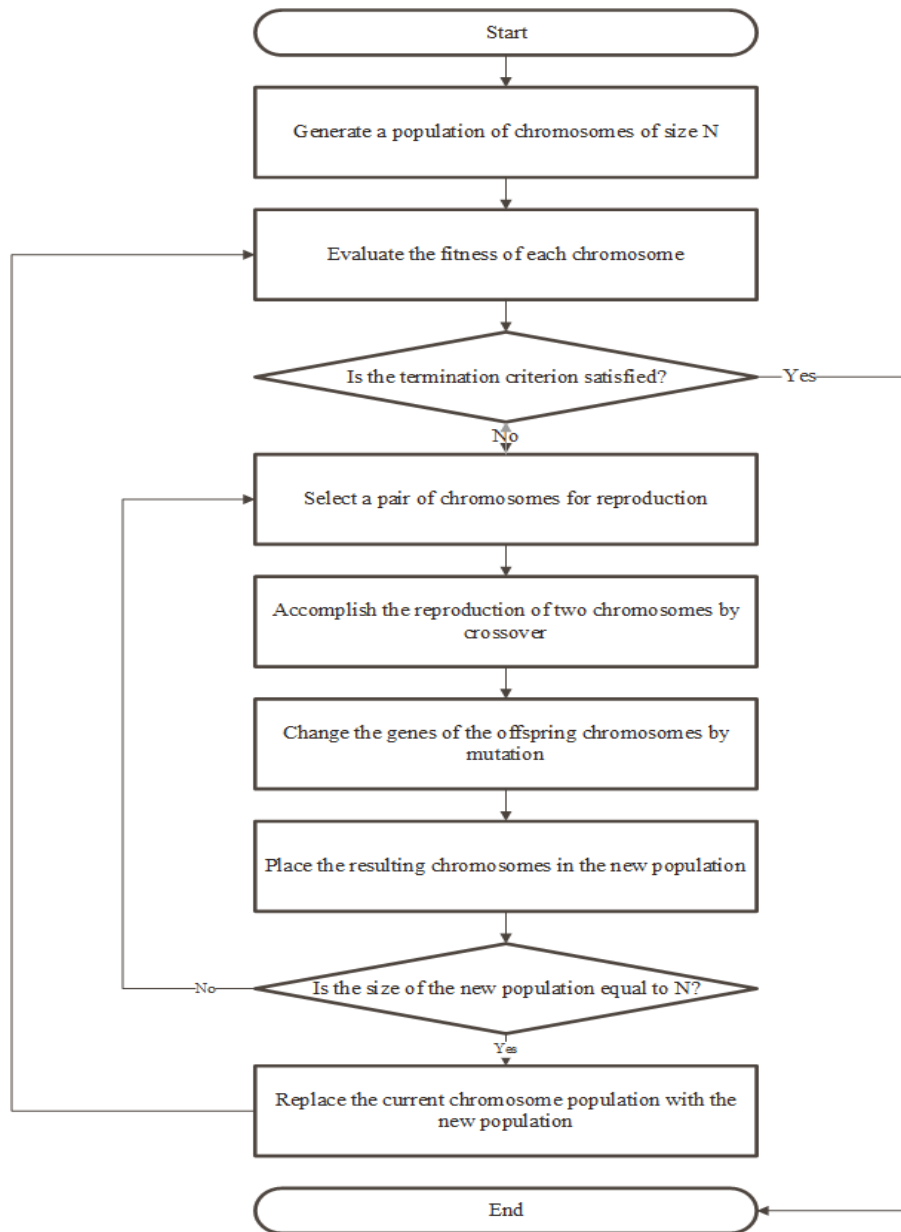
Fig. 3.11. Flowchart for GA based optimization approach.

In the following sub-sections, the design and implementation of GA, specifically defined for optimizing the relay settings and coordination are presented:

3.5.1.1   Initialization

At the very beginning stage of GA, a preliminary pool of random chromosomes referred to "parents" is generated. Parents are essentially several sets of random relay settings that must satisfy the defined constraints. Each set of relay setting is packed into a chromosome hence, each chromosome contains TMS for all the relays in the wind farm. The number of TMS sets are referred as population size which must be set properly during initialization. The higher population size selected, the more TMS sets are generated, as a result better setting for relay may be achieved at the end of GA process; however, if an enormous population size is opted, a much longer time should be provided for the GA to process all the parents based on the selected constraints and may not be suitable for some online applications that high operation speed is required. Thus, a sensible population size based on the optimization problem should be designated. The constraints defined for chromosomes, is fundamentally the constraints that should be defined for the protective relays. In this research, the constraints for overcurrent relay coordination have been defined as:

$$\Delta t_{mb} = t_b - t_m - CTI \geq 0 \qquad (3.1)$$

$$0.05 \leq TMS \leq 1 \qquad (3.2)$$

$$TMS_{imin} \leq TMS_i \leq TMS_{imax} \qquad (3.3)$$

In these equations, Δt_{mb} represents discrimination time between the backup and main overcurrent relay, t_b and t_m are the operation time for backup and main relay respectively, and CTI

is the coordination time interval between the main and backup relay. Furthermore, the range of TMS has also been defined which varies from 0.05 to 1 according to the standards. It's obvious that TMS can't afford to be 0 as the relay will operate instantaneously and causes miscoordination. Finally, the relation between TMS of each relay with other relays have also been formulated as a constraint in order to avert any malfunction and miscoordination between relays.

3.5.1.2   Evaluation

The fitness of each chromosome is evaluated by fitness function or objective function (OF) so that only the most suitable chromosomes, in other words, the best relay settings are selected and processed to the next step. Since the purpose of this research is to minimize the operation time of relays and TMS of each relay to improve the performance of overcurrent relays in wind farms, it is sensible to formulate our objective as shown below:

$$OF = min \; \sum_{i=1}^{n}(t_i)^2 \tag{3.4}$$

Where, t_i is the operation time of overcurrent relays. By applying this OF, we are able to minimize the operation time of relays and accordingly obtain TMS values, however the coordination constraints are ignored which may cause miscoordination for relays in wind farm, specifically for symmetrical fault type. Hence, it is immensely vital to introduce coordination constraints to OF as defined below:

$$OF = min \; [\sum_{i=1}^{n}(t_i)^2 + \sum_{m\&b=1}^{n}(\Delta t_{mb})^2] \tag{3.5}$$

In this equation, Δt_{mb} denotes discrimination time between the backup and main overcurrent relay. In this protection study, another expression, $\beta[\Delta t_{mb} - |\Delta t_{mb}|]$ has been added in

64

order to enhance the coordination between relays and optimize the relay settings. So the entire coordination constraint is $[\Delta t_{mb} - \beta(\Delta t_{mb} - |\Delta t_{mb}|)]$. For the given equation we can consider these two states:

$$[\Delta t_{mb} - \beta(\Delta t_{mb} - |\Delta t_{mb}|)] = \begin{cases} \Delta t_{mb}, & \Delta t_{mb} > 0 \\ (1 + 2\beta)(\Delta t_{mb}), & \Delta t_{mb} < 0 \end{cases} \qquad (3.6)$$

These constraints defined for OF would help the GA selection process to grant more opportunity to the chromosomes containing TMS to survive and reproduce superior TMS values as explained in the next sub-section. So, by considering relay operation time, coordination constraints for main and backup relay and added expression for coordination improvement, the specific OF developed to optimize the is defined as:

$$OF = \alpha_1 \sum_{i=1}^{n}(t_i)^2 + \alpha_2 \sum_{m\&b=1}^{n} \left(\Delta t_{mb} - \beta(\Delta t_{mb} - |\Delta t_{mb}|)\right)^2 \qquad (3.7)$$

$$t_i = \frac{0.14 * TSM_i}{(I/Ipickup)^{0.02} - 1} \qquad (3.8)$$

The first term in the OF is the sum of OCRs operation time, second term is the coordination constraint and α_1, α_2 and β are the weighting factors, which are devised to empower and increase the concentration of each section. t_i represents the operating time of OCRs which is derived from equation (3.8) based on IEC 60255-151:2009 and is accordingly replaced in equation (3.7) to calculate TMS and obtain optimal values for TMS. Finally, Δt_{mb} is the discrimination time between the main and backup protective relays.

The weighting factors α_1, α_2 and β can be customized depending on the optimization application. In every application these parameters may be changed to obtain the best results and optimize the relay performance. In this work after testing several values during GA based

simulation in MATLAB by trial-and-error method, the suitable parameters are selected as: $\alpha_1 = 1$, $\alpha_2 = 2$, $\beta = 100$ so that the OF achieves the minimum TMS values for each overcurrent relay and consequently, optimize the operation time of the relays based on IEC standards and the coordination constraints defined in GA.

3.5.1.3 Selection

Based on the values obtained by OF for each generation in the previous step which represents "parents", some "parents" are more divergent than others. With this regard, according to a concept known as elitism, those "parents" who have more optimal OF values in the "parents" chromosome pool, should be granted more opportunities to survive, hence they are enabled to spawn further offsprings. Afterwards, roulette wheel as selection method is used, so that the minimum values for OF are picked and processing to the next step. In other words, at this stage, the minimum TMS values are selected and processed to the next step.

3.5.1.4 Crossover and mutation

At this stage, "parents" will be responsible for reproduction of offsprings through genetic operation crossover and mutation process. Crossover operation is applied to combine the genetic information of 2 "parents" to reproduce a new offspring which represents a new TMS for an overcurrent relay. Mutation operator is responsible for imposing new genetic information and variation to the heterogeneous population with the purpose of improving genes which would contribute to obtaining better TMS for relays. It should be mentioned that mutation may have

counterproductive effect on genes in a way that during mutation process, a bad gene may be introduced and consequently an inferior TMS is produced. Thus, during setting GA parameters, a reasonable mutation value should be selected and a large value should be refrained. After the crossover and mutation for all the chromosomes is carried out, the entire generated offspring will be examined by constraint criteria and those who failed will be eliminated. The new offsprings are the new improved TMSs which will be qualified to go through the next step. This process is repeated until the size of the new population is equal to the size of preceding population.

3.5.1.5   Selection of Next Generation from Children and Parents

At this step, all the "parents" and offsprings (TMSs) that have satisfied the constraints and fitness criteria examined through OF, will replace the previous generation. The entire GA process is repeated until the termination criteria is satisfied as was previously illustrated in the flowchart shown in Fig. 3.14.

3.5.1.6   Termination

The GA process is terminated by the termination settings defined for GA. For this research, the termination criteria have been chosen as "reaching highest ranking solution fitness" and "successive iterations no longer produce better results" (optimal convergence), which means OF has reached its optimal value and cannot be minimized any further, subsequently, the most minimum TMS values for the relays have been attained.

3.5.1.7   GA Optimization Process Results

In this section, the GA optimization process which was developed specifically for achieving optimal coordination of OCRs is presented. After running the optimization process, Fig 3.12 – 3.15, show the proposed GA based optimized results for obtaining optimal TMS values, average distance between individuals, best and mean fitness values. The less average distance between individuals, the better the results are. Therefore, it can be clearly seen from Fig. 3.14 at the beginning of the simulation, the average distance between individuals were so big which means the results are not optimal. However, during the process, the average distance starts to diminish significantly and reach to the point where the average distance is near zero. The results have become stable and cannot become any better, and thus, the optimal values have been successfully reached. The same scenario also exists for Fig. 3.12 and 3.13 which represents the best and mean value of the objective function. At the beginning of the process the functional value is very large, however during the process this value is decreased significantly since the GA has been trying to minimize TMS values. At the end of the simulation the OF output has reached a steady point where it cannot improve anymore. At this point, the optimal values have been successfully attained by GA, by considering CTI of 0.2 s, and the optimal TMS values can be implemented to set the OCR operation time as shown in Fig. 3.15. Global optimal results are reached when the results are not attained any better. The GA optimization is forced to stop and GA declares that the obtained results are the best and optimal values. In this work the stopping criteria has been set as "reaching highest ranking solution' fitness" and "successive iterations no longer produce better results (optimal convergence)".
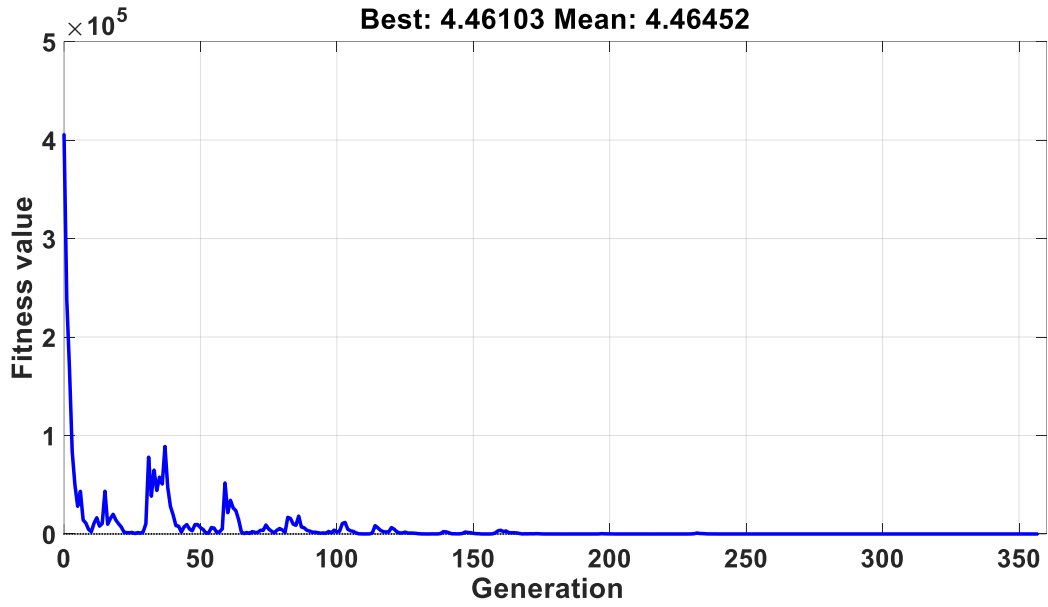
Fig. 3.12. Best and mean fitness values obtained by GA.
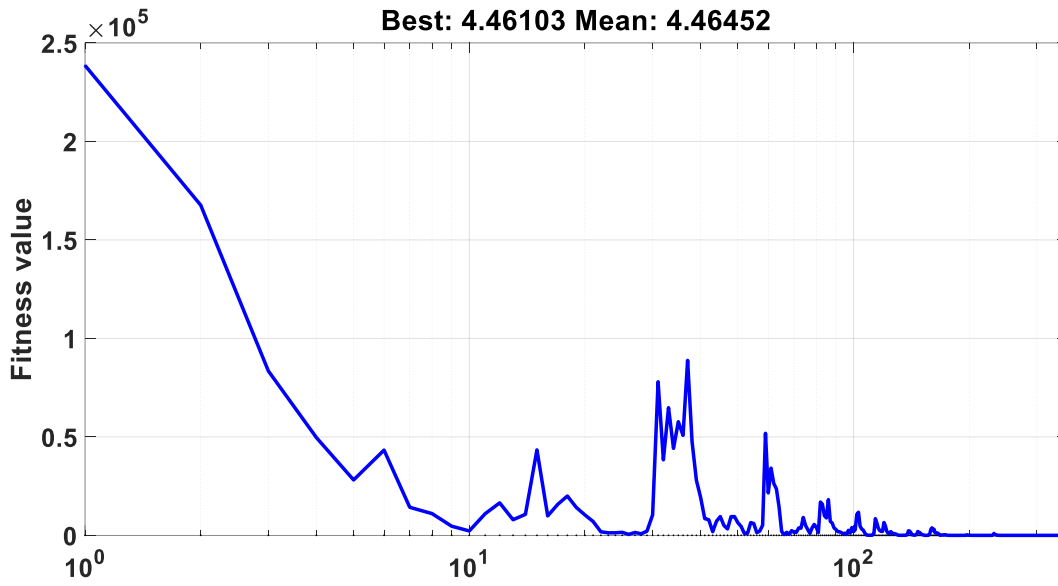
Fig. 3.13. Logarithmic representation of best and mean fitness values obtained by GA.
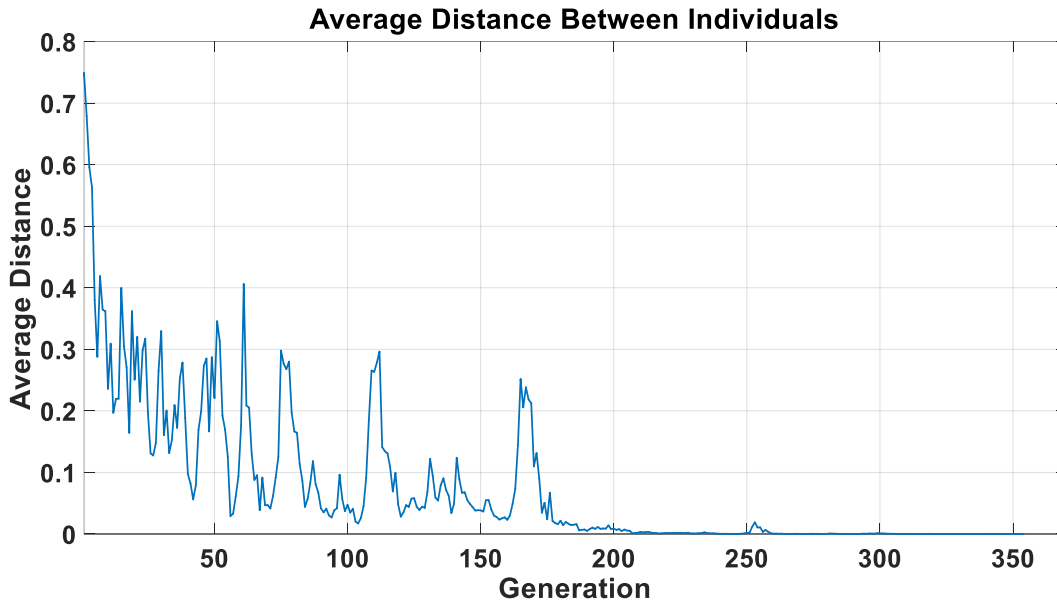
Fig. 3.14. Average distance between individuals attained by GA.
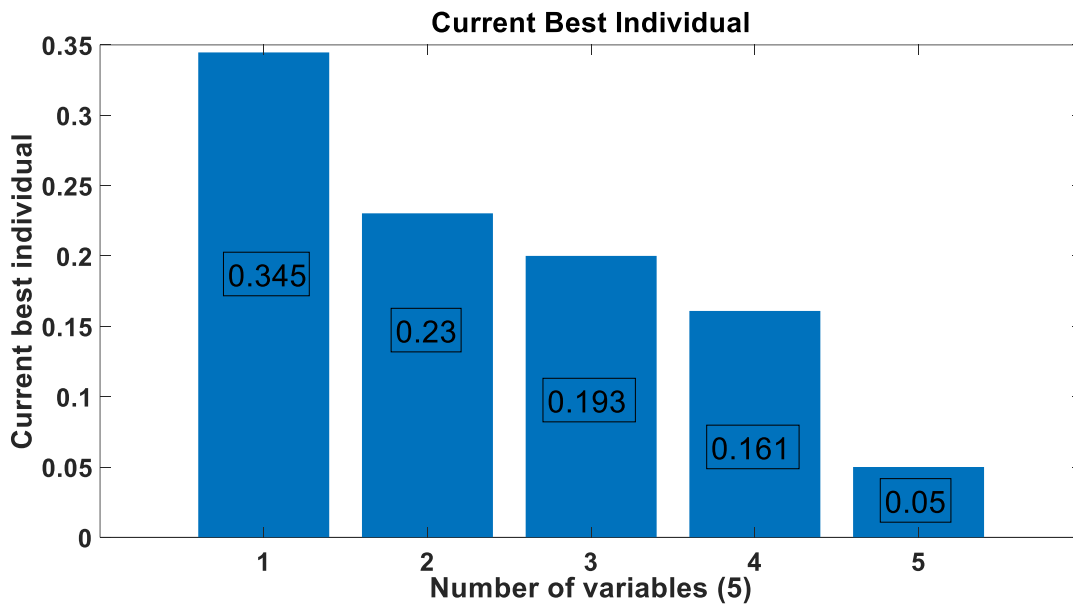
Fig. 3.15. Best individuals of TMS obtained by GA.

3.5.2   Grey Wolf Optimization-based Optimal Solution for OCR Settings

GWO is a new advanced optimization method that can be used for a variety of applications mainly for the purpose of optimizing different variables of a formulated problem, including non-convex optimization problems. GWO is inherently a meta-heuristics technique which provides the optimal solution by posing these advantages along the way: local optima avoidance, reaching global optimum value, derivative-free mechanism, flexibility and simplicity [105], [106]. It is a population-based optimization algorithm which is motivated by leadership and hunting behavior of Grey wolf as shown in Fig. 3.16. In nature, grey wolf (Canis lupus) is considered to be residing at the top in the food chain and at a top level of predators. Gray wolves live in a pack which consists of 5-12 members on an average [107]. In the group, strict dominant hierarchy is practiced, the leader of the pack in order is, α, β, δ, and γ as shown in Fig. 3.17.

In the GWO method, the best solution is α, while β provides the second-best solution followed by the position of δ members. The rest of the solutions are considered as γ that includes the remaining members of the entire population which are mainly frail and feeble members of the group and are the most replaceable among the rest [108]. The flow chart for GWO algorithms is shown in Fig. 3.18.
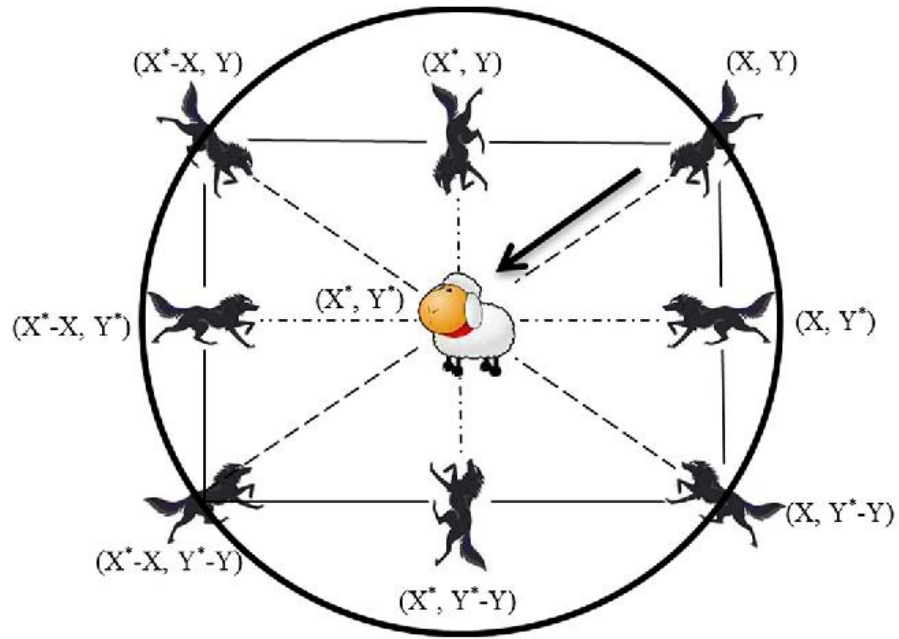
Fig. 3.16. Grey wolf hunting mechanism.
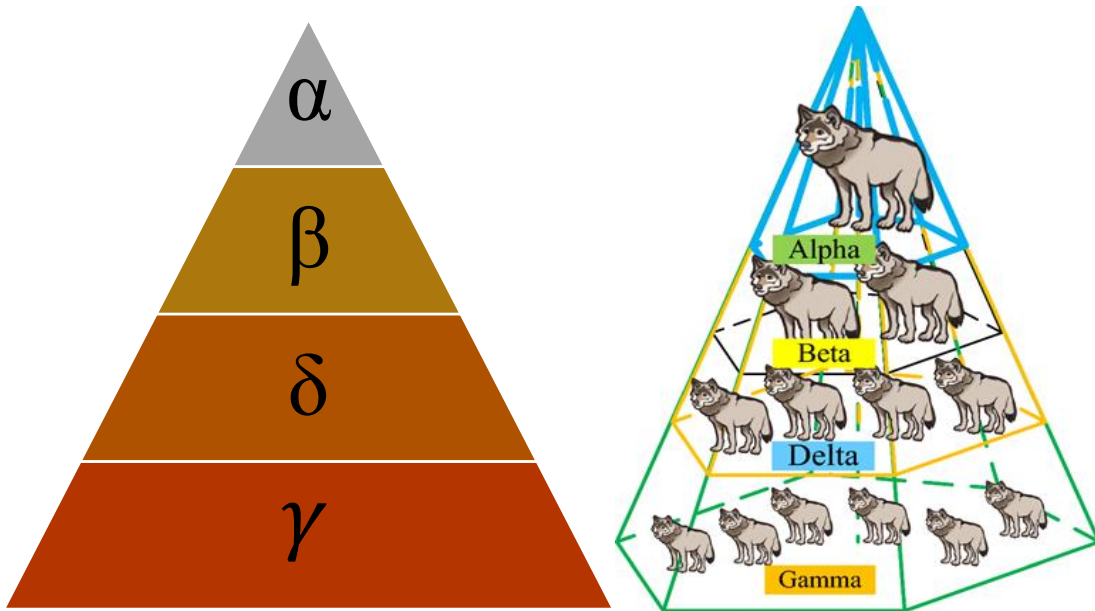
Fig. 3.17. Grey wolf social hierarchy.
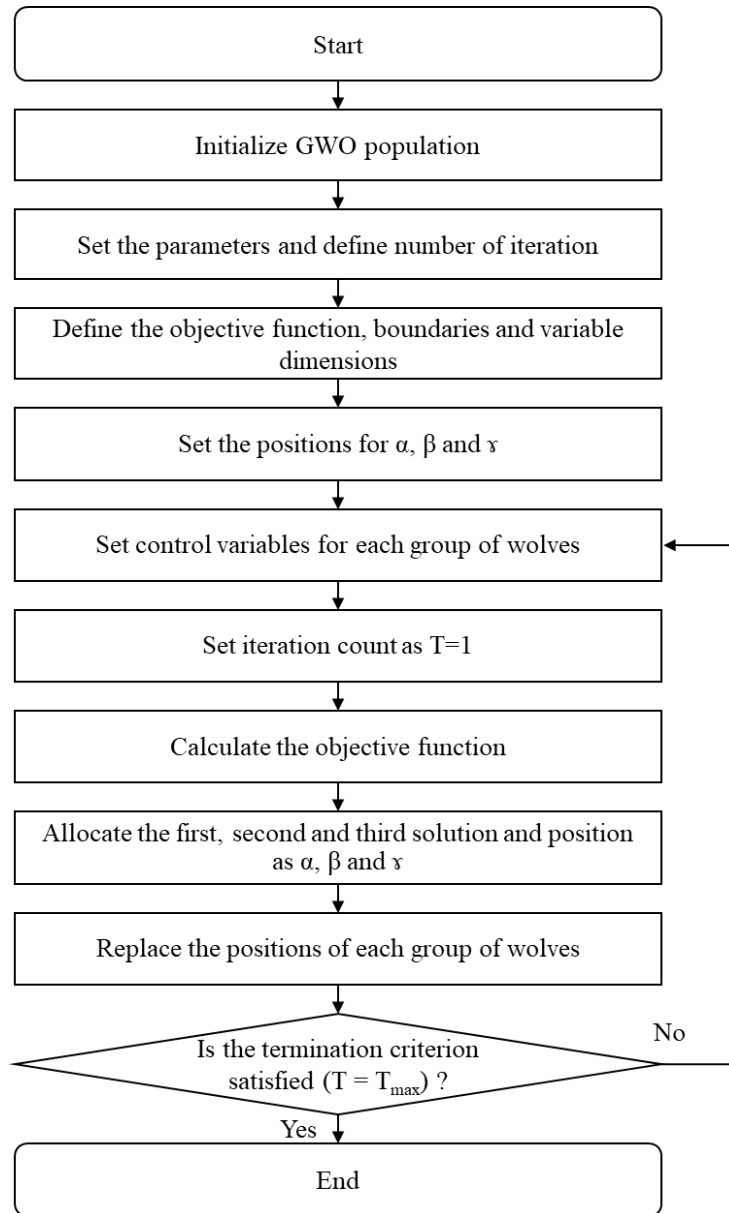
Fig. 3.18. General flow chart for grey wolf optimizer algorithm.

3.5.2.1   The Mathematical Model of GWO

In the course of hunting, grey wolves have the tendencies to encircle the prey and it's possible to devise the mathematical model for this type of behavior as below:

$$\vec{E} = \left| \vec{C} \cdot \vec{x}_P(t) - \vec{A} \cdot \vec{X}(t) \right| \tag{3.9}$$

$$\vec{X}(t+1) = \vec{x}_P(t) - \vec{A} \cdot \vec{D} \tag{3.10}$$

In these equations, E is the encircling pattern vector and therefore should have a positive value, A and C are coefficient vectors, t is known as current iteration, X_P and X are prey and grey wolf position vectors, respectively. The vector D is random, and adaptive, and provides the exploration and exploitation for the GWO algorithm. This vector also defines exploration if it has a value greater than 1.

Both A and C coefficient vectors are calculated as the following:

$$\vec{A} = 2\vec{a} \cdot \vec{r}_1 \cdot a \tag{3.11}$$

$$\vec{C} = 2 \cdot \vec{r}_2 \tag{3.12}$$

The value of 'a' decreases linearly from 2 to 0 over the course of iteration while r_1 and r_2 are random vectors in [0, 1]. Next, the most 3 optimal solutions are selected and the rest of the agents including gamma solutions start updating their positions based on their best previous positions. The formulation of this stage can be written as:

$$\vec{E}_\alpha = \left| \vec{C}_1 \cdot \vec{X}_\alpha - \vec{X} \right| \tag{3.13}$$

$$\vec{E}_\beta = \left| \vec{C}_2 \cdot \vec{X}_\beta - \vec{X} \right| \tag{3.14}$$

$$\vec{E}_\partial = \left| \vec{C}_3 \cdot \vec{X}_\partial - \vec{X} \right| \tag{3.15}$$

$$\vec{X}_1 = \vec{X}_\alpha - \vec{A}_1 \cdot (\vec{X}_\alpha) \tag{3.16}$$

$$\vec{X}_2 = \vec{X}_\beta - \vec{A}_2 \cdot (\vec{X}_\beta) \tag{3.17}$$

$$\vec{X}_3 = \vec{X}_\partial - \vec{A}_3 \cdot (\vec{X}_\partial) \tag{3.18}$$

$$\vec{X}(t+1) = \frac{\vec{X}_1 + \vec{X}_2 + \vec{X}_3}{3} \tag{3.19}$$

The procedure in which GWO is implemented for obtaining the optimal solution for OCRs are avoided in the section as it is exactly the same as the one that was defined for GA. However, the coding which was used to define the GWO in Matlab, is shown in Appendix A. 7.

3.5.2.2   GWO Optimization Process Results

At the beginning of the optimization process, the fitness value is drastically high which is similar to the GA, since no optimal value for the relays were attained. However, as the optimization process continues and more iterations are processed, the fitness value of coordination between relays starts to diminish to the point that, it no longer gets any smaller. This process is shown in Fig. 3.19, and the logarithmic minimized fitness value of the GWO optimization process is also shown in Fig. 3.20. At the end of the optimization, after around 100 iterations, no significant improvement was observed, however the process was conduced for 250 iterations to ensure the GWO has reached the global minimization for the protective relays and absolutely the most optimal TMS settings, by considering CTI of 0.2 s, have been achieved for each relay. The optimal TMS settings accomplished by GWO is shown in Fig. 3.21. The results clearly show that GWO has managed to provide better relay settings compared to GA and the conventional nonlinear time-current relay characteristic optimization method. This comparison with respect to the relay operation will be discussed in the next section.
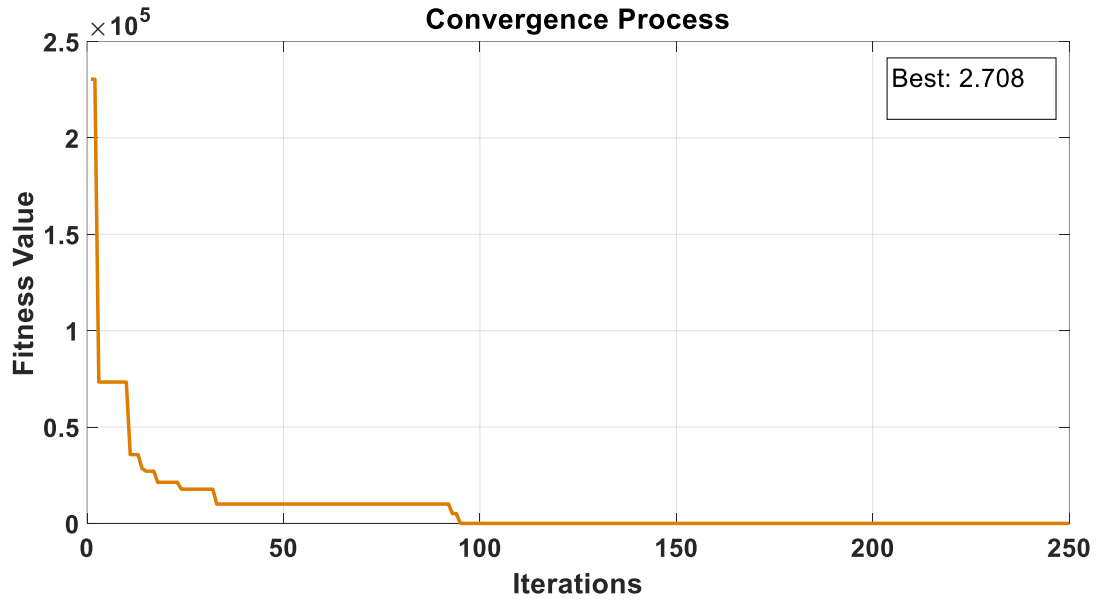
Fig. 3.19. Optimized fitness value attained by GWO.
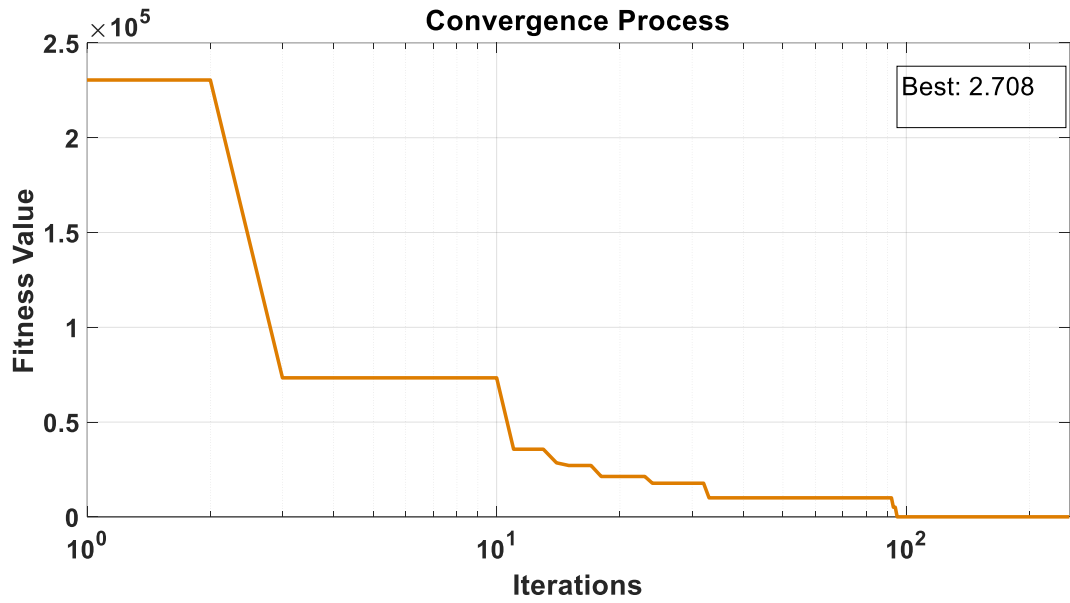
Fig. 3.20. Logarithmic optimized fitness value attained by GWO.
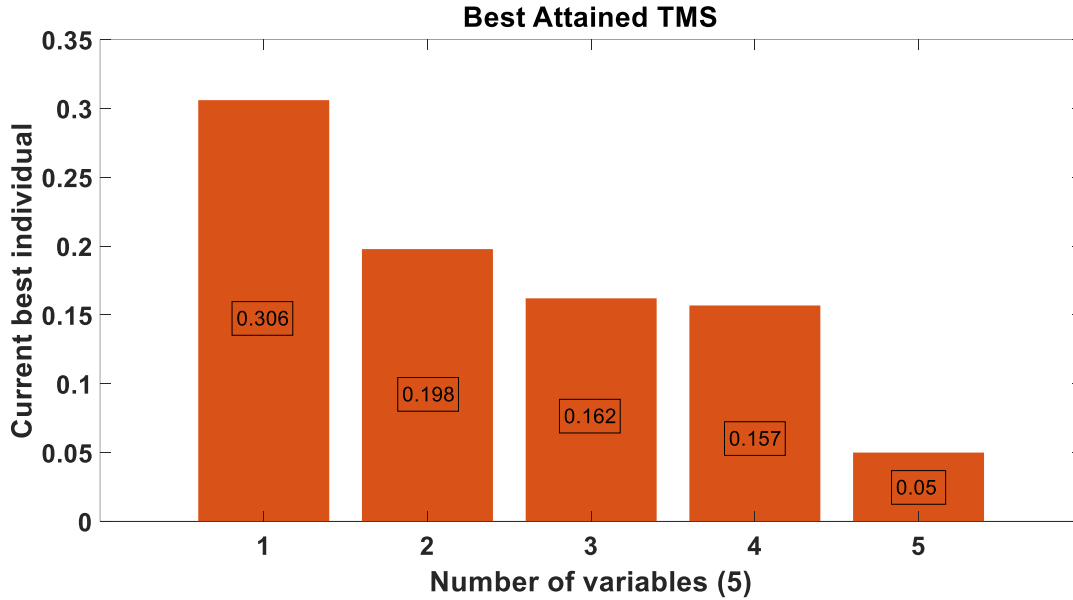
Fig. 3.21. Best individuals of TMS obtained by GWO.

3.6 Relay Improved Operation Comparison Between GWO, GA and Conventional Method

In the previous sections, GA and GWO based AI optimization techniques were developed and applied to attain optimal relay settings by minimizing the TMS settings of the relays. In this section, a comparison between GA, GWO and the conventional time-current relay characteristic methods is presented with respect to the relay operation time improvement which is presented in Table 3.3.

According to this table, although the conventional method was able to coordinate the relay settings, however, the relay settings is non-optimal and the operation time of the relays are extremely long, specifically for the far end line. However, by applying GA, the TMS settings of the relays were significantly improved, and as a result the operation time of the relay were also enhanced, where the relays were able to detect the faults much faster. The total reduction of relay

77

operation time was 7.81 s which is much less compared to 11.02 s attained by conventional approach. GA managed to improve the overall OCR protection and coordination of the wind farm by 29.12%. However, this improvement was even further improved up to 39.38 % after applying GWO, which is a astonishing enhancement of relay operation. The total operation time of the relays were recorded to be only 6.68 S which stems from the better optimization process of GWO compared to GA, which was able to minimize the TMS settings of the relays more efficiently, and as a result, better relay operation and protection for wind farms are achieved. Thus, GWO is a better approach compared to GA and conventional methods and could be a suitable solution for wind farm protection and coordination problems. In order to understand the effectiveness of proposed GWO method over the conventional method, a visual comparison based on their coordination using TCC curves are shown in Fig. 3.22.

Table 3.3 Comparison between GWO, GA and conventional methods for relay coordination

Relay	TMS (conv.)	TMS (GA)	TMS (GWO)	T (conv.)	T (GA)	T (GWO)	Operation Time Improvement by GA (%)	Operation Time Improvement by GWO (%)
1-40	0.05	0.05	0.05	0.06	0.06	0.06	0%	0%
41-44	0.2	0.2	0.15	0.45	0.45	0.34	0%	24%
45	0.2	0.2	0.15	0.86	0.86	0.64	0%	25%
46	0.55	0.25	0.2	2.78	1.26	1.01	54%	63%
47	0.75	0.35	0.3	3.18	1.49	1.27	53%	60%
-	-	-	-	11.02	7.81	6.68	29.12% Improvement	39.38% Improvement
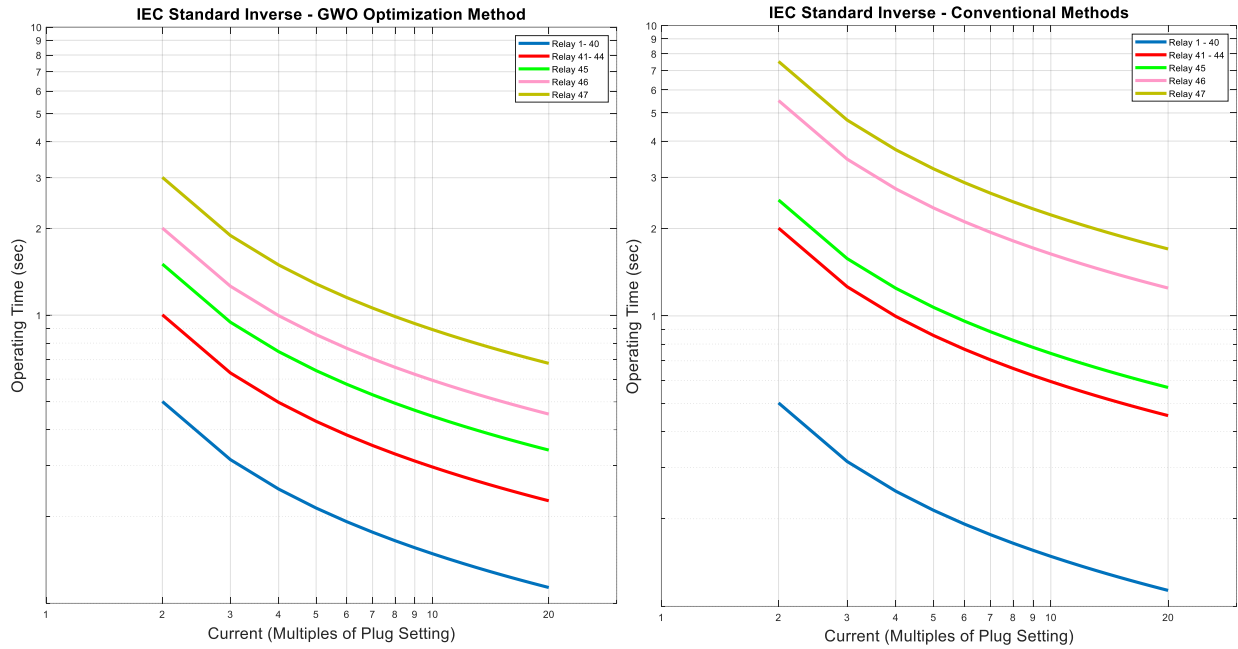
Fig. 3.22. Comparison between GWO and conventional approach in terms of coordination of OCRs shown on standard TCC curves.

Also, the operation of the relays with the new and old settings are tested for the wind farm by imposing a bolted three phase fault as the most severe fault, at the wind turbine feeder, where the fault current and voltage of the fault incidence at the wind turbine feeder is shown in Fig. 3.23. Due to severity of the fault, the voltage is near 0 V, while the fault current is extremely high, where the protective relays should detect the fault as early as possible, with respect to the settings associated with each one. The performance of the relay that was developed in this research, and also a comparison between the AI techniques and conventional technique embedded to each relay, with their exact timing, is shown in Fig. 3.24. According to this figure, the proposed protection scheme is able to accurately detect the faults with 100 % accuracy, however, as expected the operation time of each relay is completely different. By applying conventional method, the relay coordination is extremely long due to its non-optimal relay settings, however, the proposed GA-

79

based protection scheme improved the operation of the relay drastically. Finally, GWO-based protection scheme surpassed all other proposed protection techniques and is able to detect the fault at the shortest possible time with 100 % accuracy.
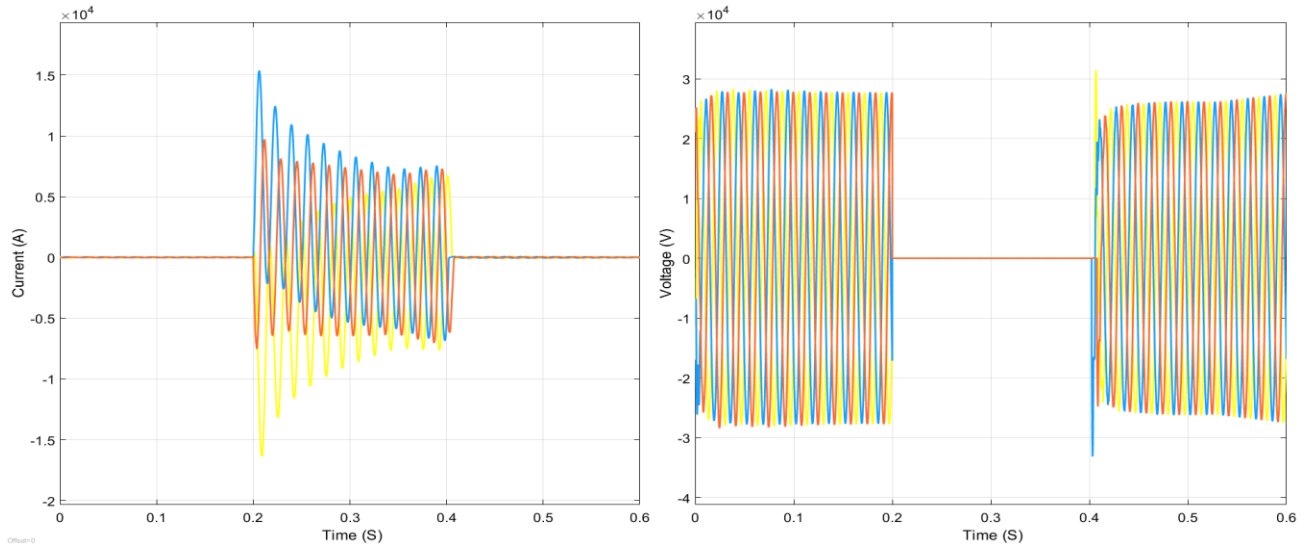
Fig. 3.23. A bolted three phase fault occurrence at the wind turbine feeder.
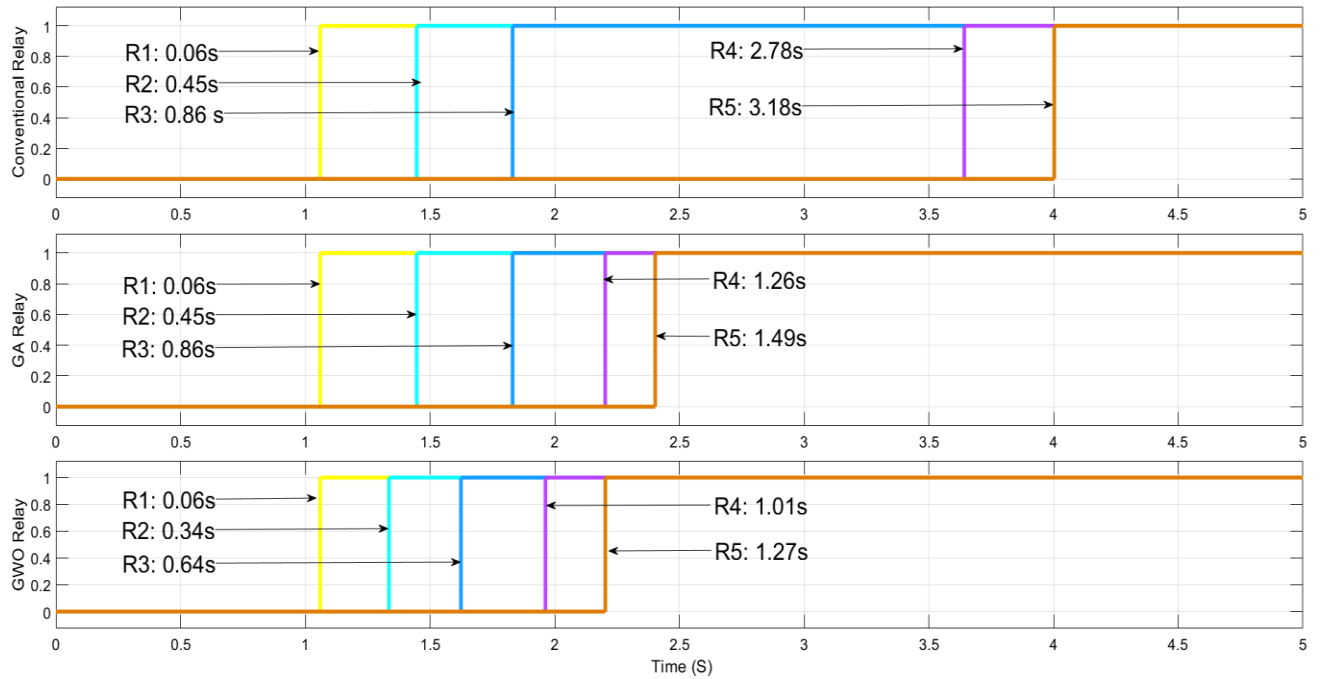
Fig. 3.24. Coordinated relay operation time comparison between GWO, GA and conventional method.

3.7 Conclusion

In this Chapter, the design and development of OCRs along with determining the settings for each relay, as well as their coordination was discussed in detail. Moreover, a few samples of hand calculations for relay settings and coordination were presented. The application of two artificial intelligence optimization technique e.g., GA and GWO, along with their coding, objective function formulation, and their development in this research were explained thoroughly. Additionally, their application on optimizing the relay settings with the optimization process was presented. Finally, a comparison between the proposed AI protection scheme and the conventional nonlinear time-current relay characteristic optimization method was made, where the operation of optimal overcurrent protection and coordination was tested and analyzed to validate the developed protection scheme. It was inferred that GWO-based optimal protection and coordination scheme, was able to provide the best protection compared to GA and conventional methods. Thus, the proposed GWO based optimal protection method can provide better security and reliability of large-scale wind farms. Another contribution of the proposed method is that, the AI-based relay settings, can replace the tedious conventional hand calculation approach for coordination of OCRS, which can significantly simplify the power engineers' job and also help them to set the best and optimal possible protection settings for each relay with maximum accuracy.

Chapter 4

Adaptive Overcurrent Protection and Coordination Schemes for Wind Farms

4.1   Background

In conventional power systems, where the main sources of power generations were synchronous generators and the power generated was typically stable, the protection and coordination could be simply carried out defining only one group of settings for relays. However, nowadays in modern power systems, with the penetration of renewable energy resources, such as wind and solar energy, the main source of power generation is not always stable, rather fluctuates drastically with weather conditions. This problem is even more evident for large-scale wind farms that a noticeable change in wind speed can proportionally affect the power generation on the grid side [109]. Moreover, due to unexpected event of unavailability of wind, or wind turbine maintenance, one or several feeders may not be in operation. Hence, the generated power and current characteristics of wind farms may drastically differ at different months or seasons of the year [110].

The aforementioned scenarios, could create serious issues for power system protective relays, coordination and their performance during both fault scenarios and normal operation. For example, if there is maintenance taking place on one of the sub-feeders of the wind farm, the feeder would be basically offline and will not provide any power to the grid. Thus, the generated current

characteristics, as well as fault current contribution on the main feeder of the wind farm would be absolutely different from the time that all wind turbines are in service and feeds bulk of power to the grid. In such cases if the relays are static, and they do not adapt their settings according to the dynamic behavior of the wind farm, it would result in miscoordination, insensitivity, blinding and maloperation of protective relays. As a result, some healthy sections of the wind farm may be disconnected unnecessarily from the grid, and some other sections of the wind farm have to undergo fault without the relays taking any action. This is indeed a catastrophe, as it could seriously damage the power apparatus, exacerbate the power quality, stability, security and reliability of wind farms.

Therefore, in this chapter, a novel intelligent protection scheme that relies on both optimal and adaptive protection, with quadruple (as the reason will be discussed later) group settings for the relays are proposed. In order to do that, a hybrid GWO-FLC protection scheme is developed, where GWO is implemented to attain optimal OCR coordination for all the relays' group settings at various wind speed, while the FLC is developed to provide adaptive feature for the relays so that the OCR settings are updated and optimal group settings for each relay are adopted according to the dynamic behaviour of the wind farm. Finally, in a laboratory environment, the proposed protection scheme is implemented in real-time using FPGA DE2-115 board equipped with Cyclone IV-E device (EP4CE115F29C7). It is found from both simulation and experimental results that the performance of the proposed hybrid GWO-FLC is robust, reliable, efficient and extremely satisfactory.

4.2   Adaptive Protection Schemes using Fuzzy Logic Controller

The fuzzy logic controller (FLC) has been widely utilized in many applications including motor drives, air conditioners, washing machines, antiskid braking systems to more complex applications such as image processing, multi-objective optimization of power systems, etc. due to its ability to adapt with unknown system disturbances [111]. Thus, in this work the FLC is employed as an intelligent adaptive protection scheme to enhance the security and reliability of power systems for large-scale wind farms. In this approach, after the entire group settings for each OCR according to specific wind speed is calculated, and the coordination settings is optimized by GWO, then FLC is employed to select proper group settings for each OCR at various wind speeds.

For the proposed FLC, the measured three phase output currents of wind generator are defined as inputs, both PS and TMS which are the relay settings, are defined as the outputs. Wind speed and the measured three phase currents near each zone to be protected by OCR, based on its magnitude is categorized into 4 groups named as "poor", "average", "good" and "excellent" as shown in Table 4.1.

Table 4.1 Defined inputs for FLC based adaptive protection

Category	Wind speed (m/s)	Measured 3-phase current
Excellent	14-25	I_a, I_b, I_c
Good	12-13	I_a, I_b, I_c
Average	10-11	I_a, I_b, I_c
Poor	6-9	I_a, I_b, I_c

As one of the possible outcomes of FLC, PS settings for a typical OCR is varied in the range between 25% to 200 % in steps of 25% (based on IEC standard), while TMS is varied in the

range of 0.05 to 1 in a step of 0.05, where the definition of the outputs are shown in the Table 4.2

and 4.3 below. The overview of the proposed FLC-based adaptive protection scheme for wind

farm is illustrated in Fig. 4.1. For each OCR, a unique FLC was developed, as an example, the

membership functions of input-output variables for OCR47, which is the last relay near the power

grid are shown in Figs. 4.2 - 4.4 The fuzzy rules are designed in a way that as the wind speed

changes and the generated current measured at each relay also changes, therefore the relay settings

should also be changed and updated according to the dynamic behavior of wind farm. In other

words, FLC will adopt the best group settings for each relay when there has been a huge difference

in wind speed and generated current. The definition and specification of the FLC parameters, and

the development of FLC-based centralized adaptive overcurrent protection and coordination, based

on both Mamdani and Sugeno types are presented in Appendix A. 8 – 14.

Table 4.2 Defined output 1 for FLC based adaptive protection

Output 1	PS value (%)
PS1	[0, 25, 50]
PS2	[25, 50, 75]
PS3	[50, 75, 100]
PS4	[75, 100, 125]
PS5	[100, 125, 150]
PS6	[125, 150, 175]
PS7	[150, 175, 200]

Table 4.3 Defined output 2 for FLC based adaptive protection

Output 2	TMS value
TMS1	[0, 0.05, 0.1]
TMS2	[0.05, 0.1, 0.15]
TMS3	[0.1, 0.15, 0.2]
TMS4	[0.15, 0.2, 0.25]
TMS5	[0.2, 0.25, 0.3]

TMS6	[0.25, 0.3, 0.35]
TMS7	[0.3, 0.35, 0.4]
TMS8	[0.35, 0.4, 0.45]
TMS9	[0.4, 0.45, 0.5]
TMS10	[0.45, 0.5, 0.55]
TMS11	[0.5, 0.55, 0.6]
TMS12	[0.55, 0.6, 0.65]
TMS13	[0.6, 0.65, 0.7]
TMS14	[0.65, 0.7, 0.75]
TMS15	[0.7, 0.75, 0.8]
TMS16	[0.75, 0.8, 0.85]
TMS17	[0.8, 0.85, 0.9]
TMS18	[0.85, 0.9, 0.95]
TMS19	[0.9, 0.95, 1]
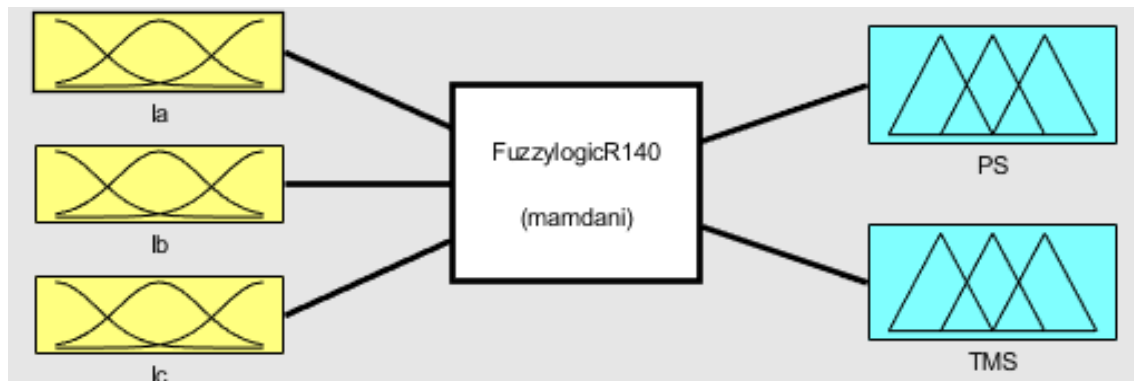
Fig. 4.1. Overview of the FLC-based adaptive protection for wind farms.
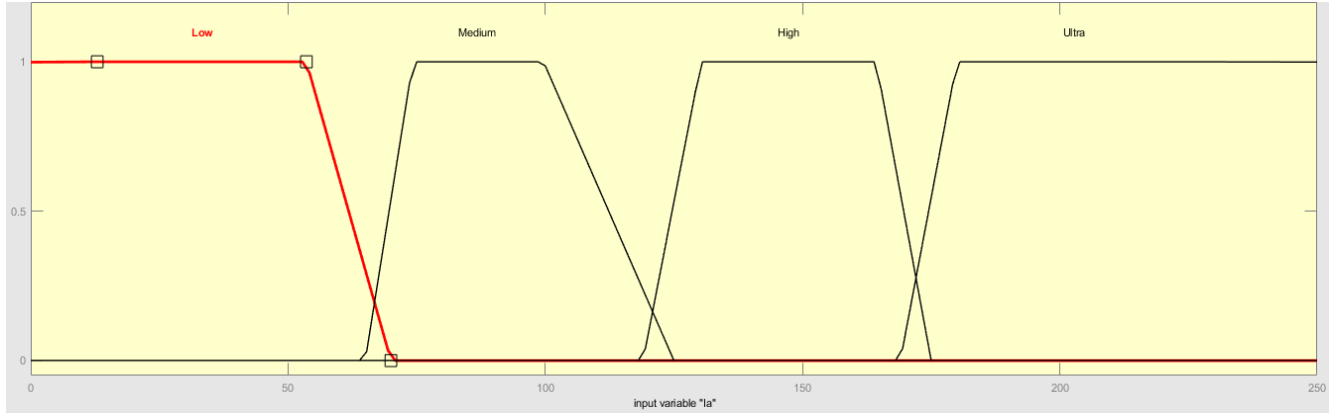
Fig. 4.2. FLC membership functions of input (current classification based on wind speed behavior).
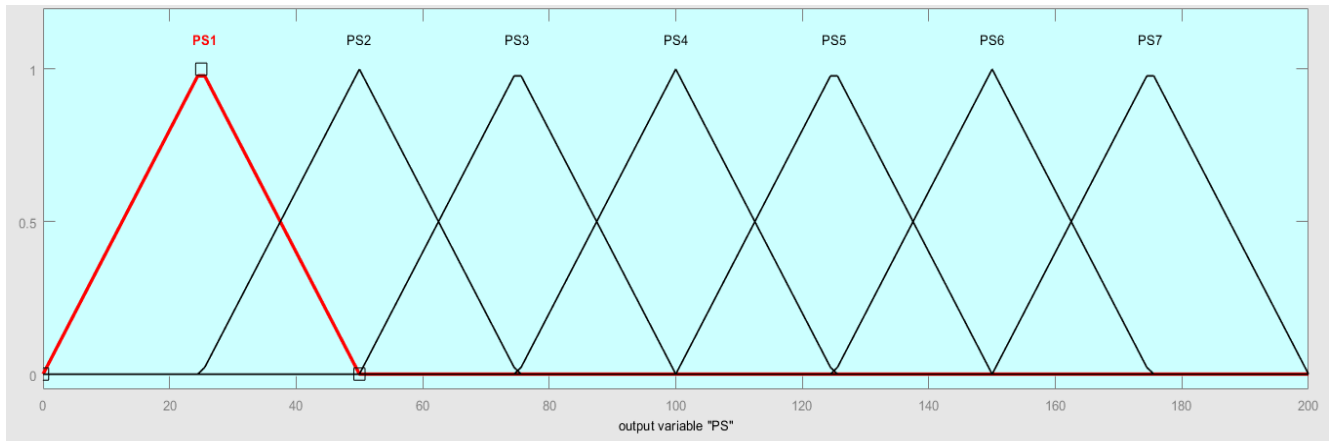
Fig. 4.3. FLC membership functions of output (PS settings).
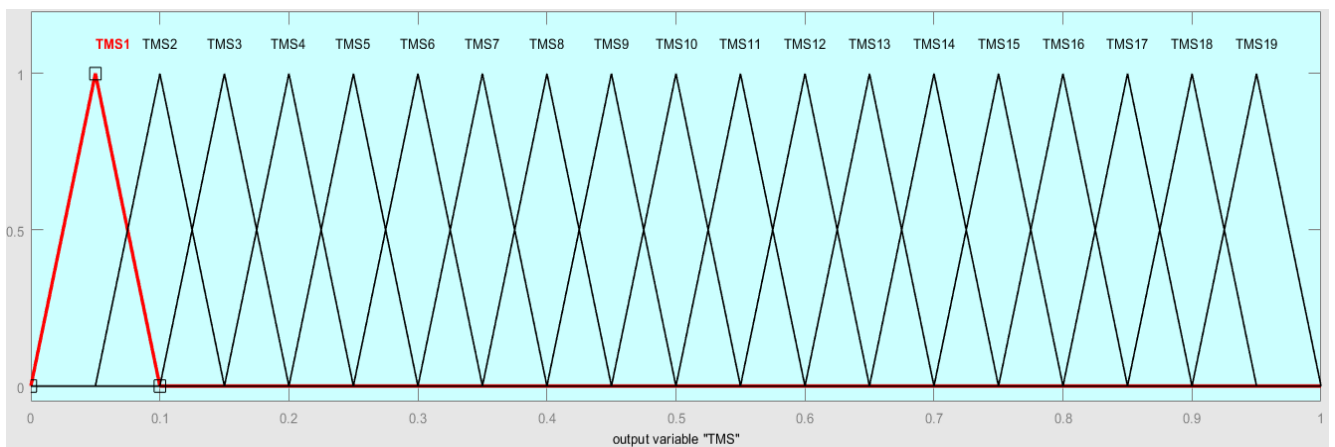
Fig. 4.4. FLC membership functions of output (TMS settings).

87

4.3 Proposing Quadruple Group Settings and Coordination for Relays

As was pointed out in the beginning of this chapter, due to dynamic behavior of wind farms, OCR settings and coordination become an extremely challenging task. Thus, the existing single group setting for the entire wind farm is not acceptable and also can cause severe miscoordination, maloperation, false tripping or even delayed tripping during fault incidence. In this work, a quadruple group setting of OCRs are calculated according to wind profile. As discussed before, wind speed is categorized into 4 groups, A, B, C and D, where each relay settings are calculated accordingly as depicted in Tables 4.4 – 4.7. At each table, the current measured at each Current Transformer (CT), the CT ratio, Relay Settings Current (RSI), pickup current (I_{pickup}), PS, PMS, TMS and operation time of the relay (T) are presented for each relay at different wind speed category. Since the OCR1-40 are located at each wind turbine, and the rating of each turbine is identical, the setting for each relay is the same. Also, the collector lines for each relay have the same rating which are protected by OCR41-44 and they have the same relay settings.

The behavior of the wind farm during wind speed variation, and its effect on the generated power generation and current profile, for a duration of 90 s is presented in Fig. 4.5. As the wind speed decreases, the wind farm generated current at different sections of the plant also decreases accordingly. The I_{pickup}, RSI, PS and PMS also changes accordingly resulting in adjustments of TMS and operation time of each relay. Therefore, only one group setting of relays is not suitable for proper protection wind farms and various group settings should be calculated.

Table 4.4 Group settings A for wind farm OCR coordination during wind speed at 14 – 25 m/s

Relay	I	CT	RSI	I_{pickup}	PS	PMS	TMS	T
1-40	28.69	50/5	37.5	3.75	75%	241.37	0.05	0.06
41-44	287.32	450/5	450	5	100%	19.25	0.2	0.45
45	1145.06	2000/5	1500	3.75	75%	4.93	0.2	0.86
46	181.6	300/5	300	5	100%	3.92	0.55	2.78
47	178.51	300/5	225	3.75	75%	5.06	0.75	3.18

Table 4.5 Group settings B for wind farm OCR coordination during wind speed at 12 – 13 m/s

Relay	I	CT	RSI	I_{pickup}	PS	PMS	TMS	T
1-40	25.99	50/5	37.5	3.75	75%	241.37	0.05	0.06
41-44	260.19	450/5	337.5	3.75	75%	25.67	0.2	0.42
45	1036.47	2000/5	1500	3.75	75%	4.93	0.2	0.86
46	164.32	300/5	225	3.75	75%	5.23	0.6	2.5
47	161.03	300/5	225	3.75	75%	5.06	0.7	2.97

Table 4.6 Group settings C for wind farm OCR coordination during wind speed at 10 – 11 m/s

Relay	I	CT	RSI	I_{pickup}	PS	PMS	TMS	T
1-40	15.83	50/5	25	2.5	50%	362.06	0.05	0.05
41-44	158.58	450/5	225	2.5	50%	38.51	0.2	0.38
45	630.06	2000/5	1000	2.5	50%	7.4	0.25	0.86
46	99.65	300/5	150	2.5	50%	7.85	0.7	2.33
47	97.65	300/5	150	2.5	50%	7.59	0.8	2.71

Table 4.7 Group settings D for wind farm OCR coordination during wind speed at 6 – 9 m/s

Relay	I	CT	RSI	I_{pickup}	PS	PMS	TMS	T
1-40	8.59	50/5	12.5	1.25	25%	724.12	0.05	0.05
41-44	86.14	450/5	112.5	1.25	25%	77.03	0.25	0.38
45	340.33	2000/5	500	1.25	25%	14.8	0.3	0.76
46	53.56	300/5	75	1.25	25%	15.7	0.75	1.85
47	52.48	300/5	75	1.25	25%	15.18	0.9	2.25
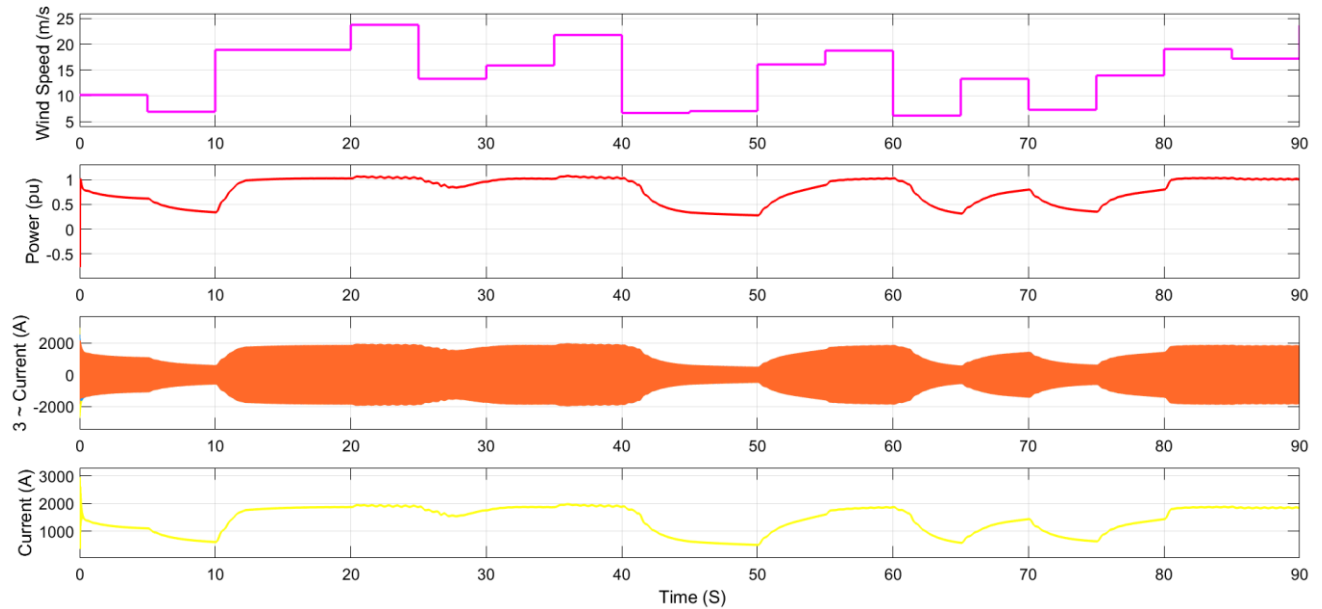
Fig. 4.5. Detrimental effect of dynamic behavior of wind farms on current settings of OCRs: (a) Wind speed, (b) pu value of generated power, (c) 3-phase current characteristic of a single DFIG, (d) Magnitude of the current profile.

4.4 Optimizing the Quadruple Group Settings for Adaptive Protection Implementing GWO Technique

In the last section, a quadruple group setting according to the dynamic behavior of the wind farms was proposed and calculated for each relay. In other words, the best relay settings with respect to current settings, PS and PMS was calculated. However, the TMS and operation time of these relay settings are not optimal, and we could still improve each relay group settings and coordination by implementing AI techniques as was successfully carried out in chapter 3. In order to do that, GWO is applied to optimize the relay settings by minimizing the TMS and operation time of all the protective relays in the wind farm. Since GWO was already explained thoroughly before, only the optimized results are shown here, where the optimal group settings for each relay,

and its improvement compared to the non-optimal relay group settings are tabulated and presented in Table 4.8 below. The CTI of 0.2 s have been selected for the purpose of coordination.

Table 4.8 The comparison between the optimal and non-optimal relay group settings.

Wind speed (m/s)	Relay	TMS (conventional)	TMS (GWO)	T (conventional)	T (GWO)	Operation Time Improvement (%)
14-25	1-40	0.05	0.05	0.06	0.06	0%
	41-44	0.2	0.15	0.45	0.34	24%
	45	0.2	0.15	0.86	0.64	25%
	46	0.55	0.2	2.78	1.01	63%
	47	0.75	0.3	3.18	1.27	60%
12-13	1-40	0.05	0.05	0.06	0.06	0%
	41-44	0.2	0.15	0.42	0.31	26%
	45	0.2	0.2	0.86	0.86	0%
	46	0.6	0.3	2.5	1.24	50%
	47	0.7	0.35	2.97	1.48	51%
10-11	1-40	0.05	0.05	0.05	0.05	0%
	41-44	0.2	0.2	0.38	0.38	0%
	45	0.25	0.2	0.86	0.68	21%
	46	0.7	0.3	2.33	0.99	57%
	47	0.8	0.4	2.71	1.35	51%
6-9	1-40	0.05	0.05	0.05	0.05	0%
	41-44	0.25	0.25	0.38	0.38	0%
	45	0.3	0.25	0.76	0.63	17%
	46	0.75	0.4	1.85	0.98	47%
	47	0.9	0.5	2.25	1.25	44%

4.5   Wind Farm Adaptive Protection Scheme Results

The FLC based adaptive protection scheme to adjust the PS and TMS settings for all relays are carried out. A large number of results can be derived from the proposed method, however, only a few samples of results are shown below. An extreme wind speed variation model is utilized to test the effectiveness of the proposed adaptive protection under harsh circumstances. As shown in Figs. 4.6 and 4.7, proper PS and TMS are being selected and consequently updating the relays as the wind speed changes. The results for hybrid GWO-FLC technique, where FLC intelligently select the proper optimized TMS relay settings previously obtained by GWO, is shown in Fig. 4.8. The proposed GWO-FLC technique utilizes the same inputs and outputs as the previous case where only FLC was used, however, the fuzzification and rules are different to ensure properly optimized TMS values are selected. Again, during the coordination calculation, the TMS for the first relay should always be selected as the minimum which is 0.05 in this work, that is why in in Fig. 4.8, the TMS values for the OCRs 1-40 (responsible for protection of wind turbines), are selected to be a discrete value of 0.05 and is illustrated as a flat line. It should also be mentioned that during any type of fault, when the wind speed is falling or rising, the most recent updated TMS and PS settings before the occurrence of fault would be selected for the relays. After the fault is cleared, the adaptive protection scheme will still keep updating the relay settings to ensure best settings are provided for each relay.

The proposed method was also tested for some more sensitive protection zone of the wind farm, where the operation of the relays was more susceptible to the wind farm dynamic behaviour. For example, the sample results for DFIG group settings relay containing both PS and TMS, and also the wind farm collector line protective relay group settings are shown in Fig. 4.9 and 4.10. These two protection zones are extremely important and the relays must be able to react fast

92

according to the changes occurring in the wind farm characteristics. The results clearly shows that the proposed GWO-FLC was able to react, and hence protective relays are updated with new relay group settings, even during harsh wind speed discrepancy.

The results obtained from both FLC and hybrid GWO-FLC clearly show that the adaptive protection can be successfully implemented for large-scale wind farms and OCRs settings can be properly selected and updated according to the wind farm dynamic behavior. Thus, the proposed GWO-FLC provides more reliable, secure and optimized performance for OCRs operation in wind farm.
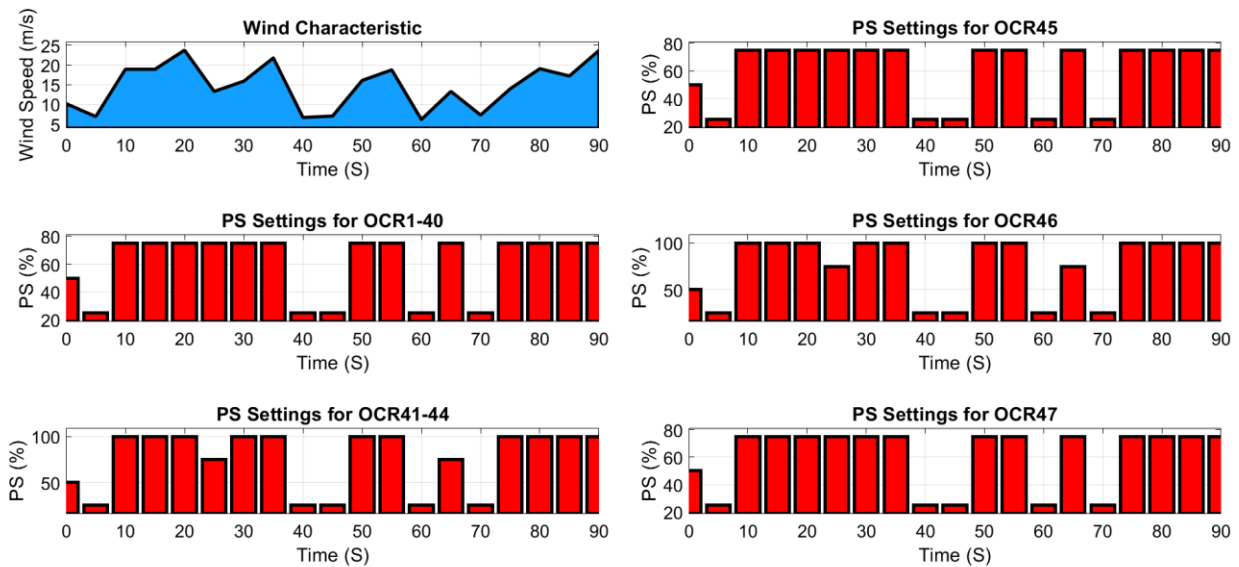
Fig. 4.6. FLC adaptive protection for selecting proper PS settings for OCRs during extreme wind speed variation: (a) wind speed profile, (b) PS settings for OCRs 1-40, (c) PS settings for OCRs 41-44, (d) PS settings for OCR 45, (e) PS settings for OCR 46, (f) PS settings for OCR 47.
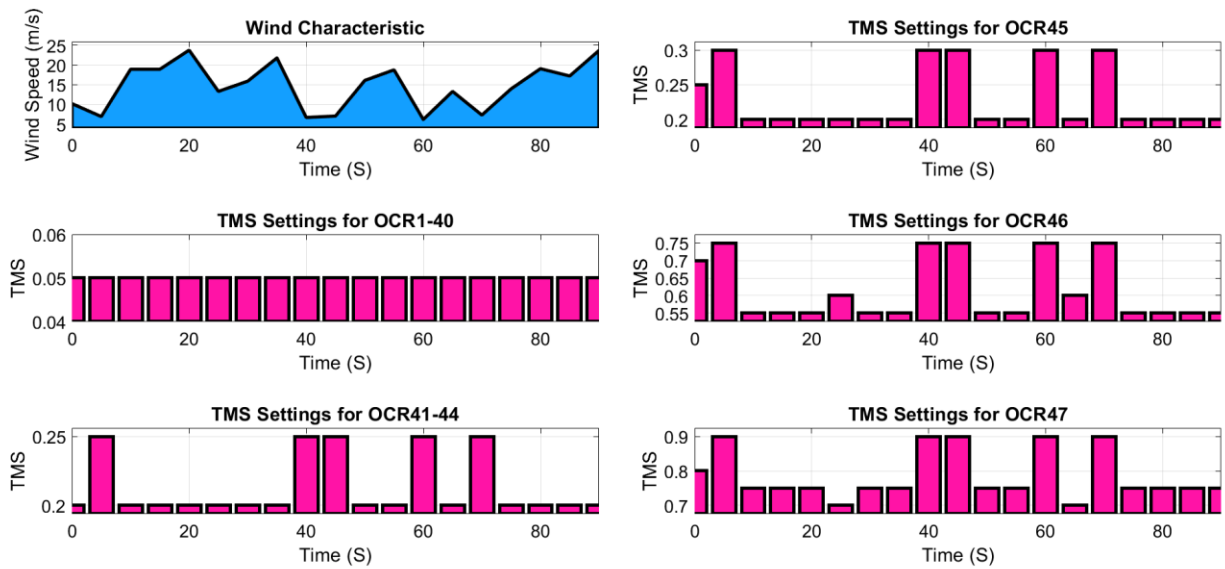
Fig. 4.7. FLC adaptive protection for selecting proper TMS settings for OCRs during extreme wind speed variation: (a) wind speed profile, (b) TMS settings for OCRs 1-40, (c) TMS settings for OCRs 41-44, (d) TMS settings for OCR 45, (e) TMS settings for OCR 46, (f) TMS settings for OCR 47.
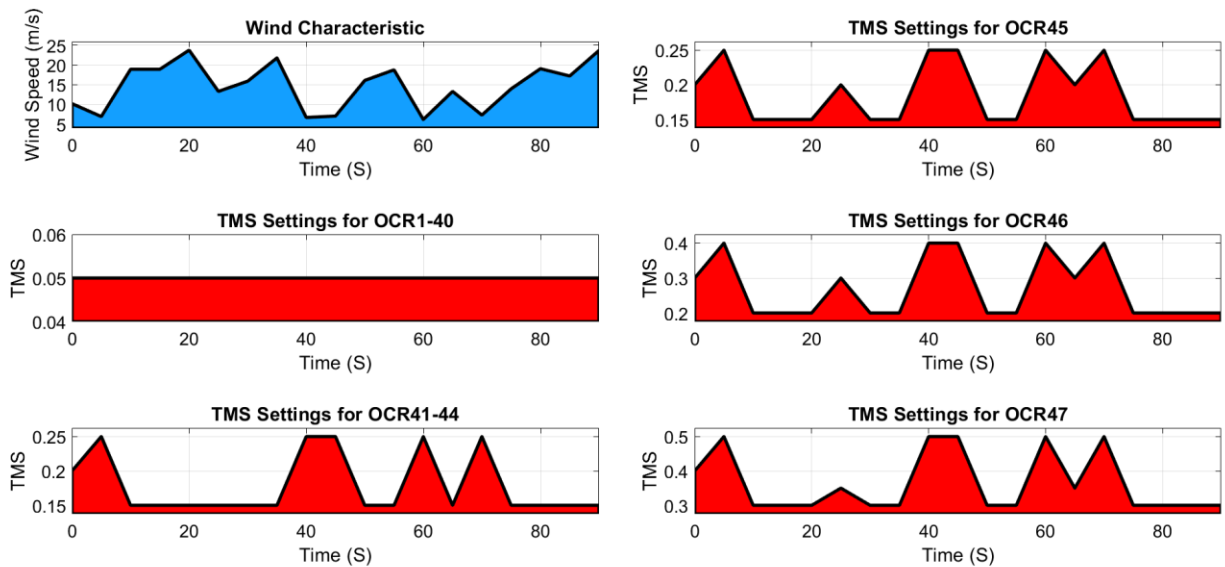
Fig. 4.8. Hybrid GWO-FLC optimal and adaptive protection for selecting proper TMS settings for OCRs during extreme wind speed variation: (a) wind speed profile, (b) TMS settings for OCRs 1-40, (c) TMS settings for OCRs 41-44, (d) TMS settings for OCR 45, (e) TMS settings for OCR 46, (f) TMS settings for OCR 47.

94
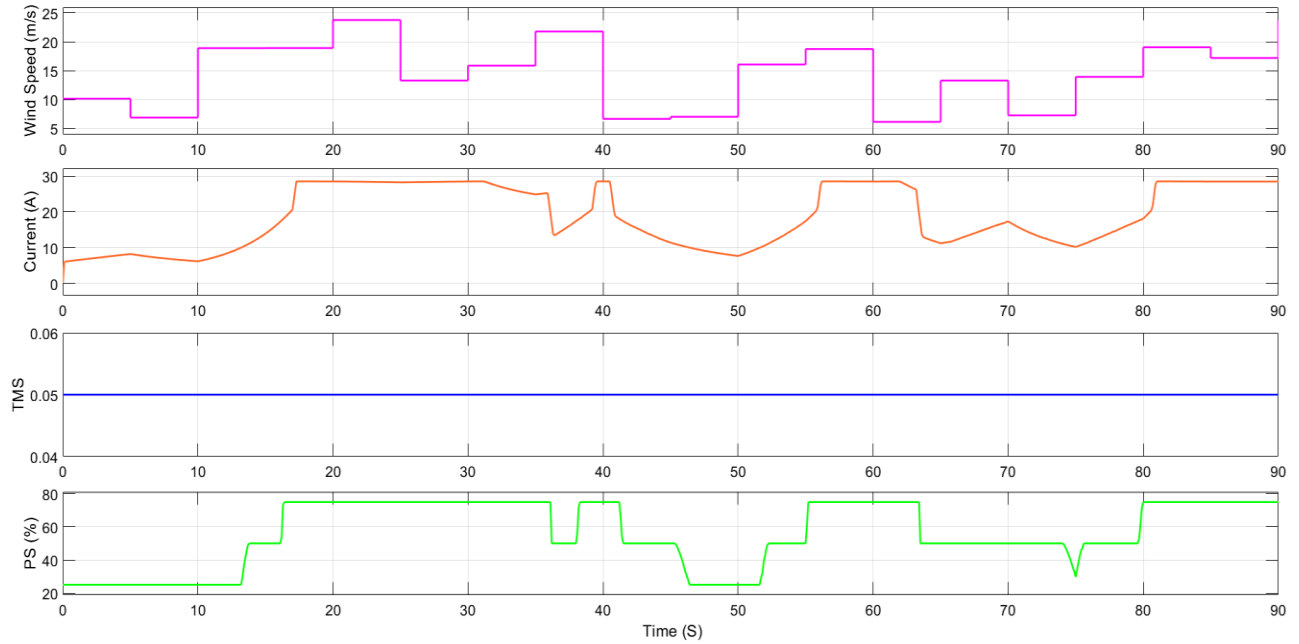
Fig. 4.9. Adaptive protection for the DFIG relay during extremely harsh wind behavior. (a) wind speed profile, (b) dynamic current characteristic behaviour, (c) adaptive TMS settings the DFIG relay, (d) adaptive PS settings for DFIG relay.
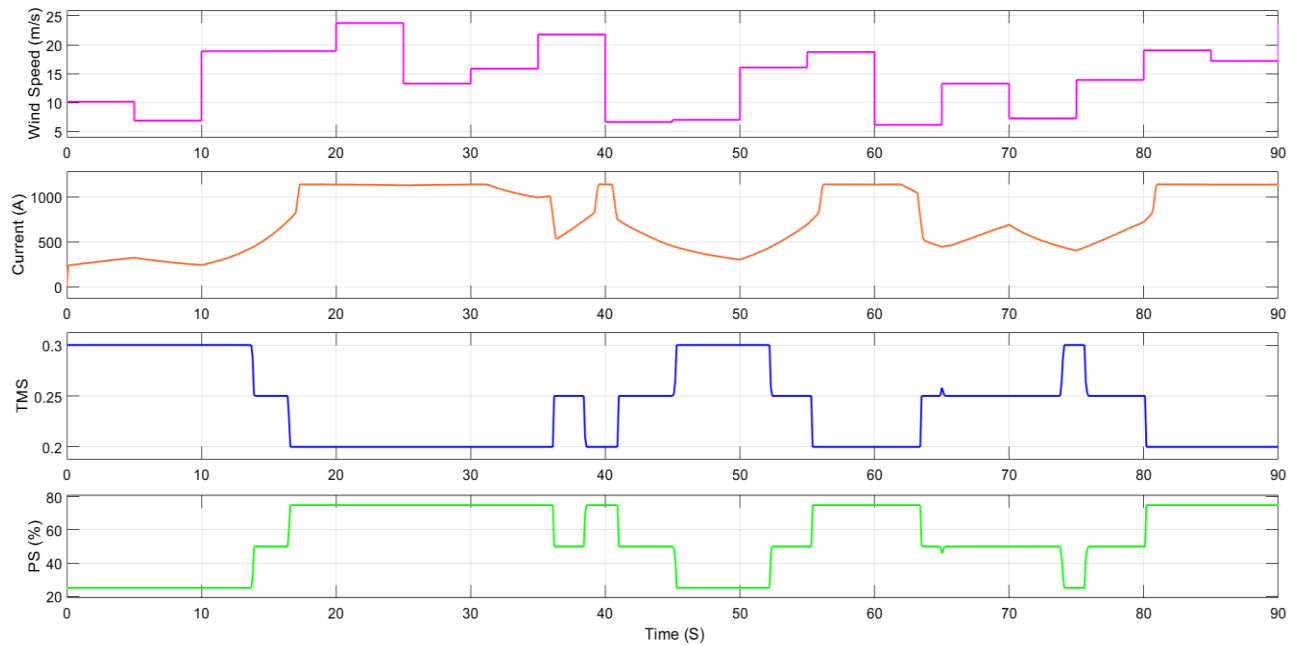
Fig. 4.10. Adaptive protection for the wind farm collector line relay during extremely harsh wind behavior: (a) wind speed profile, (b) dynamic current characteristic behaviour, (c) adaptive TMS settings the collector line relay, (d) adaptive PS settings for collector line relay.

95

4.6   Experimental Results: Real-time Implementation of FPGA-in-the-loop Operation of Protective Relays

In this section, the performance of the proposed protection scheme for the wind farms are experimentally validated in the laboratory environment, using FPGA DE2-115 board equipped with Cyclone IV-E device (EP4CE115F29C7). An overview of the real-time implementation is presented in Fig. 4.11. At first, an FPGA-based central protection scheme is developed that include all the 47 protection relays in the wind farm, and coded using Verilog hardware description language (HDL) on Modelsim. Thereafter, the entire protection algorithm is built on the FPGA using Quartus Prime, where the FPGA board itself is connected to a host computer through JTAG and Ethernet cables, and is run in real-time with the developed wind farm model which was earlier developed and analyzed in Matlab. In this way, the proposed protection scheme actually operates in FPGA-in-the-loop (FIL) as a central protection unit that eliminates the necessity to install numerous protection relays in the wind farm, which consequently reduce the costs significantly. During testing the performance of relays, various types of faults, at different locations, at different wind speed was considered to ensure the proposed protection scheme is robust enough during various conditions.

A sample of the validated operation of the protection relays with the updated settings of the proposed hybrid GWO-FLC is shown in Fig. 4.12. As an example, a bolted three-phase fault near one of the wind turbines was considered. During the fault incidence, due to the severe fault current magnitude, the active power on the faulted wind turbine has dipped near zero. As expected, the responsible relays for this protection zone, were able to detect the fault at the shortest possible time, in a well-coordinated manner, without causing any miscoordination or maloperation. In another analysis, a case of two faults occurring at the wind farm, next to two different wind turbines

was considered, where the operation of the relays is presented in Fig. 4.13. For this case, since there are two faults incidence at two different wind turbines, the protection relays for these two wind turbines operate exactly at the same time to ensure the fault at two different locations are cleared effectively. In case of the relay's failure, the backup relays would operate with some delay, as was shown in the figure.

Furthermore, in order to ensure the sensitivity of each relay, several different types of faults at different locations, near each protective relay is considered and the operation of each pair primary and backup relays are analyzed. Samples of single line to ground fault, and double line to ground fault, and line to line faults and the operation of the corresponding relays are also presented in Figs 4.14 – 4.16. It was observed from all these fault events, the backup relays were able to detect the fault and hence, operated in a well-coordinated matter with respect to the primary relay, assuming the primary relay is blinded.

Thus, the performance of the proposed adaptive and optimal overcurrent protection and coordination based on hybrid GWO-FLC, has been successfully validated and could be a robust and efficient protection scheme for modern large-scale wind farms.
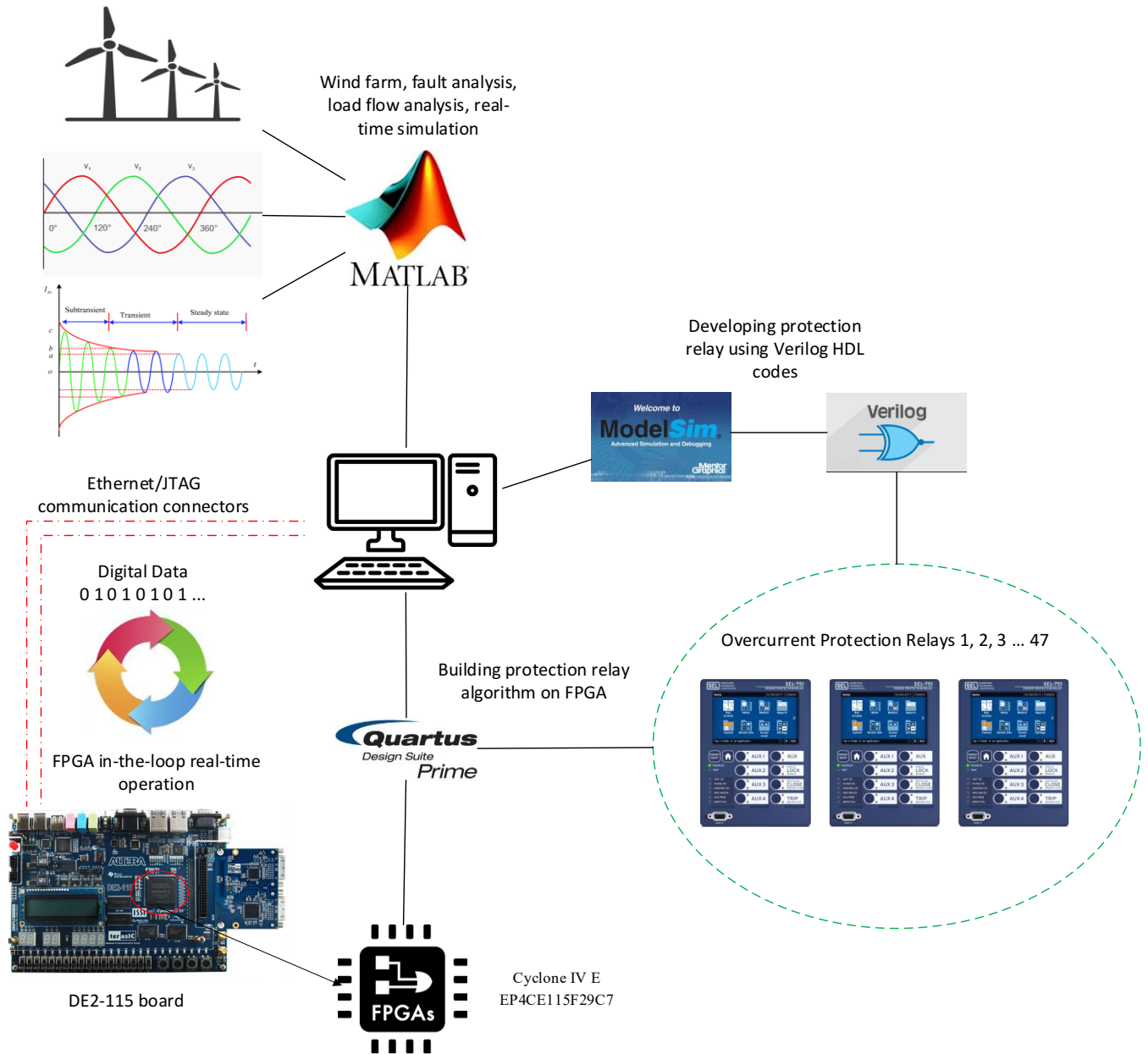
Fig. 4.11. Overview of the real-time implementation of the central FPGA based protection through FIL operation.

98
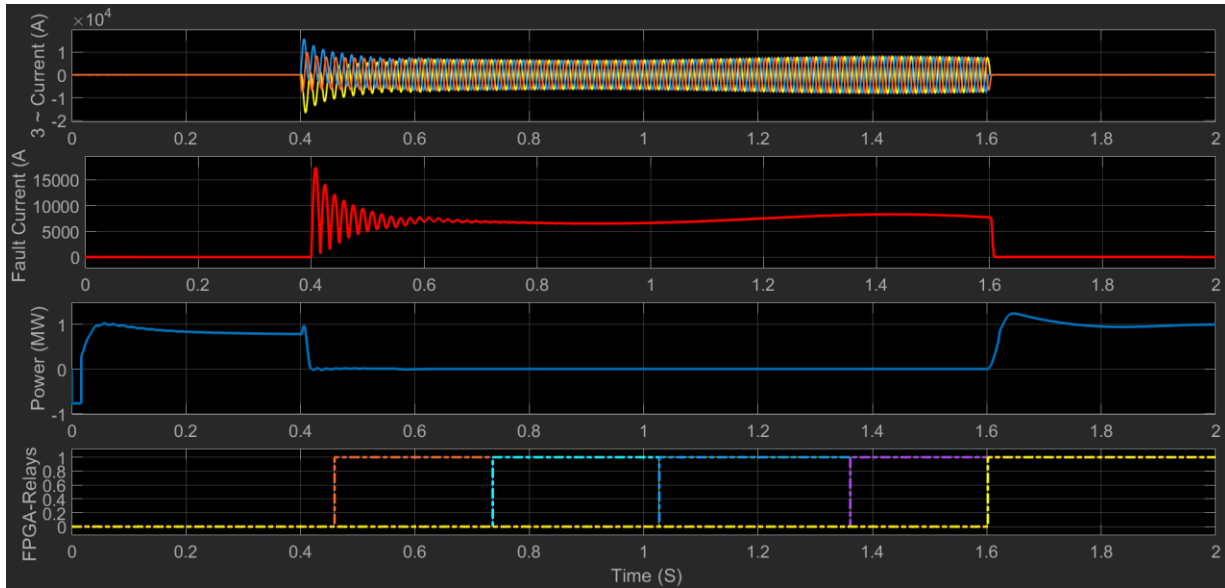
Fig. 4.12. A sample of successful operation of 5 protection relays and their coordination in the wind farm for a fault near one of the wind turbines: (a) 3-phase fault current characteristic, (b) Magnitude of the fault current, (c) Active power characteristic, (d) Operation and coordination of protective relays.
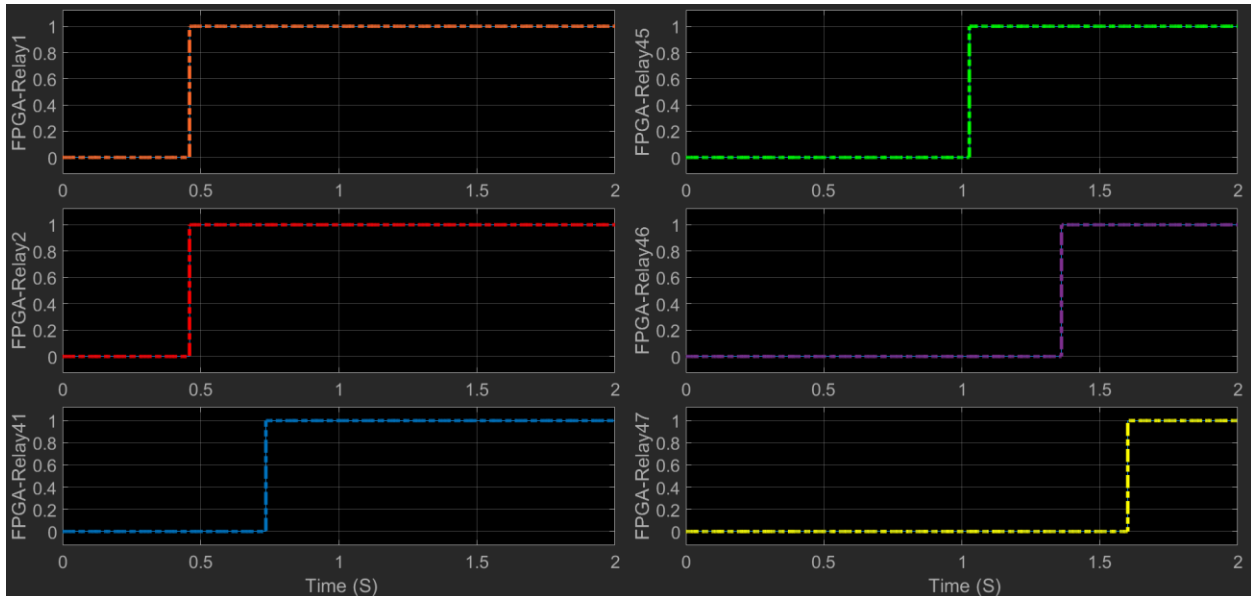
Fig. 4.13. Successful operation of several protection relays and their coordination in the wind farm for the case of two faults near two different wind turbines: (a) OCR1 (primary relay) operation located near the first wind turbine, (b) OCR2 (primary relay) operation located near the second wind turbine, (c) OCR41-44 (backup relay) operation located near each sub-feeder, (d) OCR45 (backup relay) operation located near the entire wind farm, (e) OCR46 (backup relay) operation near the power transformer, f OCR47 (backup relay) operation near the transmission line.

99
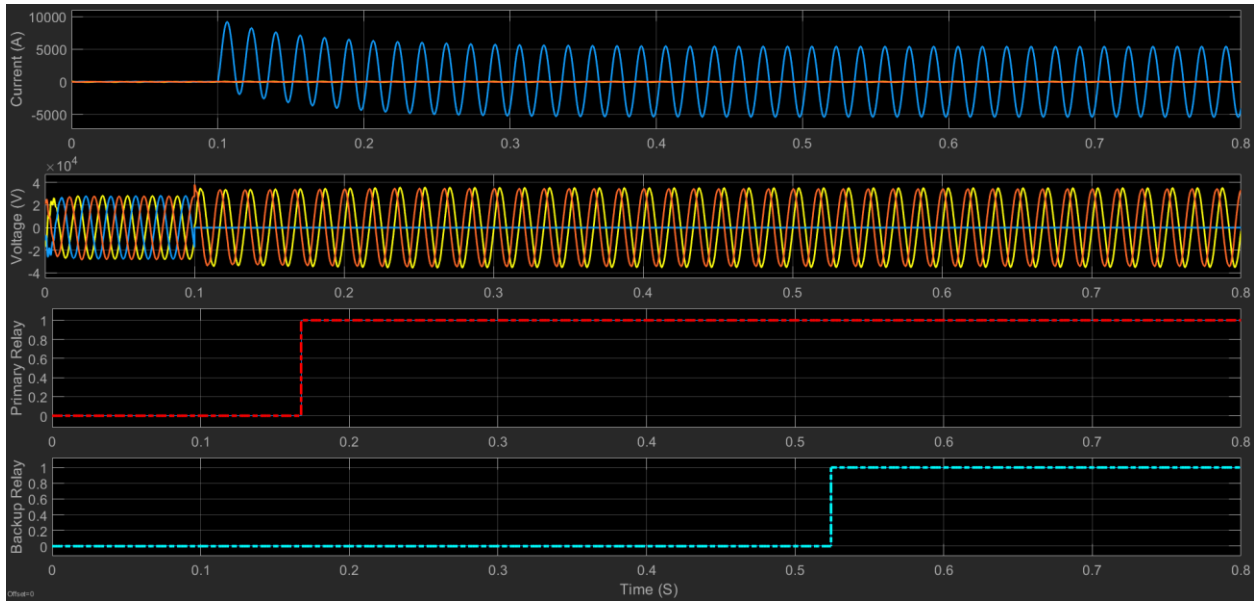
Fig. 4.14. Performance of pair primary and backup relays for a L-G fault near a wind turbine: (a) single line to ground fault current characteristic, (b) single line to ground fault voltage characteristic, (c) Primary relay operation, (d) Backup relay operation.
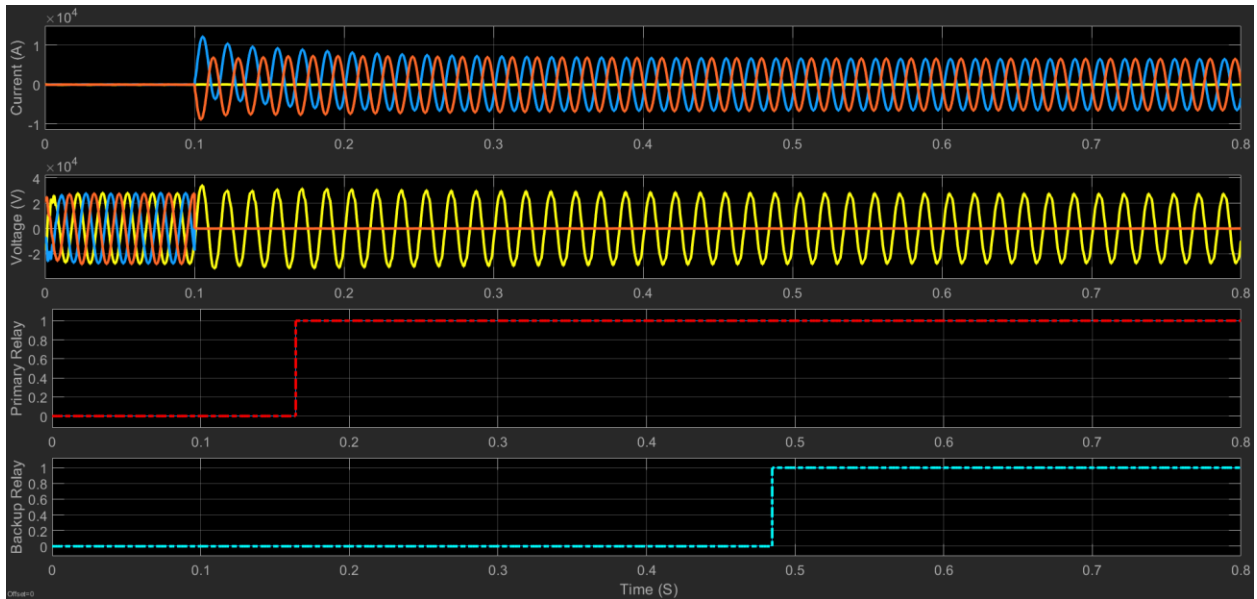
Fig. 4.15. Performance of pair primary and backup relays for a LL-G fault near a wind turbine: (a) double line to ground fault current characteristic, (b) double line to ground fault voltage characteristic, (c) Primary relay operation, (d) Backup relay operation.
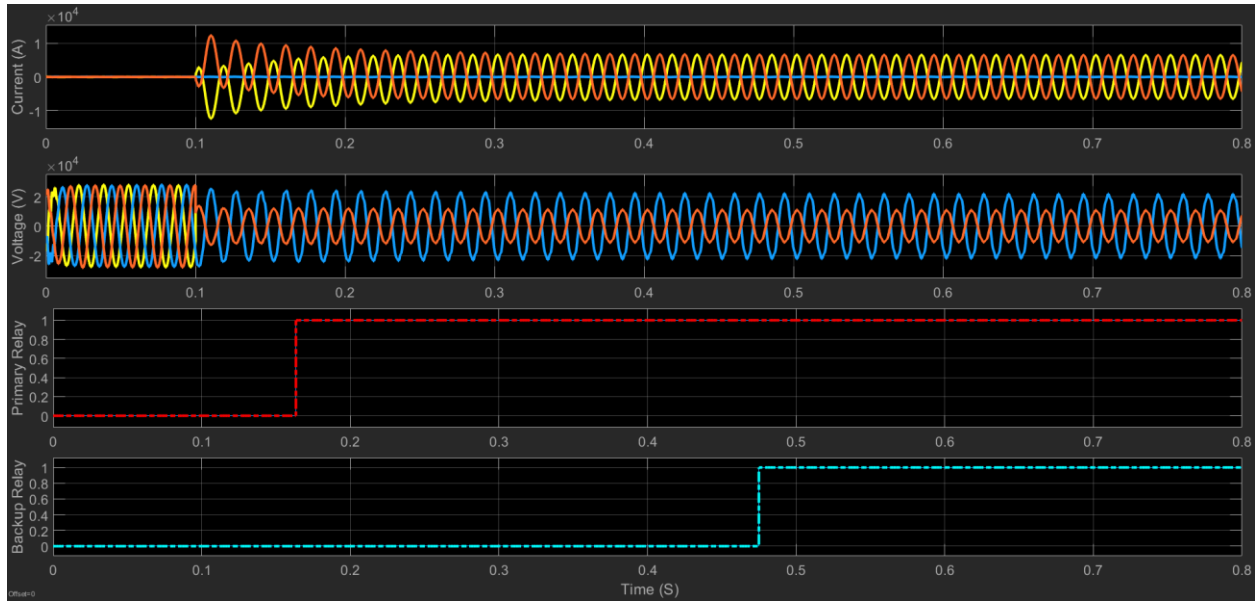
Fig. 4.16. Performance of pair primary and backup relays for a L-L fault near a wind turbine: (a) line-to-line fault current characteristic, (b) line-to-line fault voltage characteristic, (c) Primary relay operation, (d) Backup relay operation.

4.7   Conclusion

A novel hybrid GWO-FLC based adaptive and optimal overcurrent protection of large-scale wind farm was presented in this chapter. A quadruple group setting for OCRs was proposed and calculated according to wind farm dynamic behavior and wind profile at various speed to ensure flexibility. The current settings-optimized group settings of relays were further enhanced by optimizing the TMS and operation time of the relays by implementing GWO. The performance of the proposed GWO was also compared to the non-optimal relay group settings to ensure the effectiveness of the applied method, where the proposed GWO demonstrated a substantial improvement in the operation time of OCRs for the designed wind farm.

Furthermore, FLC was developed explicitly for online adaptation of the previously optimized (by GWO) OCRs settings and coordination according to the dynamic behavior of wind

farm, particularly, wind speed. Thus, the proposed GWO-FLC based protection avoids any miscoordination, maloperation, false tripping or even delayed tripping during fault incidence. The performance of the protective relays with the hybrid GWO-FLC settings were also tested and validated experimentally through FIL real-time implementation. Therefore, the proposed GWO-FLC performance was found to be robust, efficient and satisfactory and could be a potential protection technique for large-scale wind farm.

Chapter 5

Intelligent and Cost-effective Digital Differential Protection Schemes for Wind Farms

5.1 Introduction

The intertie section of wind farms where the bulk of power generation is fed to the grid through a main power transformer and transmission line, is usually protected by distance protection relays. However, as was discussed in chapter 1, the implementation of distance relays in wind farms has been found to be extremely unreliable. Therefore, in this thesis, several novel differential protection schemes based on the principle of differential relays, are proposed and suggested as a replacement for unreliable distance protective relays, in order to provide reliability and robust protection for wind farms, particularly for the intertie protection zone.

5.2 Differential Protection Relay

Differential protective relays are usually employed to provide protection for a single unit commonly employed for power transformers, generators, buses, and most recently, power transmission lines. However, in wind farms since there is a necessity to provide adequate protection for several zones rather than only a single unit, differential zone protection including ideal numbers of relays and measurement sensors i.e., CTs and VTs, for each specific zone must

be implemented [112]. Differential protection operation is reliably fast, usually close to 5ms, which could contribute to fast tripping and provide robust security for the wind farm intertie section.

The protection technique implemented for power transformers relies on the power rating of the transformer. Usually, protective fuses are employed for small size power transformer with the apparent power rating is less than 10 MVA, whereas, differential relays are usually used for transformers with apparent power rating above 10 MVA. A conventional differential protection for a 2-winding power transformer is illustrated in Fig. 5.1. N_1 and N_2 are the winding turns of primary and secondary side, respectively; I_1 is the incoming current that enters the primary side of the winding while I_2 is the outgoing current from the secondary side of the transformer. I_1' and I_2' are the currents measured by the respective CTs, indicated as CT_1 and CT_2, respectively. Relay restraining coil and relay operating coil are indicated as R and O, respectively, which are the fundamental structure of the balance beam differential relay as shown in Fig. 5.2. By symbolizing the CT turn ratios of the primary and secondary as $1/n_1$ and $1/n_2$ (CT with 1 primary turn and n secondary turn), respectively, the CT secondary currents and the current passing through the relay operating coil would be:

$$I_1' = \frac{I_1}{n_1} \tag{5.1}$$

$$I_2' = \frac{I_2}{n_2} \tag{5.2}$$

$$I' = I_1' - I_2' = \frac{I_1}{n_1} - \frac{I_2}{n_2} \tag{5.3}$$

Differential relays are simply designed in a way that for the internal faults where $I' = I_1' - I_2' \neq 0$, the relay should trip and send a signal to the corresponding circuit breaker to disconnect

the faulty section. However, for external faults where $I' = I_1' - I_2' = 0$ the relay should not operate.

According to Fig. 5.2, the electromagnetic force on the right and left side are proportional to $[N_0(I_1' - I_2')]^2$ and $[N_r(I_1' + I_2')/2]^2$, respectively. Thus, the differential relay operation condition can be verified as below [113]:

$$[N_0(I_1' - I_2')]^2 > [N_r(I_1' + I_2')/2]^2 \tag{5.4}$$

By defining $K = \frac{N_r}{N_0}$ as slope ratio, the above equation is simplified as follows:

$$|I_1' - I_2'| > K|(I_1' + I_2') / 2| \tag{5.5}$$

This equation represents the tripping condition of differential relay and the relay will only trip if an internal fault occurs within the protection zone. The schematic of such relay behavior with respect to the fault location, either external or internal fault, for a typical power transformer are shown in Figs. 5.3 and 5.4 respectively.
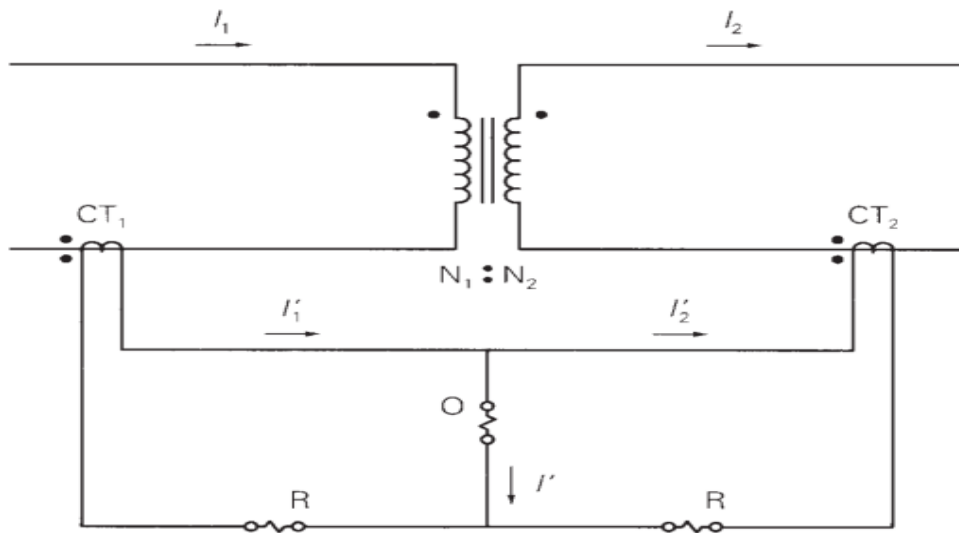
Fig. 5.1. Differential protection for a 2-winding power transformer.
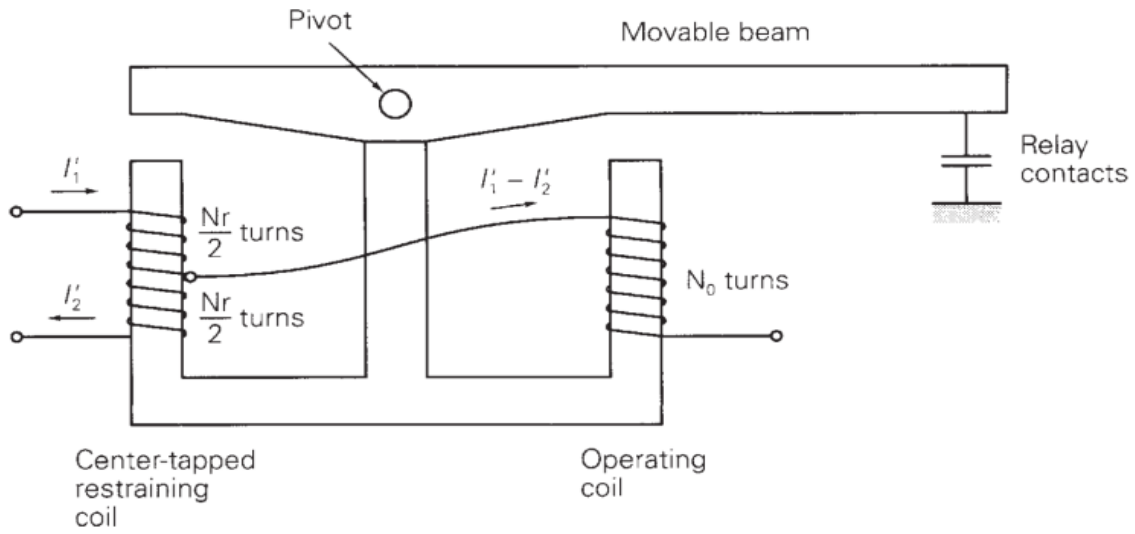
Fig. 5.2. Balance beam differential protection relay structure [113].
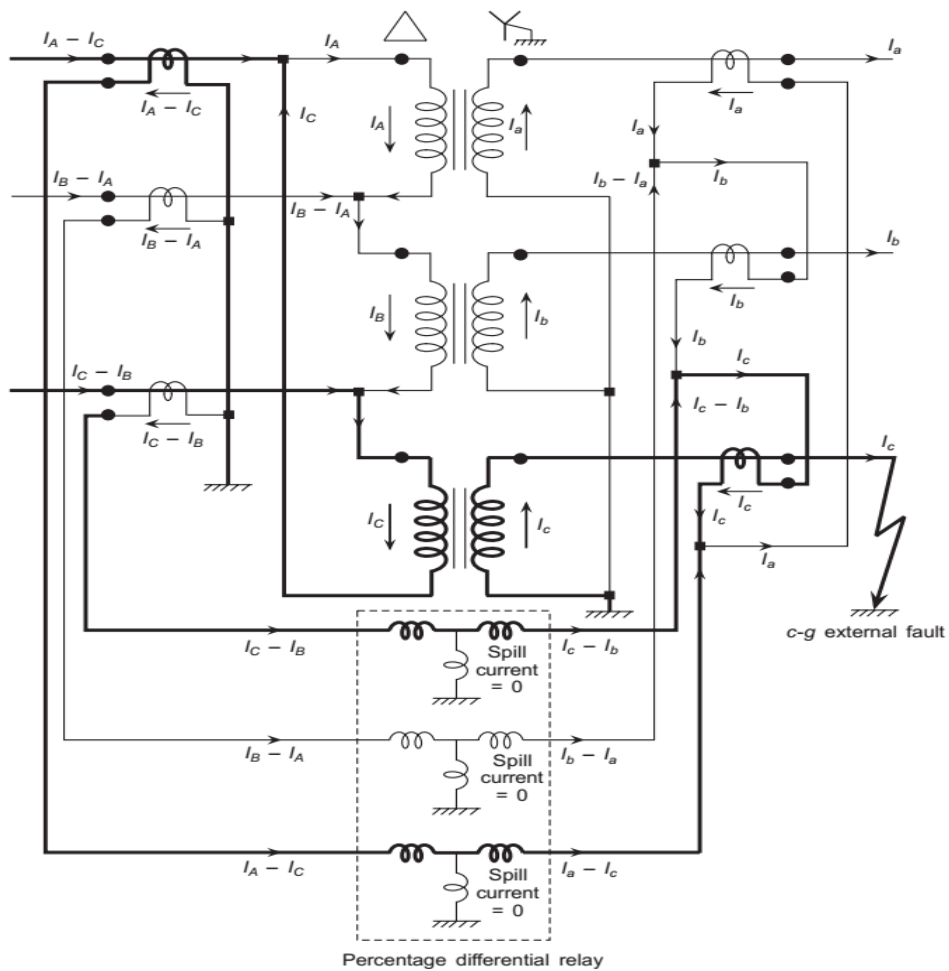
Fig. 5.3. Schematic of differential relay for a typical transformer during external L-G fault (phase "c") [66].
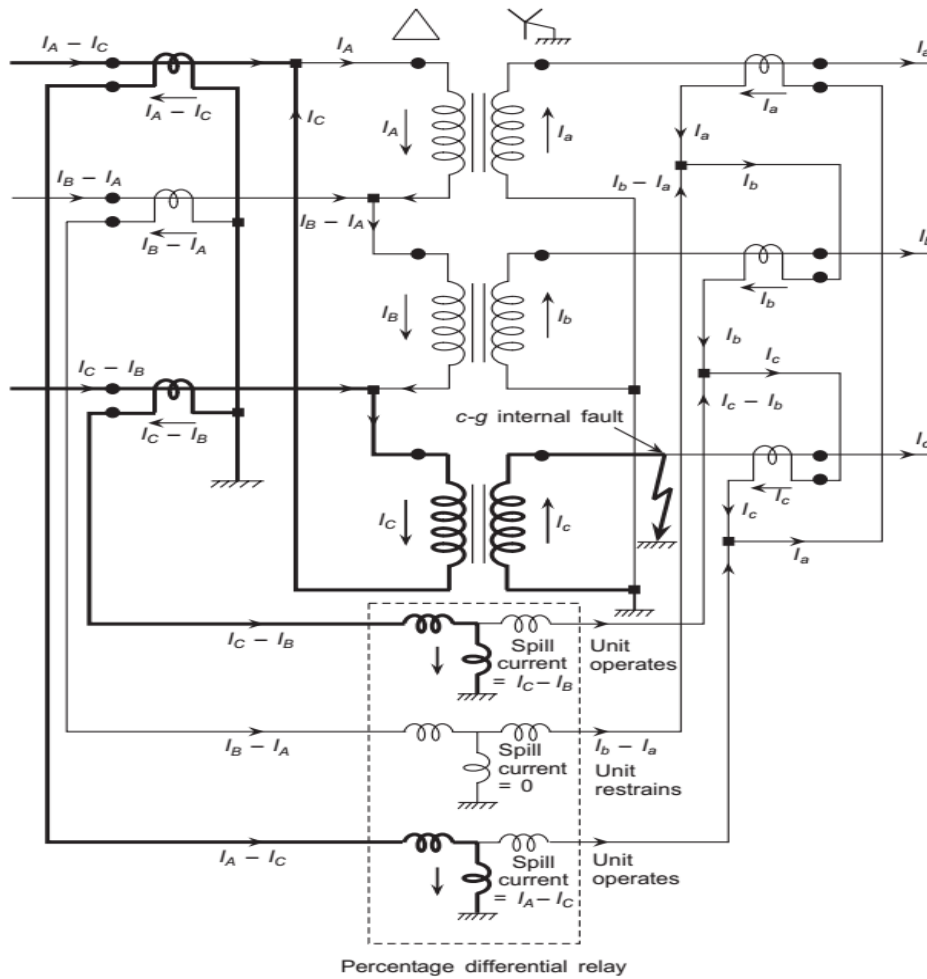
Fig. 5.4. Schematic of differential relay for a typical transformer during internal L-G fault [66].

Nowadays, microprocessor-based digital protection relays (MDPR) are mainly used for wind farm protection. The fundamental principal of digital differential relays is the same as the electromechanical relays, however, their method of measuring and processing the input signal is completely different. This would provide massive advantages compared to electromechanical and static relays which include: swift operation usually less than ½ cycle or less, flexibility, reliability, sensitivity, compact size, multi-function, multi-group settings, and adaptive protection capabilities. Moreover, the feasibility of digital communication with the substation, main control

unit or other protective relays is among other advantages of MDPR. A simple block diagram of MDPR is shown in Fig. 5.5. In these relays, the input analog current signals measured by the two CTs are converted to proportional voltage using current to voltage converters. Thereafter, AC voltage is converted to DC voltage signals through the precision rectifier and is subsequently passed to a multiplexer (MUX). Then, the analog signals are converted to digital signals using analog to digital converter (ADC) and sent to a microprocessor unit. Finally, the microprocessor unit will process and evaluate the data based on the formula derived in (5.5) and would send a trip signal to the corresponding circuit breakers when the statement in (5.5) is true.

Although, microprocessor-based protective relays are highly reliable and are blessed with numerous advantages, the major drawback is the limitations it imposes on the size of data, sequentially processing data, overheating, and most importantly their high costs, specifically, if they require large numbers of microprocessors. Unfortunately, that is always the case for large-scale wind farms connected to the power grid, that their size is gradually increasing and so are the costs of implementing, installing and maintenance of modern protective relays.
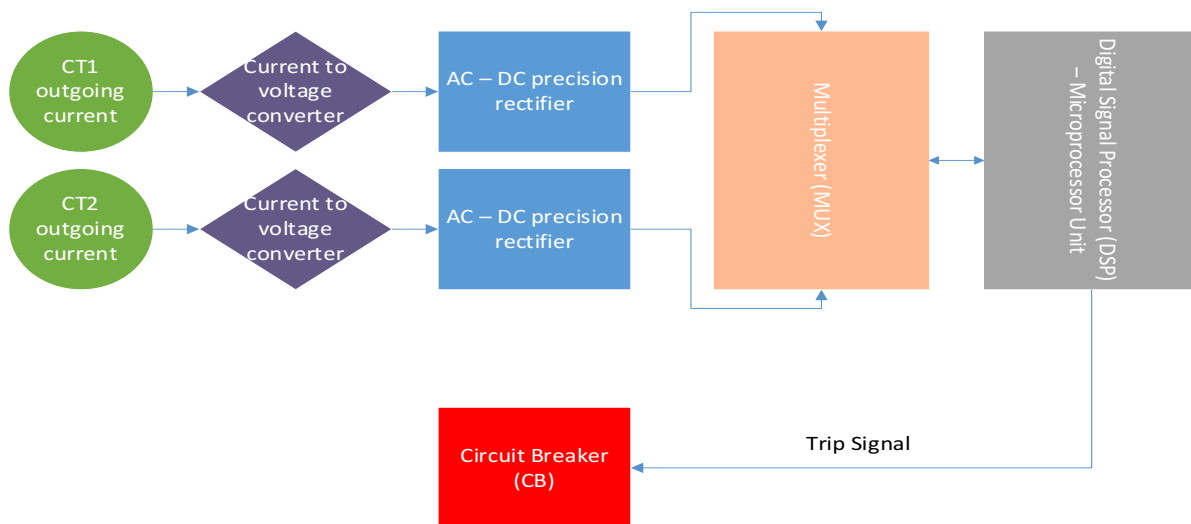
Fig. 5.5. Block diagram of the digital differential protection relay.

108

5.3 Proposed Digital Differential Protection Scheme for Wind Farms

In this research, three novel intelligent digital differential protection relays (DDPR) are proposed as a replacement to distance protection relays, which are sequentially named as differential-based protection scheme (DBPS), Field-programmable gate array-based digital differential protection scheme (FPGA-DDPS), and finally, support vector machine-based digital differential protection scheme (SVM-DDPS). The development and explanation of each proposed protection scheme are discussed in the following sub sections.

5.3.1 Differential-based Protection Scheme

In order to realize the effectiveness of differential relay, a differential-based protection scheme (DBPS) is developed in MATLAB/Simulink by considering the differential relay theory presented in previous section. An overview of the model, along with the developed user-friendly graphical interface of this relay are shown in Figs. 5.6 and 5.7 respectively. The extended version of the developed DBPS for the intertie section of the wind farm is shown in Appendix A. 15 and A. 16.

In order to set the DBPS in Fig. 5.7, the CT primary and secondary settings of both incoming and outgoing currents to the protected power apparatus, along with slope ratio, pickup current and operation time settings must be determined accurately. In this method, the CT primary of both incoming and outgoing current should be calculated, and then the ratio of the CT is set according to IEC or IEEE standards, which are defined based on the $I_{maxload}$ and I $_{SCC}$. $I_{maxload}$ is the maximum current flowing through the relay during normal operation mode of wind farm, where I $_{SCC}$ is maximum fault current to be seen by the respective CT. The secondary current of

CTs is usually selected as either 1 or 5 A. Slope ratio (K), has also been added to the developed relay to increase or decrease the sensitivity of the relay performance against fault current. Differential relay slope ratio usually varies in range of 0.1 to 0.4 based on the protection setting needed. Furthermore, the pickup current is a part of the relay setting in which the relay should operate for the current above the pre-set threshold value. Pickup current is usually set as 1.25 to 1.5 times of maximum load current. Finally, in order to provide coordination between differential relay and overcurrent relay as backup protection, an operation time setting has been devised, so that the relay would operate after a delayed time or even instantaneously based on the defined settings.

The developed relay logic function operates according to (5.5), however, the pickup current (I_{Pickup}) and CT ratio (CT_r) need to be introduced to the formula to generalize the developed differential-based protection scheme for various power systems including power transformer and transmission line within the intertie section of wind farms. Additionally, the incoming and outgoing current to a power apparatus (I_1 & I_2) are used instead of incoming and outgoing current of CT (I_1' & I_2'). Thus, the relay logic operation formula is modified as:

$$\left|\frac{I_1-I_2}{CT_r}\right| \geq K \left|\frac{I_1+I_2}{2CT_r}\right| + \frac{I_{Pickup}}{CT_r} \tag{5.6}$$

According to (5.6), if the statement is true, meaning an internal fault has occurred, then the relay would send a trip signal, otherwise, the relay will not operate as either there is no fault incidence or an external fault has occurred and the relay should ignore that. This relay operation conditions, along with the revised relay operation based on the defined slop ratio K, are illustrated in Figs. 5.8 – 5.10.
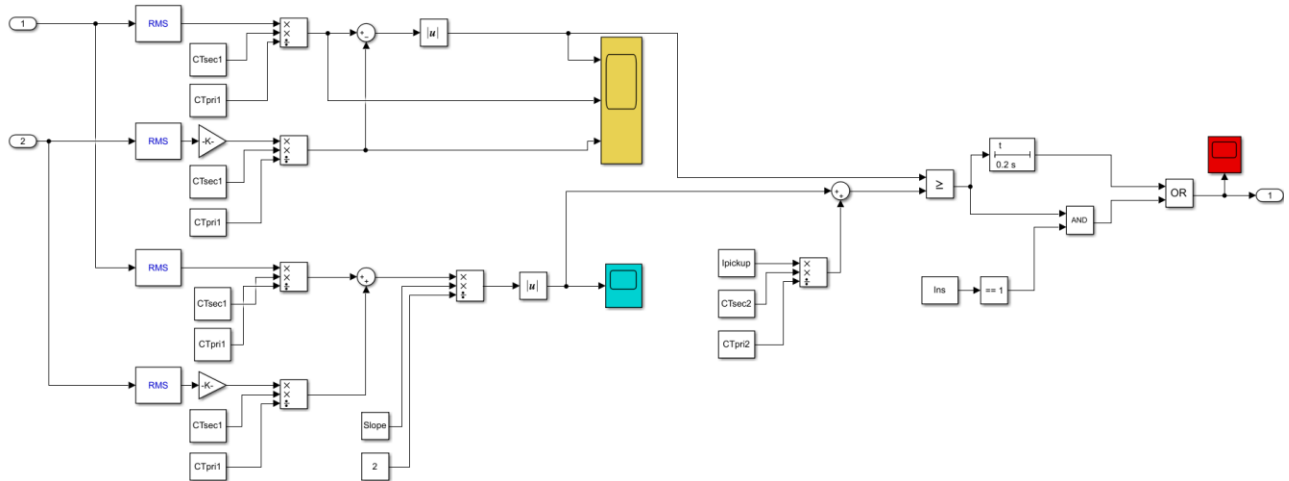
Fig. 5.6. Simulink model of developed digital DBPS for intertie zone protection of wind farm.
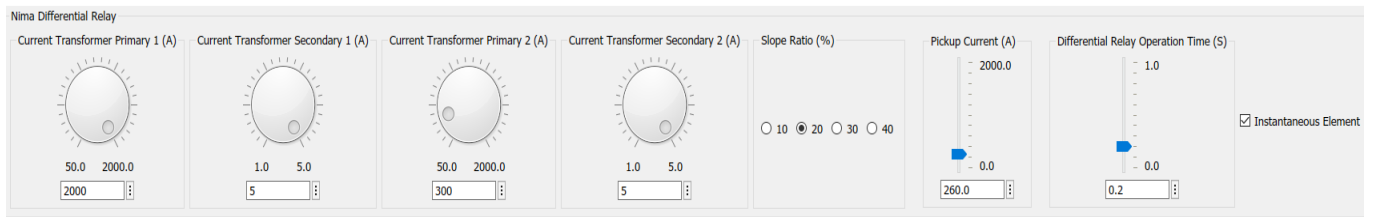
Fig. 5.7. Developed graphical interface of digital DBPS for intertie zone protection of wind farm.
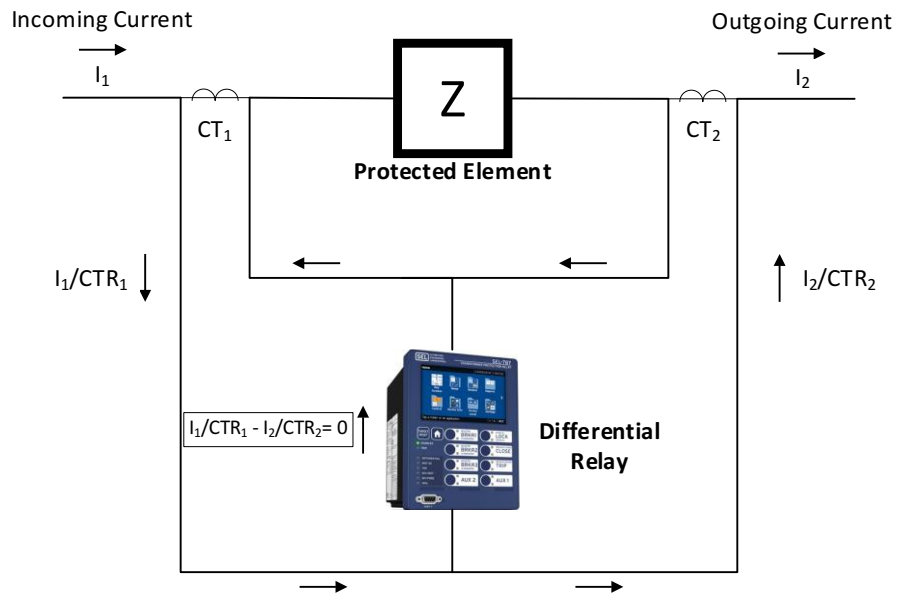
Fig. 5.8. DBPS during normal operation.

111
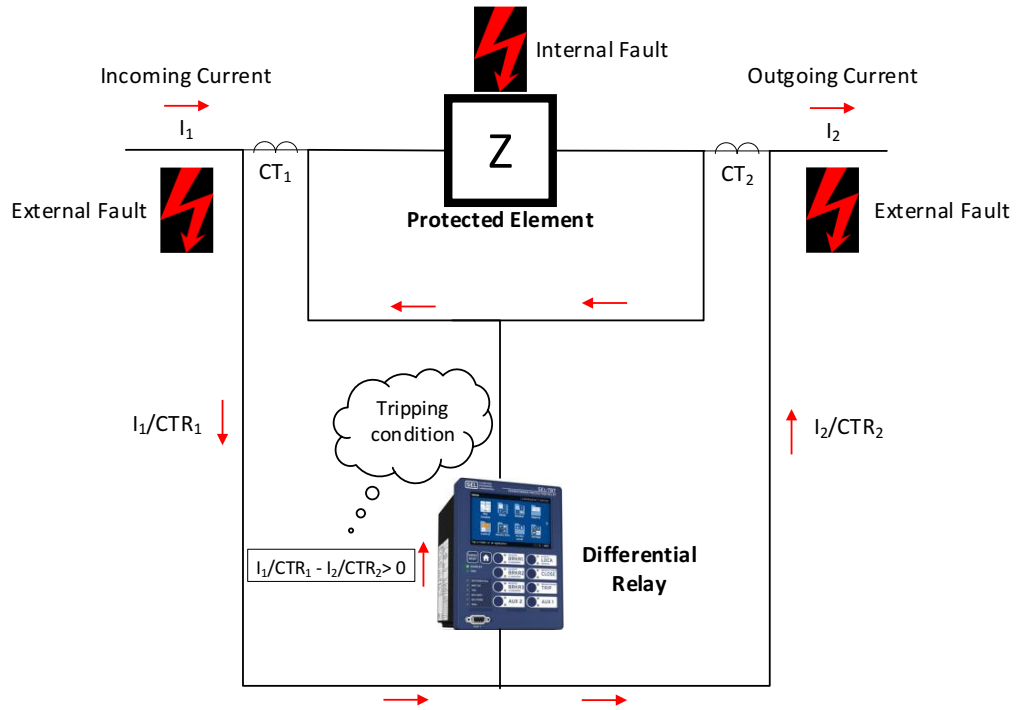
Fig. 5.9. Tripping condition of DBPS during internal and external faults.
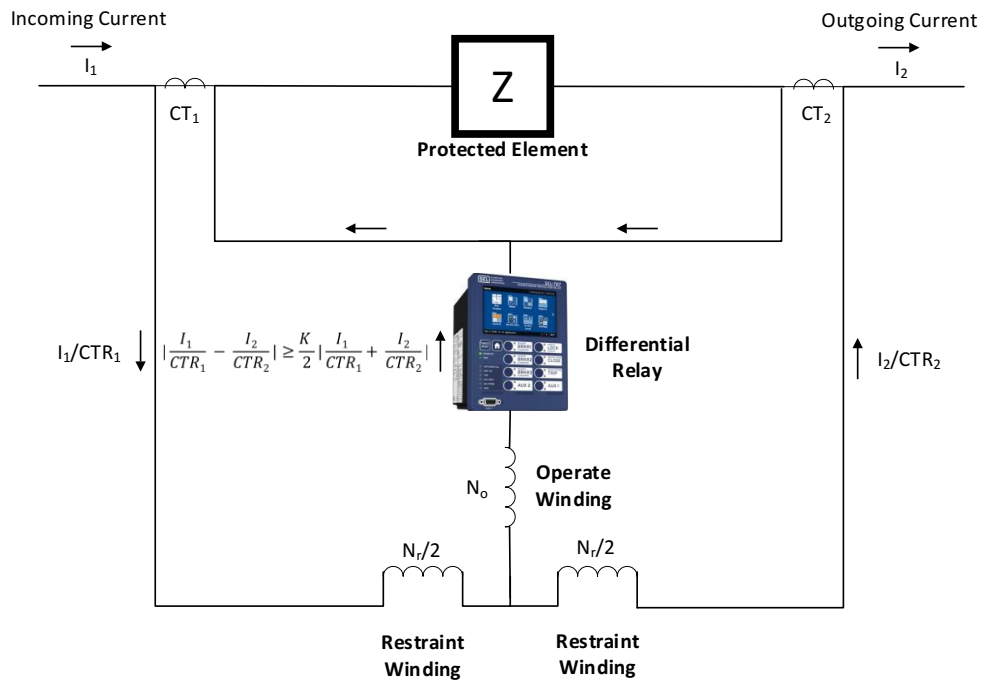
Fig. 5.10. Consideration of slope ratio K in the developed DBPS operating condition.

5.3.2   FPGA-based Digital Differential Protection Scheme

The second differential protection scheme proposed in this thesis, is FPGA-DDPS, which is developed in FPGA and its operation is based on the protection scheme that was proposed in the previous section. Field-programmable gate array (FPGA) is an integrated circuit (IC) that can be programmed and customized by the designer according to the needs of a specific task. The significant advantage of FPGA compared to microprocessor-based units and digital signal processing (DSP) units is that it is cost-effective, and also have a fast performance with minimum operation delay, which are ideal for protective relays [114]. The prominent advantages of using FPGAs as a proposed protective relay are:

- Cost-effective

- Flexible and reprogrammable

- Simultaneous parallel processing

- Swift performance with low operation delay

- Reliable and efficient

- Versatile applications

- Simple design

Therefore, in this research a differential protection relay is designed and developed in a FPGA using Modelsim software and Verilog hardware description language (HDL). Then, its effectiveness and performance are verified through FPGA-in-the-loop operation using DE2-115 FPGA board where the layout of this board is shown in Fig. 5.11 below.
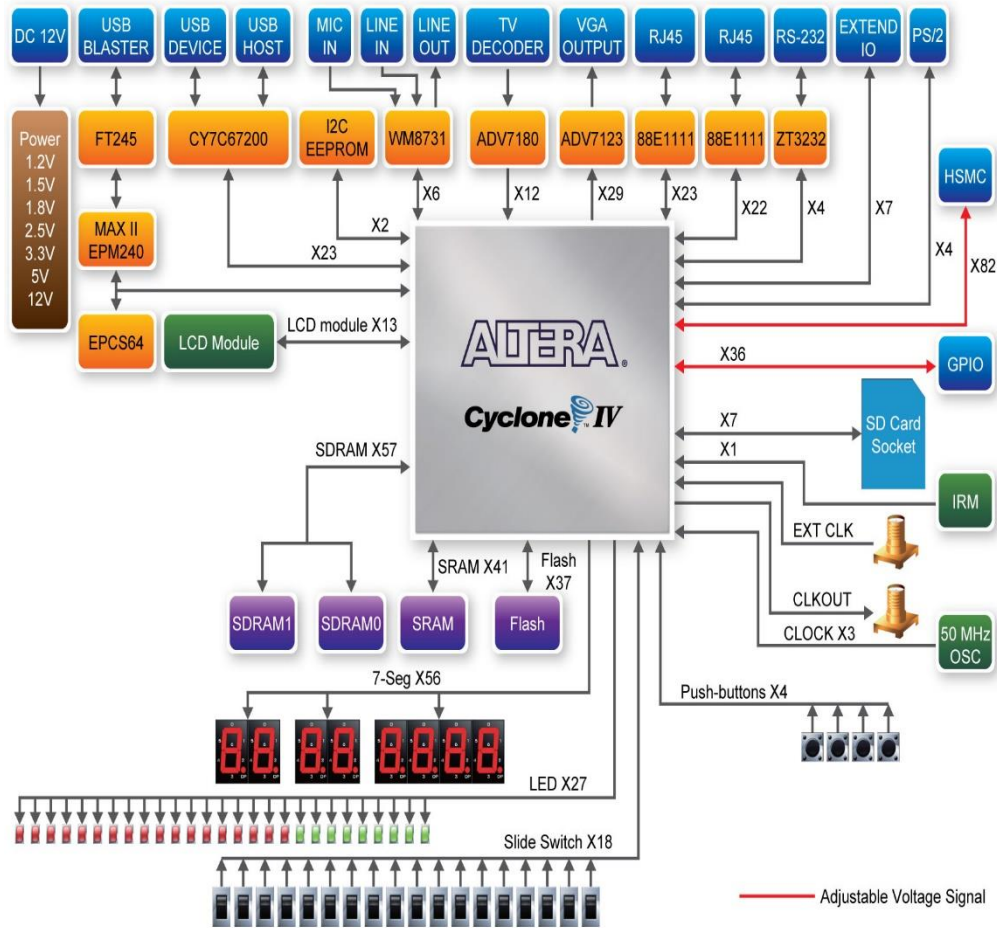
Fig. 5.11. Layout of Cyclone IV FPGA board.

In this research, in order to develop an FPGA-based digital differential relay, the following steps are taken:

5.3.2.1   Definition of Inputs and Outputs

Since, the differential relay is sensitive to the difference between the measured currents from the CTs at two points, the inputs are defined as I_1 and I_2, which are the outgoing currents from the CTs at the beginning and ending of a protection zone, and can be customized according

114

to the exact location that needs to be protected. Other inputs are, pickup current (I_{pickup}) and slope ratio (K), where, K is designed in a way that can be altered in the range of 10% - 40% to provide accurate operation of differential relay. Finally, the tripping status of the relay is defined as the output represented in digital quantity and can be either "1" (trip signal) or "0" (no trip signal).

5.3.2.2　FPGA Design and Coding for the Protection Relay Logic

The most important and challenging step is the design and coding of the relay. At this stage, the relay logic is programmed using Verilog HDL in Modelsim software and then, it is programmed at the FPGA using Quartus prime software. The relay logic defined at the relay is based on the relay characteristic operation that was earlier presented in DBPS section. The relay must be able to distinguish between internal and external faults, where during internal faults within the defined zone of protection, the relay should operate and trip i.e., the relay logic is "1", while during external faults, meaning faults that has occurred outside the defined protection zone, the relay should not react, therefore its logic should be "0". Based on the above statement, the relay logic designed and coded in FPGA is defined as in the equation below.

$$\text{Relay logic} = \begin{cases} 1, & \mid I_1 - I_2 \mid \geq K \left| \frac{(I_1 + I_2)}{2} \right| + I_{pickup} \\ 0, & \mid I_1 - I_2 \mid < K \left| \frac{(I_1 + I_2)}{2} \right| + I_{pickup} \end{cases} \qquad (5.7)$$

5.3.2.3　DE2-115 FPGA Board

The FPGA board implemented in this research is Altera DE2-115 board that is equipped with Cyclone IV E (EP4CE115F29C7), where the relay algorithm is programmed, as presented in

Appendix A. 17. The flowchart of the developed digital differential relay algorithm and the specific

FPGA board implemented in this work are shown in Figs. 5.12 and 5.13, respectively. 32-bit

fixpoint format, 16 bits for integer and 16 bits for fraction has been chosen to provide the accurate

measurement from CTs.
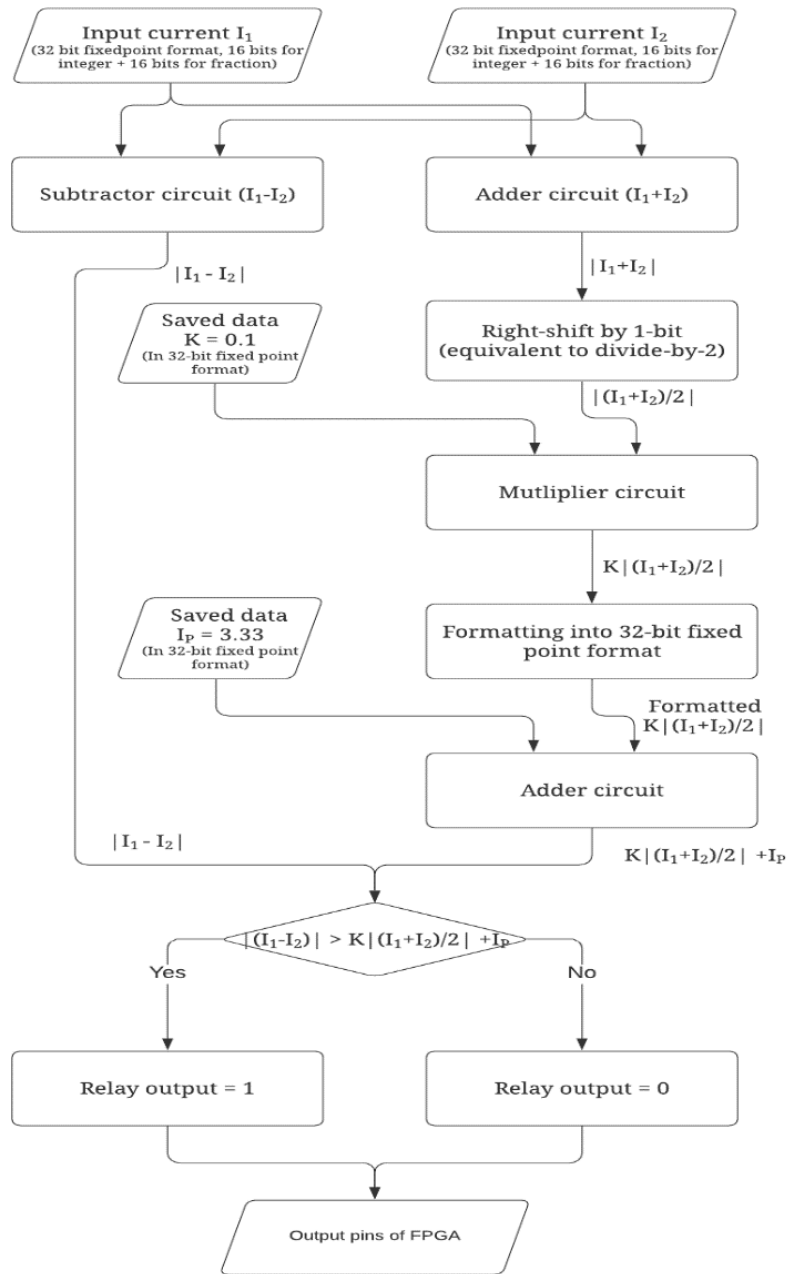
Fig. 5.12. Flowchart of the developed FPGA-DDPS.
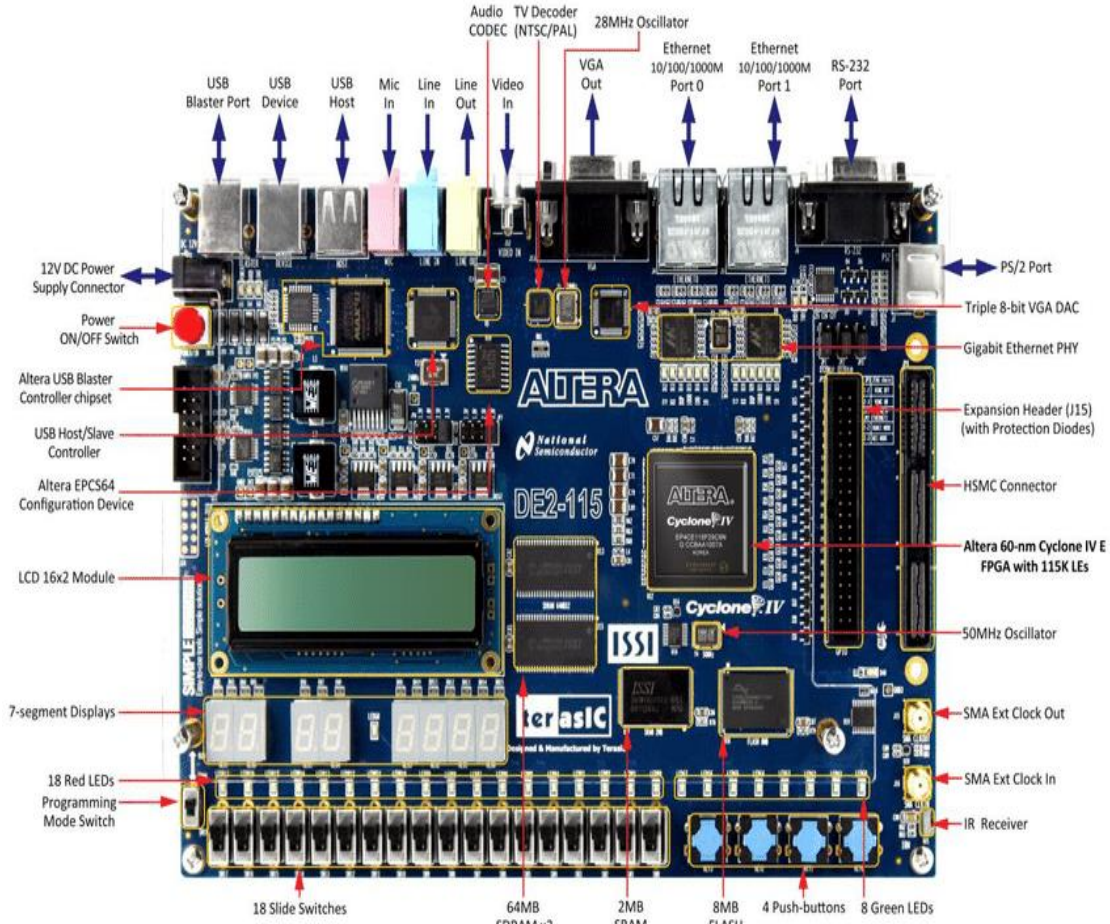
Fig. 5.13. Altera DE2-115 FPGA board implemented in this research.

5.3.2.4   FPGA-in-the-loop Operation

In order to test the effectiveness of the proposed FPGA-based digital differential protection scheme, MATLAB software is used to run the FPGA-in-the-loop (FIL) operation. The overview of the real-time FIL operation of the developed protection scheme is shown in Fig. 5.14. Also, a large-scale grid-connected wind farm model is also designed in MATLAB/Simulink, with exact rating and parameters as was shown in previous chapters, to test the proposed protection scheme

which is shown in Fig. 5.15. Since, the relay is designed in the FPGA, then by conducting FIL, or in other words, relay-in-the-loop (RIL) operation is actually taking place.
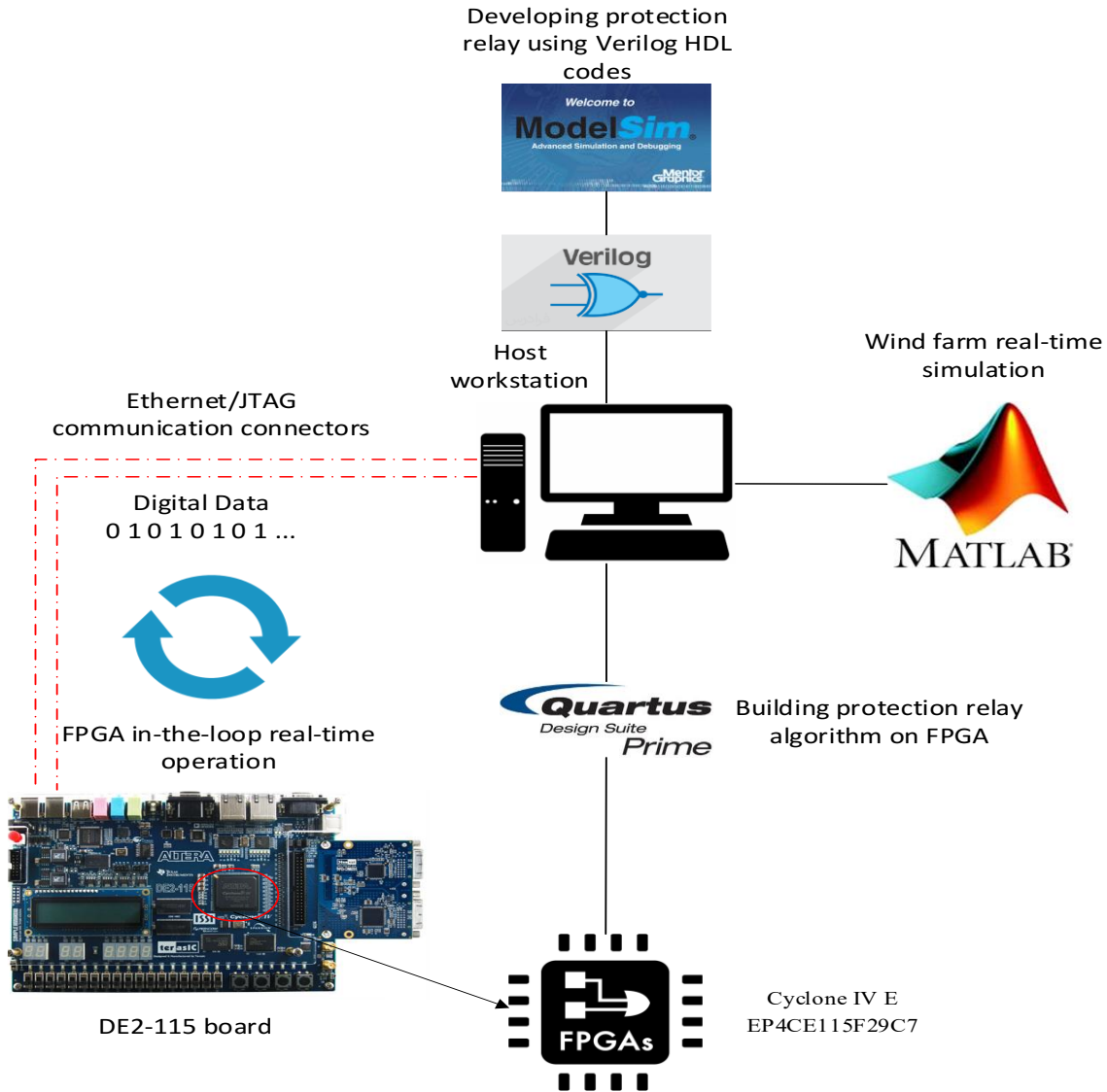
Fig. 5.14. FIL operation for FPGA-based digital protection relay.
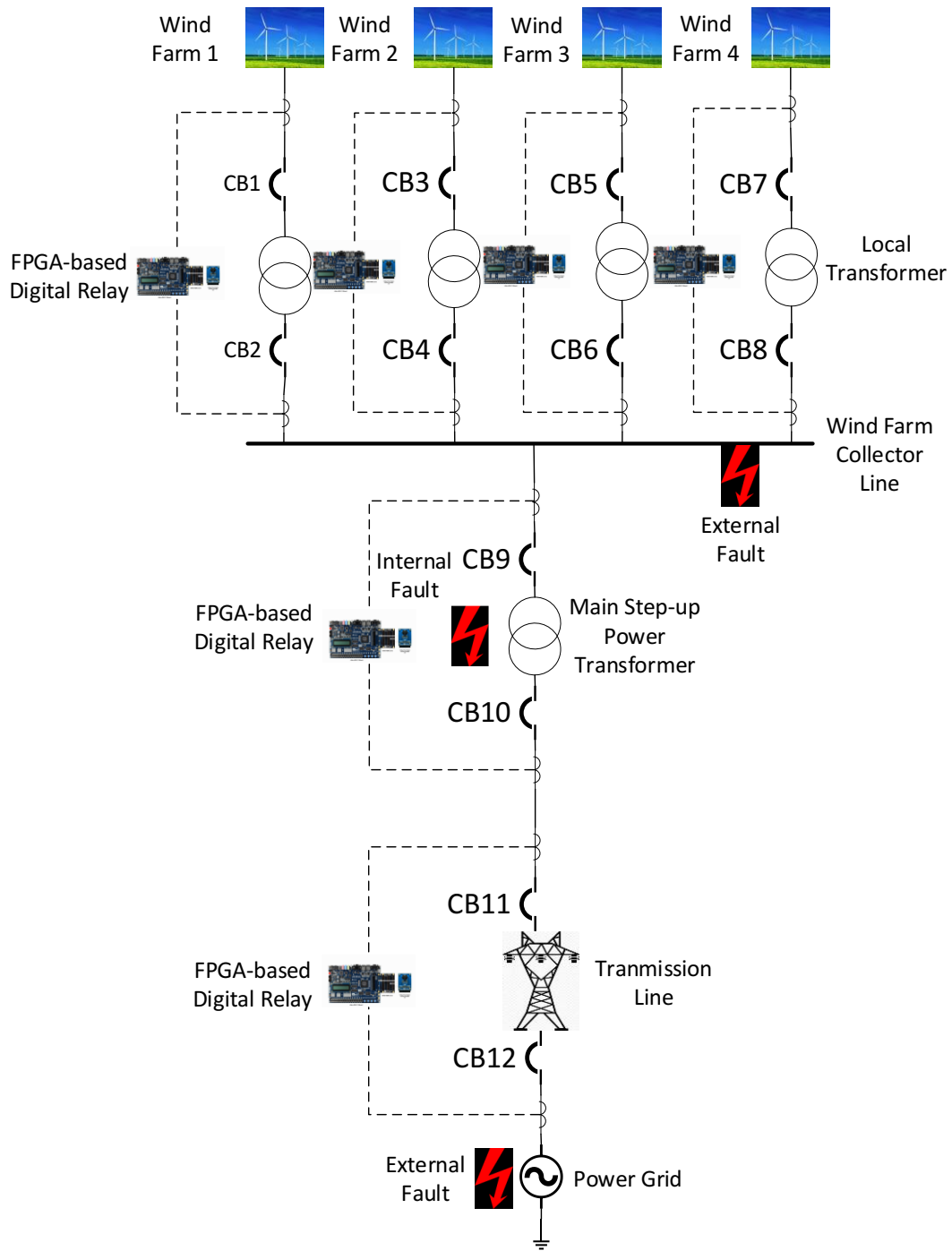
Fig. 5.15. Overview of the large-scale wind farm model under protection study for FPGA-DDPS.

5.3.2.5   Experimental Results

The performance of the proposed FPGA-DDPS is tested in real-time to verify the effectiveness and reliability of the protection scheme for a large-scale wind farm at different operating conditions. Various faults such as symmetrical three-phase fault, and unsymmetrical faults including double line to ground (LL-G), line to line (L-L), and single line to ground (L-G) are imposed at the system. Furthermore, three different values of fault resistances such as, zero resistance (bolted fault), 10 Ω and 70 Ω was selected arbitrarily and the details are presented below.

At first, the real-time operation of the relay is tested through FIL for the designed wind farm during normal operation where no fault is occurred. As expected, the relay does not detect any abnormality in the network and the FPGA-based relay logic remains zero during entire simulation, as shown in the figure below.
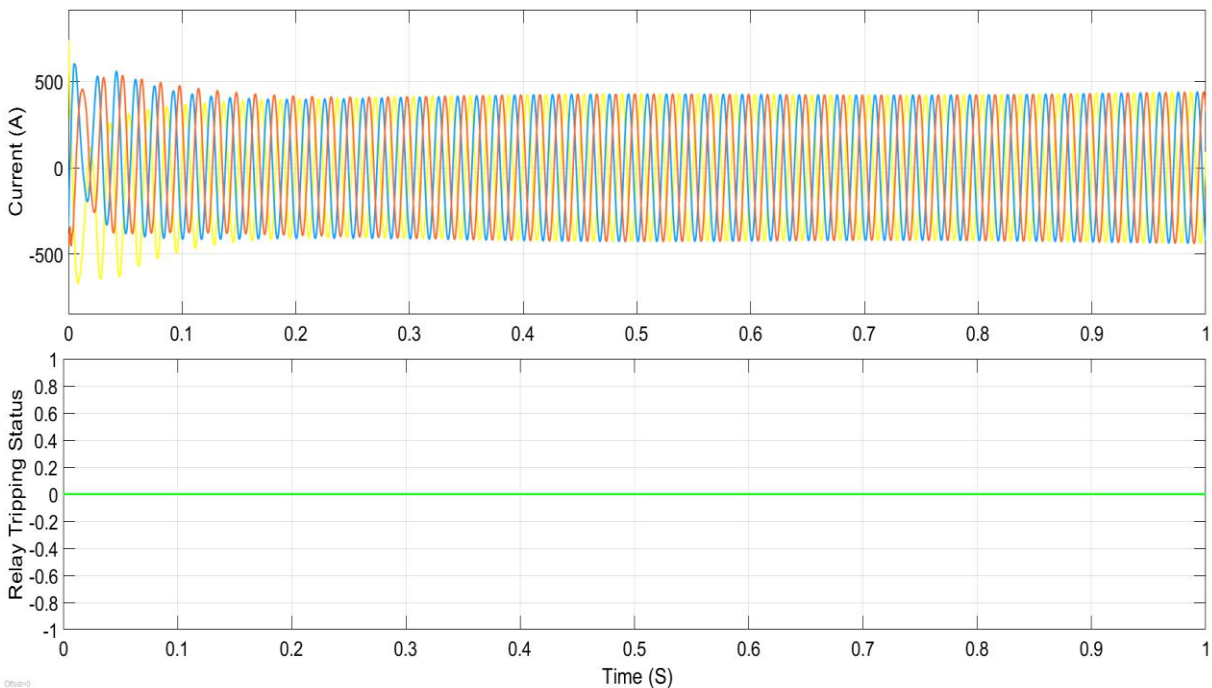
Fig. 5.16. Wind farm behavior and performance of the relay during no fault incidence: (a) Wind farm current, (b) trip signal from FPGA-DDPR.

In another test, internal faults with zero resistance (bolted fault) at the main step-up power transformer, near the grid is analyzed. As shown in Fig. 5.17, during three-phase fault incidence at time 0.4s until 0.5s, the relay successfully detects the fault, and hence, generates the trip signal accordingly. The same scenario is repeated for LL-G and L-G faults, and the proposed FPGA-DDPS reacts flawlessly, which are shown in Figs. 5.18 and 5.19 respectively. It should be mentioned that, the L-L fault exhibits almost the same behavior as LL-G, the results are not presented for L-L fault.
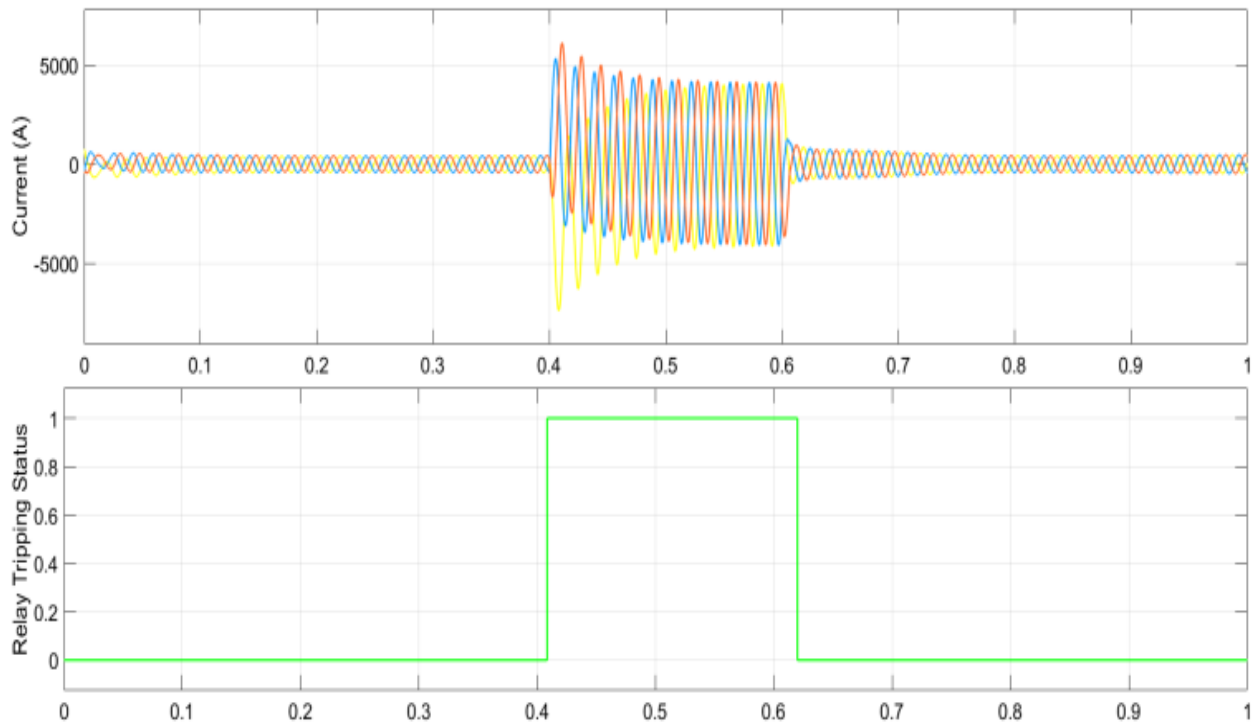
Fig. 5.17. Wind farm behavior and performance of the relay during bolted three phase fault: (a) Wind farm current, (b) trip signal from FPGA-DDPS.
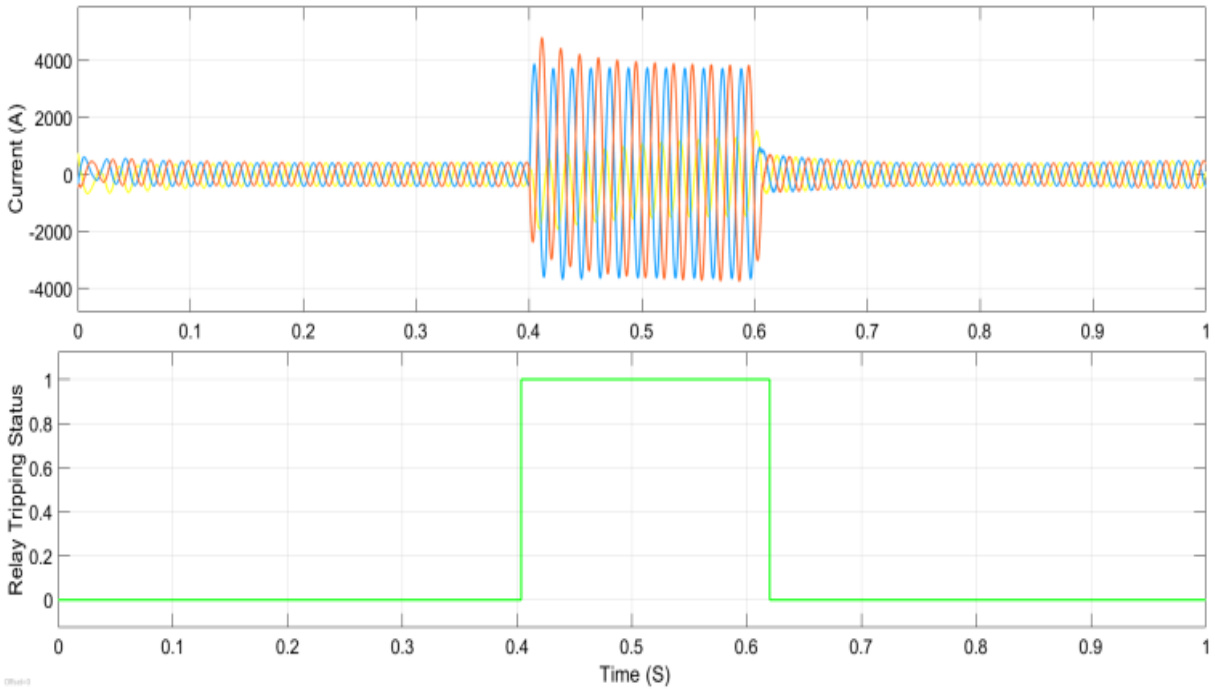
Fig. 5.18. Wind farm behavior and performance of the relay during line-line-ground fault: (a) Wind farm current, (b) trip signal from FPGA-DDPS.
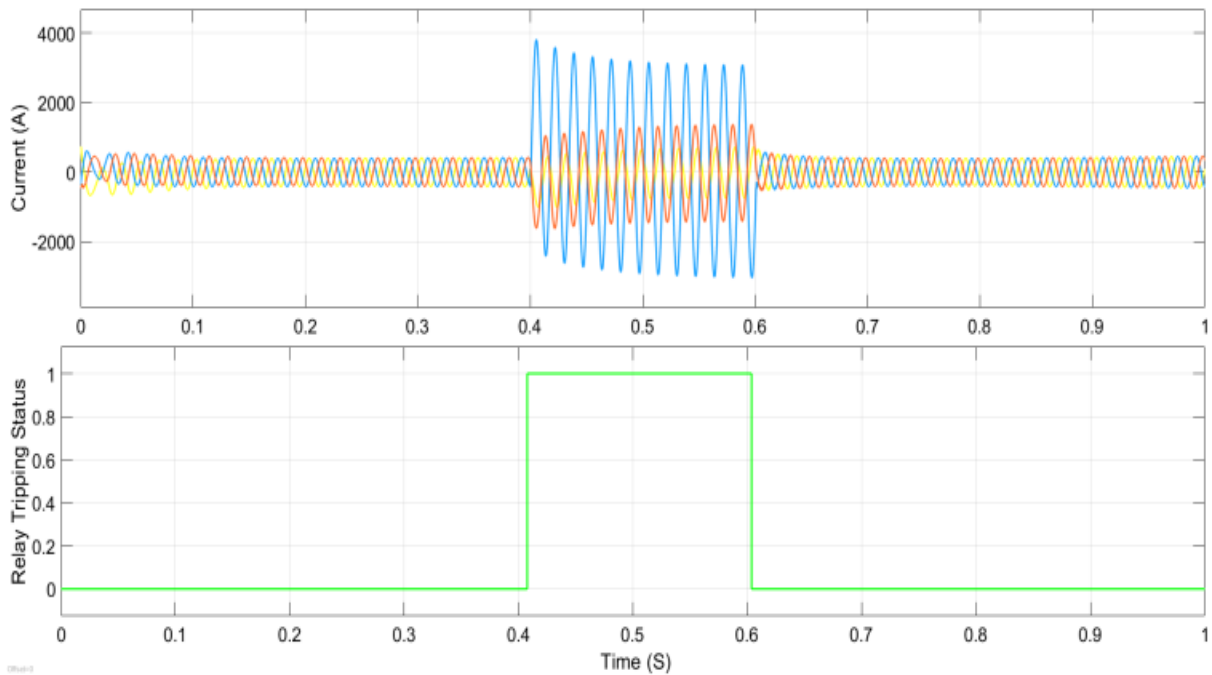
Fig. 5.19. Wind farm behavior and performance of the relay during single line to ground fault: (a) Wind farm current, (b) trip signal from FPGA-DDPS.

In general, since protective relays are sensitive to the variation of currents, during fault events with high resistance, the relay may not be able to detect the fault correctly as the current magnitude is not high enough, even if the fault is an internal fault and takes place within the zone of protection. However, in this research, during designing of FPGA-DDPS two other inputs, pickup current (I_{pickup}) and slope ratio (K) were introduced, where by adjusting these parameters and selecting the correct value for each zone of protection, the relay would be able to successfully detect the high impedance fault and trip accordingly in order to isolate the faulty section. Meanwhile, the effectiveness of the relay is also tested during high impedance faults and as a sample, two cases are presented in Figs. 5.20 and 5.21. As shown in these figures, since the fault resistance is high, the fault current has diminished significantly compared to the bolted faults where the fault had no resistance. In both of the cases, where fault resistance is 10 Ω and 70 Ω, the relay still properly detects the faults and generates the trip signal for the circuit breaker to isolate the faulty section. The pickup current and slope ratio was selected as 3.3 and 0.4 respectively, and the wind speed in the following results have been varied.
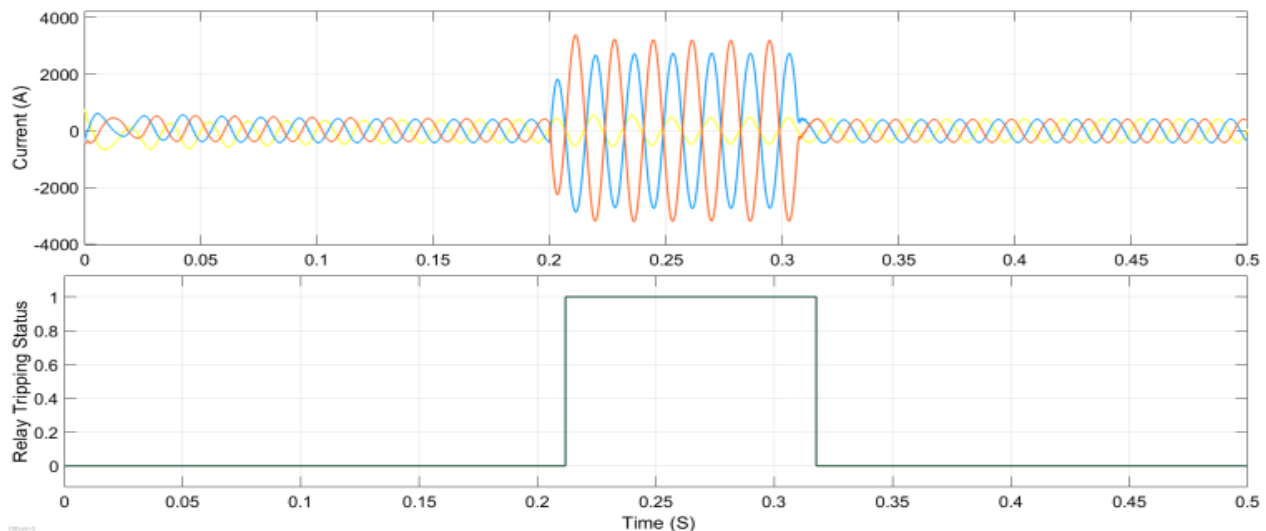
Fig. 5.20. Wind farm behavior and performance of the relay during 10 Ω LL-G fault at the power transformer: (a) Wind farm current, (b) trip signal from FPGA-DDPS.
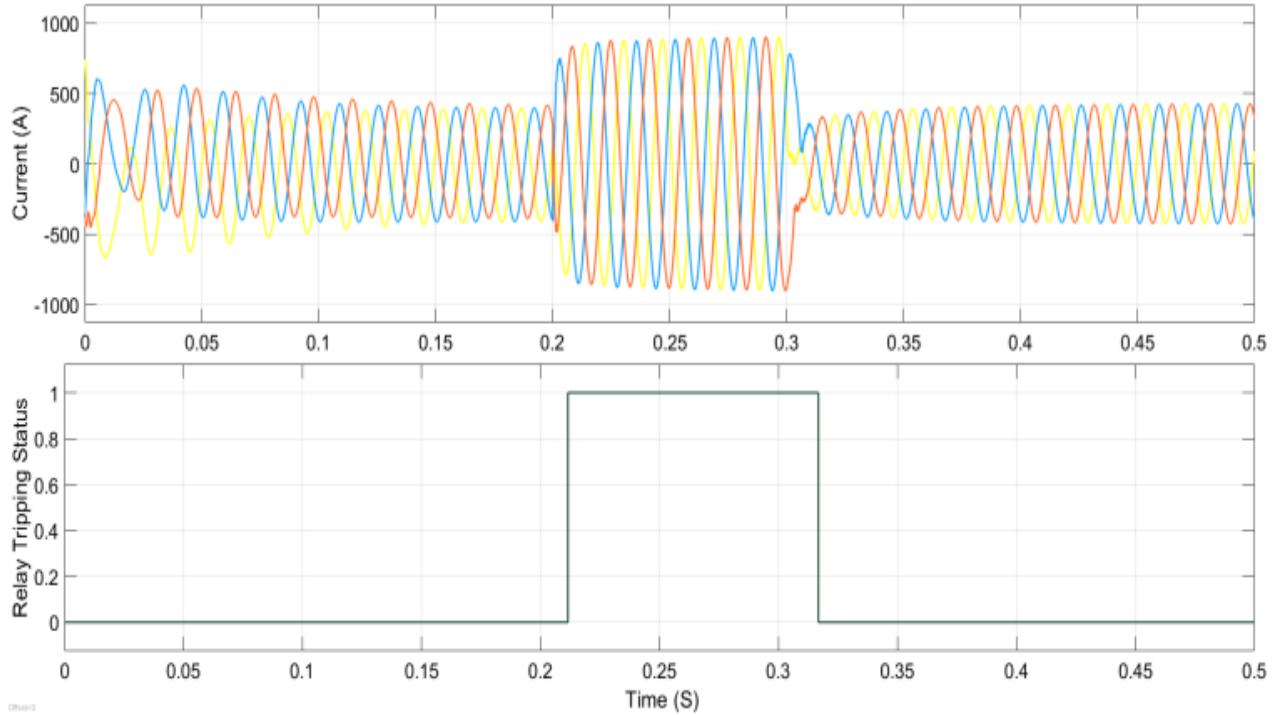
Fig. 5.21. Wind farm behavior and performance of the relay during 70 Ω LL-G fault at the power transformer: (a) Wind farm current, (b) trip signal from FPGA-DDPS.

Finally, performance of the proposed FPGA-DDPS is also tested for external fault (outside of the protection zone) and the corresponding result is shown in Fig. 5.22. As an example, a three-phase fault event on the aggregated wind farm collector is considered, where the performance of relay at the main power transformer, next to the grid is analyzed. During an external fault at the wind farm collector line, the excessive current causes the both measured current at the power transformer to increase proportionally, thus, the difference would be marginal. Slope ratio and pickup current for each differential relay should be carefully selected so the relay is able to detect the fault correctly. This selection depends mainly on the fault current, fault resistance and also the location of the fault. For example, in the relay mentioned above, a higher threshold for pickup current and also 10% sensitivity for the slope ratio K was chosen to cope with the transformer

124

transient operation during inrush current and energization procedure to prevent relay maloperation. As a result, the relay successfully ignores the external fault and did not trip at all, which is evident in this figure. Thus, the proposed FPGA-DDPS operation through real-time FIL is analyzed, and found to be reliable, fast, efficient. It is found from experimental results that the proposed FPGA-based relay is able to detect internal faults quickly and generates trip signals accordingly, while it ignores external faults. Thus, the proposed FPGA-DDPR relay could be a cost-effective substitute to the costly microprocessor-based differential relay scheme to provide fast and reliable protection for wind farms.

The application of the proposed differential protection scheme is not restricted to the intertie protection zone of wind farms, but it can also be applicable as a robust and cost-effective protection scheme in any power system that, a fast and reliable operation from protective relays is expected.
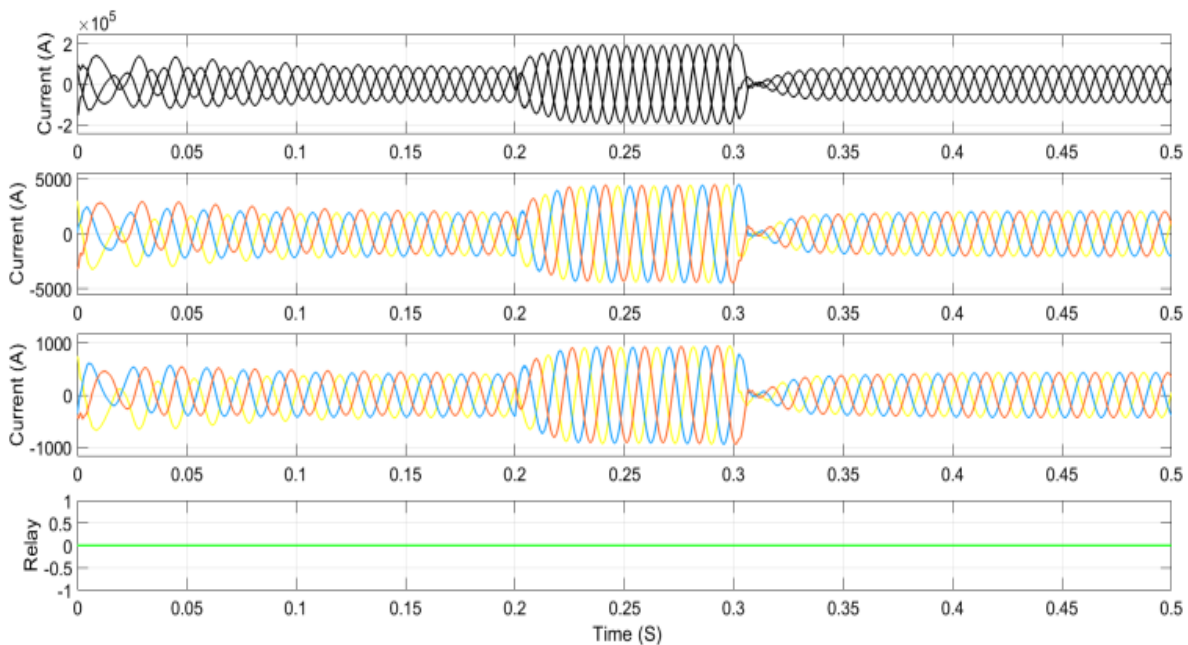
Fig. 5.22. Relay successfully ignores a 3-phase external fault on the wind farm collector line: a) wind farm collector line current, b) incoming current to the relay, c) outgoing current to the relay, d) relay tripping status.

5.3.3 Machine Learning Classifier Based Digital Differential Protection

The third novel protection scheme proposed in this thesis is SVM-DDPS, which is based on the machine learning (ML) algorithms and the DDPS that was proposed initially. This type of protection has been proposed particularly for the intertie section of the wind farm to provide a robust and effective security for such protection zone, where the present distance relays have appallingly failed to provide. The specific intelligent machine learning algorithm that was used is SVM, and its operation is designed based on the operation of differential protection schemes.

5.3.3.1 Support Vector Machine

Support vector machine (SVM) is a supervised machine learning technique used for classification and regression purposes. The SVM model aims to provide prediction to determine if a particular set of data belongs to a specific class or group by defining a separating hyperplane. To construct the separating hyperplane for a set of labeled training patterns in a feature space, the data should be transformed into N dimensional feature vector where it can be carried out by using Kernel function, also known as Kernel trick [115]. Kernel functions can be used in many applications as they provide a simple bridge from linearity to non-linearity for algorithms which can be expressed in terms of dot products, which will be more explained later in this Chapter. Therefore, SVM has two main objectives which are:

- Finding a hyperplane in a N-dimensional space with the purpose of classifying two groups from each other using Kernel method, which is shown in Fig. 5.23.
- Finding the optimal hyperplane through maximum margin between classes to improve the classification accuracy rate as shown in Fig. 5.24.
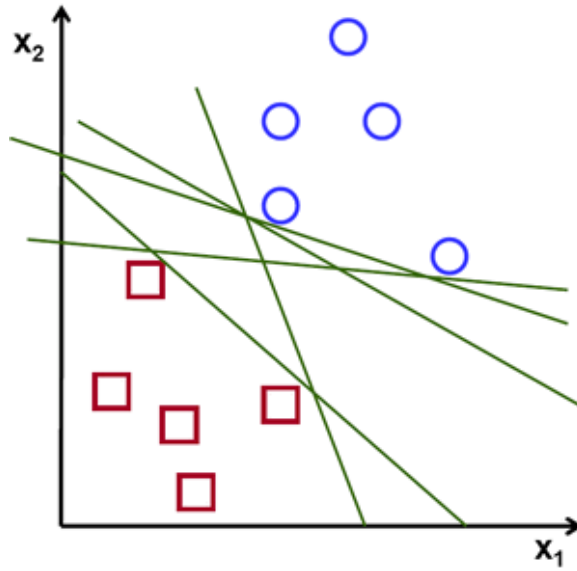
Fig. 5.23. Various possible hyperplanes for the purpose of classification between two specific groups [116].
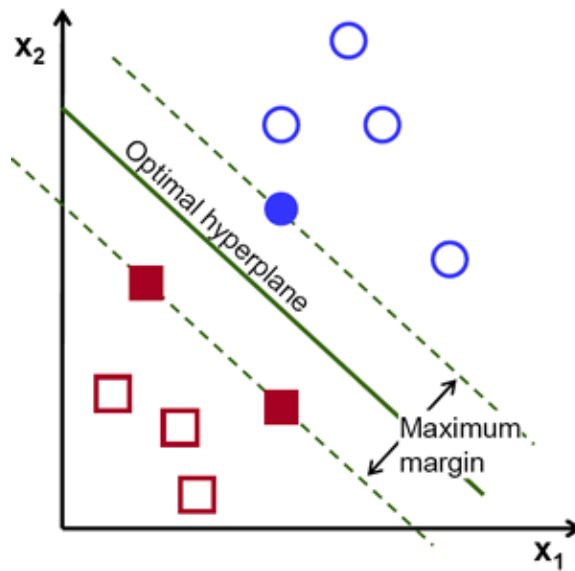
Fig. 5.24. Optimal hyperplane for the purpose of accurate classification between two specific groups [116].

In SVM, by specifying the number of features as N, and considering the value of each feature as the value of a specific coordinates, each data item could be plotted as a point in N-dimensional space. The coordinates of these individual observations are called support vectors

which can be seen in both Fig. 5.23 and 5.24, and the ultimate goal of SVM is to find the best line (hyperplane) that could segregates these data from each other as accurately as possible. Thus, this research is motivated to apply SVM based machine learning algorithm to develop an efficient and reliable protection scheme for wind farm that would differentiate between various types of operations and fault systems on the intertie section of wind farms, coping with system uncertainties such as various wind speeds and loading conditions.

5.3.3.2   Development of SVM-DDPS

For the proposed SVM-DDPS scheme first, a DDPR scheme is designed based on a newly developed generalized formula for relay logic function in order to help the relay to correctly send a tripping signal during the event of a fault. Next, an SVM classifier algorithm is modelled to improve the performance of the proposed differential protection scheme by distinguishing between internal and external faults. Furthermore, the effect of drastic change in wind speed and the corresponding variation in the generated current has also been thoroughly taken into account and properly formulated in the process of SVM machine learning model to maximize the performance of DDPR. Finally, the decision-making algorithm for the proposed hybrid SVM-DDPS scheme is significantly improved by optimizing the SVM model through the utilization of a Bayesian-based optimization technique. Therefore, SVM-DDPS is designed to operate as a decision-making method to distinguish between internal fault, external fault and normal operation for the intertie section of wind farms. Avert maloperation and false tripping during external faults and normal operation and also provide correct tripping during internal fault [117].

In this study, SVM is implemented as a classifier algorithm in order to predict and decide if a differential protection relay should trip the corresponding circuit breaker and disconnect the intertie zone or not for a given condition. Therefore, the developed SVM should be properly trained for various wind speed and generated current conditions during normal operation and fault events. This hypothesis can be successfully realized by introducing four variable inputs such as, wind speed, incoming current and outgoing current from respective CTs, and the difference between the measured currents as a part of DDPR operation. Finally, the output is defined as the proper relay tripping status as formulated below which is identical to the output relay that was earlier proposed for the FPGA-DDPS:

$$
\text{Relay logic} = \begin{cases} 1, & \mid I_1 - I_2 \mid \geq K \left| \frac{(I_1 + I_2)}{2} \right| + I_{\text{pickup}} \\ 0, & \mid I_1 - I_2 \mid < K \left| \frac{(I_1 + I_2)}{2} \right| + I_{\text{pickup}} \end{cases} \tag{5.8}
$$

Thus, the proposed SVM algorithm efficiently learns how a wind farm behaves during various condition with respect to change in wind speed and the generated current profile as shown in Fig. 5.25. Moreover, the training data during internal and external faults is also introduced to the algorithm to be capable of distinguishing between normal operation, internal faults and external faults. At the end, six possible output states are defined for the proposed hybrid SVM-DDPS, classified as: "Trip – Transformer", "No Trip – Transformer", "Warning – Transformer", "Trip – Line", "No Trip – Line", "Warning – Line" as illustrated in Table 5.1 shown below. According to the table, the wind farm intertie transformer and transmission line protection relays are trained in a way that they only operate and send a trip signal if an internal fault has occurred within the defined zone, and will not operate during normal operations, even though the wind speed and current behavior has drastically changed. Moreover, during an external fault, neither the transformer relay, nor the transmission line relay operates and they would only send a warning

signal to indicate that there is an abnormality in the wind farm. A simplified overview of the proposed hybrid SVM-DDPS is shown in Fig. 5. 26.
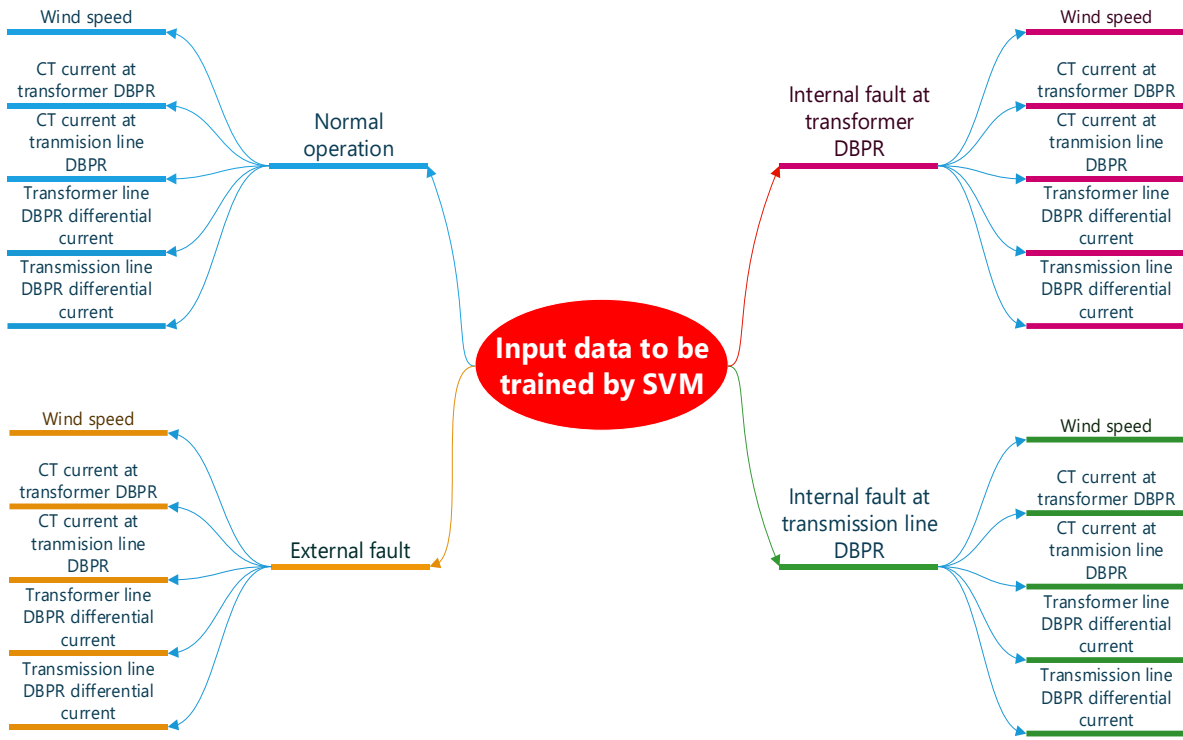
Fig. 5.25. Preparing input data for SVM classification.

Table 5.1: Output classification for training of the proposed SVM

#	Classified Relay Status	Explanation
1	Trip – Transformer	Transformer relay operates during internal fault occurred at the transformer
2	No Trip – Transformer	Normal operation, no fault
3	Warning – Transformer	External fault
4	Trip – Line	Transmission line relay operates during internal fault occurred at the transmission line
5	No Trip – Line	Normal operation, no fault
6	Warning – Line	External fault
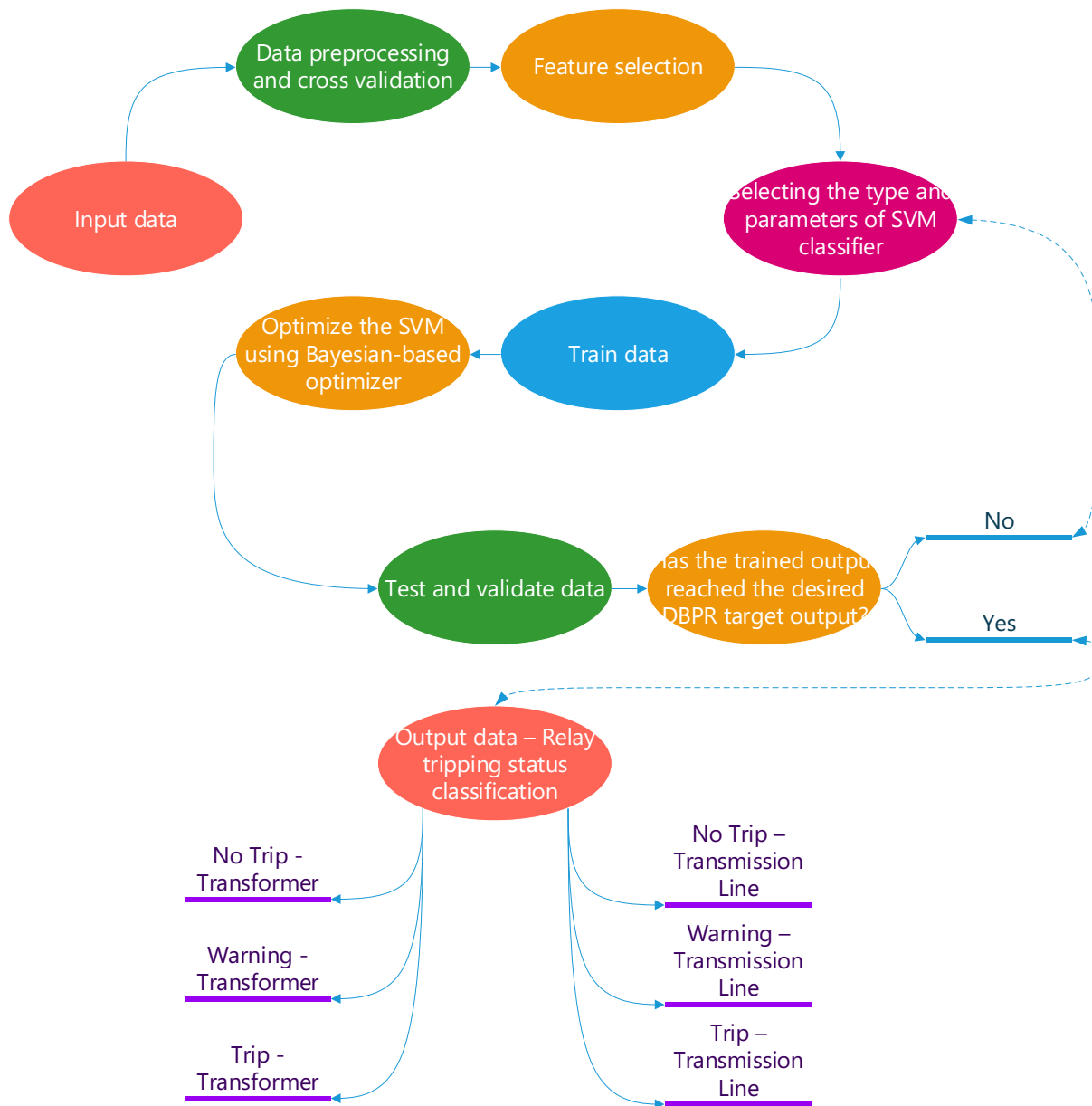
Fig. 5.26. An overview of relay decision making process by the proposed SVM-DDPS protection scheme.

For the sake of understanding the proposed SVM-DDPS a simplified mathematical expression is presented below. Assume, there are binary data (+ and -), and the goal of our protection scheme is to separate these data into two groups (fault, or no-fault) by defining a

hyperplane. So, in the event that SVM classifies the data as "fault", the logic output would be "1", therefore the relay would trip the circuit breaker. On the contrary, in the event that the data are classified as "no-fault", then the logic output would be "0", and the relay would not trip. Thus, by considering "w" as a perpendicular line to the median, and considering "u" as the data we would like to classify, therefore it is obvious that the dot product of (w . u) would represent scalar projection of u onto w. And for the cases that (w . u) is greater than a constant "c", then it actually crosses the median line, therefore it is mathematically sensible to write [118]:

$$w \cdot u \geq c \tag{5.9}$$

$$\Rightarrow \quad w \cdot u + b \geq 0 \tag{5.10}$$

Where u is +, and by considering a constant "b", c = -b.

Now by introducing a positive sample as x^+ and also a negative sample as x^-, we can introduce more constraints on the classification between "fault" and "no-fault" in the protection zone and hence we shall have:

$$w \cdot x^+ + b \geq 1 \tag{5.11}$$

$$w \cdot x^- + b \geq -1 \tag{5.12}$$

Now in order to simplify the mathematical model for the above classification scenario for protective relays, a new variable as y_i is introduced and its value behaves as shown below:

$$y_i = \begin{cases} +1, & for + data \\ -1, & for - data \end{cases} \tag{5.13}$$

As a result, the equations 5.11 and 5.12 are simplified for any x_i as:

$$y_i \left(x_i \cdot w + b \right) \geq 1 \tag{5.14}$$

$$\Rightarrow\ y_i\,(x_i\,.\,w + b) - 1 \geq 0 \qquad\qquad (5.15)$$

So far, the margin between "fault" and "no-fault" incidents are well classified, however, the ultimate goal for power system protection engineers is to make sure the relay always detects the fault, no matter what! Thus, the protection scheme should be able to discriminate between "fault" and "no-fault" incidents with the highest accuracy. In order to do that, the width between these two types of data which are gathered from wind farms CTs and fed to the SVM, should be as maximum as possible to avoid any relay maloperation and false tripping. So, by defining a width between these two positive and negative margins, we shall have:

$$Width = (x^+ - x^-)\,.\,\frac{w}{\|w\|} \qquad\qquad (5.16)$$

Where, $\|w\|$ is the magnitude of the vector "w", and the term $\frac{w}{\|w\|}$ is added to the equation to turn the w term in to unit vector. The assumption here is that one data point will exactly satisfy the upper constraint and one will satisfy exactly the negative constraint with equality. By referring to equation 5.15, and considering it in 5.16, the above equation is revised as shown below:

$$Width = \frac{(1-b)+(1+b)}{\|w\|} \qquad\qquad (5.17)$$

Or in other words:

$$Width = \frac{2}{\|w\|} \qquad\qquad (5.18)$$

Therefore, the goal would be to maximize the $\frac{2}{\|w\|}$, which means minimizing the magnitude of w, $\|w\|$. And to make it mathematically convenient, minimization of $\frac{\|w\|^2}{2}$ should be considered. There are several possible methods in order to perform the minimization of this term, such as employing quadratic programming (QP), verification by using the Karush-Kuhn -Tucker (KKT)

conditions, or using modified Lagrange multipliers (MLP) method. However, in this work, the MLP approach is implemented for the purpose of minimization of the width. Thus, by implementing the MLM a new term is defined as:

$$L = \frac{1}{2} \|w\|^2 - \sum_i \alpha_i \left[y_i \left(x_i . w + b \right) - 1 \right] \tag{5.19}$$

In this equation the second term is added with the purpose of adding constraints in a way that the constraints in brackets would be restricted to zero. Now by differentiating the expression of 'L' with respect to 'w' and 'b' and equating those to zero the following expressions can be found:

$$\frac{d}{dw} L = w - \sum \alpha_i \, y_i \, x_i = 0 \tag{5.20}$$

$$w = \sum \alpha_i \, y_i \, x_i \tag{5.21}$$

$$\frac{d}{db} L = \sum \alpha_i \, y_i = 0 \tag{5.22}$$

$$\sum \alpha_i \, y_i = 0 \tag{5.23}$$

Now by placing the above equations back in equation 5.19, the minimization problem would be abridged as follows:

$$L = \frac{1}{2} \left[\sum \alpha_i \, y_i \, x_i \right] . \left[\sum \alpha_j \, y_j \, x_j \right] - \left[\sum \alpha_i \, y_i \, x_i \right] . \left[\sum \alpha_j \, y_j \, x_j \right] - \sum \alpha_i \, y_i \, b - \sum \alpha_i \tag{5.24}$$

$$L = - \sum \alpha_i - \frac{1}{2} \sum_i \sum_j a_i \, a_j \, y_i \, y_j \left(x_i \cdot x_j \right) \tag{5.25}$$

Finally, for any unknown data to be classified, for example u, the decision rule for any u that is + would be:

134

$$\sum_i \alpha_i \; y_i \; (x_i . u) \; + \; b \geq 0 \tag{5.26}$$

The above expression still has the x term, or to be more accurate, $\varphi(x)$ which is the mapping the point on a complex feature space x. Equation (5.26) can be easily solved by Kernelization method or in other words utilizing Kernel trick. This method avoids the explicit mapping that is required to enable the machine learning algorithm to learn a nonlinear function or decision boundary. In Kernel trick, the mapping occurs as a dot product in both training as well as testing. Every kernel function can be expressed as a dot product in a possibly infinite dimensional feature space, which is based on Mercer's theorem [119]. So for all the x and y in the input space φ, certain function k (x , y) can be expressed as an inner product in another space, for example ψ. where since k (x , y) is equivalent to the dot product of the mapping, we can avoid explicit mapping to the higher dimension. Thus, it can be simply shown as:

$$w: \; \varphi \rightarrow \psi \tag{5.27}$$

$$k \; (x , y) = (w(x) , w(y)) \; \psi \tag{5.28}$$

Now according to the definition of the Kernel, by considering x_i and x_j, and substituting these values:

$$\varphi^T(x_i) \; \varphi(x_j) = k \; (x_i, x_j) \tag{5.29}$$

By substituting (5.29) back into (5.25), and considering the defined Kernel approach to SVM, the new equation would be:

$$L = - \sum \alpha_i - \frac{1}{2} \sum_i \sum_j a_i \; \alpha_j \; y_i \; y_j \; \varphi^T(x_i) \; \varphi(x_j) \tag{5.30}$$

$$\rightarrow L = - \sum \alpha_i - \frac{1}{2} \sum_i \sum_j a_i \, \alpha_j \, y_i \, y_j \, k \left(x_i, x_j \right) \qquad (5.31)$$

And again, as for similar case as explained earlier in equation (5.26), for any unknown data to be classified, for example u, by using Kernel approach for SVM:

$$w^T \varphi(x) = \left[\sum_i a_i \, y_i \, \varphi(x_i) \right]^T \varphi(x) \rightarrow \Sigma_i \, a_i \, y_i \, \varphi^T(x_i) \varphi(x) \rightarrow \Sigma_i \, a_i \, y_i \, k(x_i, u) \qquad (5.32)$$

Thus, the SVM-DDPS would be able to classify any given data either as "fault", "no-fault" or "warning", and for the data that is classified as fault, the output of the intelligent controller would be "1" and quite opposite, for the data that is classified as no fault, the output of the protection scheme would be "0". Also, for the data that is classified as "warning", still the output of the protection scheme would be "0", however the warning signal is still sent to indicate the there is still an external fault or abnormality in the system, but the specific differential relay is not responsible to take any action as the fault is outside its protection zone. Therefore, in this case, the closest relay to the fault location would trip, and only the limited faulty section is disconnected from the power grid, not the entire wind farm. Finally, these digital logic data would be sent to the respective circuit breakers located on the intersection of wind farm, and based on the decision made by SVM-DDPS, it would accordingly trip or not.

5.3.3.3 Further Improvement of SVM Classification Accuracy

In this section, two different approaches are conducted in order to improve the classification accuracy of the SVM. First, several different types of Kernel function are defined and implemented for SVM classification process, the second approach is to use an optimization technique to find the optimal hyperplane.

There are various types of Kernel functions available, however in this work with the focus on SVM classification for differential relay, and fast operation required for SVM processing implemented for the relays, 5 different types of nonlinear Kernel function named as coarse Gaussian, fine Gaussian, medium Gaussian, quadratic and cubic functions are selected and defined in Table 5.2 [120]. These functions are then used in the SVM training process as was defined in the previous section, to test the classification accuracy for various fault location conditions. The results of the training performance and their analysis are presented in section 5.3.3.5.

Table 5.2: Defined functions for each type of Kernel approach for SVM [120]

Type of SVM Kernel function	Function
Coarse Gaussian	$k(x,y) = \exp\left(-\frac{\|x-y\|^2}{2\sigma^2}\right) = \exp\left(-\Upsilon\|x-y\|^2\right)$ σ or Υ are adjustable parameter which defines coarse, fine and medium Gaussian types. For coarse Gaussian, $\Upsilon = 4\sqrt{n}$ is considered. Also, n is the number of features or the dimension size of x.
Fine Gaussian	$k(x,y) = \exp\left(-\frac{\|x-y\|^2}{2\sigma^2}\right) = \exp\left(-\Upsilon\|x-y\|^2\right)$ For fine Gaussian, $\Upsilon = \sqrt{\frac{n}{4}}$
Medium Gaussian	$k(x,y) = \exp\left(-\frac{\|x-y\|^2}{2\sigma^2}\right) = \exp\left(-\Upsilon\|x-y\|^2\right)$ For medium Gaussian, $\Upsilon = \sqrt{n}$
Rational Quadratic	$k(x,y) = 1 - \dfrac{\|x-y\|^2}{\|x-y\|^2 + c}$ c: constant, where $c \geq 0$
Cubic (General form for degree "d" Polynomial)	$k(x,y) = (\alpha x^T y + c)^d$ α: Slope, adjustable parameter d: Polynomial degree c: constant, where $c \geq 0$

The classifier algorithm of the proposed SVM scheme is further optimized to find the optimal separating hyperplane by way of maximizing the margins between data and hence, minimizing the error in order to properly classifies the training data. In other words, the relay

operates more reliably with respect to various wind farm conditions. There are several optimization models available for achieving optimal hyperparameter where the most common methods are: grid search, random search, gradient-based and evolutionary optimization models. However, these optimization methods have a tendency to roam the full space of available parameter values by ignoring the attained past results. Consequently, it would be extremely time consuming to optimally tune the parameters, most specifically for large-scale wind farms that requires enormous parameters spaces. In this work, Bayesian-based optimization model is utilized as it inherently diminishes the time spent to obtain the best possible set of parameters by taking into account information on the hyperparameter combinations it has seen. Therefore, this method is faster, more efficient and is able to achieve smaller validation set errors compared to previous optimization methods.

Hyperparameter tuning is an optimization problem where the objective function of optimization is unknown or a black-box function. Traditional optimization techniques like Newton method or gradient descent cannot be applied. However, Bayesian optimization is a very effective optimization algorithm in solving this kind of optimization problem [121]. Bayesian-based optimization only considers the previously obtained results to create a probabilistic model mapping hyperparameters that provides a score on the objective function: P (score | hyperparameters). This model is known as surrogate. The hyperparameter optimization can be formulated as explained below:

If f(x) is defined as an acquisition function, which determines the sampling points in the search space, the goal would be maximizing the acquisition function in order to find the next sampling point. For a given inputs x, y, the samples would be [122]:

$$D_{1:\,t-1} = \{(x_1,\, y_1),\, ...,\, (x_{t-1},\, y_{t-1})\} \tag{5.33}$$

138

Therefore, the hyperparameter optimization function is defined as:

$$x_t = arg\ max_x\ u\ (x\mid D_{1:t-1})$$ (5.34)

Bayesian optimization operation is based on the Bayes' theorem, meaning that for a given evidence data E, the posterior probability P (M | E) of a model M is proportional to the likelihood P (E | M) of overserving E given model M multiplied by the prior probability of P (M). The above statement is the core idea of Bayesian optimization, which can can be expressed as:

$$P\ (M\mid E) \sim P\ (E\mid M)\ P\ (M)$$ (5.35)

The principle of Bayesian optimization is to combine the prior distribution of the function f(x) with the sample information or in other words, evidence, to obtain the posterior of the function. Thereafter, the posterior information is used to find where the function f(x) is maximized according to a criterion. The criterion is represented by a utility function u which is also called acquisition function. The function u is used to determine the next sample point in order to maximize the expected utility. When searching the sampling area, it is necessary to take into account both explorations, meaning sampling from the areas of high uncertainty, and also exploitation, meaning sampling from that with high values [123]. That will help to reduce the number of sampling. Furthermore, the performance might be improved even when the function has multiple local maxima. In addition to the sample information, Bayesian optimization depends on the prior distribution of the function f, which is an indispensable element in the statistical inference of the posterior distribution of the function f. A priori distribution does not have to be an objective basis, either partially or entirely based on subjective beliefs. It is generally assumed that Gaussian process is well suited to the prior distribution of Bayesian optimization. Gaussian process is highly flexible

and easy to handle, so Bayesian optimization applies Gaussian process to fit data and update the posterior distribution.

The process of Bayesian-based optimization for SVM is commenced repeatedly, where the overview of the process is conducted in the following stages:

1. For $t = 1, 2, 3 \ldots$

2. Maximize the acquisition function over Gaussian Process (GP) in order to find the next sampling point x_t, where $x_t = arg\ max_x\ u\ (x \mid D_{1:\ t-1})$.

3. Sample the objective function $y_t = f(x_t)$, in other words, create a "noisy" sample $y_t = f(x_t) + e_t$ from $f(x_t)$.

4. Add the obtained sample with the previous samples, where, $D_{1:\ t} = \{D_{1:\ t-1}, (x_t, y_t)\}$ and GP is updated accordingly (updates the posterior of function f).

5. End

The GP mentioned above, is a generalization of the Gaussian probability distribution, whereas a probability distribution describes random variables which are scalars or vectors (for multivariate distributions), a stochastic process governs the properties of functions [124]. GP assumes that similar input produces similar output, and thus assumes a statistical model of the function. The same as Gaussian distribution defined by mean and covariance, GP is similarly defined by its mean function m, and its covariance function k. Therefore, the GP process is denoted as:

$$f(x) \sim GP(m(x), k(x, y)) \tag{5.36}$$

For convenience, it is assumed that the GP mean function $m(x) = 0$. For the covariance function k, the exponential square function is a popular choice, thus:

$$f(x) \sim GP\ (m\ (x)\ ,\ k\ (x\ ,\ y))\tag{5.37}$$

$$k\ (x_i\ ,\ x_j) = exp\ (-\ 1/2\ \left\|x_i - x_j\right\|^2)\tag{5.38}$$

Where the same as we had earlier, x_i and x_j are the ith and jth samples. As x_i and x_j get

closer to each other, the value of k, approaches 1, and quite on the contrary, as x_i and x_j get farther

away from each other, the value of k, gets closer to 0. When two sampling points are close to each

other, they have a strong correlation and a mutual influence; when they get further apart, the mutual

influence is weak.

In order to determine the posterior distribution of f (x), at first, sample t observations as the

training set $D_{1:t} = \{x_n\ ,\ f_n\}$, where $f_n = f(x_n)$ are considered. It is assumed that the function values

f are drawn according to the multivariate normal distributions f ~ (0 , K), where K is the matrix of

all different x_i and x_j, and each element k in this matrix is simply computed according to equation

(5.38) as was defined earlier. The function k measures the degree of approximation between two

samples. Obviously, the diagonal element k $(x_i\ ,\ x_j) = 1$ without considering the effect of noise.

Finally, based on the function f, the function value $f_{t+1} = f(x_{t+1})$ at the new sample point x_{t+1} is

computed. According to the assumption of Gaussian process, $f_{1:t}$ in the training set plus the

function value f_{t+1} follows the t + 1 dimensional normal distribution as shown below:

$$\left| \begin{matrix} f_{1:t} \\ f_{t+1} \end{matrix} \right| \sim N\ (0\ ,\ \left| \begin{matrix} K & k \\ k^T & k(x_{t+1}\,,x_{t+1}) \end{matrix} \right|)\tag{5.39}$$

Where, $f_{1:t} = [f_1, f_2, ..., f_t]^T$ and $k = [k(x_{t+1}\,, x_1, k(x_{t+1}\,, x_2, ..., k(x_{t+1}\,, x_t]$. Moreover, f_{t+1}

simply follows the normal distribution, meaning $f_{t+1} \sim N\ (\mu_{t+1}\ ,\ \sigma_{t+1}^2)$. By referring to the properties of

the join Gaussian, normal distribution:

$$\mu_{t+1}\ (x_{t+1}) = k^T\ K^{-1}\ f_{1:t}\tag{5.40}$$

$$\sigma^2_{t+1}(x_{t+1}) = -k^T K^{-1} k + k(x_{t+1}, x_{t+1}) \tag{5.41}$$

It is obvious from the above equations that GP does not return a scalar value for $,f_{t+1},$ instead it returns the probability distribution over all possible values of f_{t+1}. If the training set is large enough, GP is able to obtain a decent estimate of the function f (x) distribution.

After finding the posterior distribution of the objective function, Bayesian optimization utilizes the acquisition function u to derive the maximum of the function f. Usually, it is assumed that the high value of the acquisition function corresponds to the large value of the objective function f. As a result, maximizing the acquisition function is the same as to maximizing the function f. Meaning that $x^+ = $ arg $\max_x$ u (x | D) which is very similar to what was earlier defined in equation (5.34).

There are three major functions used for acquisition function (f): Upper Confidence Bound (UCB), Maximum Probability of Improvement (MPI) and Expected Improvement (EI), where the latter is more efficient and is used in this work. Therefore, EI is expressed as below:

$$EI\ (x) = E\ (max\ (f\ (x) - f\ (x^+),\ 0)) \tag{5.42}$$

where, the values for the best samples are defined as f (x+) and the location of the sample is x+. The evaluation of EI is then represented as:

$$EI\ (x) = (\mu(x) - f\ (x+) - \varepsilon)\ \alpha(z) + \sigma(x)\ \beta(z) \tag{5.43}$$

Where in the following formula, Z is defined as:

$$Z = \frac{\mu(x) - f\ (x+) - \varepsilon}{\sigma(x)} \tag{5.44}$$

In the above equations, $\mu(x)$ and $\sigma(x)$ are the mean and standard deviation, respectively, while α and β are the cumulative distribution function (CDF) and probability density function (PDF) of the standard distribution. Finally, ε is a small constant parameter that is chosen as 0.01.

The process continues until maximum iterations or, the error has been minimized where no more improvement can be achieved. At this point, the SVM hyperparameter is successfully trained and optimized by Bayesian-based optimization method, and can contribute to significant improvement of DBPR performance with respect to the wind farm various operation modes as will be shown in section 5.3.3.5.

5.3.3.4   Wind Farm Model under SVM-DDPS Evaluation Study

For simplicity of the design and also for faster and smoother simulation analysis, an aggregated model of the wind farm that was studied earlier for both overcurrent and differential protection is considered where all the 40 DFIG wind turbines are modelled as only one wind turbine, which is a common practice among researchers for conducting fault analysis and protection study. The simplified version of designed wind farm model for intuitive comprehension is illustrated in Fig. 5.27. Circuit Breakers are indicated as CB1 to CB5 where CB3 and CB4 are the intertie breakers that are exclusively responsible for disconnecting the power transformer and transmission line, respectively, by receiving tripping signal from the developed digital DBPR scheme during internal fault incidence as shown in the figure. Moreover, a grounding transformer is also installed next to the intertie line in order to manage the unbalanced load on the power system as well as to handle high magnitude of excessive current during ground faults by providing a

grounding path. The designed ML protection scheme for the wind farm under study is shown in Appendix A.18.
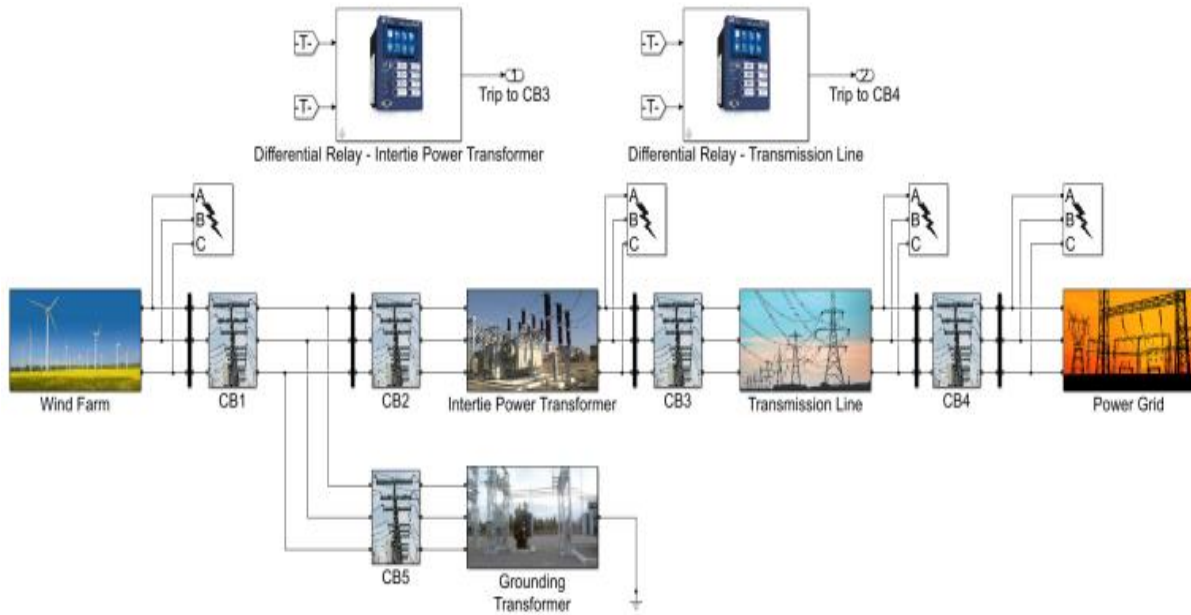
Fig. 5.27. Large-scale centralized DFIG-based aggregated wind farm model.

5.3.3.5   Training Performance of the Proposed SVM-DDPS

In order for training of the proposed SVM based DDPS several types of Kernel functions such as, coarse Gaussian, fine Gaussian, medium Gaussian, quadratic and cubic functions are chosen. The performance of these Kernel functions is compared to see their effectiveness for fault classification and training efficiency for various wind farm operation modes such as, normal operation, external and internal fault conditions. The corresponding results are shown in Figs 5.28 – 5.34.

It is seen from Fig. 5.28 below that the coarse Gaussian SVM is only successful in detecting external faults, meanwhile it failed to detect internal faults for transmission line and had a disappointing 17% success rate for the transformer. On average, it can achieve only 60% accuracy rate which is not acceptable for a high-performance DDPR.
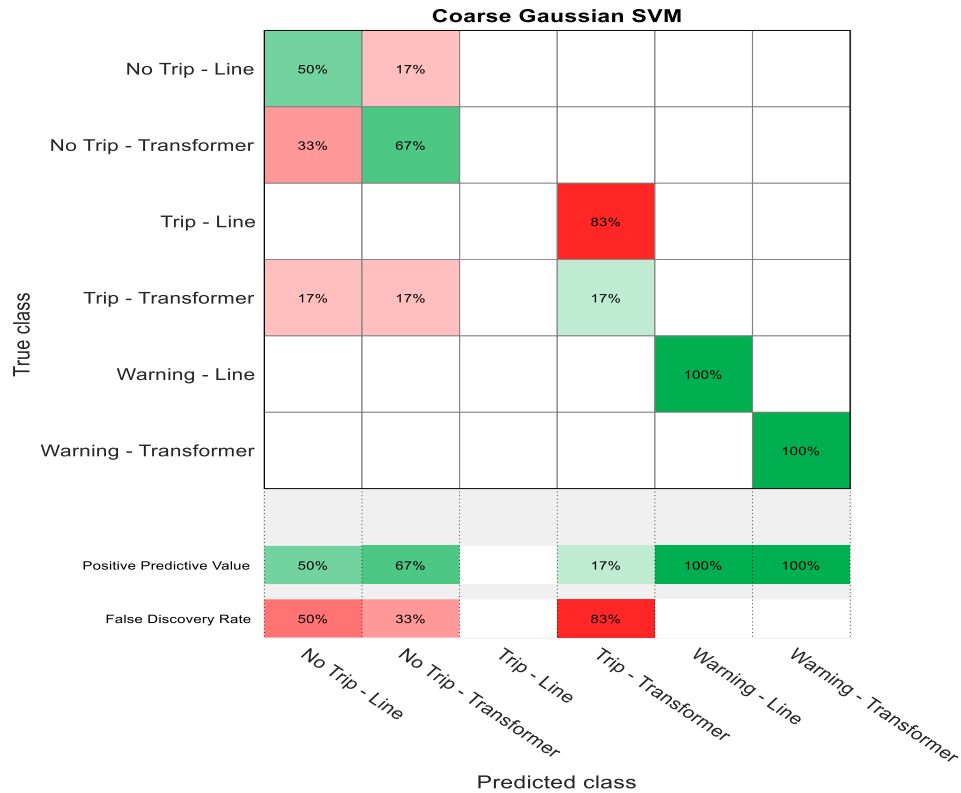
Fig. 5.28. Performance validation for Coarse Gaussian SVM.

Again, the fine Gaussian SVM successfully detects all internal faults for both the transformer and transmission line which can be seen from the Fig. 5.29 below. However, the success rate for detecting the external faults is only 40% and hence, not reliable for protection of wind farm intertie section.
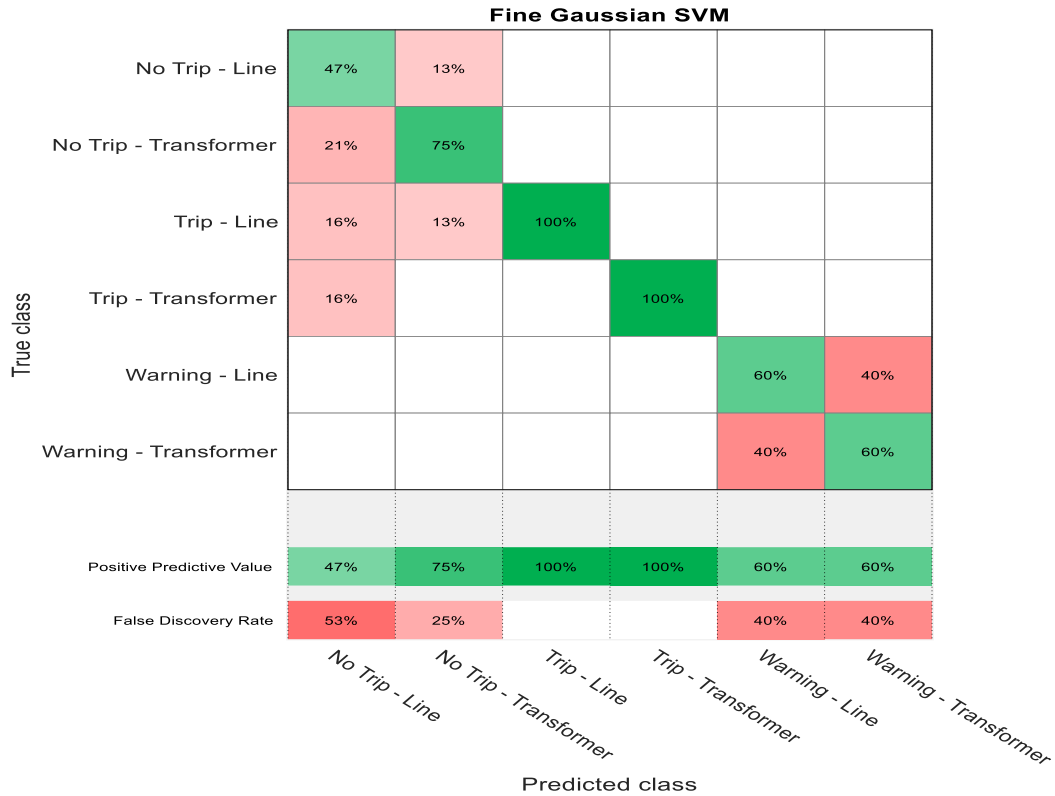
Fig. 5.29. Performance validation for Fine Gaussian SVM.

Satisfactory results as shown in Figs. 5.30 – 5.32 were attained by using three different SVMs including medium Gaussian, quadratic and cubic SVM where the accuracy rate accomplished for these methods were 90%, 92.5% and 95%, respectively. They were all 100% successful for tripping during internal faults, however, only medium Gaussian and cubic SVM managed to detect the external properly, while the quadratic SVM failed to identify 17% of external faults for the power transformer. However, these SVM techniques failed to provide a satisfactory result when the wind speed was drastically changing, which is still considered as normal operation for wind generators.
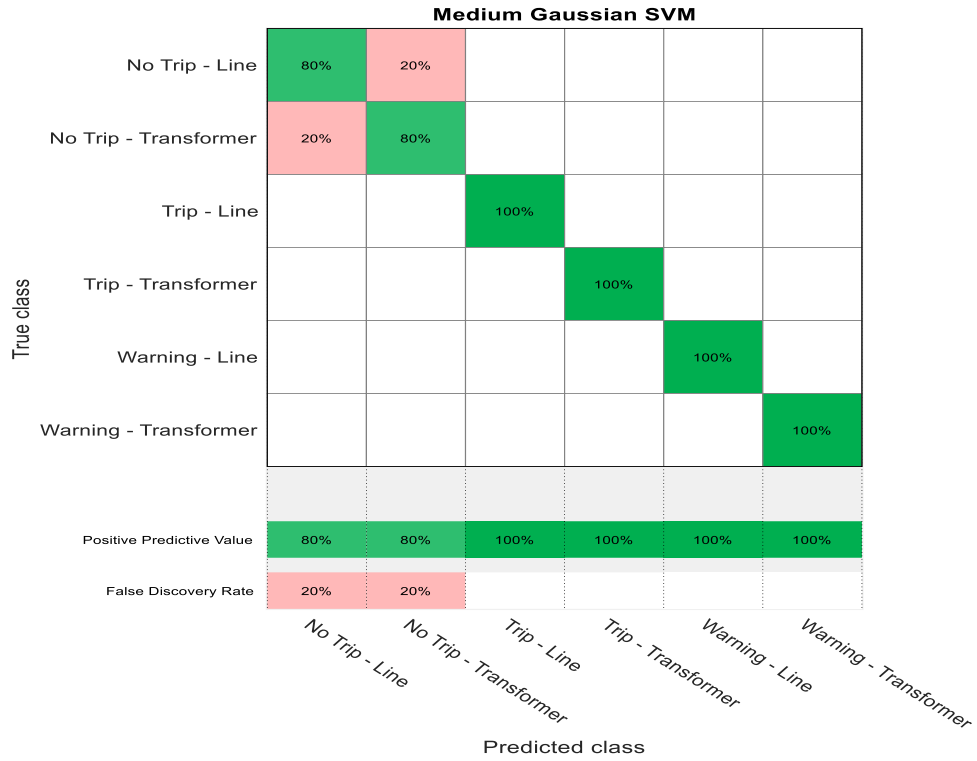
Fig. 5.30. Performance validation for Medium Gaussian SVM.
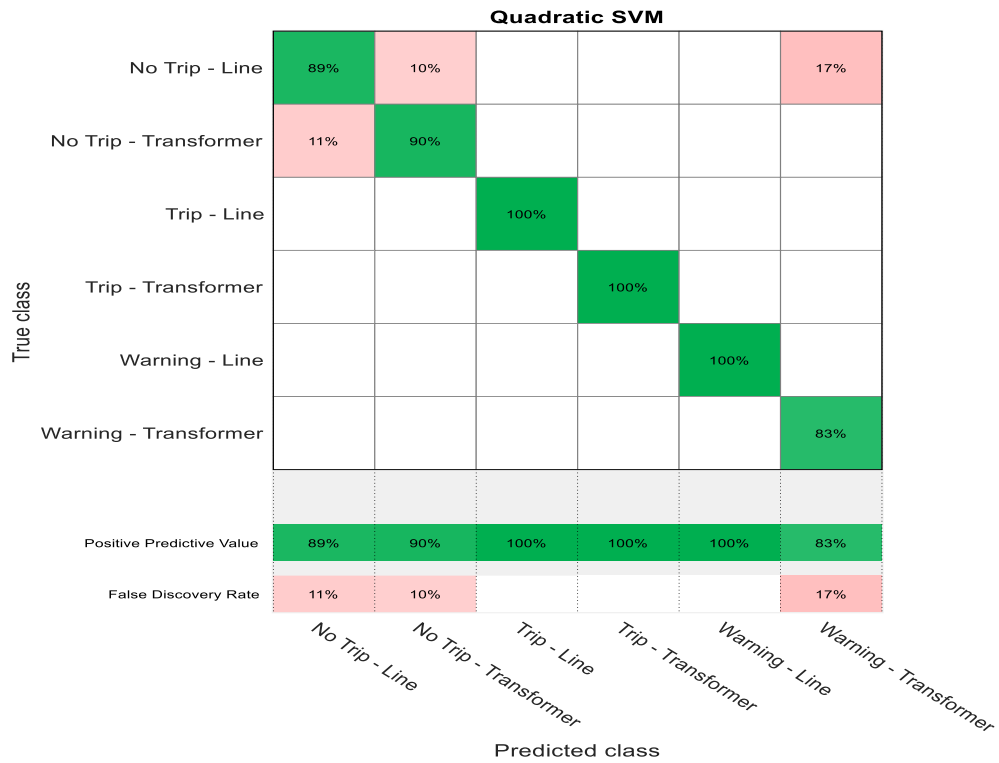
Fig. 5.31. Performance validation for Quadratic Gaussian SVM.
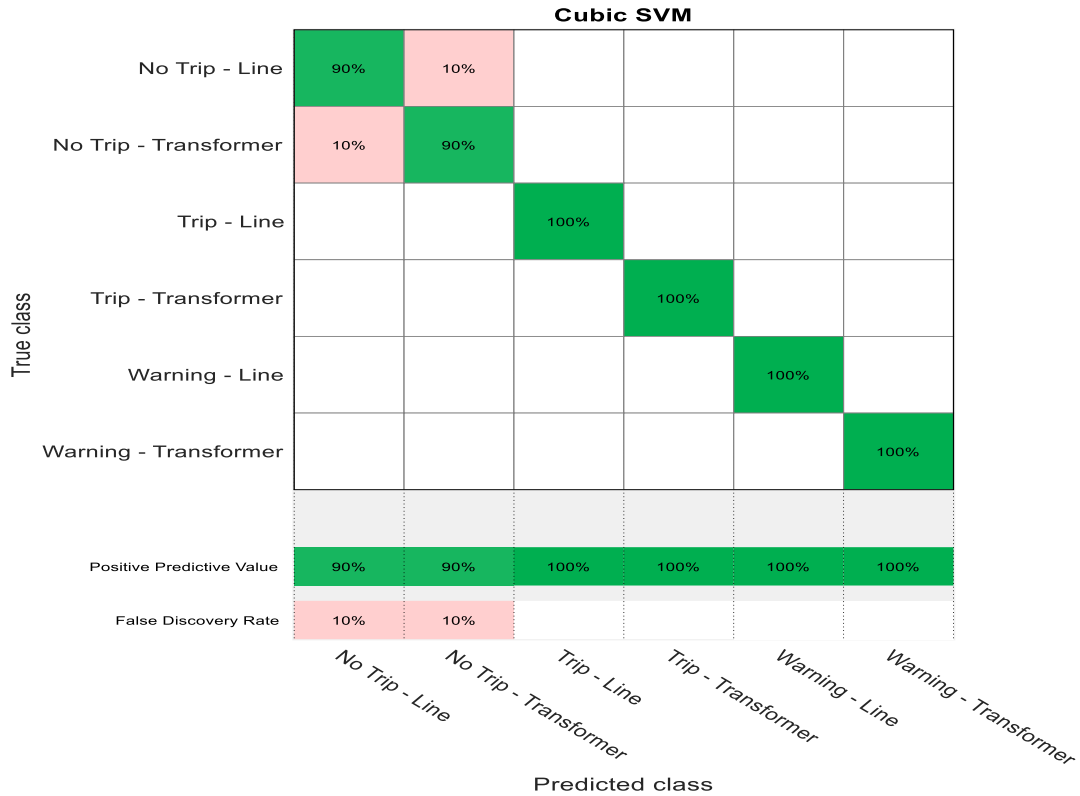
Fig. 5.32. Performance validation for Cubic Gaussian SVM.

Therefore, in this work a Bayesian-based optimization technique is used to find the best hyperparameter for SVM that result in improving the training process by minimizing both the observed and predicted errors. The maximum number of iterations is set to be 30 and minimum classification errors and best hyperplane for SVM are achieved only after 16 iterations, which is shown in Fig. 5.31. It is found from Fig. 5.32 that the performance of Bayesian-based optimization method is significantly better than any previous methods. It successfully trips the transformer and transmission line relays during the corresponding internal faults and sends a warning signal during external faults. It is also tested for a drastic change in wind speed and the proposed Bayesian-based optimization method for SVM achieves a success rate of 100% and 91% for power transmission line and power transformer DBPRs operations, respectively. The average accuracy rate of the

148

proposed Bayesian-based optimized SVM-DDPS is found to be 97.5%. Although this performance is greatly acceptable, it should be noted that the accuracy of protection schemes should be extremely high and cannot afford to misclassify any normal condition in the grid as a fault condition and vice versa. Therefore, the accuracy of any protection scheme should be as close to 100% as possible. Although, it may not be practically feasible to reach to this ultimate level of accuracy, it may be possible to reach near this high accuracy by improving the training data which are fed to the machine learning algorithm. In order to do that, in this work the principal component algorithm (PCA) method was implemented to improve the training process, hence increasing the accuracy of the SVM. PCA is essentially a common method in machine learning that aims to reduce the dimensionality of large set data sets by transforming a large set of variables and features into a smaller one that could still maintain the essential information. In other words, its an effective method that attempts to simplify the data by getting rid of repetitive and redundant data, hence, it would enhance the ML training process. The PCA mathematical approach is out of scope of this research, and the application of such technique is used in this research. All the mathematical derivation are fully documented in [125], therefore it is not mentioned here again.

In this work, after implementing PCA, the previously mentioned Bayesian-based optimized SVM was analyzed again and as expected, improved operation by the SVM-based protection scheme was resulted which are presented in Fig. 5.35 and 5.36. The improved optimization process of the proposed Bayesian-based SVM after implementing PCA is shown in Fig. 5.35, and compared to the previous SVM method without applying PCA (Fig. 5.33), it is evident that training process and optimization of SVM has been improved in terms of finding the best point hyperparameter. Furthermore, the actual performance validation for the SVM-based protection scheme after implementation of PCA is shown in Fig. 5.36, where compared to the one without

PCA (Fig. 5.34), it can be clearly seen that accuracy of the proposed protection scheme has been improved and almost no misclassification is observed. The accuracy attained is 99.8% which is a relatively good performance, where compared to the one without PCA (accuracy 97.5%), a 2.3% improved accuracy was achieved. This improvement in accuracy is very important since the relays shall never have a false tripping and the misclassification should be avoided as much as possible. Thus, the proposed protection scheme has achieved the salient objective of this research.

The comparison summary among different classifier techniques conducted in this research is shown in Table 5.3. Also, the performance of the proposed SVM was also compared with other common ML techniques such as: Decision trees, K-nearest neighbour, Naïve Bayes, boosted trees and random forest, which are tabulated in Table 5.4. Thus, the proposed scheme can be utilized as an intelligent and adaptive machine learning-based protection scheme for providing improved security and reliability for intertie section of wind farms.
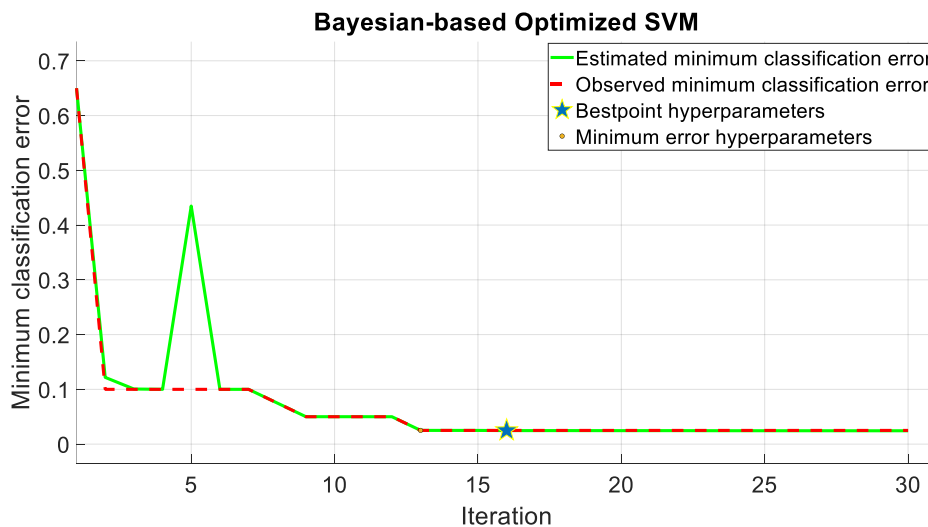
Fig. 5.33. Optimization process of Bayesian-based SVM.
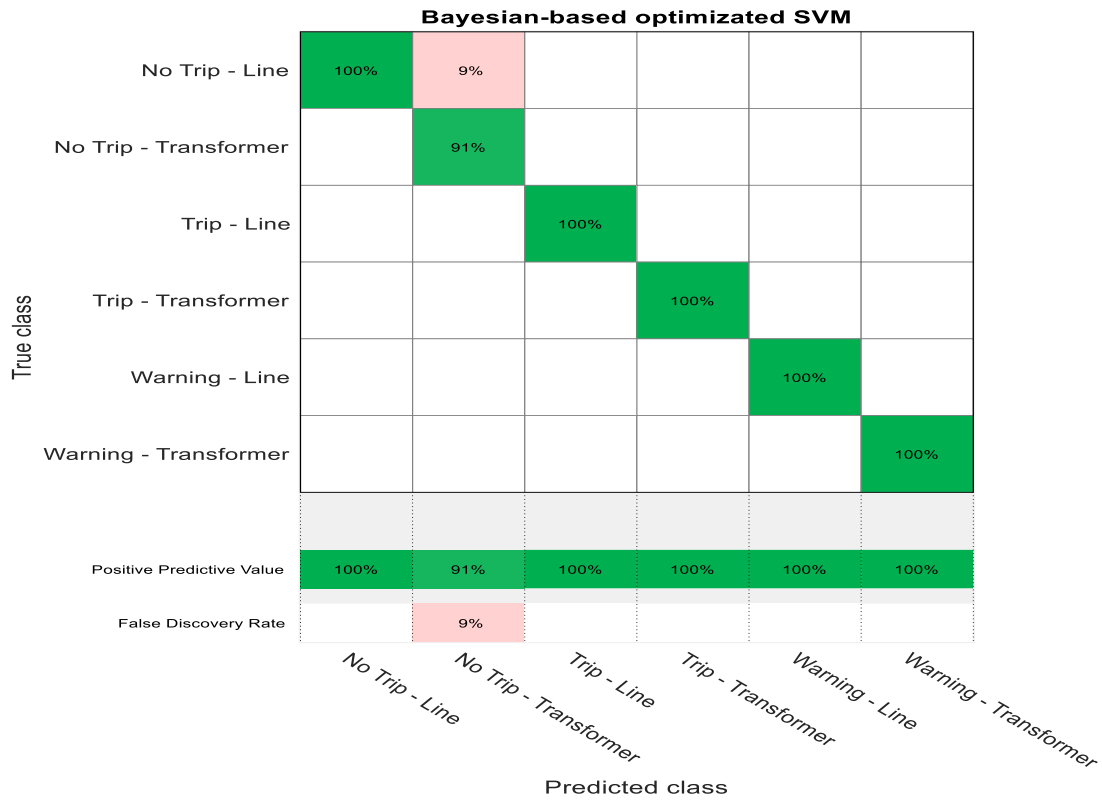
Fig. 5.34. Performance validation for Bayesian-based optimized SVM.
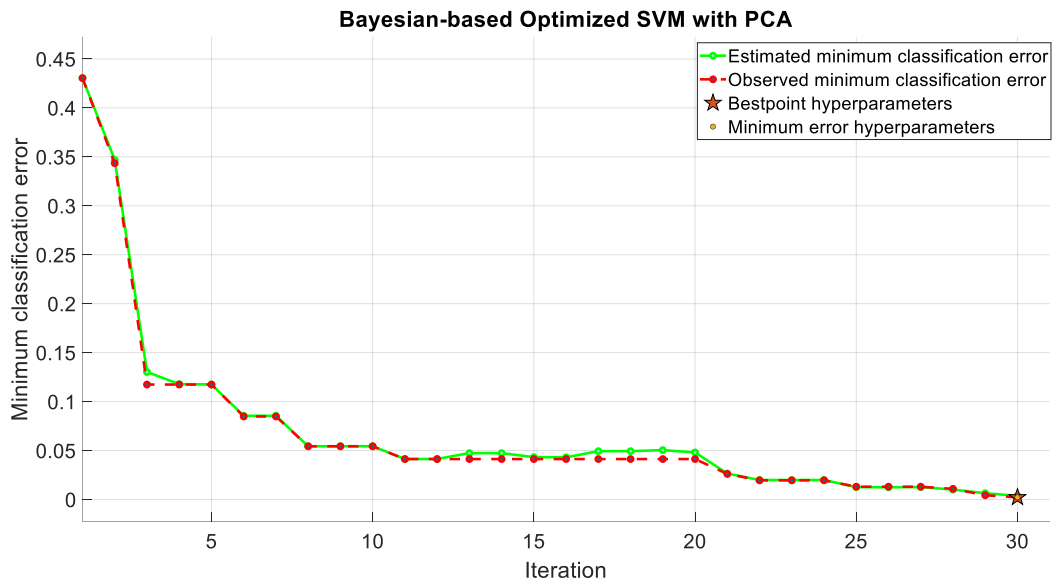
Fig. 5.35. Improved optimization process of Bayesian-based SVM after implementation of PCA.

151

Bayesian-based Optimized SVM with PCA

True class						
No Trip - Line	100%	<1%				
No Trip - Transformer		>99%				
Trip Line			100%			
Trip Transformer				100%		
Warning Line					100%	
Warning Transformer						100%
Positive Predictive Value	100%	>99%	100%	100%	100%	100%
False Discovery Rate		<1%				

Predicted class
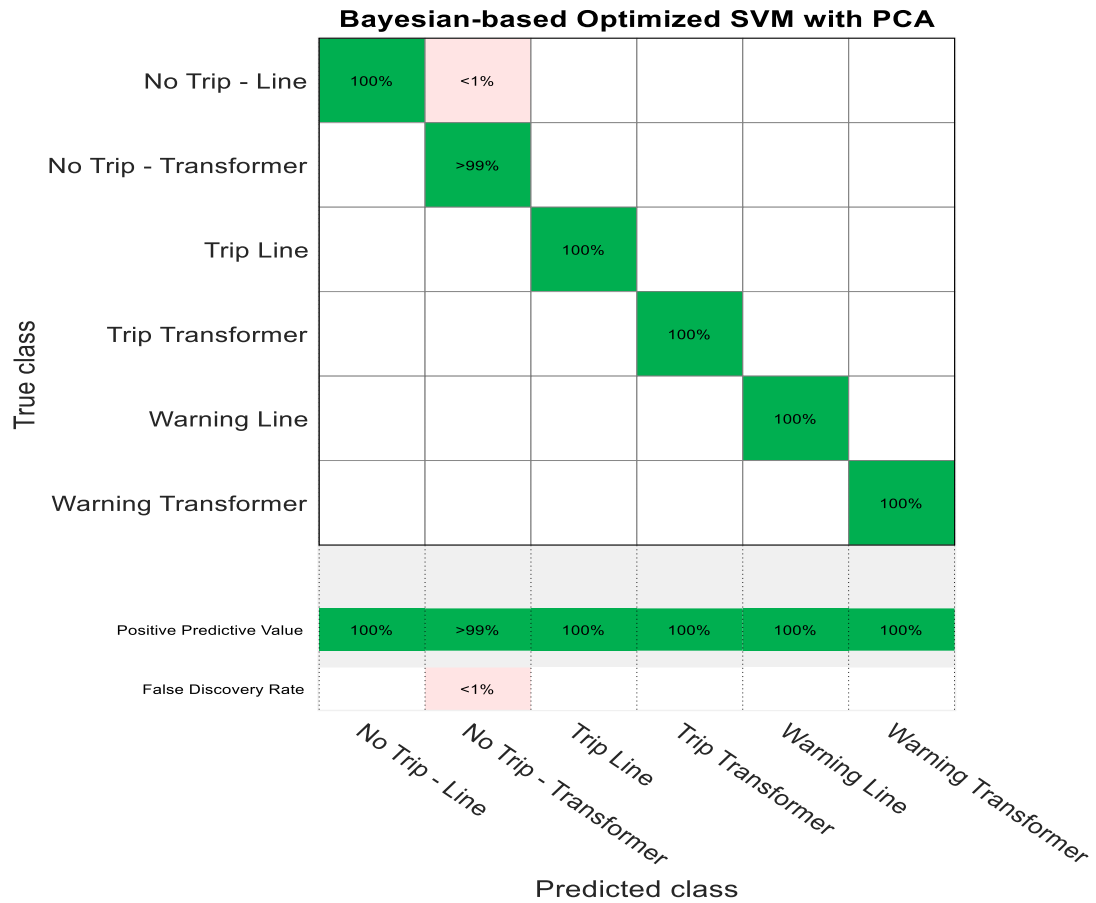
Fig. 5.36. Performance improvement of Bayesian-based optimized SVM after implementation of PCA.

Table 5.3 Comparison among various classifier-based training of SVM

#	SVM Classification Method	Accuracy Rate (%)	Ranking
1	Coarse Gaussian SVM	60%	Worst
2	Fine Gaussian SVM	65%	-
3	Medium Gaussian SVM	90%	-
4	Quadratic SVM	92.5%	-
5	Cubic SVM	95%	-
6	Bayesian-Based Optimized SVM	97.5%	
7	Bayesian-Based Optimized SVM with PCA	99.8%	Best

152

Table 5.4 A comparison between the proposed SVM-DDPS and other popular ML classification techniques

#	ML-based Classification Techniques	Prediction Speed	Training Speed	Memory Usage	Accuracy Rate (%)
1	Decision Trees	Fast	Fast	Small	45%
2	K-Nearest Neighbour	Medium	Slow	Medium	65%
3	Naïve Bayes	Fast	Fast	Medium	88%
4	Boosted Trees	Medium	Slow	Large	93%
5	Random Forest	Medium	Medium	Medium	95%
6	Bayesian-Based Optimized SVM	Fast	Very Slow	Medium	99.8%

5.4 A Comparison between the Real-time Performance of the Proposed Protection Schemes for Wind Farms

In this section, the effectiveness and robustness of the proposed protection schemes are tested for various fault types, fault location, and even faults with high resistance that present distance protection relays in wind farms usually fail to detect correctly. Also, a comparison between all the three proposed differential protections schemes, which were DBPS, FPGA-DDPS, and SVM-DDPS, in terms of functionality, accuracy and operation speed are investigated thoroughly.

At first, the performance of protection relays is tested for during normal operation where no fault, or grid disturbance is present. This analysis is shown in Fig. 5.37, where the current waveform on the transformer, and transmission line, within the intertie section of the wind farm shows no abnormalities. On (a) and (b), the incoming and outgoing current to the transformer is shown, where by considering the transformer ratio, the current on both ends would be almost the same. Therefore, the protective relay has not detected any abnormalities, thus a constant "0" logic

data is provided to the circuit breaker as shown in (c). The same scenario can be seen for the transmission line, as illustrated on (d) and (e). The incoming and outgoing current at the both end of the line is almost the same (on the far end side, the outgoing current might be slightly smaller than the incoming current due to some minor power loss and the impedance of the line, however this slight difference is negligible), therefore the relay does not trip, depicted in (f).
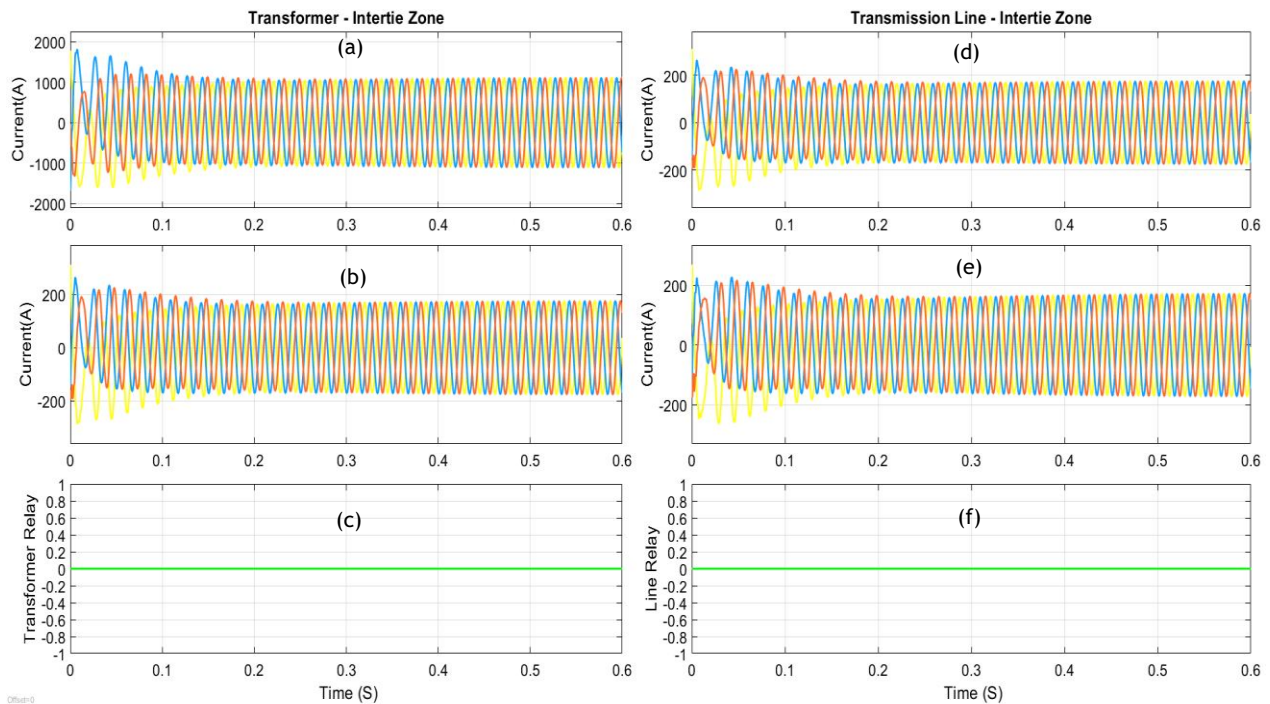
Fig. 5.37. Relay performance during normal operation (steady state): (a) Transformer incoming current, (b) Transformer outgoing current, (c) Transformer relay operation, (d) Line incoming current, (e) Line outgoing current, (f) Line relay operation.

Next, the performance of protective relays is tested for an external fault on the collector line, which this incidence is common in wind farms. This fault event is shown in Fig. 5.38. Since the fault has occurred outside the protection zone of the intertie section, therefore, the developed protection scheme must be able to detect the fault, but consider it as an external fault, therefore the relays should not trip at all. It is evident from this figure that relays on the transformer and the

transmission line has not operated, since the incoming and outgoing current is exactly the same, thus the relay has successfully considered them as external fault and avoided maloperation.
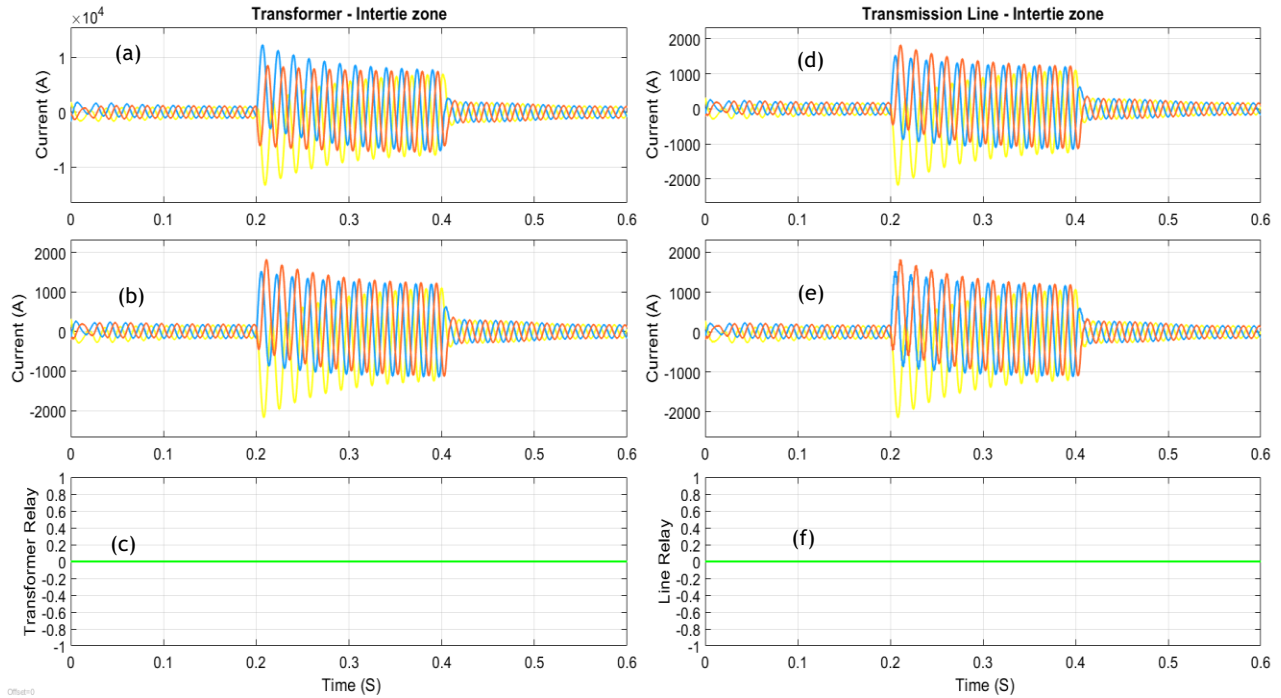
Fig. 5.38. Relay performance external fault at the wind farm collector line (abnormal condition): (a) Transformer incoming current, (b) Transformer outgoing current, (c) Transformer relay operation, (d) Line incoming current, (e) Line outgoing current, (f) Line relay operation.

The protection relays must be able to quickly detect internal faults defined in the protection zone, and trip the circuit breaker as soon as possible. Failure to do so, may cause serious damage to power equipment and diminish the power quality. The performance of all proposed protection schemes for such internal faults is evaluated in real-time which are shown in Fig. 5.39 – 5.43.

First, the worst-case scenario, which is a bolted three phase fault on the power transformer is analyzed as shown in Fig. 5.39. During this fault, the fault current is significantly high, and also there is significant difference between the incoming and outgoing current sensed by the protection

relay in the transformer protection zone. Therefore, as shows in "c", all the proposed protection schemes have successfully detected the internal faults and tripped accordingly. However, since this fault has occurred in the power transformer, it would be an external fault on the transmission line, therefore the line protection relay has successfully ignored this fault as shown in "f" and has not falsely tripped, which shows the intelligence, effectiveness and accuracy of the proposed protection scheme. Moreover, in this analysis, the operation speed of the protection relays has also been compared as shown in "c". The first relay which is actually the proposed DBPS, has operated almost instantly, since it is developed based on the theory of differential relays and is considered as an ideal relay, or reference point for the other developed relays. On the other hand, the developed FPGA-DDPS, has also tripped extremely fast, within only 4 ms, and finally the SVM-DDPS has also successfully operated and detected the fault correctly, but with a bit longer time, 32 ms.

The reverse scenario has been analyzed for a bolted three phase fault on the transmission line as shown in Fig. 5.40, where again all the proposed protection relays were able to detect the fault on the line successfully, while the relay on the transformer ignored the fault, since it detects it as external fault. In terms of tripping speed, the DBPS (ideal relay, reference relay) tripped almost instantly, while FPGA-DDPS tripped in 4 ms, and SVM-DDPS tripped after 29 ms.
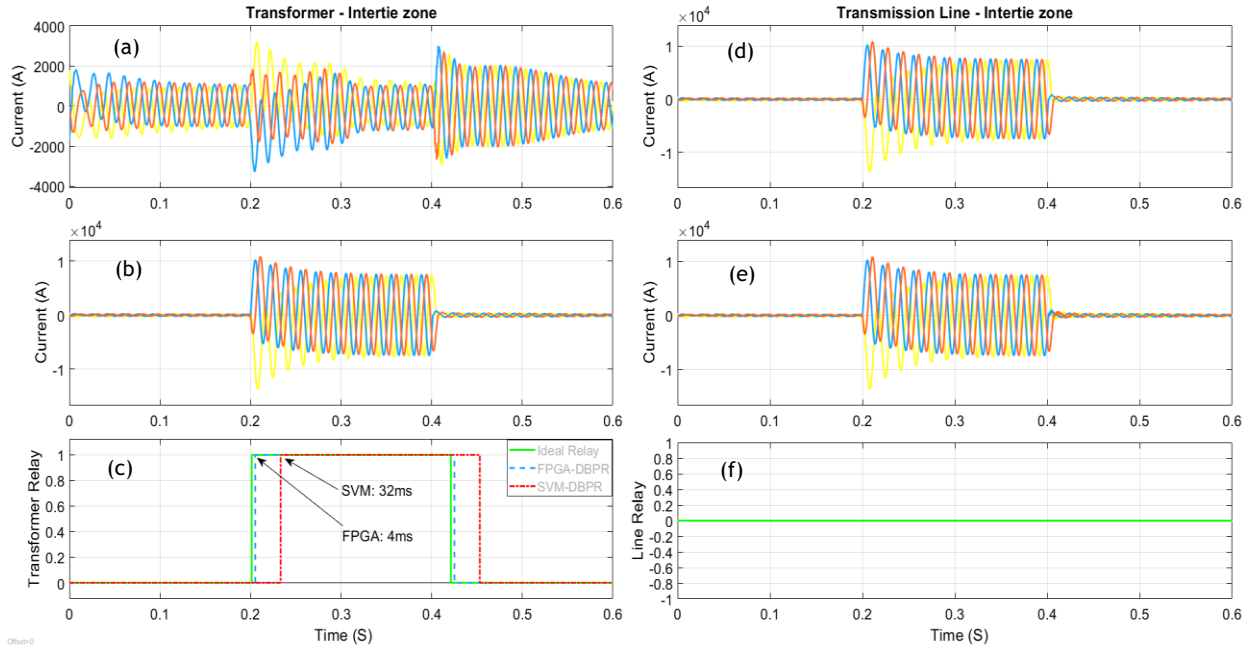
Fig. 5.39. Relays performance during 3-phase bolted internal fault at the transformer: (a) Transformer incoming current, (b) Transformer outgoing current, (c) Transformer relay operation, (d) Line incoming current, (e) Line outgoing current, (f) Line relay operation.
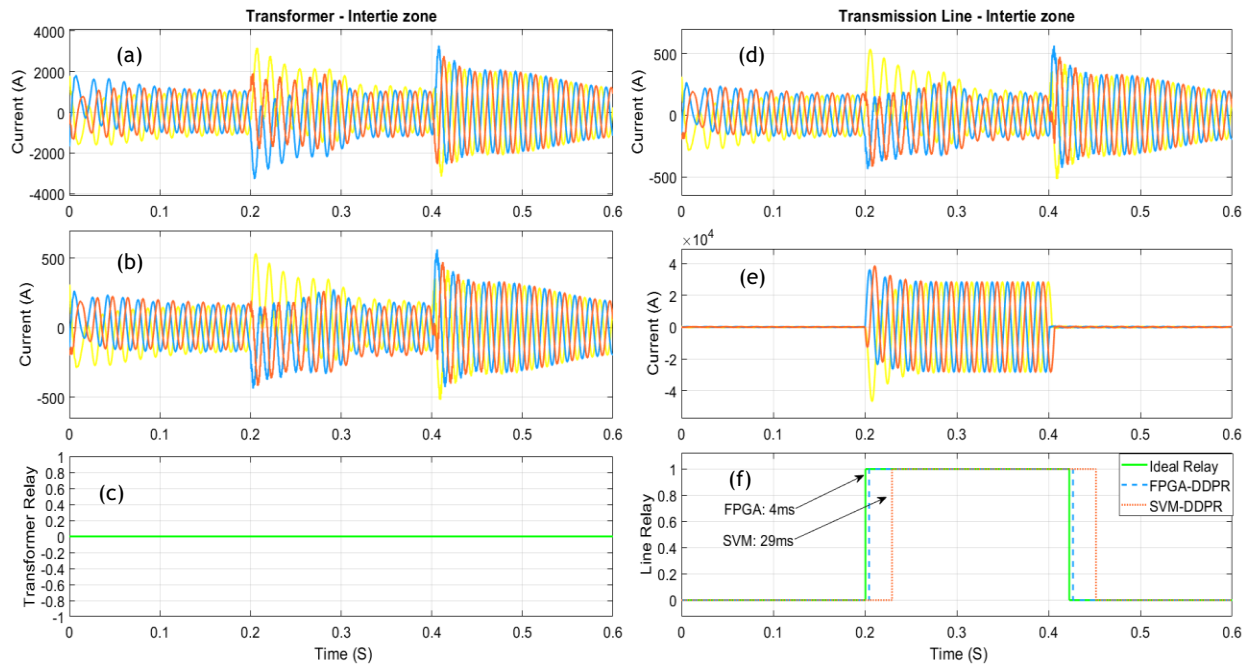
Fig. 5.40. Relay performance 3-phase bolted internal fault at the transmission line: (a) Transformer incoming current, (b) Transformer outgoing current, (c) Transformer relay operation, (d) Line incoming current, (e) Line outgoing current, (f) Line relay operation.

157

In order to ensure the protection relays are robust and sensitive enough, several different types of faults, such as double line to ground, line-to-line and single line to ground faults, and the response from the relays were analyzed as shown in Figs. 5.41 and 5.42.

First a double line to ground fault on the power transformer was imposed, where all the protection relays detected the fault an internal fault correctly within a very short time, where for DBPR, FPGA-DDPS, and SVM-DDPS, the operation time the relays were recorded to be, instantaneously, 4ms and 31 ms respectively. This analysis is shown in Fig. 5.41. The relay on the transmission line did not operate since the protection mechanism detected the fault as an external fault correctly.
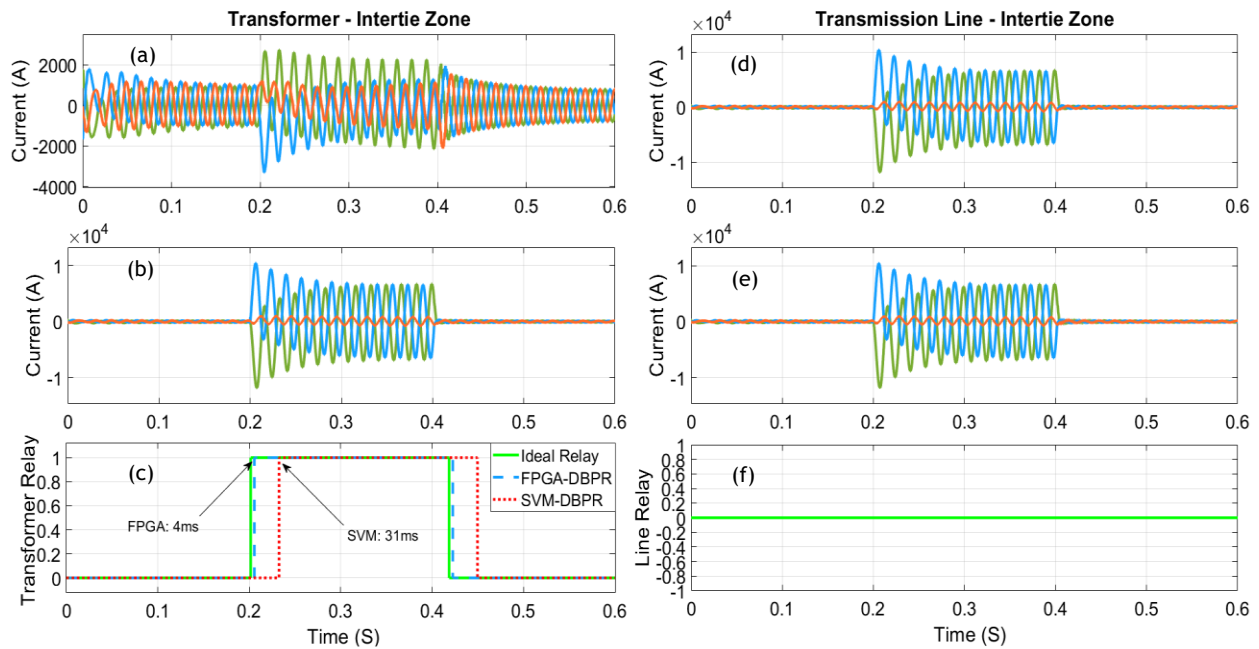
Fig. 5.41. Relays performance during L-L-G internal fault at the transformer fault at the transformer: (a) Transformer incoming current, (b) Transformer outgoing current, (c) Transformer relay operation, (d) Line incoming current, (e) Line outgoing current, (f) Line relay operation.

In another test, a single line to ground fault on the transmission line was considered as depicted in Fig. 5.42, where as expected the protective relays on the power transformer successfully ignores the fault by considering it as external fault. However, the developed protection relays on the transmission line, were able to accurately detect the internal fault and trip as the shortest possible time.
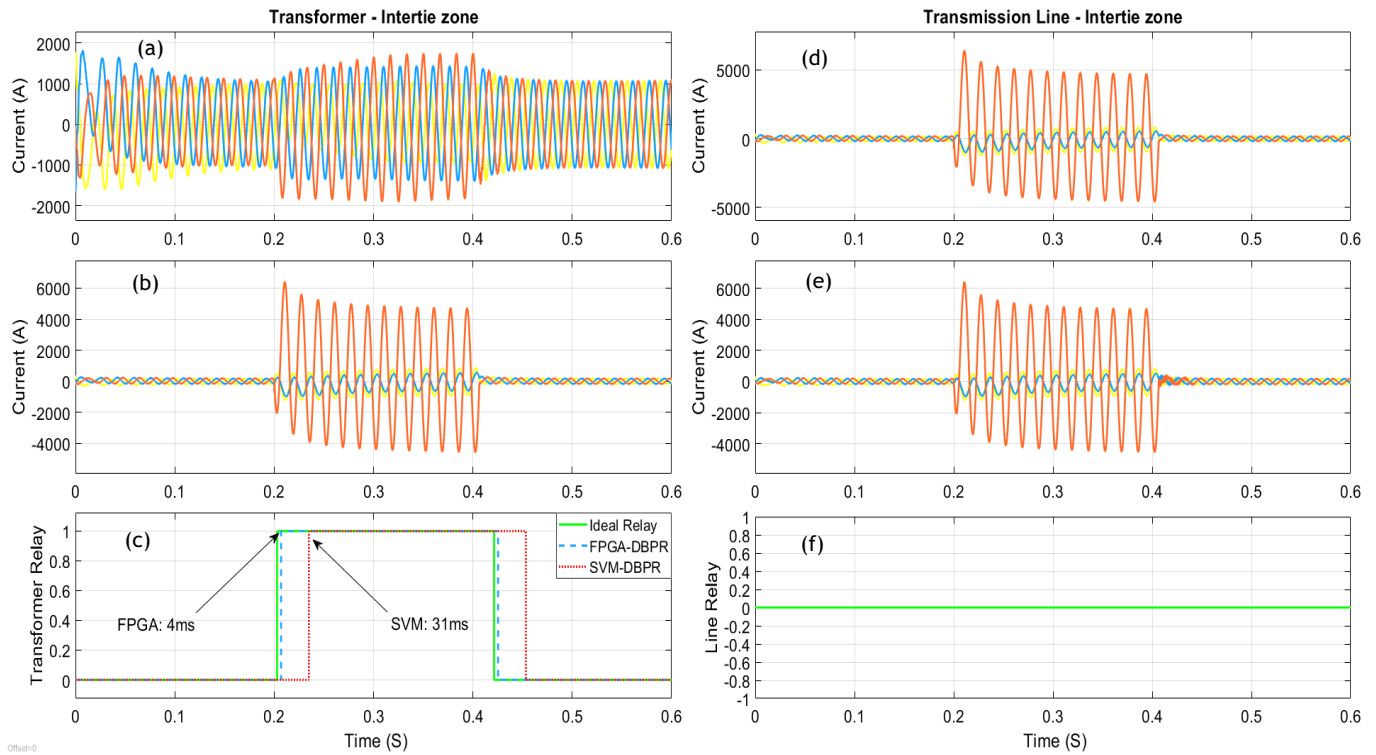
Fig. 5.42. Relays performance during single line to ground internal fault at the transformer: (a) Transformer incoming current, (b) Transformer outgoing current, (c) Transformer relay operation, (d) Line incoming current, (e) Line outgoing current, (f) Line relay operation.

Finally, a very extreme case, where a very high resistance line-to-line fault (70 Ώ) on the power transmission line was analyzed. Normally, such faults with extreme fault resistance are drastically difficult for relays to detect due to reduced fault current magnitude, and normally distance protection relays which are the most common types of protection mechanism for

transmission line in wind farms, fails to detect the fault correctly. However, all the proposed differential protection schemes in this research, were effectively able to not only detect the fault accurately, but also trip in a very short time as shown in Fig. 5.43. Additionally, the relay on the power transformer were also able to successfully ignores the fault since it has considered it as an external fault.

Thus, in this work, the effectiveness and accuracy of all the developed proposed protection scheme for the intertie section of wind farms have been tested, validated, and therefore could be considered as a robust protection mechanism as a substitution for distance protection relays.
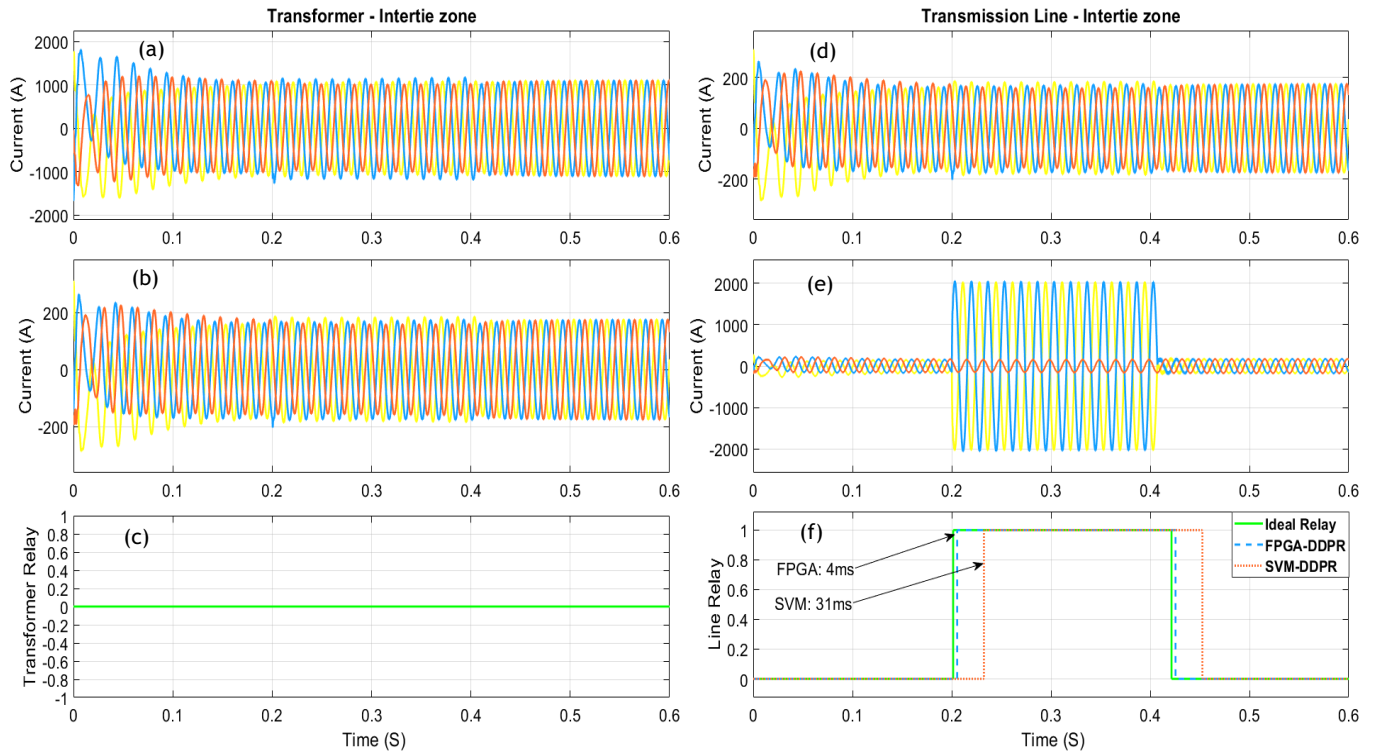
Fig. 5.43. Relays performance during 70 Ὡ L-L internal fault at the transmission line (high resistance fault): (a) Transformer incoming current, (b) Transformer outgoing current, (c) Transformer relay operation, (d) Line incoming current, (e) Line outgoing current, (f) Line relay operation.

5.5 Conclusion

This Chapter extensively focused on proposing various differential protections schemes as an alternative to unreliable distance protections that are presently implemented in wind farms. In the first part of this chapter a DBPS was developed utilizing the principle of conventional differential protection. This type of protection was proposed as an ideal protection scheme for wind farms and was designed to be implemented as a reference point for the two other intelligent and cost-effective protection schemes that was proposed which are: FPGA-DDPS and SVM-DDPS.

In the second part of this research, an FPGA-based digital differential protection relay was proposed as a cost-effective and robust protection scheme to provide a secure and reliable protection of a wind farm. An algorithm for the proposed differential relay was created in an FPGA using Modelsim software and Verilog HDL codes. The experimental testing was carried out in the laboratory environment through real-time FPGA-in-the-loop, where the FPGA acts like a differential protection relay. The DE2-115 FPGA board equipped with Cyclone IV E (EP4CE115F29C7) was utilized in this work. Several types of faults as well as faults with different fault resistances at different locations were imposed to verify the effectiveness of the proposed FPGA-DDPR. It was found from experimental results that the proposed FPGA-based relay was able to detect internal faults quickly and generates trip signals accordingly, while it ignored external faults. Thus, the proposed FPGA-DDPR relay could be a cost-effective substitute to the costly microprocessor-based differential relay scheme to provide fast and reliable protection for wind farms.

Finally, in the third part of this chapter, a novel hybrid machine learning based digital DBPR protection scheme was developed to provide a reliable protection for intertie zone of wind farm that overcomes the limitations of conventional DBPR and distance relays. A machine learning based support vector machine was used as a decision-making algorithm for the proposed DBPR by classifying various possible relay states with respect to wind farm operation modes. Based on the performance and accuracy comparison among various classifier methods, a Bayesian-based optimization algorithm was utilized for optimizing the hyperparameter of SVM to maximize the effectiveness of the SVM-DBPR scheme. The proposed protection technique was found successful (average accuracy of 99.8%) in both simulation and real-time to isolate the faulty section during internal fault while ignores any external fault or a drastic change in wind speed which is still considered as a normal operating condition. Thus, the proposed SVM-DBPR protection scheme could be utilized for intertie zone protection of real-life wind farms. With the proper standardization and communication structures, machine learning based digital protection scheme could be a cost-effective alternative for expensive analog differential relays in the near future which would revolutionize the effectiveness of power system protection.

Chapter 6

Conclusion

6.1   Summary

A comprehensive study on various novel power system protection schemes for large-scale wind farms have been outlined in this thesis. An overview of power system protection and its challenges were provided, while a thorough and concise analytical review on existing protection methods proposed for wind farms was also presented. Wind farm modelling, mathematical fault calculation, and overcurrent relay settings and coordination calculation were studied for a typical wind farm model. Development and design of OCRs, optimal coordination of protective relays and development of GA and GWO-based artificial intelligence techniques, in conjunction with adaptive and intelligent quadruple group settings-based overcurrent protection and coordination of relays, proposed as GWO-FLC protection scheme were illustrated in detail. Also, development of several novel differential protection relays, including DBPS, FPGA-DDPS and SVM-DDPS for intertie protection zone of wind farms, was studied in depth. Finally, a comprehensive fault analysis for testing the effectiveness of all the proposed protection schemes were also carried out.

First, an overview of wind farm operation, and associated protection challenges with these entities was presented. Furthermore, a brief but comprehensive literature review on specific wind farm protection issues was provided with thorough explanation, and the research motivation for each specific protection scheme was also presented at the end of each section. Finally, the main

objectives of this research with respect to addressing the present problems in wind farm protection, was also mentioned concisely.

Next, Chapter 2 was focused on design of the wind farm model as a case study for protection analysis. Moreover, short-circuit current contribution of various types of wind turbines, with emphasis on DFIG type was explained. Finally, with regards to short-circuit current calculation for a DFIG, a sample of hand calculation for short-circuit current of a DFIG as a verification for the software analysis was also provided.

In Chapter 3, the design and development of OCRs, determining the settings for each relay, along with their coordination was fully detailed. Moreover, a few samples of hand calculations for relay settings and coordination were provided. Furthermore, the application of two artificial intelligence optimization technique e.g., GA and GWO, along with their coding, objective function formulation, and their development were explained thoroughly. Additionally, their application on optimizing the relay settings with the optimization process was presented. Finally, the operation of optimal overcurrent protection and coordination was tested and analyzed to validate the developed protection scheme.

In Chapter 4, the proposed intelligent adaptive protection and coordination for large-scale wind farms, and development of hybrid GWO-FLC was presented. Furthermore, the performance of this protection scheme under test and validation for various wind speed cases even during drastic wind speed variation for examining the robustness and effectiveness of the proposed method was also illustrated.

Finally, Chapter 5 covered several topics including, design and development of differential protection specific for intertie zone of wind farms, digital differential protection scheme, cost-

effective FPGA-DDPS, and Intelligent SVM-DDPS. All of these techniques were explained thoroughly and the step-by-step design and development of each technique were also illustrated. Additionally, the performance of each novel protection scheme was inspected for various types of fault, at different locations and different fault resistance. Besides, the experimental hardware-in-the-loop operation of FPGA-based protection using FPGA DE2-115 board to validate the developed protection scheme and simulation results, were also provided.

6.2   Major Contributions of the Thesis

The major contributions of this thesis are pointed out below:

- An optimal overcurrent protection and coordination based on GA and GWO as AI and NIA-based techniques were designed and developed. The proposed optimal OCRs were managed to improve the operation of overcurrent protection in terms of speed and accuracy, by optimizing the TMS and current settings of all protective relays in a wind farm. The performance of the proposed relays was compared to the conventional non-linear time-current curves settings approach for OCRs, and it was evident that the proposed protection schemes provided significantly improved performance.

- A novel adaptive and intelligent overcurrent protection and coordination based on GWO-FLC was proposed as a smart controlling mechanism to continuously update the relay settings with the best possible optimal parameters for various wind speed in wind farms at different dynamic conditions, such as loading, connection or disconnection of wind turbine from the plant, and etc. Moreover, a quadruple group setting for all the 47 relays in the wind farm was calculated and proposed, where the optimized settings were provided to the

FLC, that was designed specifically for the adaptive protection purpose. It was inferred that by implementing such protections scheme, the relay settings are constantly adapted to the dynamic behavior of wind farms, therefore, false tripping would be avoided.

- Several cost-effective and novel intelligent differential protection schemes such as DBPS, FPGA-DDPS, and SVM-DDPS were proposed as an effective protection mechanism for the intertie section of wind farms. All the differential protection schemes developed in this research were rigorously tested and examined for various conditions such as normal condition, external faults, internal faults, different types of severe and less severe faults, faults with high or low resistance, and faults at different locations. All of the protective relays were able to successfully detect the faults with high accuracy within a very short time. Thus, the proposed protection schemes can be successfully implemented in the intertie section of wind farms that would overcome the limitations of conventional distance relays.

- In general, all the protection schemes developed and designed in this thesis was intended to be a simple but effective controlling mechanism to improve the protection, security, reliability and stability of wind farms compared to their counterparts.

6.3   Future Scope of Work

This thesis developed several different types of protection techniques to be applicable for different protection zones. However, as a future scope of work, the following studies could be carried out:

- All of the developed protection schemes in this thesis have only been applied for wind farms. However, with proper modification and standardization these protections schemes can also be applied for various modern power systems, such as smart grids, microgrids, and in various sectors of power networks including: generation, transmission and distribution.

- The grid standards for LVRT and FRT of wind turbines are constantly evolving and improving every year, therefore, the wind farm integrated standards for power system protection must also evolve accordingly to provide a more reliable and stable power system. Thus, in future, more research needs to be carried out to incorporate the latest standards of LVRT and FRT in the developed protection schemes for wind farms.

- Nowadays, with ever increasingly dependency of power system on communications in smart grids, the number of malicious cyber-attacks have also been significantly amplified. This problem is even more serious and vital for digital relay-based power system protection as the online manipulation of any parameter in the relay settings, could cause catastrophic consequences in the power networks. For example, a cyber-attack was reported at Ukraine power grid in 2015, where Russian hackers compromised information systems of three energy distribution companies, and temporarily disrupted the electricity supply to consumers. During this attack, 30 substations at the high and medium voltage level (110kv and 35kv) were switched off, and also about 230,000 customers were without electricity for a period from 1 to 6 hours. Imagine what such cyber-attack could impose to a large-scale power network that is interconnected between several regions, or countries, where the disruption of such power system is not tolerated even for a few seconds. Thus, in the future research, more focus will be devoted on developing more robust and anti-cyber-attack protection relays for smart grids.

6.4   Concluding Remarks

In this thesis, various novel protection schemes applicable for present and future large-scale wind farms were developed and tested in both simulation and real-time laboratory environment. Starting from overcurrent protection to more advanced protection techniques such as AI-based intelligent relays, GA and GWO-based optimized coordination between numerous overcurrent protective relays for a large-scale wind farm, fuzzy logic and NIA-based adaptive protection schemes, several cost-effective and smart differential protection schemes including DBPS, FPGA-DDPS, and SVM-DDPS were considered in this work. Through the successful application of the developed protection techniques various protection and security-related challenges in existing wind farms have been successfully solved. Thus, the proposed protection schemes would significantly benefit the reliability, security, protection, stability and cost of wind farms if the models are implemented in the real-life power systems.

References

[1]   A. K. Tamer, M. Naema, and I. T. Abd El-Maksoud, "Performance evaluation of conventional protection systems for wind farms," in *IEEE Power and Energy Society 2008 General Meeting: Conversion and Delivery of Electrical Energy in the 21st Century, PES*, 2008, doi: 10.1109/PES.2008.4596765.

[2]   S. Heier, *Grid integration of wind energy: onshore and offshore conversion systems*. John Wiley & Sons., 2014.

[3]   S. Gsänger, "World Wind Energy Association - World wind capacity at 650,8 GW," 2020.

[4]   B. K. Sahu, "Wind energy developments and policies in China: A short review," *Renew. Sustain. Energy Rev.*, vol. 81, pp. 1393–1405, Jan. 2018, doi: 10.1016/J.RSER.2017.05.183.

[5]   S. M. Islam, C. V. Nayar, A. Abu-Siada, and M. M. Hasan, *Power Electronics for Renewable Energy Sources*. Butterworth-Heinemann, 2018.

[6]   C. V. Nayar, S. M. Islam, H. Dehbonei, K. Tan, and H. Sharma, "Power Electronics for Renewable Energy Sources," in *Alternative Energy in Power Electronics*, 2011, pp. 1–79.

[7]   M. A. Hyams, *Wind energy in the built environment*. Woodhear Publishing, 2012.

[8]   I. Dincer and M. F. Ezzat, *Renewable Energy Production*. Comprehensive Energy Systems, Elsevier, 2018.

[9]   GE Renewable Energy, "Haliade-X offshore wind turbine," 2021. https://www.ge.com/renewableenergy/wind-energy/offshore-wind/haliade-x-offshore-turbine.

[10] T. Kawady, C. Feltes, I. Erlich, and A. M. I. Taalab, "Protection system behavior of DFIG based wind farms for grid-faults with practical considerations," in *IEEE PES General Meeting, PES 2010*, 2010, doi: 10.1109/PES.2010.5589854.

[11] X. Xie, W. Liu, H. Liu, Y. Du, and Y. Li, "A system-wide protection against unstable SSCI in series-compensated wind power systems," *IEEE Trans. Power Deliv.*, vol. 33, no. 6, pp. 3095–3104, Dec. 2018, doi: 10.1109/TPWRD.2018.2829846.

[12] H. Zhang, F. Gruson, D. M. F. Rodriguez, and C. Saudemont, "Overvoltage Limitation Method of an Offshore Wind Farm With DC Series-Parallel Collection Grid," *IEEE Trans. Sustain. Energy*, vol. 10, no. 1, pp. 204–213, Jan. 2019, doi: 10.1109/TSTE.2018.2829929.

[13] R. G. Deshagoni, T. Auditore, R. Rayudu, and C. P. Moore, "Factors Determining the Effectiveness of a Wind Turbine Generator Lightning Protection System," *IEEE Trans. Ind. Appl.*, vol. 55, no. 6, pp. 6585–6592, Nov. 2019, doi: 10.1109/TIA.2019.2931866.

[14] J. Liao, X. Zhu, and Q. Wang, "Transient current similarity-based protection for interconnecting transformers in wind farms," *IEEE Access*, vol. 7, pp. 45744–45757, 2019, doi: 10.1109/ACCESS.2019.2909063.

[15] T. S. Ustun, C. Ozansoy, and A. Zayegh, "Modeling of a centralized microgrid protection system and distributed energy resources according to IEC 61850-7-420," *IEEE Trans. Power Syst.*, vol. 27, no. 3, pp. 1560–1567, 2012, doi: 10.1109/TPWRS.2012.2185072.

[16] T. A. Kawadi, N. M. Mansour, and A. I. Taalab, "Wind farm protection systems: state of the art and challenges.," in *Distributed Generation*, 2010, pp. 265–288.

[17] B. Chen, A. Shrestha, F. A. Ituzaro, and N. Fischer, "Addressing protection challenges

associated with Type 3 and Type 4 wind turbine generators," in *2015 68th Annual Conference for Protective Relay Engineers*, 2015, pp. 335–344, doi: 10.1109/CPRE.2015.7102177.

[18]   J. Cardenas, V. Muthukrishnan, D. McGinn, and R. Hunt, "Wind farm protection using an IEC 61850 process bus architecture," in *IET Conference Publications*, 2010, vol. 2010, no. 558 CP, doi: 10.1049/cp.2010.0285.

[19]   Z. X. Zheng, C. J. Huang, R. H. Yang, X. Y. Xiao, and C. S. Li, "A Low Voltage Ride Through Scheme for DFIG-Based Wind Farm with SFCL and RSC Control," *IEEE Trans. Appl. Supercond.*, vol. 29, no. 2, Mar. 2019, doi: 10.1109/TASC.2019.2891687.

[20]   A. M. Rauf, V. Khadkikar, and M. S. El Moursi, "A New Fault Ride-Through (FRT) Topology for Induction Generator Based Wind Energy Conversion Systems," *IEEE Trans. Power Deliv.*, vol. 34, no. 3, pp. 1129–1137, Jun. 2019, doi: 10.1109/TPWRD.2019.2894378.

[21]   H. Sun and R. Chen, "A two-level distributed approach to power network modeling," *IEEE Trans. Power Deliv.*, vol. 30, no. 3, pp. 1496–1504, Jun. 2015, doi: 10.1109/TPWRD.2014.2381877.

[22]   D. Jones and J. J. Kumm, "Future distribution feeder protection using directional overcurrent elements," *IEEE Trans. Ind. Appl.*, vol. 50, no. 2, pp. 1385–1390, 2014, doi: 10.1109/TIA.2013.2283237.

[23]   S. Guobing, W. Xiaobo, C. Zhongxue, T. Jisi, and P. Liu, "A novel protection method of collecting power lines in PMSG wind farm," in *Asia-Pacific Power and Energy Engineering Conference, APPEEC*, Dec. 2016, vol. 2016-December, pp. 2086–2090, doi:

10.1109/APPEEC.2016.7779854.

[24]   D. Jones and K. Bennett, "Wind farm collector protection using directional overcurrent elements," in *Proceedings of the IEEE Power Engineering Society Transmission and Distribution Conference*, 2012, doi: 10.1109/TDC.2012.6281532.

[25]   W. Wei, L. Zhang, B. Gao, Y. Tang, N. Chen, and L. Zhu, "Frequency inconsistency in DFIG-based wind farm during outgoing transmission line faults and its effect on longitudinal differential protection," in *4th Annual IEEE International Conference on Cyber Technology in Automation, Control and Intelligent*, 2014, pp. 25–30.

[26]   S. H. Horowitz and A. G. Phadke, *Power system relaying*. Wiley/Research Studies Press, 2008.

[27]   R. Mohammadi, H. A. Abyaneh, H. M. Rudsari, S. H. Fathi, and H. Rastegar, "Overcurrent relays coordination considering the priority of constraints," *IEEE Trans. Power Deliv.*, vol. 26, no. 3, pp. 1927–1938, Jul. 2011, doi: 10.1109/TPWRD.2011.2123117.

[28]   A. I. Atteya, A. M. E. Zonkoly, and H. A. Ashour, "Optimal relay coordination of an adaptive protection scheme using modified PSO algorithm," in *2017 19th International Middle-East Power Systems Conference, MEPCON 2017 - Proceedings*, Feb. 2018, vol. 2018-February, pp. 689–694, doi: 10.1109/MEPCON.2017.8301256.

[29]   F. A. Albasri, A. R. Alroomi, and J. H. Talaq, "Optimal Coordination of Directional Overcurrent Relays Using Biogeography-Based Optimization Algorithms," *IEEE Trans. Power Deliv.*, vol. 30, no. 4, pp. 1810–1820, 2015, doi: 10.1109/TPWRD.2015.2406114.

[30]   S. Das Manohar Singh, B.K. Panigrahi, A.R. Abhyankar, "Optimal coordination of

directional over-current relays using informative differential evolution algorithm," *J. Comput. Sci.*, vol. 5, no. 2, pp. 269–276, 2014.

[31]   D. Birla, R. P. Maheshwari, and H. O. Gupta, "Time-Overcurrent Relay Coordination: A Review," *Int. J. Emerg. Electr. Power Syst.*, vol. 2, no. 2, 2005.

[32]   M. H. Hussain, S. R. A. Rahim, and I. Musirin, "Optimal Overcurrent Relay Coordination: A Review," in *Malaysian Technical Universities Conference on Engineering & Technology 2012, MUCET 2012 Part 1- Electronic and Electrical Engineering*, 2013, pp. 332–336.

[33]   M. H. Hussain, I. Musirin, S. R. A. Rahim, and A. F. Abidin, "Computational Intelligence Based Technique in Optimal Overcurrent Relay Coordination: A Review," *Int. J. Eng. Sci.*, vol. 2, no. 1, pp. 1–9, 2013.

[34]   M. Singh, B. K. Panigrahi, and A. R. Abhyankar, "Optimal overcurrent relay coordination in distribution system," in *2011 International Conference on Energy, Automation and Signal*, 2011, pp. 1–6.

[35]   A. J. Urdaneta, H. Restrepo, S. Márquez, and J. Sánchez, "Coordination of directional overcurrent relay timing using linear programming," *IEEE Trans. Power Deliv.*, vol. 11, no. 1, pp. 122–128, 1996, doi: 10.1109/61.484008.

[36]   A. S. Noghabi, H. R. Mashhadi, and J. Sadeh, "Optimal coordination of directional overcurrent relays considering different network topologies using interval linear programming," *IEEE Trans. Power Deliv.*, vol. 25, no. 3, pp. 1348–1354, Jul. 2010, doi: 10.1109/TPWRD.2010.2041560.

[37]   P. N. Korde and P. P. Bedekar, "Optimal overcurrent relay coordination in distribution

system using nonlinear programming method," in *International Conference on Electrical Power and Energy Systems, ICEPES 2016*, May 2017, pp. 372–376, doi: 10.1109/ICEPES.2016.7915960.

[38] V. A. Papaspiliotopoulos, G. N. Korres, and N. G. Maratos, "A Novel Quadratically Constrained Quadratic Programming Method for Optimal Coordination of Directional Overcurrent Relays," *IEEE Trans. Power Deliv.*, vol. 32, no. 1, pp. 3–10, Feb. 2017, doi: 10.1109/TPWRD.2015.2455015.

[39] A. A. Kida, A. E. Labrador Rivas, and L. A. Gallego, "An improved simulated annealing–linear programming hybrid algorithm applied to the optimal coordination of directional overcurrent relays," *Electr. Power Syst. Res.*, vol. 181, p. 106197, Apr. 2020, doi: 10.1016/j.epsr.2020.106197.

[40] A. Darabi, M. Bagheri, and G. B. Gharehpetian, "Highly reliable overcurrent protection scheme for highly meshed power systems," *Int. J. Electr. Power Energy Syst.*, vol. 119, p. 105874, Jul. 2020, doi: 10.1016/j.ijepes.2020.105874.

[41] S. Tirumala Pallerlamudi Srinivas and K. Shanti Swarup, "Optimal Protection Coordination of Nonstandard Overcurrent Relays Using Hybrid QCQP Method," *Electr. Power Components Syst.*, 2020, doi: 10.1080/15325008.2020.1829187.

[42] A. Darabi, M. Bagheri, and G. B. Gharehpetian, "Dual feasible direction-finding nonlinear programming combined with metaheuristic approaches for exact overcurrent relay coordination," *Int. J. Electr. Power Energy Syst.*, vol. 114, p. 105420, Jan. 2020, doi: 10.1016/j.ijepes.2019.105420.

[43] T. Amraee, "Coordination of Directional Overcurrent Relays Using Seeker Algorithm,"

IEEE Trans. Power Deliv., vol. 27, no. 3, pp. 1415–1422, Jul. 2012, doi: 10.1109/TPWRD.2012.2190107.

[44] F. A. Albasri, A. R. Alroomi, and J. H. Talaq, "Optimal Coordination of Directional Overcurrent Relays Using Biogeography-Based Optimization Algorithms," *IEEE Trans. Power Deliv.*, vol. 30, no. 4, pp. 1810–1820, Aug. 2015, doi: 10.1109/TPWRD.2015.2406114.

[45] A. Chawla, B. R. Bhalja, B. K. Panigrahi, and M. Singh, "Gravitational Search Based Algorithm for Optimal Coordination of Directional Overcurrent Relays Using User Defined Characteristic," *Electr. Power Components Syst.*, vol. 46, no. 1, pp. 43–55, Jan. 2018, doi: 10.1080/15325008.2018.1431982.

[46] P. P. Bedekar and S. R. Bhide, "Optimum coordination of overcurrent relay timing using continuous genetic algorithm," *Expert Syst. Appl.*, vol. 38, no. 9, pp. 11286–11292, Sep. 2011, doi: 10.1016/j.eswa.2011.02.177.

[47] M. M. Mansour, S. F. Mekhamer, and N. El-Kharbawe, "A Modified Particle Swarm Optimizer for the Coordination of Directional Overcurrent Relays," *IEEE Trans. Power Deliv.*, vol. 22, no. 3, pp. 1400–1410, Jul. 2007, doi: 10.1109/TPWRD.2007.899259.

[48] J. Diego, D. C. Pico, and G. Ramos, "Protection coordination analysis under a real-time architecture for industrial distribution systems based on the Std IEEE 242-2001," in *2015 IEEE Industry Applications Society Annual Meeting*, 2015, pp. 1–6, doi: 10.1109/IAS.2015.7356956.

[49] M. G. M. Zanjani, K. Mazlumi, and I. Kamwa, "Application of μPMUs for adaptive protection of overcurrent relays in microgrids," *IET Gener. Transm. Distrib.*, vol. 12, no.

18, pp. 4061–4069, Oct. 2018, doi: 10.1049/iet-gtd.2018.5898.

[50]   S. Teimourzadeh, F. Aminifar, M. Davarpanah, and M. Shahidehpour, "Adaptive Protection for Preserving Microgrid Security," *IEEE Trans. Smart Grid*, vol. 10, no. 1, pp. 592–600, 2019, doi: 10.1109/TSG.2017.2749301.

[51]   A. A. Balyith, H. M. Sharaf, M. Shaaban, E. F. El-Saadany, and H. H. Zeineldin, "Non-Communication Based Time-Current-Voltage Dual Setting Directional Overcurrent Protection for Radial Distribution Systems With DG," *IEEE Access*, vol. 8, pp. 190572–190581, Oct. 2020, doi: 10.1109/access.2020.3029818.

[52]   M. N. Alam, "Adaptive Protection Coordination Scheme Using Numerical Directional Overcurrent Relays," *IEEE Trans. Ind. Informatics*, vol. 15, no. 1, pp. 64–73, Jan. 2019, doi: 10.1109/TII.2018.2834474.

[53]   A. Rahmati, M. A. Dimassi, R. Adhami, and D. Bumblauskas, "An overcurrent protection relay based on local measurements," in *IEEE Transactions on Industry Applications*, May 2014, vol. 51, no. 3, pp. 2081–2085, doi: 10.1109/TIA.2014.2385933.

[54]   S. Shen, D. Lin, and B. He, "An Adaptive Protection Scheme for Distribution Systems with DGs Based on Optimized Thevenin Equivalent Parameters Estimation," *IEEE Trans. Power Deliv.*, vol. 32, no. 1, pp. 411–419, Feb. 2017, doi: 10.1109/TPWRD.2015.2506155.

[55]   H. Muda and P. Jena, "Superimposed Adaptive Sequence Current Based Microgrid Protection: A New Technique," *IEEE Trans. Power Deliv.*, vol. 32, no. 2, pp. 757–767, Apr. 2017, doi: 10.1109/TPWRD.2016.2601921.

[56]   T. S. S. Senarathna and U. Hemapala, "Review of adaptive protection methods for

microgrids," *AIMS Energy*, vol. 7, no. 5, pp. 557–578, 2019, doi: 10.3934/energy.2019.5.557.

[57]   P. H. A. Barra, D. V. Coury, and R. A. S. Fernandes, "A survey on adaptive protection of microgrids and distribution systems with distributed generators," *Renewable and Sustainable Energy Reviews*, vol. 118. Elsevier Ltd, p. 109524, Feb. 01, 2020, doi: 10.1016/j.rser.2019.109524.

[58]   E. Sorrentino and M. Navas, "Two improvements related to overcurrent functions for bus protection in distribution systems," *IEEE Trans. Power Deliv.*, vol. 30, no. 3, pp. 1634–1635, Jun. 2015, doi: 10.1109/TPWRD.2015.2394509.

[59]   B. Polajžer, M. Pintarič, M. Rošer, and G. Štumberger, "Protection of MV Closed-Loop Distribution Networks with Bi-Directional Overcurrent Relays and GOOSE Communications," *IEEE Access*, vol. 7, pp. 165884–165896, 2019, doi: 10.1109/ACCESS.2019.2952934.

[60]   R. Jain, D. L. Lubkeman, and S. M. Lukic, "Dynamic Adaptive Protection for Distribution Systems in Grid-Connected and Islanded Modes," *IEEE Trans. Power Deliv.*, vol. 34, no. 1, pp. 281–289, Feb. 2019, doi: 10.1109/TPWRD.2018.2884705.

[61]   V. A. Papaspiliotopoulos, G. N. Korres, V. A. Kleftakis, and N. D. Hatziargyriou, "Hardware-In-the-Loop Design and Optimal Setting of Adaptive Protection Schemes for Distribution Systems with Distributed Generation," *IEEE Trans. Power Deliv.*, vol. 32, no. 1, pp. 393–400, Feb. 2017, doi: 10.1109/TPWRD.2015.2509784.

[62]   M. Kavi, Y. Mishra, and M. Vilathgamuwa, "Morphological Fault Detector for Adaptive Overcurrent Protection in Distribution Networks With Increasing Photovoltaic

Penetration," *IEEE Trans. Sustain. Energy*, vol. 9, no. 3, pp. 1021–1029, Jul. 2018, doi: 10.1109/TSTE.2017.2759158.

[63]   M. Y. Shih, A. Conde, Z. Leonowicz, and L. Martirano, "An Adaptive Overcurrent Coordination Scheme to Improve Relay Sensitivity and Overcome Drawbacks due to Distributed Generation in Smart Grids," *IEEE Trans. Ind. Appl.*, vol. 53, no. 6, pp. 5217–5228, Nov. 2017, doi: 10.1109/TIA.2017.2717880.

[64]   F. Coffele, C. Booth, and A. Dyśko, "An Adaptive Overcurrent Protection Scheme for Distribution Networks," *IEEE Trans. Power Deliv.*, vol. 30, no. 2, pp. 561–568, Apr. 2015, doi: 10.1109/TPWRD.2013.2294879.

[65]   P. M. Anderson, *Power system protection*. Wiley-IEEE Press, 1998.

[66]   Y. G. Paithanker and S. R. Bhide, *Fundamentals of power system protection*. PHI Learning Pvt. Ltd., 2010.

[67]   J. Ma, W. Zhang, J. Liu, and J. S. Thorp, "A novel adaptive distance protection scheme for DFIG wind farm collector lines," *Int. J. Electr. Power Energy Syst.*, vol. 94, pp. 234–244, 2018, doi: 10.1016/j.ijepes.2017.07.008.

[68]   M. Dewadasa, A. Ghosh, and G. Ledwich, "An inverse time admittance relay for fault detection in distribution networks containing DGs," *IEEE Reg. 10 Annu. Int. Conf. Proceedings/TENCON*, pp. 1–6, 2009, doi: 10.1109/TENCON.2009.5396204.

[69]   B. J. Brearley and R. R. Prabu, "A review on issues and approaches for microgrid protection," *Renew. Sustain. Energy Rev.*, vol. 67, pp. 988–997, 2017, doi: 10.1016/j.rser.2016.09.047.

[70] V. Phadke, S. Pathradkar, A. Rajput, S. Unde, and S. Dambhare, "Distance protection of lines connected to doubly fed induction generator based wind farms," *2016 IEEE 7th Power India Int. Conf. PIICON 2016*, pp. 1–6, 2017, doi: 10.1109/POWERI.2016.8077177.

[71] G. H. Li, B. H. Zhang, J. Wang, and T. Yip, "Wind Farm Electromagnetic Dynamic Model and Outgoing Line Protection Relay RTDS Testing," *Univ. Power Eng. Conf. (UPEC), Proc. 2011 46th Int.*, no. September, pp. 1–6, 2011.

[72] A. Hooshyar, M. A. Azzouz, and E. F. El-Saadany, "Distance protection of lines connected to induction generator-based wind farms during balanced faults," *IEEE Trans. Sustain. Energy*, vol. 5, no. 4, pp. 1193–1203, 2014, doi: 10.1109/TSTE.2014.2336773.

[73] J. M. Dewadasa, A. Ghosh, and G. Ledwich, "Distance Protection Solution for a Converter Controlled Microgrid," *Power*, no. December, pp. 586–591, 2008, doi: 10.1016/j.socscimed.2015.03.020.

[74] H. Lin, C. Liu, J. M. Guerrero, and J. C. Vasquez, "Distance protection for microgrids in distribution system," *IECON 2015 - 41st Annu. Conf. IEEE Ind. Electron. Soc.*, pp. 731–736, 2015, doi: 10.1109/IECON.2015.7392186.

[75] A. M. Tsimtsios, G. N. Korres, and V. C. Nikolaidis, "A pilot-based distance protection scheme for meshed distribution systems with distributed generation," *Int. J. Electr. Power Energy Syst.*, vol. 105, pp. 454–469, Feb. 2019, doi: 10.1016/j.ijepes.2018.08.022.

[76] D. Khalifa and M. Nour, "Assessment of transmission line protection with integrated offshore wind farm in UAE," in *IET Conference Publications*, 2016, vol. 2016, no. CP671, doi: 10.1049/cp.2016.0062.

[77]   G. Feng, G. Zhe, S. Zhang, J. Zhang, and J. Dou, "Influence on transmission line relay protection under Dfig-based wind farm intergration," in *Proceedings of the 5th IEEE International Conference on Electric Utility Deregulation, Restructuring and Power Technologies, DRPT 2015*, Mar. 2016, pp. 290–295, doi: 10.1109/DRPT.2015.7432244.

[78]   Z. Lv, Z. Wang, and W. Xu, "Transient Waveform Characteristics Based Current Differential Protection of Wind Farm Outgoing Line," in *APAP 2019 - 8th IEEE International Conference on Advanced Power System Automation and Protection*, Oct. 2019, pp. 1713–1718, doi: 10.1109/APAP47170.2019.9224684.

[79]   D. P. Bandaru and A. G. Shaik, "Wind Farm Connected Distribution System Protection Using Wavelet-Alienation Coefficient Technique," in *2018 3rd International Conference for Convergence in Technology, I2CT 2018*, Nov. 2018, doi: 10.1109/I2CT.2018.8529579.

[80]   H. Nguyen-Duc and Y. Nakanishi, "Effect of DFIG Wind Farm Fault Currents on the Transformer Differential Relaying Performance," in *International Conference on Innovative Smart Grid Technologies, ISGT Asia 2018*, Sep. 2018, pp. 916–921, doi: 10.1109/ISGT-Asia.2018.8467823.

[81]   G. Yang, M. Dong, and C. Zhou, "The influences and countermeasures of transmission line differential protection and auto-reclosing when wind farm connected," in *China International Conference on Electricity Distribution, CICED*, 2012, doi: 10.1109/CICED.2012.6508672.

[82]   K. Jia, Y. Li, Y. Fang, L. Zheng, T. Bi, and Q. Yang, "Transient current similarity based protection for wind farm transmission lines," *Appl. Energy*, vol. 225, pp. 42–51, Sep. 2018, doi: 10.1016/j.apenergy.2018.05.012.

[83] A. Mohamed, A. E. Sayed, S. Moussa, and A. Elsamahy, "Central Relaying Unit for Wind Farm Based on Directional Angle and Differential Current," in *IEEE Conference on Power Electronics and Renewable Energy, CPERE 2019*, Oct. 2019, pp. 186–193, doi: 10.1109/CPERE45374.2019.8980127.

[84] R. P. Medeiros and F. B. Costa, "A Wavelet-Based Transformer Differential Protection with Differential Current Transformer Saturation and Cross-Country Fault Detection," *IEEE Trans. Power Deliv.*, vol. 33, no. 2, pp. 789–799, Apr. 2018, doi: 10.1109/TPWRD.2017.2764062.

[85] F. Song and C. F. Ten, "Application of differential protection to offshore wind farm for earth fault detection with substantially unbalanced charging current," *J. Eng.*, vol. 2018, no. 15, pp. 836–840, Oct. 2018, doi: 10.1049/joe.2018.0201.

[86] L. Zheng, K. Jia, T. Bi, Z. Yang, and Y. Fang, "A Novel Structural Similarity Based Pilot Protection for Renewable Power Transmission Line," *IEEE Trans. Power Deliv.*, vol. 35, no. 6, pp. 2672–2681, Dec. 2020, doi: 10.1109/TPWRD.2020.2973505.

[87] MATLAB 9.7.0.1190202 (R2019b), "Natick, Massachusetts: The MathWorks Inc." 2019.

[88] J. J. Grainger and W. D. Stevenson, *Power System Analysis*. McGraw-Hill Education, 1994.

[89] J. C. Das, *Power system analysis: short-circuit load flow and harmonics (Vol. 1)*. CRC Press, 2017.

[90] P. M. Anderson, *Analysis of faulted power systems*. New York: IEEE press., 1995.

[91] A. Nayir, E. Rosolowski, and L. Jedut, "Analysis of short circuit faults in a system fed by wind turbine," in *2012 International Conference on Renewable Energy Research and*

Applications (ICRERA), 2012, pp. 1–4, doi: 10.1109/ICRERA.2012.6477275.

[92]   A. M. Sadati, H. K. Karegar, P. Saadat, and N. Niassati, "Short circuit current analysis for different types of wind turbines," in *2012 IEEE International Conference on Cyber Technology in Automation, Control, and Intelligent Systems (CYBER)*, 2012, pp. 292–296, doi: 10.1109/CYBER.2012.6392568.

[93]   S. Y. Liu, C. M. Pimenta, H. A. Pereira, and V. F. Mendes, "Aggregated inverters wind farm harmonic propagation analysis c," no. October 2014, pp. 5180–5186, 2012, doi: 10.13140/2.1.3148.0326.

[94]   S. Chandrasekar and R. Gokaraju, "Dynamic Phasor Modeling of Type 3 DFIG Wind Generators (Including SSCI Phenomenon) for Short-Circuit Calculations," *IEEE Trans. Power Deliv.*, vol. 30, no. 2, pp. 887–897, 2015, doi: 10.1109/TPWRD.2014.2365587.

[95]   F. D. Kanellos and J. Kabouris, "Wind Farms Modeling for Short-Circuit Level Calculations in Large Power Systems," *IEEE Trans. Power Deliv.*, vol. 24, no. 3, pp. 1687–1695, 2009.

[96]   J. Morren and S. Haan, "Short-Circuit Current of Wind Turbines With Doubly Fed Induction Generator," *IEEE Trans. Energy Convers.*, vol. 22, no. 1, pp. 174–180, 2007.

[97]   ABB, "Doubly-fed electrical drivetrain package." https://new.abb.com/motors-generators/segments/wind-power/doubly-fed-electrical-drivetrain-package.

[98]   J. M. Haan and S. W. H. De, "Short-Circuit Current of Wind Turbines With Doubly Fed Induction Generator," *IEEE Trans. Energy Convers.*, vol. 22, no. 1, pp. 174–180, 2007, doi: 10.1109/TEC.2006.889615.

[99]   E. Muljadi and V. Gevorgian, "Short-circuit modeling of a wind power plant," *2011 IEEE Power Energy Soc. Gen. Meet.*, pp. 1–9, 2011, doi: 10.1109/PES.2011.6039068.

[100]   M. Y. Shih, C. A. Castillo Salazar, and A. Conde Enríquez, "Adaptive directional overcurrent relay coordination using ant colony optimisation," *IET Gener. Transm. Distrib.*, vol. 9, no. 14, pp. 2040–2049, 2015, doi: 10.1049/iet-gtd.2015.0394.

[101]   N. Rezaei, M. N. Uddin, I. K. Amin, M. L. Othman, and M. Marsadek, "Genetic Algorithm Based Optimization of Overcurrent Relay Coordination for Improved Protection of DFIG Operated Wind Farms," in *2018 IEEE Industry Applications Society Annual Meeting (IAS)*, Sep. 2018, pp. 1–8, doi: 10.1109/IAS.2018.8544534.

[102]   N. Rezaei, M. N. Uddin, I. K. Amin, M. L. Othman, and M. Marsadek, "Genetic Algorithm-Based Optimization of Overcurrent Relay Coordination for Improved Protection of DFIG Operated Wind Farms," *IEEE Trans. Ind. Appl.*, vol. 55, no. 6, pp. 5727–5736, 2019, doi: 10.1109/TIA.2019.2939244.

[103]   IEEE Std 242-2001, *IEEE Recommended Practice for Protection and Coordination of Industrial and Commercial Power Systems*. 2001.

[104]   J. Diego, D. C. Pico, and G. Ramos, "Protection Coordination Analysis Under a Real-Time Architecture for Industrial Distribution Systems Based on the Std IEEE 242-2001," *IEEE Trans. Ind. Appl.*, vol. 52, no. 4, pp. 2826–2833, 2016.

[105]   S. Mirjalili, S. M. Mirjalili, and A. Lewis, "Grey Wolf Optimizer," *Adv. Eng. Softw.*, vol. 69, pp. 46–61, Mar. 2014, doi: 10.1016/j.advengsoft.2013.12.007.

[106]   S. Mirjalili, S. Saremi, S. M. Mirjalili, and L. D. S. Coelho, "Multi-objective grey wolf

optimizer: A novel algorithm for multi-criterion optimization," *Expert Syst. Appl.*, vol. 47, pp. 106–119, Apr. 2016, doi: 10.1016/j.eswa.2015.10.039.

[107] M. N. Uddin, I. K. Amin, N. Rezaei, and M. Marsadek, "Grey Wolf optimization based power management strategy for battery storage of dfig-wecs in standalone operating mode," *2018 IEEE Ind. Appl. Soc. Annu. Meet. IAS 2018*, pp. 1–7, 2018, doi: 10.1109/IAS.2018.8544633.

[108] N. Rezaei, M. N. Uddin, I. K. Amin, M. L. Othman, and I. Z. Abidin, "Grey Wolf Optimization based Improved Protection of Wind Power Generation Systems," in *2018 IEEE Industry Applications Society Annual Meeting (IAS)*, Sep. 2018, pp. 1–8, doi: 10.1109/IAS.2018.8544502.

[109] N. Rezaei and M. N. Uddin, "State-of-the-Art Microgrid Power Protective Relaying and Coordination Techniques," *2020 IEEE Ind. Appl. Soc. Annu. Meet.*, pp. 1–8, 2020.

[110] N. Rezaei and M. N. Uddin, "Fuzzy Logic Based Adaptive Overcurrent Protection for Wind Farms," *ICREST 2021 - 2nd Int. Conf. Robot. Electr. Signal Process. Tech.*, pp. 225–228, 2021, doi: 10.1109/ICREST51555.2021.9331173.

[111] M. N. Uddin, T. S. Radwan, and M. A. Rahman, "Performances of fuzzy-logic-based indirect vector control for induction motor drive," *IEEE Trans. Ind. Appl.*, vol. 38, no. 5, pp. 1219–1225, Sep. 2002, doi: 10.1109/TIA.2002.802990.

[112] N. Rezaei, M. N. Uddin, I. K. Amin, M. L. Othman, and M. Marsadek, "Novel Differential-based Protection Scheme for Intertie Zone of Large-Scale Centralized DFIG Wind Farms," in *2019 IEEE Industry Applications Society Annual Meeting (IAS)*, 2019, pp. 1–8.

[113] T. Glover, J. D., Sarma, M. S., & Overbye, *Power system analysis & design*. Cengage Learning, 2012.

[114] M. N. Uddin and N. Rezaei, "An FPGA-based Cost-effective Digital Differential Relay for Wind Farm Protection," *2020 IEEE Ind. Appl. Soc. Annu. Meet. IAS 2020*, pp. 1–8, 2020, doi: 10.1109/IAS44978.2020.9334863.

[115] K. Koutroumbas and S. Theodoridis, *Pattern Recognition*, 4th ed. Elsevier, 2008.

[116] D. Bhalla, "Support Vector Machine Simmplified using R," *Listen Data - Make you data tell a story*. https://www.listendata.com/2017/01/support-vector-machine-in-r-tutorial.html.

[117] N. Rezaei, M. N. Uddin, I. K. Amin, M. L. Othman, M. B. Marsadek, and M. M. Hasan, "A Novel Hybrid Machine Learning Classifier-Based Digital Differential Protection Scheme for Intertie Zone of Large-Scale Centralized DFIG-Based Wind Farms," *IEEE Trans. Ind. Appl.*, vol. 56, no. 4, pp. 3453–3465, 2020, doi: 10.1109/TIA.2020.2990584.

[118] L. Nguyen, "Tutorial on support vector machine," *Appl. Comput. Math.*, vol. 4, no. 4–1, pp. 1–15, 2017.

[119] J. C. Ferreira and V. A. Menegatto, "Eigenvalues of integral operators defined by smooth positive definite kernels," *Integr. Equ. Oper. Theory*, vol. 64, no. 1, pp. 61–81, 2009.

[120] C. Savas and F. Dovis, "The Impact of Different Kernel Functions on the Performance of Scintillation Detection Based on Support Vector Machines," *Sensors*, vol. 19, no. 5219, pp. 1–16, 2019.

[121] B. Betrò, "Bayesian methods in global optimization," *J. Glob. Optim.*, vol. 1, no. 1, pp. 1–14, 1991.

[122] J. Wu, X. Y. Chen, H. Zhang, L. D. Xiong, H. Lei, and S. H. Deng, "Hyperparameter optimization for machine learning models based on Bayesian optimization," *J. Electron. Sci. Technol.*, vol. 17, no. 1, pp. 26–40, 2019.

[123] P. J. Lamberson, "Exploration and exploitation, Differential Evolution: In Search of Solutions," *Springer*, pp. 69–81, 2006.

[124] C. E. Rasmussen and C. K. I. Williams, "Gaussian processes for machine learning," *Springer*, vol. 103, no. 14, pp. 63–71, 2003.

[125] R. Reris and J. P. Brooks, "Principal Component Analysis and Optimization: A Tutorial," *Informs Comput. Soc.*, pp. 212–225, 2015.

Appendix
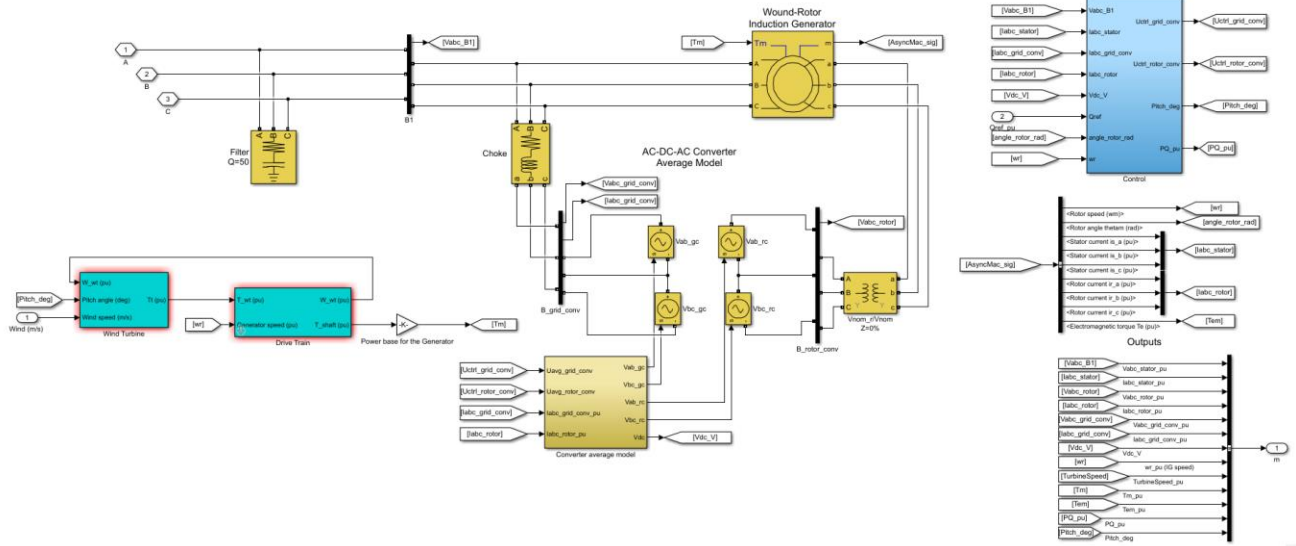
A. 1. Wind turbine generator model.

```matlab
function [NimaTime, NimaTrip] = fcn(CTpri, CTsec, Irms, PS, TMS, TDS, k, n,
clk)
 persistent OCRState OCRTrip OCRTime OCRPickupTime


if isempty(OCRState)
    OCRState = 0;
    OCRTrip = inf;
    OCRTime = inf;
    OCRPickupTime = 0;
end



CT = max(Irms/(CTpri/CTsec));
Pickup = (PS*0.25)*CTsec;



if (OCRState == 0)&&(CT > Pickup)
    OCRPickupTime = clk;
    OCRState = 1;
end



if (OCRState == 1)&&(clk>(OCRPickupTime+0.02))
    if k == 0
        OCRTime = TDS;
    else
        PMS = CT/Pickup;
        OCRTime = ((k/((PMS^n)-1))*(TMS*0.05));
    end
    OCRTrip = OCRPickupTime + OCRTime;
    OCRState = 2;
end
 NimaTrip = OCRTrip;
NimaTime = OCRTime;
```

A. 2. Matlab codes for defining the operation of OCR.

188

```matlab
TMS = str2num(get_param(gcb,'TMS'));
k = str2num(get_param(gcb,'k'));
n = str2num(get_param(gcb,'n'));
I = 1:20;
td = ((k./((I.^n)-1)))*TMS;
loglog(td);
set(gcf, 'Position', [200 150 300 500]);
switch(get_param(gcb,'TCC'))
    case 'IEC Standard Inverse'
        title('IEC Standard Inverse');
        set(gca, 'YTick', (1:10));
        ylim([0.1 10]);
    case 'IEC Very Inverse'
        title('IEC Very Inverse');
        set(gca, 'YTick', (1:2:15));
        ylim([0.01 15]);
    case 'IEC Long Time Inverse'
        title('IEC Long Time Inverse');
        set(gca, 'YTick', (0:20:120));
        ylim([0.1 120]);
    case 'IEC Extremely Inverse'
        title('IEC Extremely Inverse');
        set(gca, 'YTick', (0:5:30));
        ylim([0.01 30]);
end

set(gca, 'XTick', [1:10 20]);
xlim([1 30]);
xlabel('Current (Multiples of Plug Setting)');
ylabel('Operating Time (sec)');
grid on;
```

A. 3 Matlab codes for plotting the TCC curves for OCR.

```matlab
switch(get_param(gcb,'TCC'))
```

```matlab
case 'IEC Standard Inverse'
    set_param(gcb,'k','0.14');
    set_param(gcb,'n','0.02');

case 'IEC Very Inverse'
    set_param(gcb,'k','13.5');
    set_param(gcb,'n','1');

case 'IEC Long Time Inverse'
    set_param(gcb,'k','120');
    set_param(gcb,'n','1');

case 'IEC Extremely Inverse'
    set_param(gcb,'k','80');
    set_param(gcb,'n','2');

    otherwise
    set_param(gcb,'k','0');
    end
```

A. 4. Matlab codes for defining various OCR types based on IEC 60255-151:2009 standard.
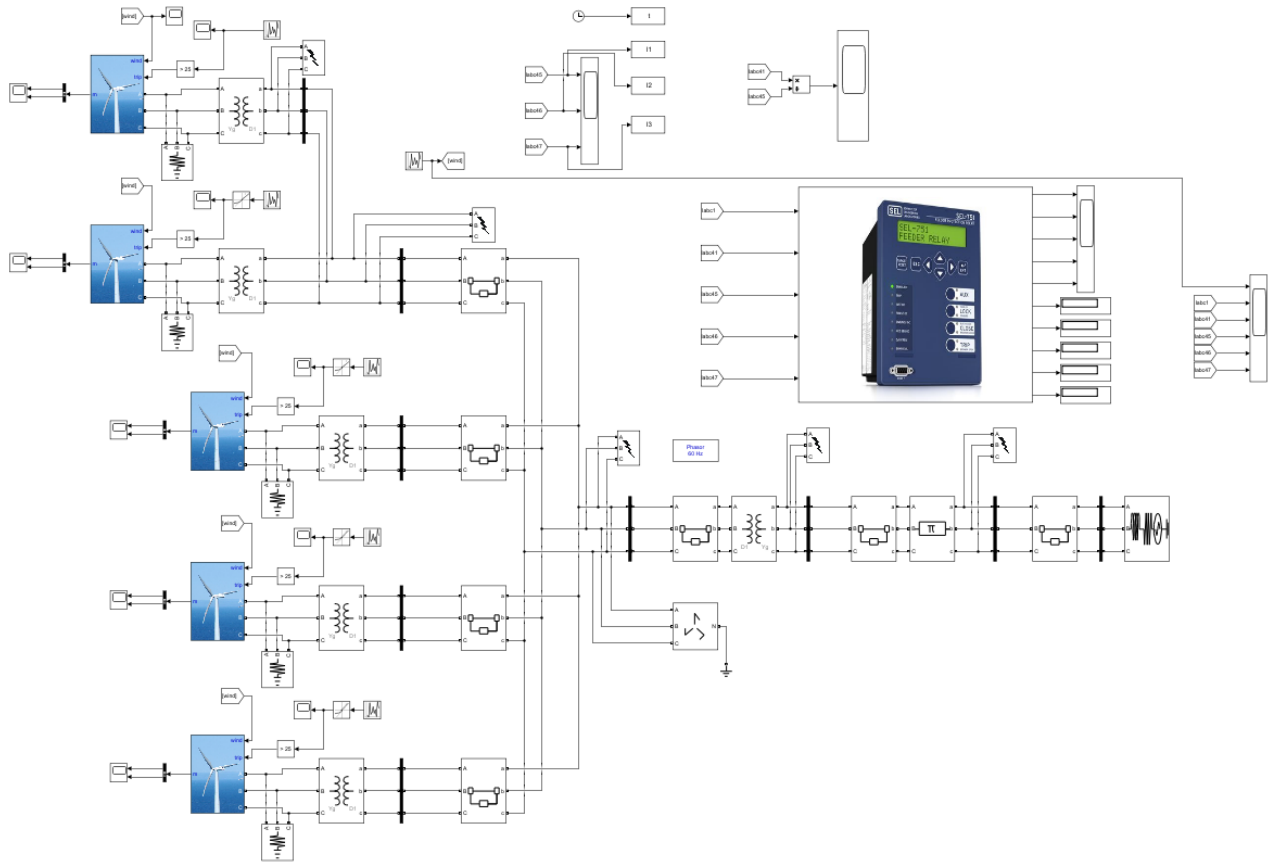
A. 5. Centralized overcurrent protection scheme.
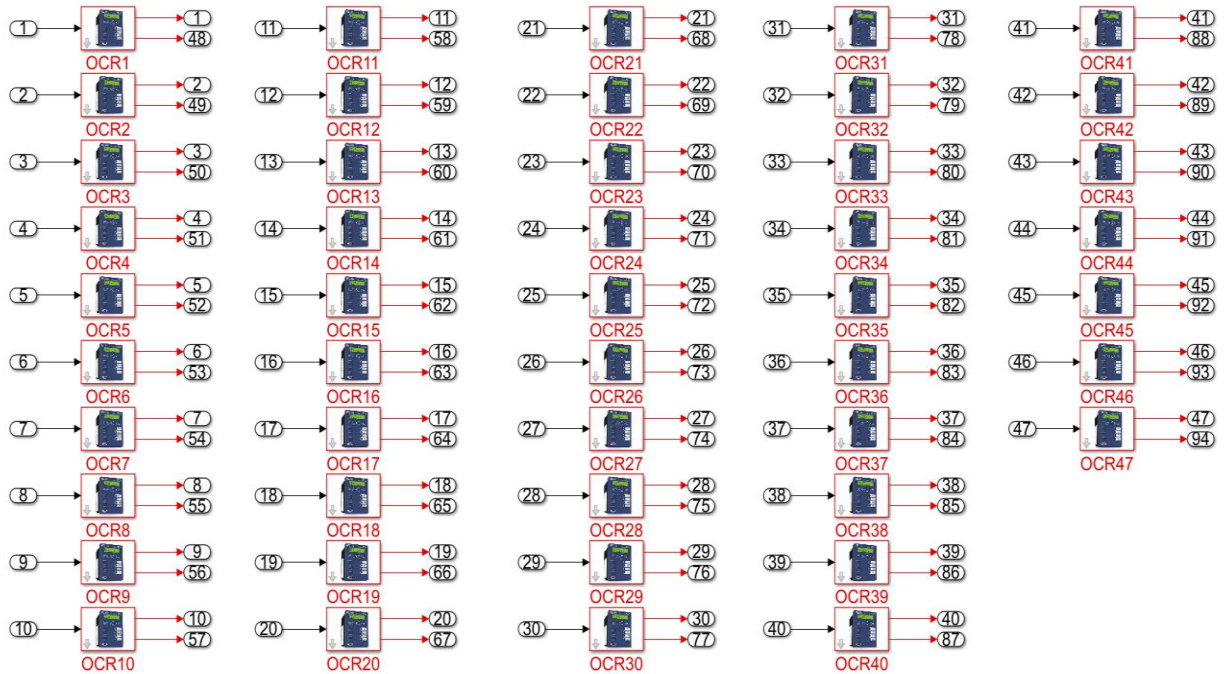
A6. Overcurrent protection relays for the wind farm.

```matlab
SearchAgents_no=300;
ub=[0.05 0.05 0.05 0.05 0.05];
lb=[1 1 1 1 1];
Max_iter=250;
dim=5;
for i=1:dim
        ub_i=ub(i);
        lb_i=lb(i);
        Positions(:,i)=rand(SearchAgents_no,1).*(ub_i-lb_i)+lb_i;
end
Alpha_pos=zeros(1,dim);
Alpha_score=inf;

Beta_pos=zeros(1,dim);
Beta_score=inf;

Delta_pos=zeros(1,dim);
Delta_score=inf;
```

```matlab
Convergence_curve=zeros(1,Max_iter);

l=0;%

while l<Max_iter
    for i=1:size(Positions,1)


        Flag4ub=Positions(i,:)>ub;
        Flag4lb=Positions(i,:)<lb;

Positions(i,:)=(Positions(i,:).*(~(Flag4ub+Flag4lb)))+ub.*Flag4ub+lb.*Flag4lb
;
a = 1;
b = 2;
c = 100;
cti = 0.3;
k = 0.14;
n = 0.02;
PSM(5) = 241.37;
PSM(4) = 19.25;
PSM(3) = 4.93;
PSM(2) = 3.92;
PSM(1) = 5.06;
t(i,5) = (Positions(i,5) * k) /((PSM(5).^n) - 1);
t(i,4) = (Positions(i,4) * k) /((PSM(4).^n) - 1);
t(i,3) = (Positions(i,3) * k) /((PSM(3).^n) - 1);
t(i,2) = (Positions(i,2) * k) /((PSM(2).^n) - 1);
t(i,1) = (Positions(i,1) * k) /((PSM(1).^n) - 1);
T(i) = t(1).^2 + t(2).^2 + t(3).^2 + t(4).^2 + t(5).^2;
TT = ((t(4) - t(5) - cti) - c*((t(4) - t(5) - cti) - abs(t(4) - t(5) -
cti))).^2 + ((t(3) - t(4) - cti) - c*((t(3) - t(4) - cti) - abs(t(3) - t(4) -
cti))).^2 + ((t(2) - t(3) - cti) - c*((t(2) - t(3) - cti) - abs(t(2) - t(3) -
cti)))^2 + ((t(1) - t(2) - cti) - c*((t(1) - t(2) - cti) - abs(t(1) - t(2) -
cti)))^2;

        fitness=a * (T) + b * (TT);
```

```matlab
        if fitness(i)<Alpha_score
            Alpha_score=fitness(i);
            Alpha_pos=Positions(i,:);
        end

        if fitness(i)>Alpha_score && fitness(i)<Beta_score
            Beta_score=fitness(i);
            Beta_pos=Positions(i,:);
        end

        if fitness(i)>Alpha_score && fitness(i)>Beta_score &&
fitness(i)<Delta_score
            Delta_score=fitness(i);
            Delta_pos=Positions(i,:);
        end
    end

    a=2-l*((2)/Max_iter);
    for i=1:size(Positions,1)
        for j=1:size(Positions,2)

            r1=rand();
            r2=rand();

            A1=2*a*r1-a;
            C1=2*r2;)

            D_alpha=abs(C1*Alpha_pos(j)-Positions(i,j));
            X1=Alpha_pos(j)-A1*D_alpha;

            r1=rand();
            r2=rand();

            A2=2*a*r1-a;
            C2=2*r2;
```

```matlab
            D_beta=abs(C2*Beta_pos(j)-Positions(i,j)); %
            X2=Beta_pos(j)-A2*D_beta;

            r1=rand();
            r2=rand();

            A3=2*a*r1-a;
            C3=2*r2;

            D_delta=abs(C3*Delta_pos(j)-Positions(i,j));
            X3=Delta_pos(j)-A3*D_delta;

            Positions(i,j)=(X1+X2+X3)/3;
          w= Positions;
        end
    end
    l=l+1;
    Convergence_curve(l)=Alpha_score;
end
```

A.7. GWO Matlab codes for optimizing the coordination of OCRs for wind farms.

[System]
Name='NimaFuzzylogicR140'
Type='mamdani'
Version=2.0
NumInputs=3
NumOutputs=2
NumRules=4
AndMethod='min'
OrMethod='max'
ImpMethod='min'
AggMethod='max'
DefuzzMethod='centroid'

[Input1]

Name='Ia'

Range=[0 35]

NumMFs=4

MF1='Low':'trapmf',[0 2.17 8.59 10.1]

MF2='Medium':'trapmf',[9.9 11.84 15.83 17.1]

MF3='High':'trapmf',[16.9 20.65 25.99 27.1]

MF4='Ultra':'trapmf',[26.9 28 30 35]

[Input2]

Name='Ib'

Range=[0 35]

NumMFs=4

MF1='Low':'trapmf',[0 2.17 8.59 10.1]

MF2='Medium':'trapmf',[9.9 11.84 15.83 17.1]

MF3='High':'trapmf',[16.9 20.65 25.99 27.1]

MF4='Ultra':'trapmf',[26.9 28 30 35]

[Input3]

Name='Ic'

Range=[0 35]

NumMFs=4

MF1='Low':'trapmf',[0 2.17 8.59 10.1]

MF2='Medium':'trapmf',[9.9 11.84 15.83 17.1]

MF3='High':'trapmf',[16.9 20.65 25.99 27.1]

MF4='Ultra':'trapmf',[26.9 28 30 35]

[Output1]

Name='PS'

Range=[0 200]

NumMFs=7

MF1='PS1':'trimf',[0 25 50]

MF2='PS2':'trimf',[25 50 75]

MF3='PS3':'trimf',[50 75 100]

MF4='PS4':'trimf',[75 100 125]

MF5='PS5':'trimf',[100 125 150]

MF6='PS6':'trimf',[125 150 175]

MF7='PS7':'trimf',[150 175 200]

[Output2]

Name='TMS'

Range=[0 1]

NumMFs=19

MF1='TMS1':'trimf',[0 0.05 0.1]

MF2='TMS2':'trimf',[0.05 0.1 0.15]

MF3='TMS3':'trimf',[0.1 0.15 0.2]

MF4='TMS4':'trimf',[0.15 0.2 0.25]

MF5='TMS5':'trimf',[0.2 0.25 0.3]

MF6='TMS6':'trimf',[0.25 0.3 0.35]

MF7='TMS7':'trimf',[0.3 0.35 0.4]

MF8='TMS8':'trimf',[0.35 0.4 0.45]

MF9='TMS9':'trimf',[0.4 0.45 0.5]

MF10='TMS10':'trimf',[0.45 0.5 0.55]

MF11='TMS11':'trimf',[0.5 0.55 0.6]

MF12='TMS12':'trimf',[0.55 0.6 0.65]

MF13='TMS13':'trimf',[0.6 0.65 0.7]

MF14='TMS14':'trimf',[0.65 0.7 0.75]

MF15='TMS15':'trimf',[0.7 0.75 0.8]

MF16='TMS16':'trimf',[0.75 0.8 0.85]

MF17='TMS17':'trimf',[0.8 0.85 0.9]

MF18='TMS18':'trimf',[0.85 0.9 0.95]

MF19='TMS19':'trimf',[0.9 0.95 1]

[Rules]

4 4 4, 3 1 (1) : 2

3 3 3, 3 1 (1) : 2

2 2 2, 2 1 (1) : 2

1 1 1, 1 1 (1) : 2

A. 8. Fuzzy logic parameters and definition for OCRs 1-40.

[System]

Name='NimaFuzzylogicR4144'

Type='mamdani'

Version=2.0

NumInputs=3

NumOutputs=2

NumRules=4

AndMethod='min'

OrMethod='max'

ImpMethod='min'

AggMethod='max'

DefuzzMethod='centroid'

[Input1]

Name='Ia'

Range=[0 350]

NumMFs=4

MF1='Low':'trapmf',[0 21.7 86.14 101]

MF2='Medium':'trapmf',[99 118.68 158.58 171]

MF3='High':'trapmf',[169 206.81 260.19 271]

MF4='Ultra':'trapmf',[269 280 300 350]

[Input2]
Name='Ib'
Range=[0 350]
NumMFs=4
MF1='Low':'trapmf',[0 21.7 86.14 101]
MF2='Medium':'trapmf',[99 118.7 158.6 171]
MF3='High':'trapmf',[169 206.8 260.2 271]
MF4='Ultra':'trapmf',[269 280 300 350]

[Input3]
Name='Ic'
Range=[0 350]
NumMFs=4
MF1='Low':'trapmf',[0 21.7 86.14 101]
MF2='Medium':'trapmf',[99 118.7 158.6 171]
MF3='High':'trapmf',[169 206.8 260.2 271]
MF4='Ultra':'trapmf',[269 280 300 350]

[Output1]
Name='PS'
Range=[0 200]
NumMFs=7
MF1='PS1':'trimf',[0 25 50]
MF2='PS2':'trimf',[25 50 75]
MF3='PS3':'trimf',[50 75 100]
MF4='PS4':'trimf',[75 100 125]
MF5='PS5':'trimf',[100 125 150]
MF6='PS6':'trimf',[125 150 175]

MF7='PS7':'trimf',[150 175 200]

[Output2]

Name='TMS'

Range=[0 1]

NumMFs=19

MF1='TMS1':'trimf',[0 0.05 0.1]

MF2='TMS2':'trimf',[0.05 0.1 0.15]

MF3='TMS3':'trimf',[0.1 0.15 0.2]

MF4='TMS4':'trimf',[0.15 0.2 0.25]

MF5='TMS5':'trimf',[0.2 0.25 0.3]

MF6='TMS6':'trimf',[0.25 0.3 0.35]

MF7='TMS7':'trimf',[0.3 0.35 0.4]

MF8='TMS8':'trimf',[0.35 0.4 0.45]

MF9='TMS9':'trimf',[0.4 0.45 0.5]

MF10='TMS10':'trimf',[0.45 0.5 0.55]

MF11='TMS11':'trimf',[0.5 0.55 0.6]

MF12='TMS12':'trimf',[0.55 0.6 0.65]

MF13='TMS13':'trimf',[0.6 0.65 0.7]

MF14='TMS14':'trimf',[0.65 0.7 0.75]

MF15='TMS15':'trimf',[0.7 0.75 0.8]

MF16='TMS16':'trimf',[0.75 0.8 0.85]

MF17='TMS17':'trimf',[0.8 0.85 0.9]

MF18='TMS18':'trimf',[0.85 0.9 0.95]

MF19='TMS19':'trimf',[0.9 0.95 1]

[Rules]

4 4 4, 4 4 (1) : 2

3 3 3, 3 4 (1) : 2

2 2 2, 2 4 (1) : 2

1 1 1, 1 5 (1) : 2

A. 9. Fuzzy logic parameters and definition for OCRs 41-44.

[System]

Name='NimaFuzzylogicR45'

Type='mamdani'

Version=2.0

NumInputs=3

NumOutputs=2

NumRules=4

AndMethod='min'

OrMethod='max'

ImpMethod='min'

AggMethod='max'

DefuzzMethod='centroid'

[Input1]

Name='Ia'

Range=[0 1500]

NumMFs=4

MF1='Low':'trapmf',[0 84.35 340.3 450]

MF2='Medium':'trapmf',[440 470.5 630.06 750]

MF3='High':'trapmf',[740 823 1036 1100]

MF4='Ultra':'trapmf',[1090 1200 1350 1500]

[Input2]

Name='Ib'

Range=[0 1500]

NumMFs=4

MF1='Low':'trapmf',[0 84.35 340.3 450]

MF2='Medium':'trapmf',[440 470.5 630.1 750]

MF3='High':'trapmf',[740 823 1036 1100]

MF4='Ultra':'trapmf',[1090 1200 1350 1500]

[Input3]

Name='Ic'

Range=[0 1500]

NumMFs=4

MF1='Low':'trapmf',[0 84.35 340.3 450]

MF2='Medium':'trapmf',[440 470.5 630.1 750]

MF3='High':'trapmf',[740 823 1036 1100]

MF4='Ultra':'trapmf',[1090 1200 1350 1500]

[Output1]

Name='PS'

Range=[0 200]

NumMFs=7

MF1='PS1':'trimf',[0 25 50]

MF2='PS2':'trimf',[25 50 75]

MF3='PS3':'trimf',[50 75 100]

MF4='PS4':'trimf',[75 100 125]

MF5='PS5':'trimf',[100 125 150]

MF6='PS6':'trimf',[125 150 175]

MF7='PS7':'trimf',[150 175 200]

[Output2]

Name='TMS'

Range=[0 1]

NumMFs=19

MF1='TMS1':'trimf',[0 0.05 0.1]

MF2='TMS2':'trimf',[0.05 0.1 0.15]

MF3='TMS3':'trimf',[0.1 0.15 0.2]

MF4='TMS4':'trimf',[0.15 0.2 0.25]

MF5='TMS5':'trimf',[0.2 0.25 0.3]

MF6='TMS6':'trimf',[0.25 0.3 0.35]

MF7='TMS7':'trimf',[0.3 0.35 0.4]

MF8='TMS8':'trimf',[0.35 0.4 0.45]

MF9='TMS9':'trimf',[0.4 0.45 0.5]

MF10='TMS10':'trimf',[0.45 0.5 0.55]

MF11='TMS11':'trimf',[0.5 0.55 0.6]

MF12='TMS12':'trimf',[0.55 0.6 0.65]

MF13='TMS13':'trimf',[0.6 0.65 0.7]

MF14='TMS14':'trimf',[0.65 0.7 0.75]

MF15='TMS15':'trimf',[0.7 0.75 0.8]

MF16='TMS16':'trimf',[0.75 0.8 0.85]

MF17='TMS17':'trimf',[0.8 0.85 0.9]

MF18='TMS18':'trimf',[0.85 0.9 0.95]

MF19='TMS19':'trimf',[0.9 0.95 1]

[Rules]

4 4 4, 3 4 (1) : 2

3 3 3, 3 4 (1) : 2

2 2 2, 2 5 (1) : 2

1 1 1, 1 6 (1) : 2

A. 10. Fuzzy logic parameters and definition for OCRs 45.

[System]

Name='NimaFuzzylogicR46'

Type='mamdani'

Version=2.0

NumInputs=3

NumOutputs=2

NumRules=4

AndMethod='min'

OrMethod='max'

ImpMethod='min'

AggMethod='max'

DefuzzMethod='centroid'

[Input1]

Name='Ia'

Range=[0 250]

NumMFs=4

MF1='Low':'trapmf',[0 12.91 53.56 70]

MF2='Medium':'trapmf',[69 74.27 99.65 120]

MF3='High':'trapmf',[119 130.3 164.3 170]

MF4='Ultra':'trapmf',[169 180 225 250]

[Input2]

Name='Ib'

Range=[0 250]

NumMFs=4

MF1='Low':'trapmf',[0 12.91 53.56 70]

MF2='Medium':'trapmf',[69 74.27 99.65 120]

MF3='High':'trapmf',[119 130.3 164.3 170]

MF4='Ultra':'trapmf',[169 180 225 250]

[Input3]

Name='Ic'

Range=[0 250]

NumMFs=4

MF1='Low':'trapmf',[0 12.91 53.56 70]

MF2='Medium':'trapmf',[69 74.27 99.65 120]

MF3='High':'trapmf',[119 130.3 164.3 170]

MF4='Ultra':'trapmf',[169 180 225 250]

[Output1]

Name='PS'

Range=[0 200]

NumMFs=7

MF1='PS1':'trimf',[0 25 50]

MF2='PS2':'trimf',[25 50 75]

MF3='PS3':'trimf',[50 75 100]

MF4='PS4':'trimf',[75 100 125]

MF5='PS5':'trimf',[100 125 150]

MF6='PS6':'trimf',[125 150 175]

MF7='PS7':'trimf',[150 175 200]

[Output2]

Name='TMS'

Range=[0 1]

NumMFs=19

MF1='TMS1':'trimf',[0 0.05 0.1]

MF2='TMS2':'trimf',[0.05 0.1 0.15]

MF3='TMS3':'trimf',[0.1 0.15 0.2]

MF4='TMS4':'trimf',[0.15 0.2 0.25]

MF5='TMS5':'trimf',[0.2 0.25 0.3]

MF6='TMS6':'trimf',[0.25 0.3 0.35]

MF7='TMS7':'trimf',[0.3 0.35 0.4]

MF8='TMS8':'trimf',[0.35 0.4 0.45]

MF9='TMS9':'trimf',[0.4 0.45 0.5]

MF10='TMS10':'trimf',[0.45 0.5 0.55]

MF11='TMS11':'trimf',[0.5 0.55 0.6]

MF12='TMS12':'trimf',[0.55 0.6 0.65]

MF13='TMS13':'trimf',[0.6 0.65 0.7]

MF14='TMS14':'trimf',[0.65 0.7 0.75]

MF15='TMS15':'trimf',[0.7 0.75 0.8]

MF16='TMS16':'trimf',[0.75 0.8 0.85]

MF17='TMS17':'trimf',[0.8 0.85 0.9]

MF18='TMS18':'trimf',[0.85 0.9 0.95]

MF19='TMS19':'trimf',[0.9 0.95 1]

[Rules]

4 4 4, 4 11 (1) : 2

3 3 3, 3 12 (1) : 2

2 2 2, 2 14 (1) : 2

1 1 1, 1 15 (1) : 2

A. 11. Fuzzy logic parameters and definition for OCRs 46 and 47.
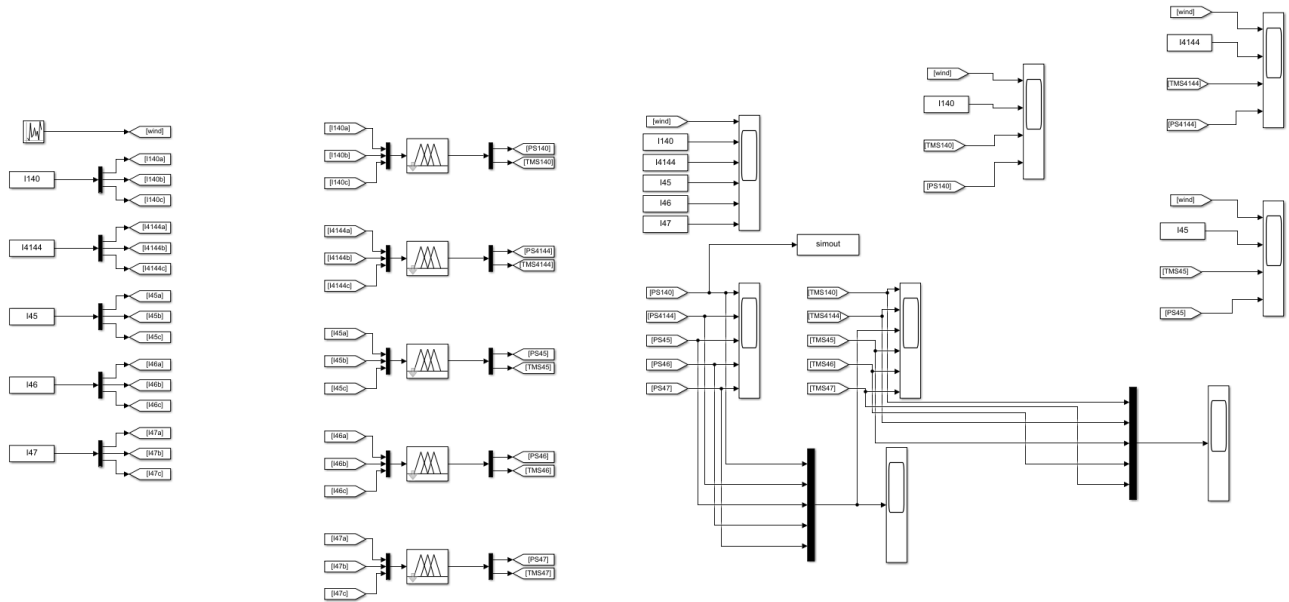
A. 12. Adaptive Fuzzy Logic Protection Scheme (Mamdani).
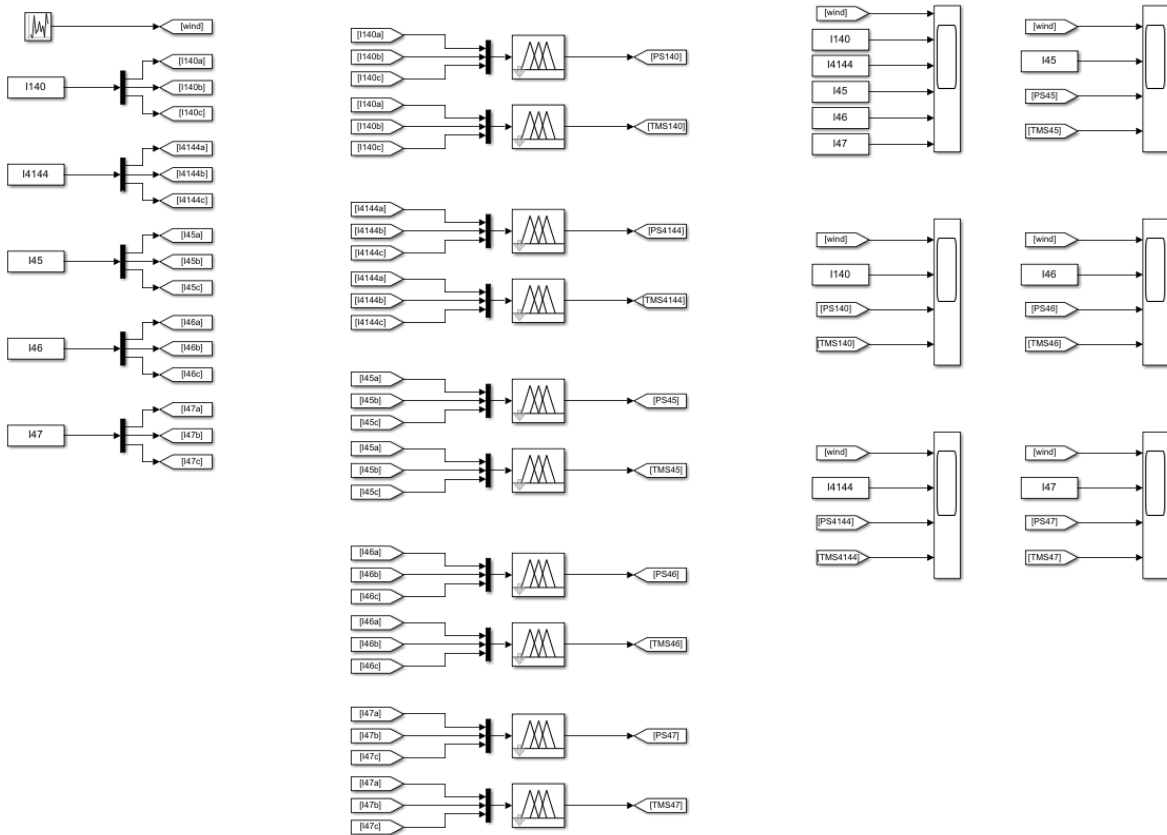
A. 13. Adaptive Fuzzy Logic Protection Scheme (Sugeno).
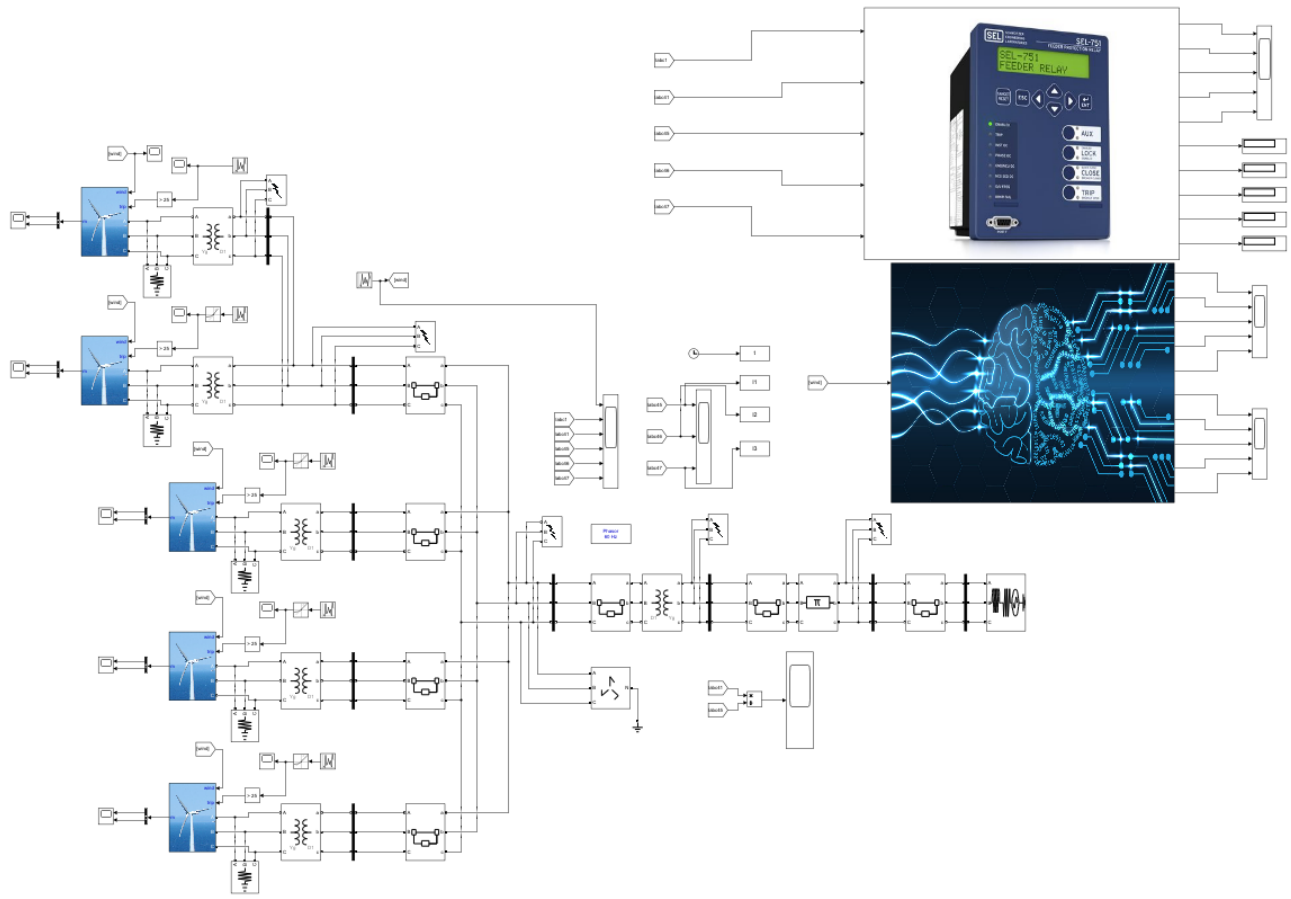
A. 14. Intelligent and adaptive centralized overcurrent protection and coordination scheme.
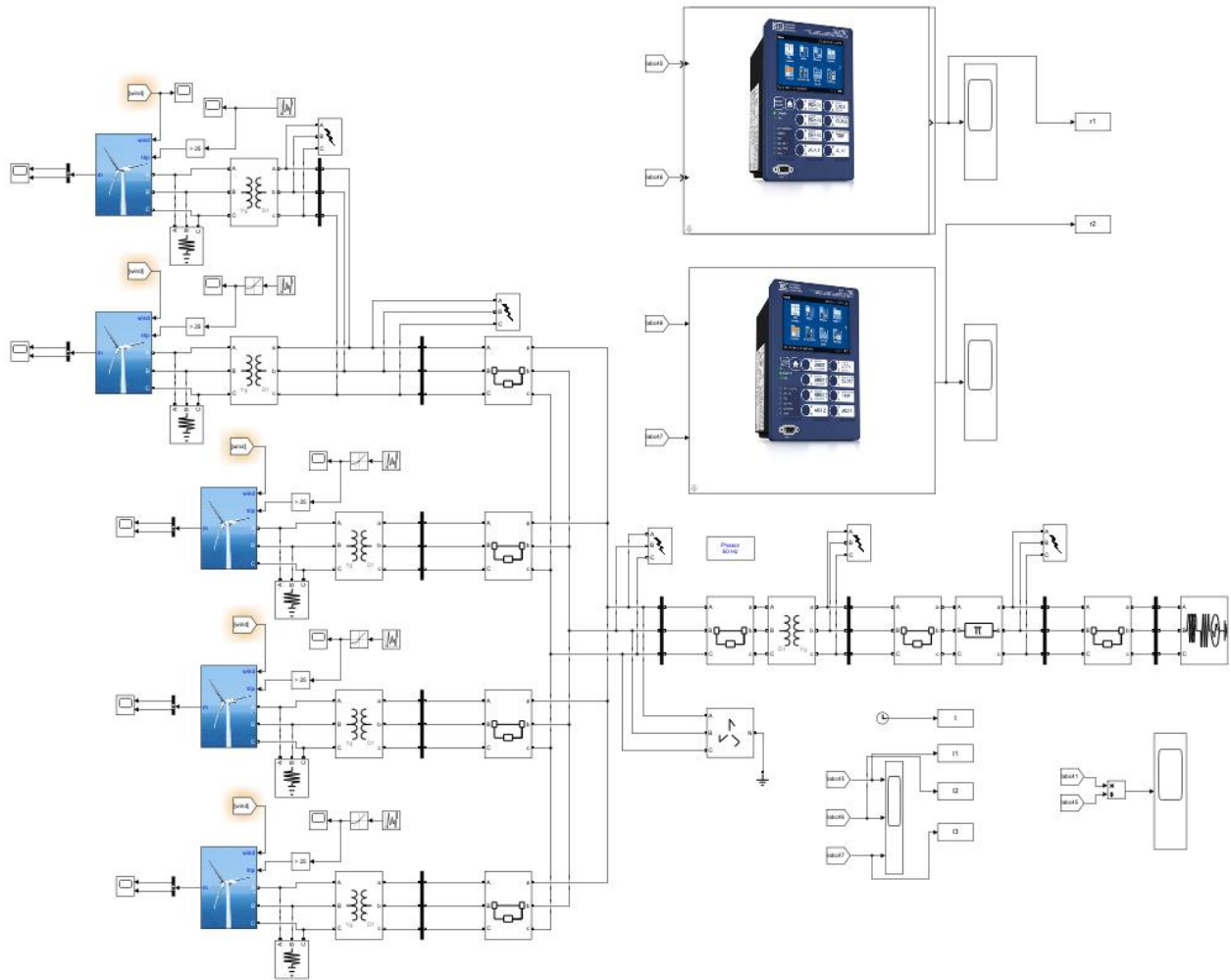
A. 15. Centralized differential protection scheme.
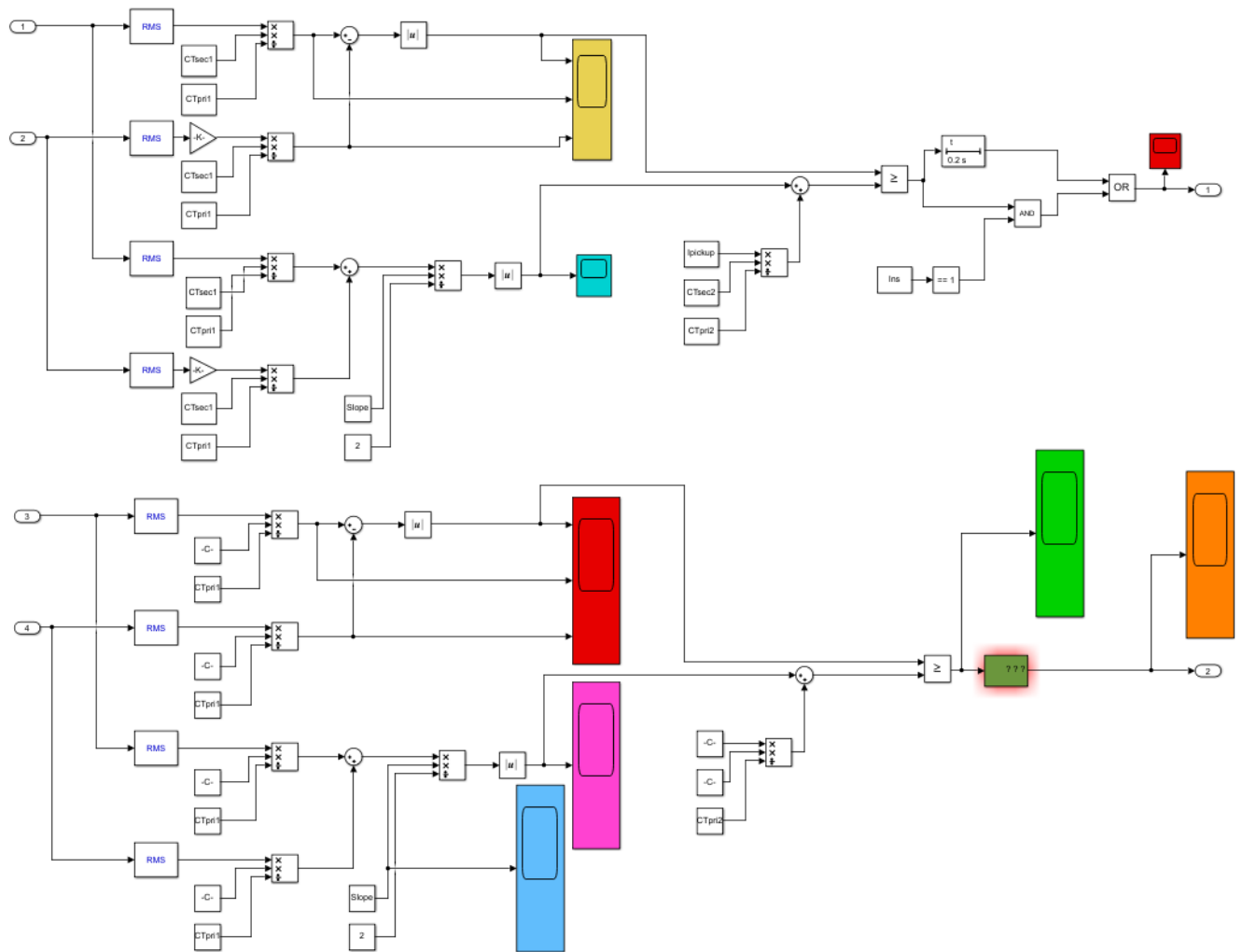
A. 16. Differential protection scheme for the intertie section of the wind farm.

module Nima_protection_relay (r, w, a, b);

parameter p = 32'b00000000_00000011_01010100_01111010;

parameter k = 32'b00000000_00000000_00011001_10011001;

input signed [31:0] a, b;

output r, w;

reg r;

reg w;

reg signed [31:0] lefthandside, currentaddition, divisionofcurrentaddition, formattedsloperatiomultiplication, righthandside;

reg signed [63:0] sloperatiomultiplication;

always @ (a, b)

begin

       lefthandside = a - b;

       currentaddition = a + b;

       divisionofcurrentaddition = {1'b0, currentaddition[31:1]};

       sloperatiomultiplication = k * divisionofcurrentaddition;

       formattedsloperatiomultiplication = sloperatiomultiplication[47:16];

       righthandside = formattedsloperatiomultiplication + p;

       if (lefthandside > righthandside)

       begin

              r = 1'b1;

              w = 1'b0;

       end

       else

       begin

```
                    r = 1'b0;

                    w = 1'b1;

            end



end



endmodule
```

A. 17. Simplified FPGA Verilog codes for the proposed FPGA-DDPS.
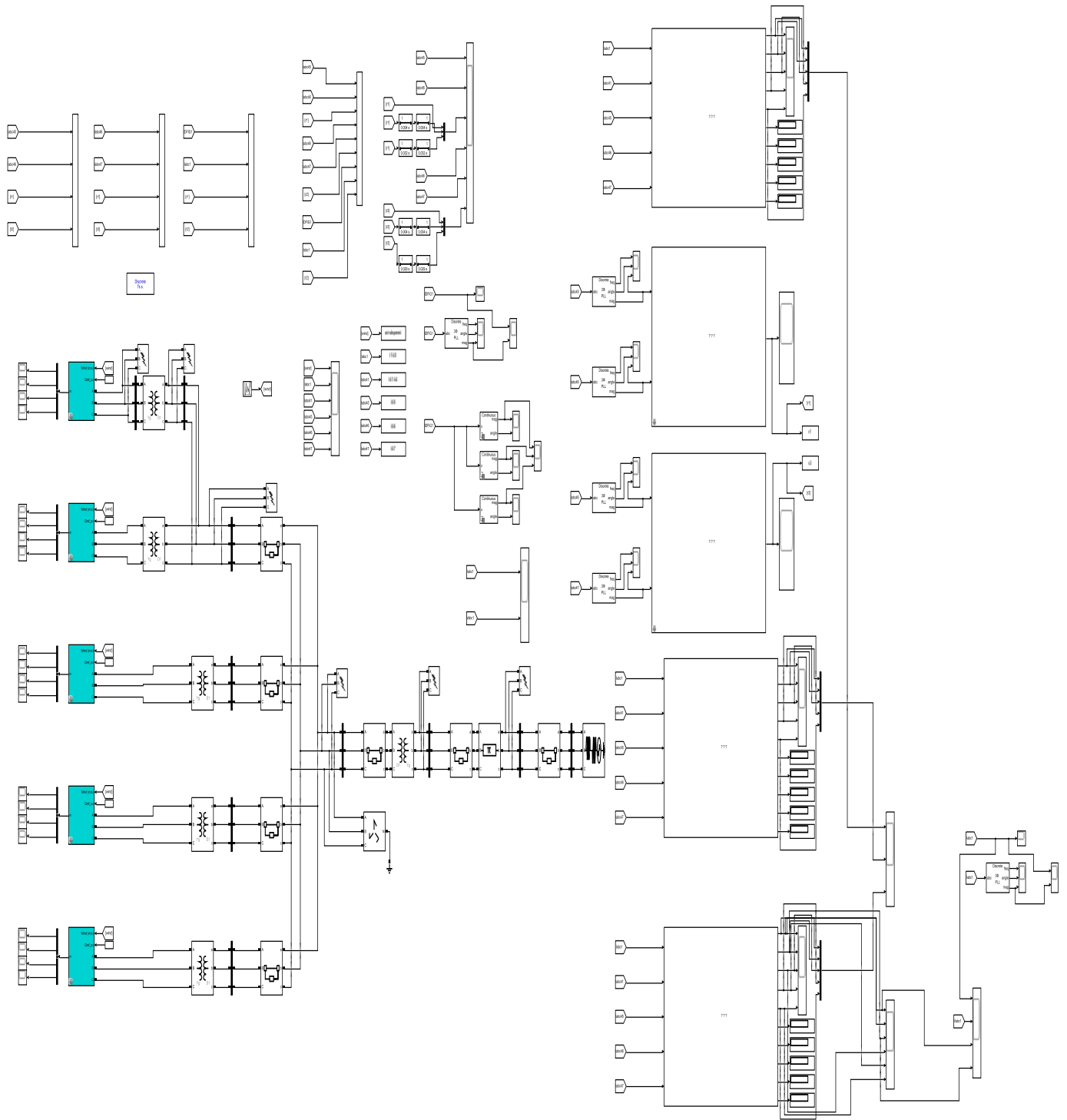
A. 18. Operation of machine learning-based protection schemes.

List of Publications

The outcome of this research was published in 11 peer-reviewed scientific journals and conferences, as listed below:

Journals

1. N. Rezaei and M. N. Uddin, "An Analytical Review on State-of-the-Art Microgrid Protective Relaying and Coordination Techniques," in IEEE Transactions on Industry Applications, vol. 57, no. 3, pp. 2258-2273, May-June 2021, doi: 10.1109/TIA.2021.3057308).

2. N. Rezaei, M. N. Uddin, I. K. Amin, M. L. Othman, M. B. Marsadek and M. M. Hasan, "A Novel Hybrid Machine Learning Classifier-Based Digital Differential Protection Scheme for Intertie Zone of Large-Scale Centralized DFIG-Based Wind Farms," in IEEE Transactions on Industry Applications, vol. 56, no. 4, pp. 3453-3465, July-Aug. 2020, doi: 10.1109/TIA.2020.2990584.

3. N. Rezaei, M. N. Uddin, I. K. Amin, M. L. Othman and M. Marsadek, "Genetic Algorithm-Based Optimization of Overcurrent Relay Coordination for Improved Protection of DFIG Operated Wind Farms," in IEEE Transactions on Industry Applications, vol. 55, no. 6, pp. 5727-5736, Nov.-Dec. 2019, doi: 10.1109/TIA.2019.2939244.

Conferences

1. M. N. Uddin, N. Rezaei, and O. Emmanuel, "Adaptive and Optimal Overcurrent Protection of Wind Farms with Improved Reliability", 2021 IEEE Industry Applications Society Annual Meeting, Vancouver, BC, Canada. (Accepted – waiting for publication).

2. N. Rezaei and M. N. Uddin, "Fuzzy Logic Based Adaptive Overcurrent Protection for Wind Farms," 2021 2nd International Conference on Robotics, Electrical and Signal Processing Techniques (ICREST), DHAKA, Bangladesh, 2021, pp. 768-771, doi: 10.1109/ICREST51555.2021.9331046.

3. N. Rezaei, M. N. Uddin "State-of-the-Art Microgrid Power Protective Relaying and Coordination Techniques," 2020 IEEE Industry Applications Society Annual Meeting, Detroit, MI, USA, 2020, pp. 1-9, doi: 10.1109/IAS44978.2020.9334901.

4. M. N. Uddin and N. Rezaei, "An FPGA-based Cost-effective Digital Differential Relay for Wind Farm Protection," 2020 IEEE Industry Applications Society Annual Meeting, Detroit, MI, USA, 2020, pp. 1-8, doi: 10.1109/IAS44978.2020.9334863.

5. N. Rezaei, M. N. Uddin, I. K. Amin, M. L. Othman and M. Marsadek, "A Novel Differential-based Protection Scheme for Intertie Zone of Large-Scale Centralized DFIG Wind Farms," 2019 IEEE Industry Applications Society Annual Meeting, Baltimore, MD, USA, 2019, pp. 1-8, doi: 10.1109/IAS.2019.8912373.

6. N. Rezaei, M. N. Uddin, I. K. Amin, M. L. Othman and M. Marsadek, "Genetic Algorithm Based Optimization of Overcurrent Relay Coordination for Improved Protection of DFIG Operated Wind Farms," 2018 IEEE Industry Applications Society Annual Meeting (IAS), Portland, OR, 2018, pp. 1-8, doi: 10.1109/IAS.2018.8544534.

7. N. Rezaei, M. N. Uddin, I. K. Amin, M. L. Othman and I. Z. Abidin, "Grey Wolf Optimization based Improved Protection of Wind Power Generation Systems," 2018 IEEE Industry Applications Society Annual Meeting (IAS), Portland, OR, 2018, pp. 1-8, doi: 10.1109/IAS.2018.8544502.

8. M. N. Uddin, I. K. Amin, N. Rezaei and M. Marsadek, "Grey Wolf Optimization based Power Management Strategy for Battery Storage of DFIG-WECS in Standalone Operating Mode," 2018 IEEE Industry Applications Society Annual Meeting (IAS), Portland, OR, 2018, pp. 1-7, doi: 10.1109/IAS.2018.8544633.